京都大学学術情報リポジトリ
KURENAI 紅
Kyoto University Research Information Repository

京都大学
KYOTO UNIVERSITY

Title	Creation and Characterization of Novel Organic Optical and Electronic Materials through Conjugation of Oligo(phenyleneethynylene) with Helical Peptides(Dissertation_全文)
Author(s)	Nakayama, Hidenori
Citation	Kyoto University (京都大学)
Issue Date	2012-03-26
URL	http://dx.doi.org/10.14989/doctor.k16805
Right	許諾条件により要旨・本文は2013-04-01に公開
Type	Thesis or Dissertation
Textversion	author

Kyoto University

Creation and Characterization of Novel Organic Optical and Electronic Materials through Conjugation of Oligo(phenyleneethynylene) with Helical Peptides

Hidenori Nakayama

2012

Science is a wonderful thing
if one does not have to earn one's living at it.
—Albert Einstein

CONTENTS

Preface

It was even before beginning of the author's very first year of the undergraduate course at Kyoto University that he decided to be supervised by Prof. Shunsaku Kimura. He had already decided to do a research on organic semiconductors for electronic and optical devices, because he was deeply impressed by researches on conducting polymers, which led to a Nobel Prize winning accomplishment by Prof. Hideki Shirakawa and his colleagues. The author was certain that such organic compounds could suggest new solutions for computing devices. Prof. Kimura's ambition was just on the line, but even more challenging and exciting: he was trying to apply biomaterials, especially helical peptides (HPs), to build up optical and electronic devices. Four years later, the author was in Prof. Kimura's office selecting his research theme with other students. No hesitation was there to decide to pick up the theme for this dissertation. The following contents are accomplishments with the author's firm determination to acquire a Ph. D degree with this theme under Prof. Kimura's supervising.

All of the researches in this dissertation have a common starting point: conjugate oligo(phenyleneethynylene) (OPEs) and HPs to obtain molecules of novel characters. It seems unwise to confine limited building blocks. In addition, the two compounds have been studied well for decades. Such confinement is, however, turned out to be effective in finding a way to exploit OPEs and HPs. The following descriptions show that there are still some new features in these well-studied compounds. The author finally found that HPs can tune the properties of OPEs in unique ways. This dissertation will tell the readers that discovery of a new functional molecule is not always equal to seeking new molecular skeletons or way of substitutions, but it can be just trying new combination of well-known

functional structures.

The dissertation also deals with synthetic schemes of the OPE-HP conjugates as well as the properties of the conjugates. The schemes have been optimized over countless number of trials. These will be helpful for those who challenge synthesizing complex compounds based on HPs and OPEs.

The contents of each chapter are nearly identical to corresponding articles. The introduction of each chapter is revised so that development of the author's research can be easily followed by the readers.

The author cited a considerable amount of articles on OPEs and HPs in General Introduction. They are chronologically introduced so that the development of the researches becomes clear to the readers. The author hopes General Introduction as well as each of the chapters will help the readers in locating the historical position of the dissertation and inspire them with their own researches.

List of Abbreviations

^{1}H NMR	proton nuclear magnetic resonance
^{1}H–^{1}H COSY	proton–proton correlation spectroscopy
Ac	acetyl
AcOH	acetic acid
AFM	atomic force microscopy
Aib	α-aminoisobutyric acid
Ala	L-alanine
APS	(3-aminopropyl)trimethoxysilane
aq.	aqueous solution
Asp	L-asparatic acid
B3LYP	Becke's three parameter hybrid functional and Lee–Yang–Parr correlation
BA*n*M	Boc-(Ala-Aib)$_{n/2}$-OMe
Boc	*tert*-butyloxycarbonyl
CD	circular dichroism
CuI	copper(I) iodide
CV	cyclic voltammetry
C10	1-decanethiol
C12	1-dodecanethiol
DCC	dicyclohexylcarbodiimide
DCE	1,2-dichloroethane
D–D	dipole–dipole
DFT	density functional theory
DIA	diisopropylamine
DIEA	diisopropylethylamine
DMAP	*N*,*N*-dimethylaminopyridine
DMF	*N*,*N*-dimethylformamide
DMPEB	*p*-di(*p*-methylphenylethynyl)aromatic
DMSO	dimethylsulfoxide
DTT/TG	dithiotheriol/α-thioglycerol (1/2, v/v)

EI	electron ionization
EtOAc	ethyl acetate
Et_2O	diethyl ether
EtOH	ethanol
FAB	fast atom bombardment
FET	field effect transistor
Glu	L-glutamic acid
HA*n*M	H-(Ala-Aib)$_{n/2}$-OMe
HATU	*O*-(7-azobenzotriazol-1-yl)-1,1,3,3-tetramethyluronium hexafluorophosphate
HOAt	1-hydroxy-7-azabenzotriazole
HP	helical peptide
HPLC	high performance liquid chromatography
iPr_2O	diisopropyl ether
IR	infrared
IR-RAS	infrared reflection-absorption spectroscopy
LB	Langmuir–Blodgett
LED	light-emitting device
NBA	3-nitrobenzylalcohol
NLO	non-linear optical
MeOH	methanol
NDR	negative differential resistance
MS	mass spectrometry
OMe	methyl ester
OPac	phenacyl ester
OPE	oligo(phenyleneethynylene)
OPV	oligo(phenylenevinylene)
Orn	L-ornithine
O^{t}Bu	*tert*-butyl ester
$Pd(PhCN)_2Cl_2$	bis(benzonitril)palladium(II) dichloride
$Pd(PPh_3)_2Cl_2$	bis(triphenylphosphine)palladium(II) dichloride
PPE	poly(*p*-phenyleneethynylene)
PPP	poly(*p*-phenylene)
PPV	poly(*p*-phenylenevinylene)

PT	polythiophene
RBF	round-bottomed flask
RT	room temperature
SAM	self-assembled monolayer
SPM	scanning probe microscope
SHG	secondary harmonic generation
SSA*n*H	$\overline{\text{SSCH}_2\text{CH}_2\text{CH}}(\text{CH}_2)_4\text{CO-(Ala-Aib)}_{n/2}\text{-OH}$
STM	scanning tunneling microscopy
TBAF	tetrabutylammonium fluoride
TD-DFT	time dependent-density functional theory
TFA	trifluoroacetic acid
TFE	2,2,2-trifluoroethanol
THF	tetrahydrofurane
TLC	thin layer chromatography
TMSA	trimethylsilylacetylene
UV	ultraviolet
Val	L-valine
λ_{max}	maximum absorbance wavelength
π–*A*	surface pressure–surface area

List of Experimental Equipments

Absorption spectroscopy: Shimadzu UV-2450PC spectrometer (for transmission measurements), System Instruments SIS-50 surface and interface spectrometer (for measurements with an optical waveguide)

CD spectroscopy: JASCO J-600 CD spectropolarimeter

Computational calculation: Gaussian, Inc. Gaussian 03 program on a Fujitsu HX600 cluster (operation system: RedHat Enterprise Linux AS V4)

CV: BAS model 604

EI-MS: JEOL JMS-MS700

Ellipsometry: MIZOJIRI DHA-OLS/S auto-ellipsometer

FAB-MS: JEOL JMS-HX110A

Fluorescence and excitation spectroscopy: JASCO FP-6600 spectrometer

Fluorescence lifetime measurement: Spectra Physics Tsunami (Ti:sapphire laser); Spectra Physics Millennia Xs (diode laser); Spectra Physics model 3980 (pulse selector); JASCO M10 (monochromator); Hamamatsu model C3360 (photomultiplier)

Graphical user interface for computation: Semichem, Inc. Gaussview program Ver. 4.1.2 and 5.0.8

HPLC: TOSOH DP-8020 (pump); SD-8022 (degasser); UV-8020 (UV detector); and RI-8020 (reflective index detector)

IR spectroscopy: Nicolet Magna 850 fourier transform infrared spectrometer

IR-RAS: Nicolet Magna 850 fourier transform infrared spectrometer with Harrick RMA-1DG/VRA reflection attachment

NMR: Bruker DPX-400 spectrometer

MALDI-MS: Thermo LTQ ORBITRAP XL

STM: UNISOKU USM-1100SA connected by RHK Technology SPM 100 and PMC 100

STM controller: RHK Technology XPM Pro Ver. 1.2.3.4

Vapor deposition of metals: Osaka Vacuum N-KS350 metal deposition system

π−*A* Isotherm and LB layer preparation: USI 3-22N Langmuir film balance with a trough of a 100 × 278 mm area

General Introduction

Learning molecular designing from creatures

Better materials make our physical life easier. This has been true since human beings began creation of tools. Iron enabled our ancestors to construct a society of far higher productivity than ever before. Papers drastically raised both quality and quantity of our knowledge. Synthetic fibers and resins have made our lives much more comfortable. Science and technology on materials are thus essential to maintain and improve our civilization.

Organic materials are currently among of the most promising materials. As well as further progress of traditional organic materials such as polymers, the application range of organic materials is expanding to the area where inorganic materials have exclusively dominated. This is observed as a rapid development of semiconductors and biomedical materials based on organic materials. One reason for such expansion is our requirement for more energy efficient and environmentally benign products. Organic semiconductor devices are thought to consume less power than inorganic ones and can be free from harmful inorganic elements. Organic medical materials can be highly biocompatible since our body is mainly organic. Another reason is splendid development on organic synthesis in the last century, which followed the year of development of the Grignard reagents.[1] Inventors of the Diels-Alder reaction,[2–4] the Ziegler-Natta catalyst,[5–7] hydroboration,[8,9] the Wittig reaction,[10–12] solid state synthesis,[13,14] the concept of retrosynthesis,[15–17] asymmetric catalysts,[18–22] olefin metathesis,[23–25] and cross coupling reactions[26–28] are laureates of the Nobel prize.

To secure the development of organic materials, a plenty of strategies in molecular designing have been iinvented. However, no matter what reactions we take, we have used

only three strategies to design organic molecules. Creation of novel skeletons is one of them. Alternation of atomic arrangements can drastically change properties of a compound.[29] A famous example is fullerene.[30–32] Even though it is composed only of carbon and hydrogen, the topology distinguishes it from that of other π-conjugate compounds. Fullerene derivatives are now gathering great attention as stable electron-acceptors in organic electronics[33,34] and photovoltaic cells,[35–38] and carriers of small atoms, molecules, or ions.[39] The second strategy is substitution. It has been the first choice for chemist to select substituents to obtain compounds of desired solubility, reactivity, or electronic state. Systematic analysis of electronic effect of substituents has thus been one of the main concerns in organic chemistry since Hammett firstly reported the relationship of substituents and reactivity in aromatic compounds in 1935.[40–42] Not only substituting a hydrogen with a functional group but also a carbon with a heteroatom is frequently adopted. The third one is combination of two or more skeletons. Many kinds of copolymers have been synthesized since their properties are different from that of the mixtures of polymers composed of corresponding monomers. Molecular devices and machines, a recent trend in organic functional materials, are mostly made of several skeletons each of which has a specific role.[43]

Then, a question would arise: is there another way for molecular designing? To have an answer, it is wise to be aware that not only has human intelligence been in quest of better organic materials, but also creatures have also continuously been searching for them. After billions of years of evolution, creatures acquired materials which support the state-of-the-art mechanisms to maintain their lives. Their strategies on molecular design include ours: diversity of skeletons are used for vitamins; more than twenty groups exist as substituents on the α-carbon of amino acids; and biopolymers such as polysaccharides and DNAs containing several types of skeletons as monomer units.

Another strategy do creatures adopt to design molecules: alignment of relatively rigid secondary structures. Proteins are good examples.[44] Diversity and relative rigidness in three-dimensional structures are characteristics of proteins. Muscles, skins, enzymes, ion channels, and other countless numbers of body parts consist of them. Tens of thousands of protein structures have been determined up to date.[45] The basic structures to construct proteins are, however, highly limited: helices, sheets and loops. Diversity in spatial alignment of the basic structures emerges diversity in structure and function of proteins. Helices and sheets are potentially multifunctional, and it is their positions in a protein that determines which function should be expressed.

It is the author's objective to demonstrate the effectiveness of this strategy, a rarely adopted way in artificial molecular designing, on fabricating diverse functional molecules. This strategy enables fabrication of a wide range of functional molecules from limited numbers of simple secondary structures. Not do skeletons and substituents dominate the cardinal functions in this strategy. They just give variations to functions. It is some of intrinsic functions of the basic structures expressed according to the alignment of the structures that determine the nature of the compound. In other words, several compounds of highly different properties can be prepared just by alternating the relative positions of the structural components. This strategy is thus advantageous against the other strategies.

In this dissertation, HPs and OPEs are adopted as basic structures for creation of diverse noble organic optical and electronical materials. This choice has three reasons. Firstly, both compounds take clear and simple structures: a helix structure for a HP and a rod structure for a OPE. Secondly, the synthesis methods on the both compounds are well established: liquid-phase and solid-phase synthesis for peptides and Sonogashira cross coupling for OPEs. Thirdly, they have several functional characters. For HPs, those are dipole, chirality, and self-assembling ability. For OPEs, those are optical and electronic

characters originated from semiconductor-like electronic structure. Details will be discussed in the following two sections.

Helical peptides

History. HPs have gathered attentions from molecular biologists and chemists since suggestion of 3_{10}-helical structure by Taylor[46] and by Huggins[47] in 1940s and the structure of an α-helix was determined by Pauling et al. in 1951.[48] The main interests of molecular biologists are location of the HPs in a protein and their functions.[49,50] Countless of protein crystals are analyzed by X-rays and NMR. One of the greatest achievements using this approach is the discovery on the mechanism of ion selectivity in potassium ion channels by R. MacKinnon.[51–53] The core of the channel is found to be consisted of several helices. Rigid-rod structure of helix is indispensable for building up a channel and aligning carbonyl oxygens at a specific point to select potassium ions. Studies on interaction of HPs with cell membrane have been another great interest.[54–57] Helical structure is suitable to pierce a lipid bilayer membrane.

Chemists have focused on finding out how and why some peptides form a certain helix (3_{10}-, α-, or π-helix).[58,59] Relationship between 3_{10}-helix and α-helix is especially of high importance.[60] 3_{10}-helix is less stable than α-helix but the two helices shares most of their regions in the Ramachandran map. It is thus suggested that 3_{10}-helix is an intermediate in α-helix folding.[61–63] One of the trends in the study is using Aib in the sequences since Aib can promote a helical structure due to steric interactions involving the two methyl groups on the α-carbon. Karle et al.,[64–66] Toniolo et al.,[67,68] and Kimura et al.[69] have synthesized Aib containing oligopeptides to determine the condition of transition of helices from 3_{10}- to α-helical structure. Recent study by Toniolo et al. showed a homo-peptide of (αMe)Val makes a reversible 3_{10}-/α-helix transition.[70]

Some chemists are ambitious for fabricating well stabilized HPs from short peptides. One of the tactics is introducing intra-bridges over side chains. The bridges can be a salt bridge,[71] an ionic bond,[72] a disulfide bond,[73] a hydrogen bond,[74,75] and a covalent bond.[76–80] Secondary interactions such as aromatic–aromatic interactions,[81] cation-π interactions,[82,83] hydrophobic interactions[84,85] are also utilized. Another strategy presented by Arora et al. is replacing one of the intramolecular hydrogen bonds in α-helix with a covalent bond (named hydrogen bond surrogate or HBS helices).[86,87] Fujita et al. applied their technique of coordination chemistry to construct a hydrophobic cavity which induce α-helix to a short peptide having two hydrophobic residues.[88–91]

These stabilized helices can be used to fundamental research and control of the gene expression. Verdine et al. demonstrated upregulation of p53 expression and activation of the apoprotic siglnal[92] and repression of Notch-mediated[93] gene expression with adequately designed helices stabilized by olefin methathesis reaction between side chains. Arora et al. succeeded in synthesizing a HBS helix that has strong affinity to Bci-xL.[94] Recently, they designed HBS helices which inhibit gp41-mediated cell fusion[95] and transcription of hypoxia inducible genes in cell culture,[96] respectively.

Dipole. One of the earliest reviews on the nature of the helix dipole was reported by A. Wada in 1976.[97] W. G. J. Hol elucidated that the electric field generated from the dipole of a HP has three important contributions to protein functions.[98–100] He introduced three instances in his paper for *Nature* in 1978.[98] The first point is on bindings. Negatively charged groups interact favorably with the helix field and bind at the N-terminus of a HP. The second point is on attraction. He pointed out that a long-range attraction of charged substrates is possible especially by proteins which contain several helices running parallel to each other. The third point is on reaction rate. The helix field affects the transfer of protons away from side chains at the N-terminus of a helix. The effect of dipole on photosynthesis

was also discussed.[99]

Even though such important roles of the dipole in HPs have been widely acknowledged for decades, little researches are there on positively utilizing the dipole of HPs to fabricate functional materials and molecules. In contrast, molecular dipole has gathered great attention in the field of organic a NLO materials based on π-conjugate chemistry since 1980s.[101] Aligning π-conjugate molecules of large dipole, which has large hyperpolarizability, in the same orientation is essential to obtain NLO effect, but this alignment is generally unfavorable since dipole–dipole (D–D) interaction forces two dipoles to be antiparallel. Würthner et al. recognized that this character can be applied to a great resource for supramolecular chemistry.[102,103] They demonstrated supramolecular polymerization and hierarchical self-organization using dipolar merocyanine dye assemblies.[104,105]

Inspired by such prevalence in proteins and motivated by novelty in artificial compounds, the author set his mind on utilizing the dipole of HPs. Two ways on exploiting dipole can be suggested. One is D–D interaction. The author puts emphasis on difference of D–D interaction from a simple electrostatic interaction, which just attracts or expels charged matters. A molecule utilizing the dipole of HPs has already been proposed.[106] The molecule named **Tri9** is consisted of three HPs of nonamer. Each HP is connected to a benzene ring at the side chain of the central residue Lys via amide bond. This structure forces the three helices to be on the same plane due to D–D interaction both in solution and on substrate.

The other is an electric field. A HP can be utilized as a nano-electric field generator. This electric field can modulate the electronic structure of a π-conjugate compound when the helix is closely bonded to it (see the next section for details).

Chirality. Chirality, one of the main goals for chemists to manipulate, is another character of HPs. Owing to successful asymmetric synthetic procedures, polymers, oligomers, and

supramolecules of chiral structures are now easily accessible. Its applicability for functional materials is well proved by biomaterials such as DNAs and polypeptides. Countless number of artificial helical polymers/oligomers of high functionality have been reported so far.[107] Some of the helical compounds even show dynamic inversion in response to environmental stimuli such as solvents[108–110] and temperature.[111–113]

Compared with these carefully designed helices, two advantages of HPs can be pointed out. One is an established relationship between chirality of monomer and helix sense. Some of helical structures, including homopolymer of asparatic acid, show inversion in helix sense. Such a character may be attractive, but be cautious about enantiopurity. Most of HPs take right-handed sense when they are consisted of amino acid of L-form, and left-handed sense when D-form. This well proved facts are a solid base for constructing a chiral structure. The second point is that even short peptides can fold themselves to take a relatively stable helical structure. Most of helical structures are designed to be polymeric, and their structural stabilities are out of knowledge when they are oligomers. Thus, HPs is more secure to be used for short chiral building blocks for complicated functional molecules and for supramolecules.

This dissertation tries fabricating chiral π-conjugate molecules using the chirality of a HP. Attention toward chiral π-conjugate molecules is now increasing because it can directly emit and absorb a light of circular polarization. Circularly polarized light is otherwise generated by transmitting linearly polarized light though a 4/λ filter or reflecting non-polarized light from a cholesteric liquid crystal, which both greatly reduces original light intensity.

Self-assembly. Self-assembling ability of HPs is also a highly attractive feature. Two functional structures can be fabricated using this ability: one is molecular assemblies such as colloids, vesicles, and tubes, and the other is SAMs.

Molecular assemblies have recently gathering attentions as a smart carrier of drugs and imaging substances.[114,115] Peptides are one of the most adopted building blocks because peptides can be both hydrophobic and hydrophilic, and biocompatible.[116,117] HPs are not common as a building block for amphiphilic copolymer since intermolecular hydrogen bond found in β-sheet seems attractive for building up molecular assemblies. Recent studies, however, show that the morphology of molecular assembly prepared from hydrophobic HP–polysarcosine amphiphilic polymers can be precisely controlled by preparation temperature and mixing ratio of right-handed HP polymer and left-handed HP polymer.[118–122] This is one of successful ways of utilizing multiple aspects of HPs in an integrated way.

In this dissertation, however, SAMs are chosen as a target to utilize the self-assembly nature of HPs. This is because fundamental studies and applications for organic molecular optical and electronic devices using SAMs have been well established. One of the characters of SAMs is that they are essentially a nanostructure: fabrication of a SAM is a bottom-up method using organic molecules, which means it usually requires several nanometers in thickness and several square nanometers in area at least. Another advantage is that they can be stably formed through covalent bonds on various surfaces such as metals,[123] metal oxides, silica, and ITO substrates by changing the linker moiety. This promises a wide range of applications such as organic/molecular memories,[124–126] opto-electronic devices,[127–129] and sensors for biomolecules[130] (biochips).

SAMs of HPs have been studied well. The first phase of the study on HP-SAMs was developing procedures to fabricate a well oriented layer. The oldest examples of HP monolayers were presented by Whitesell et al.[131,132] They have synthesized α-helices directly on a gold surface by using amino acid *N*-carboxyanhydride, whose polymerization was initiated by amino groups immobilized on the gold substrate. The orientation of the

HPs was, however, found to be random. To overcome this problem, Kimura et al adopted HPs of $(Ala\text{-}Aib)_n$ sequence since they discovered that these HPs form a well packed monolayer at air/water interfaces as a result of self-assembly.[133–135] They found that oriented HP-SAM of $(Ala\text{-}Aib)_n$ can be prepared on gold using interaction between ammonium ion and 18-crown-6,[136] electrostatic interaction between ammonium ion and carboxylate,[137] and automatically forming covalent bond between gold and sulfur.[138] One of characteristic features of HP-SAMs is that the tilt angle of the HPs in the SAM can be easily determined by IR-RAS measurements.[138,139] This provides us solid bases for discussion on the structure of HP-SAMs.

In the next phase, the interest split to fundamental and applicational aspects. Typical fundamental researches were revealing electron transfer/transport mechanism through HPs. Regarding a gold substrate on which SAMs form as an electrode, electron transfer rate and conductivity of various compounds including alkyl chains,[140–148] and π-conjugate oligomers[149–152] have been determined. In a typical procedure for electron transfer over organic molecules, is analyzing redox-active SAMs on an electrode with electrochemical methods.[153] In electron transport experiments, conductance of single or several molecules is determined by STM or conductive AFM on SAMs,[154] and STM break junction.[155] From the experiments for alkanethiol and π-conjugate oligomers, the electron transfer/transport was interpreted on the basis of the electron tunneling mechanism. The same measurements for HPs, however, proposed a controversy:[156] some concluded that the electron transfer is based on the electron tunneling mechanism just as alkanethiol and π-conjugate oligomers, others on the electron hopping mechanism as DNAs.[157] Recent studies on $(Ala\text{-}Aib)_n$-Fc, where n = 4–40, revealed that both mechanisms are responsible when n = 8 and 16, and the hopping mechanism becomes prominent when $n > 24$.[158–160] Conductance measurements at a single molecule level have also been carried out. The conductance of HPs is found out to be larger

than alkanethiols but smaller than π-conjugate molecules.[161–163]

In application of HP-SAMs, dipole, easiness of functionalization, and stability of helical structure were utilized as well as self-assembling behavior. An electron transfer study of HP-SAMs revealed that the dipole of HP positively influence on the electron transfer rate.[164] Motivated by this finding, a HP-SAM acting as a photodiode of switchable photocurrent direction was fabricated.[165] HPs have also been utilized as a scaffold to align functional groups in SAMs.[166–168] HPs having naphthyl units at every three residues of its sequence were fabricated. The naphthyl groups linearly align along a helix since the peptide sequence was designed to take 3_{10}-helix structure. Enhanced photocurrent generation by the electron hopping through the naphthyl groups was clearly observed in the SAMs. The photoresponsive SAM was prepared from a compound where two HPs were connected with an azobenzene moiety.[169,170] Due to photosensitive behavior of the azobenzene unit and rigidity of HPs, the structure of the SAMs can be repeatedly switched by light irradiation.

In this dissertation the author tried to construct SAMs of some HP-OPE conjugates owing the comprehension on characterization and application of HP-SAMs described above. Molecules in a SAM are surrounded in different environments and take a different conformation from that in solution. It is thus studies of SAMs can be a good way to discover new aspects of a conjugate of OPEs and HPs.

Oligo(phenyleneethynylene)s

Overview. OPEs are among the most frequently utilized π-conjugate compounds for nano electronic material or optical material. Two reasons are there for merits of using OPEs. One is synthetic easiness and flexibility in molecular design. OPEs are easily prepared by the Sonogashira cross coupling reaction. Desired OPE derivatives are prepared just by selecting appropriate substituted benzenes as the building blocks. The other is their simple linear

rigid-rod structure. This feature is essential for building blocks for nano devices because it enables precise design of the devices.

Even though they have rigidness, OPEs have structural arbitrary: the benzene rings rotate almost freely. In dilute solutions, the rotation barrier of benzene ring is about 1 kcal mol^{-1}. [171–173] It is therefore a convolution of each property of multiple conformations that what we normally observe in spectroscopy. This makes the compound unique and inspires physical chemists to come up with some elegant experiments to determine the conformation–property relationship.

In the following two sections, development of OPE studies are briefly reviewed. The first section focuses on researches using OPEs as a nano electronic material. OPEs have significantly contributed both to fundamental studies on metal–molecule–metal junctions and to the development of molecular electronics. The second section reviews researches on optical properties of OPEs. Answering how multiconformer nature of OPEs contributes to the spectra has been the main topic. Studies for application of OPEs using their high fluorescence quantum yield are also introduced.

Nano Electronic Material. Organic electronic materials have been made of π-conjugate polymers since discovery of high conductivity in doped polyacetylenes. Poly(phenyleneethynylenes) (PPEs) are, however, not widely acknowledged as a candidate of electronic materials. It is derivatives of poly(*p*-phenylenevinylenes) (PPVs) and polythiophenes (PTs) that are traditionally utilized in organic semiconductors[174] and opto-electronic devices such as LEDs[175] and photovoltaic devices.[176–178] Although various PPEs have been synthesized and systematically characterized in 1990s[179] and some PPEs were suggested for application to LEDs in late 90s,[180–182] PPEs slipped away from the candidates of polymeric electronic and optical materials.

In contrast, OPEs have attracted a great attention as a candidate of molecular

electronics devices at the same period.[183] The fever commences in 1995 when a group led by Tour and Weiss revealed that an OPE was a highly conducting single molecular electric wire.[184] This finding made OPEs as an archetype of molecular wires. The following decade saw fundamental researches on molecular electronics based on OPEs both in experimental and in theoretical ways.[185] Such studies were recognized as of high importance for development of molecular electronics in around 2000 because there had been no comprehensive understanding on electronic phenomenon in a metal–molecule–metal junction, which is essential for designing molecular electronics devices. OPEs are an ideal compound in such studies because of their simple linear rigid-rod structure. Indeed, oligophenylenes are also popular as a molecular wire but OPVs are not, even though they have higher conductivity and electron transfer rate than OPEs.[150,151,186–189] OPEs and other linear π-conjugate compounds have been frequently used as a bridge of two electronic active moieties in complex molecular systems.[190–193]

Several examples for research on the junction are as follows. Kushmerick et al. conducted charge transport studies on OPEs using a simple crossed-wire tunnel junction technique.[194] They prepared two OPEs: One was a symmetrical OPE, which has two thiol groups at the both ends, and the other was asymmetrical one, which has one thiol group at one end. The experiments showed that the nature of metal–molecule contacts showed a definitive effect on the *I–V* character and also that such an effect can be understandable in a quantitative way. Allara et al. figured out the effect of local environment on molecular conduction using an OPE derivative.[195] They clearly demonstrated that the *I–V* curves of an OPE-SAM and those of individual OPE molecule are totally different. Haiss et al. developed an approach to monitor the electrical properties of single-molecule junctions, which involves precise control of the contact spacing and tilt angle of the molecule.[196] They found that the tilt angle dependence of the electrical conductance is a good prove to

determine the position of the Fermi energy. Zhao et al. theoretically revealed that geometry relaxation under an external electric field between two metal electrodes is essential for an accurate prediction of electron transport character using a metal–OPE–metal junction.[197]

Researches for the intrinsic electron transport character of molecules are also of great interest. Determining conductivity, electron transport mechanism, and length dependence of conductivities are of the primary interests. *I–V* curves of several alkane thiols of different length were investigated and fitted with theoretical models.[198] The studies revealed that the Simmons model[199,200] was successful for theoretical fitting of the experimental *I–V* curves, suggesting that the direct electron tunneling mechanism is dominant in molecular conduction. This methodology was immediately applied to π-conjugate wires and the fitting values were compared.[143,186,187] It was found that the electron attenuation factor of conductivity against molecular length, β, of π-conjugate wires is about the half of that in alkane molecules. Recent studies revealed that such interpretation is valid only when the molecular length is less than several nanometers.[152,201] When the length is more than that, the hopping mechanism becomes dominant. This is also applicable to the OPE wire.[202]

Through the conduction measurements, existence of multiple conformers is found to have a strong influence on the conductivity of OPEs. Tour et al. reported that the conductance of OPE-SAMs decreased at low temperatures because OPEs took a twisted conformation.[183] The detailed calculations on electron transfer through OPE-SAMs was conducted by Newton et al. They found that the large conformational distribution due to rotation of benzene rings had a significant impact on the kinetics of electron transfer through the SAM.[203] Theoretical analysis by Tomfohr and Sankey revealed that rotation of the middle ring had 3-order-impact on conductance.[204]

Another interest was substitution effect on electron conducting characters. OPEs were suitable as a framework of molecular wire in this study because of synthetic flexibility.

Tour et al. are among the earliest groups who paid attention to OPEs in this sense. They have synthesized various OPE derivatives and examined their electronic properties.[183] Some of the OPEs were found to function not just as a wire but as electronic devices, such as random-access memories[205] and NDR devices.[206–208]

Optical Materials. Both PPEs and OPEs were picked out for studies on their conformation–property relationship in optical properties. One of the oldest researches was accomplished by Le Moigne et al.[209] They alternately polymerlized two phenyleneethynylene monomers having an amino group and a carboxyl group on the phenyl ring, respectively, so that the polymer took a coplanner conformation by intramolecular hydrogen bond between neighboring phenyl rings. They confirmed that such planner conformation enables efficient electronic delocalization throughout the backbone. The following several years saw controversy of the aggregation effect and the conformational effect on spectral changes of PPEs/OPEs induced by environmental changes such as concentration, temperature, fluidity and phase transitions. While early researches tended to focus on the aggregation effect,[210–214] the conformational effect was gradually considered to have more contribution.[171,215]

It was Bunz and Garicia-Garibay's group which gave a comprehensive story of the two effects on spectra of PPEs/OPEs.[216] They used an OPE having no substitutions, which is namely 1,4-bis(phenylethynyl)benzene. After a series of photophysical measurements and AM1 calculations, they concluded that a relatively modest shift of ca. 20–30 nm in absorption spectra with preserved vibronic structure of the monomer and high emission quantum yield was due to planarization of the OPE. On the other hand, aggregation resulted in larger shifts and loss of vibronic structure.

In the same year, Swager et al. suggested an elegant method for deconvoluting the two effects.[217] They spread PPEs having hydrophobic, hydrophilic or both side chains on

air/water interface and narrowed the area monitoring the absorption and emission spectra. According to hydrophobicity of the side chain, some PPEs aggregated with their phenyl rings twisted from the neighboring ones and others took a coplananer conformation, aggregating each other in a face-to-face manner. The research clearly revealed that twist in the main chain of PPEs resulted in ca. 20 nm hypsochromic shift, while cofacial aggregation in emergence of sharp aggregation band at ca. 10 nm longer than the original maximum absorption wavelength.

Yang et al. synthesized pentiptycene-derived OPEs.[172,218] These OPEs do not take the coplanar conformation due to interference of bulky side chains. They concluded that twisting in backbone resulted in a hypsochromic shift both in absorption and in fluorescence spectra, which is consistent with the report by Bunz et al. In contrast, the fluorescence quantum yield is reported to be higher in a twisted conformation in Yang's article. They also reported that fluorescence profiles of twisted OPEs were independent of chain length. This phenomenon is explained by localized excited states upon excitation should be confined in a common segment.

Zhao et al. recently revived the hydrogen bond strategy to obtain fixed coplanar conformation.[219] The article reports that the backbone planarization results in bathochromic shift of ca. 40 nm, which is far larger than the value reported by Bunz et al.

Researches on PPEs/OPEs for application have also been active for recent two decades. A reasonable application of such compounds is fluorescence chemosensors because they have relatively high fluorescence quantum yield.[220] Swager is one of the pioneers. His first target was paraquat, which is one of the most widely used herbicides in the world. His group introduced a crown ether in the main chain of PPEs.[221,222] When paraquat is captured by a crown ether, electron transfer quenching occurs. The electron transfer quenching with a combination of photoenergy migration became a standard for the following sensors. Some

PPEs modified with crown ethers showed fluorescence quenching under potassium ion rich environment. Potassium ions induced aggregation of PPEs, which enhanced interchain excimer formation and reduced fluorescence intensity. Another example suggested by Swager is trapping an analyte compound such as trinitrotoluene (TNT) in cavities in a pentiptycene-derived PPE based film.[223,224] TNT is an electron deficient compound due to three nitro groups on the benzene ring. TNTs accepted electrons from photoexcited PPEs, resulting in quenching. Harada et al. has designed cyclodextrin-grafted PPEs. The polymer recognized adamantane derivatives and reduced or changed its fluorescence intensity.

Conjugation

The purpose of the theme is to obtain a compound of a novel character as a result of combination of corresponding specific characters of HPs and OPEs which are described above. Both HPs and OPEs have a rigid rod shape. The way of conjugation is therefore limited: H-character type (two moieties are connected at the center of each), O-character type (two moieties are connected at the both ends of each), and linear type. T-character type is also possible, but not adopted in this theme because orthogonal alignment of two functions generally yield little synergy effect. Seven researches on those conjugates have done (Figure 1). Each of seven chapters in this dissertation deals with each of the researches, respectively. Those chapters are classified into three parts.

Part I contains Chapter I and II. This part deals with researches on conformation stabilization using D–D interaction. In Chapter I, H-type conjugation was adopted so that D–D interaction between two moieties emerges. A peptide nonamer $(Ala\text{-}Aib)_2\text{-}Glu\text{-}(Ala\text{-}Aib)_2$ and an OPE on which nitro group was introduced at an end was conjugated at the center of each (**OPEn9**). Two moieties were found to take antiparallel conformation in solution and in LB film. When the OPE moiety is under the electric field

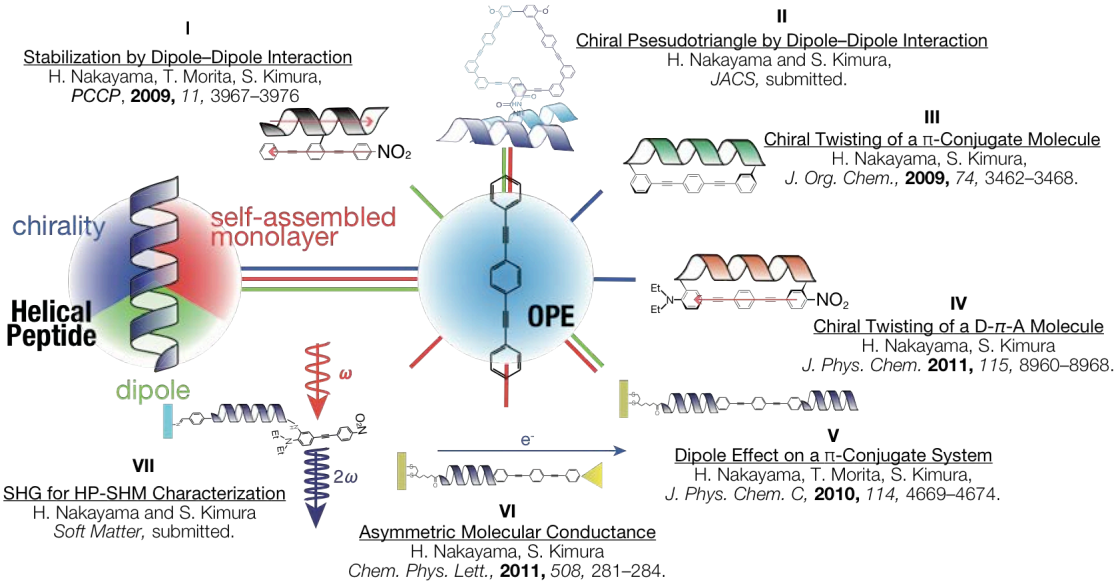

Figure 1. Seven ways for conjugation of OPE and HP.

generated by the HP moiety, its HOMO–LUMO gap decreases. This phenomenon has been proposed theoretically,[197,225–227] but not confirmed by experiments. π–*A* isotherm of **OPEn9** at air/water interface reveals that **OPEn9** does not irreversibly aggregate even when the area of the interface is compressed upto 20 mN m^{-1}, which is contrasting to **BA8M** and an OPE without the HP. A stable oriented LB film is thus available from **OPEn9** due to this nature and intermolecular D–D interaction. Based on optical spectroscopy and ab initio calculations, the electronic structure of the OPE moiety and structure of the LB film are discussed.

In Chapter II, the OPE part is extracted to be a pseudotriangle where one side was disconnected. Two HPs, $(Ala\text{-}Aib)_2$-Orn-$(Ala\text{-}Aib)_2$, are introduced at the scission site (**f-OPEBE**). When intramolecular D–D interaction works, **f-OPEBE** takes a pseudotriangle conformation by formation of a complex of the two HPs. The conformation should be chiral because association of two right-handed HP results in formation of a chiral complex.. The purpose of this chapter is thus not just utilization of dipole of HPs but also chirality of them.

Indeed, induced Cotton effect was observed at absorption region of the π-conjugate system in chloroform, suggesting a left-handed chiral arrangement of the pseudotriangle structure of the π-conjugate system. The chiral pseudotriangle structure is considered to be formed by association of two HPs due to D–D interaction in chloroform.

Part II contains Chapter III and IV. This part deals with cyclic conjugate of OPE and HP. Sinxe they hoave two connection points of the OPE moiety and the HP moiety, chirality can expand from the HP to the OPE moiety. In Chapter III, O-character type conjugation of OPE with no electron-donating or accepting substitutes and HP was designed. The compound, **C-OPE10**, was synthesized by the macrocyclization method normally used for cyclic peptide synthesis. The conformation and the optical properties of the cyclic conjugate were studied by CD, absorption, and fluoresence spectroscopies. In the cyclic conjugate, the rotational motion around the molecular axis of the OPE moiety was hindered to take a chirally twisted conformation, which is a distorted form from the coplanar conjugated structure, as revealed by observation of an induced negative Cotton effect of the OPE moiety. Molecular simulation using TD-DFT indicated a right-handed twist conformation of the OPE moiety for the negative Cotton effect. This conjugate therefore provides a new way to obtain a π-conjugated compound having a main-chain chirality. The optical properties of the OPE moiety taking the twist conformation in the cyclic conjugate are also discussed in depth.

In Chapter IV, the chirality introducing design demonstrated in the previous chapter was applied to an OPE based D–π–A system. The OPE moiety of a novel conjugate, **SSA8=OPE** was twisted by clamping both ends of the OPE with a HP. The induced twist in OPE was in a right-handed way. **SSA8=OPE** showed a weaker HOMO–LUMO band in the absorption spectrum than that of a reference compound **AcOPE** (no the helix bridge). The fluorescence quantum yield of **SSA8=OPE** was extremely low (0.0045–0.0165), which was

in contrast to **AcOPE** with a moderate quantum yield of 0.355. The fluorescence life times of **SSA8=OPE** and **AcOPE** were nearly the same. TD-DFT calculations (B3LYP/6-31G(d,p) level) on a twisted conformation of the D–π–A system qualitatively reproduced CD spectra and UV spectra of a weak oscillator strength of the HOMO–LUMO transition. Upon twisting the D–π–A system, the oscillator strength of the HOMO–LUMO transition is thus reduced.

Part III contains Chapter V, VI, and VII. This part deals with linear conjugate of OPE and HP. They form well-ordered SAMs since the OPE moiety does not disturb interaction between HPs. In Chapter V, HPs and an OPE were linearly conjugated. This configuration is suitable for fabricating a SAM. By studying absorption spectra of the OPE moiety of the SAMs of the conjugates, electric field effect on an OPE moiety was investigated. The HPs have a generalized formulation of $(\text{Ala-Aib})_{n \text{ or } m}$, which are connected to OPE in series of $(\text{Ala-Aib})_n$-OPE-$(\text{Ala-Aib})_m$ abbreviated by **2*n*OPE2*m***, (*n*, *m*) = (4, 0), (4, 4), (8, 0), (8, 4), (8, 8). The conjugates having one or two hexadecapeptides formed well-packed and vertically oriented SAMs on gold as revealed by IR-RAS, CV, and ellipsometry. Absorption spectra of the OPE moiety in the SAMs showed a bathochromic shift of ca. 25 nm from a reference SAM of the conjugate of 11-mercaptoundecanoic acid and OPE (**C11OPE**). The shift is consistent with the DFT calculations, showing that an external electric field directed along the molecular axis diminishes the HOMO–LUMO gap of OPE. The author thus concludes that the electric field generated by the peptide dipoles effectively modulate the electronic structure of the OPE moiety in the SAMs.

In Chapter VI, an electronic conduction behavior of **8OPE**, a compound used in the previous chapter was examined. This experiment is inspired by some STS measurements conducted by Kimura's group,[161–163,228,229] not by an intention to utilize the three characters of HPs described above. **8OPE** molecules were embedded in a SAM of **C10** on gold

substrate. The *I–V* profiles of **8OPE** showed an asymmetric character in terms of the bias dependence when the STM tip was put closely on the molecule, while those of **C10** retained a symmetric character irrespective of the STM tip position. The OPE moiety therefore acts as a 'molecular lead' due to the strong electron coupling between the closely positioned tip and the π-conjugate system.

In Chapter VII, linear conjugate of a HP and a D–π–A was synthesized. SHG from the D–π–A moiety was utilized for determining tilt angle and its distribution of stereocomplex and enantiopure HP-SAMs. A stereomixed SAM of a left-handed helical conjugate (**D17**) and a right-handed helical one (**L17**) showed four times larger SHG intensity than a stereomixed SAM of a left-handed helical **D17** and a right-handed HP without the D–π–A chromophore (**LA16**), which agrees well with dependence of SHG intensities on the surface densities of the D–π–A chromophore. The SHG intensities of enantiopure SAMs of **D17** and **L17** are, however, 47% and 27% of that of a stereomixed SAM of **D17** and **L17,** respectively. These differences can be explained only after taking a larger distribution of the tilt angle of the chromophore in the enantiopure SAMs than in the stereomixed SAM of **D17** and **L17**. On the basis of these analyses, it is concluded that a stereomixed SAM of a left-handed helix and a right-handed helix constitutes a well-ordered structure, where the tilt angle of the HP from the surface normal and its distribution are small, due to stereocomplex formation.

The studies clearly demonstrates that the author's strategy yields compounds of unprecedented characters. These compound are not just interesting but useful for answering some fundamental questions on photophysical characters of OPE such as electric field and twisting effects. These accomplishments thus will contribute to the development of functional molecular design and fundamental researches on π-conjugate compounds.

PART I

Stabilization of Conformation by Dipole–Dipole Interaction

Reason is, and ought only to be the slave of the passions,
and can never pretend to any other office
than to serve and obey them.
—David Hume

Chapter I

Dipole Effects on Electronic Structure and Molecular Conformation in H-shaped Oligo(phenyleneethynylene)-Helical Peptide Conjugate

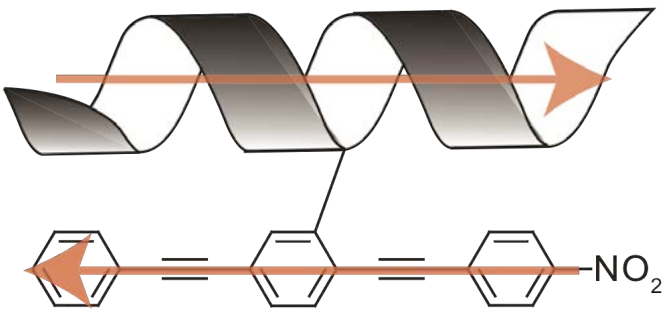

Introduction

Recent development of supramolecular chemistry[230–232] and foldamer chemistry[233,234] requires precise control of total structure. It is obviously impossible to accomplish this only with covalent bonds. Secondary interaction such as hydrophobic interactions, hydrogen-bonds, electrostatic interactions, and CH–π interactions have been used for regulation of the artificial molecular structures. Most of these ideas are inspired by highly organized biomolecular structures such as cell membrenes and proteins. Interaction generated from dipole, which is utilized in proteins as described in General Introduction, has, however, rarely intentionally utilized. Recently, Kimura's group have successfully utilized another noncovalent interaction, D–D interaction, for construction of a planar triangle geometry where three helices were circularly arranged in a head-to-tail manner.[235]

This chapter discusses on the dipole effect on stabilizing molecular conformation as well. The author reports here another example of a conformational regulation by D–D

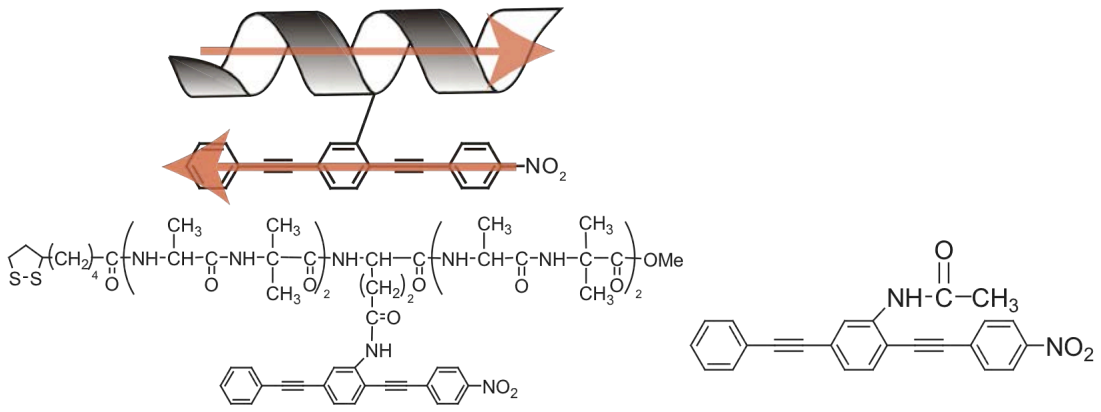

OPEn9 **OPEnAc**

Figure I-1. Schematic illustration of a D–D interaction in **OPEn9** (left top) and chemical structure of **OPEn9** (left bottom) and **OPEnAc** (right).

interaction between two different types of dipolar components in a single molecule. A novel conjugate of a helical nonapeptide and a nitro-substituted OPE is synthesized (**OPEn9,** Figure I-1). Both components have different magnitudes of dipoles. The peptide consists of an alternating sequence of Ala and Aib with an interruption of a Glu at the center of the sequence. The OPE component is connected to the peptide via the Glu. A disulfide group is attached to the N terminal of the peptide component for immobilization to gold in the case of formation of a SAM. The HP and the OPE with the nitro substitution have dipoles of ca. 20 D and ca. 3.5 D, respectively. It is expected that the peptide and the OPE components may take the antiparallel arrangement by the D–D interaction (Figure I-1) to form a planar structure. A reference compound without the peptide moiety is also prepared (**OPEnAc,** Figure I-1). Previous theoretical studies predicted that the HOMO–LUMO gap of a π-conjugate system is influenced by an external electric field.[197,225–227] Inconsistency of the absorption band of **OPEn9** with that of **OPEnAc** is thus a sign that the OPE moiety of **OPEn9** is under effect of the electric field generated by the helix dipole. The author studied the electronic structure of the OPE in the conjugate in various environments of solution, LB layers on fused quartz, and a SAM on gold using absorption spectroscopy. The films of **OPEn9** were characterized with IR-RAS and ellipsometry. On the basis of these measurement data, the author discusses the dipole effects of the peptide in those environments to demonstrate the utility of D–D interaction for regulating the molecular structure.

Experimental

Material. OPEn9 and **OPEnAc** were synthesized according to Scheme I-1. The peptide component of **OPEn9** was synthesized by the conventional liquid-phase method. The OPE component of **OPEn9** and **OPEnAc** was synthesized by the Sonogashira coupling. THF

used as the solvent in the Sonogashira coupling was distilled over calcium hydride and butylated hydroxyl toluene. The other reagents were used as purchased. All intermediates were identified by ^{1}H NMR spectroscopy and some of them were further confirmed by FAB-MS.

Spectroscopy in solution. The CD spectrum was measured at a residue concentration of 0.2 mM with an optical cell of a 0.1 cm optical path length. UV-vis absorption spectra were recorded at a concentration of less than 10 mM.

Quantum calculation. ab initio Calculations were carried out using the DFT with B3LYP method[236] with the 6-31G(d,p)[237] basis set. The geometry of **OPEnAc** was initially

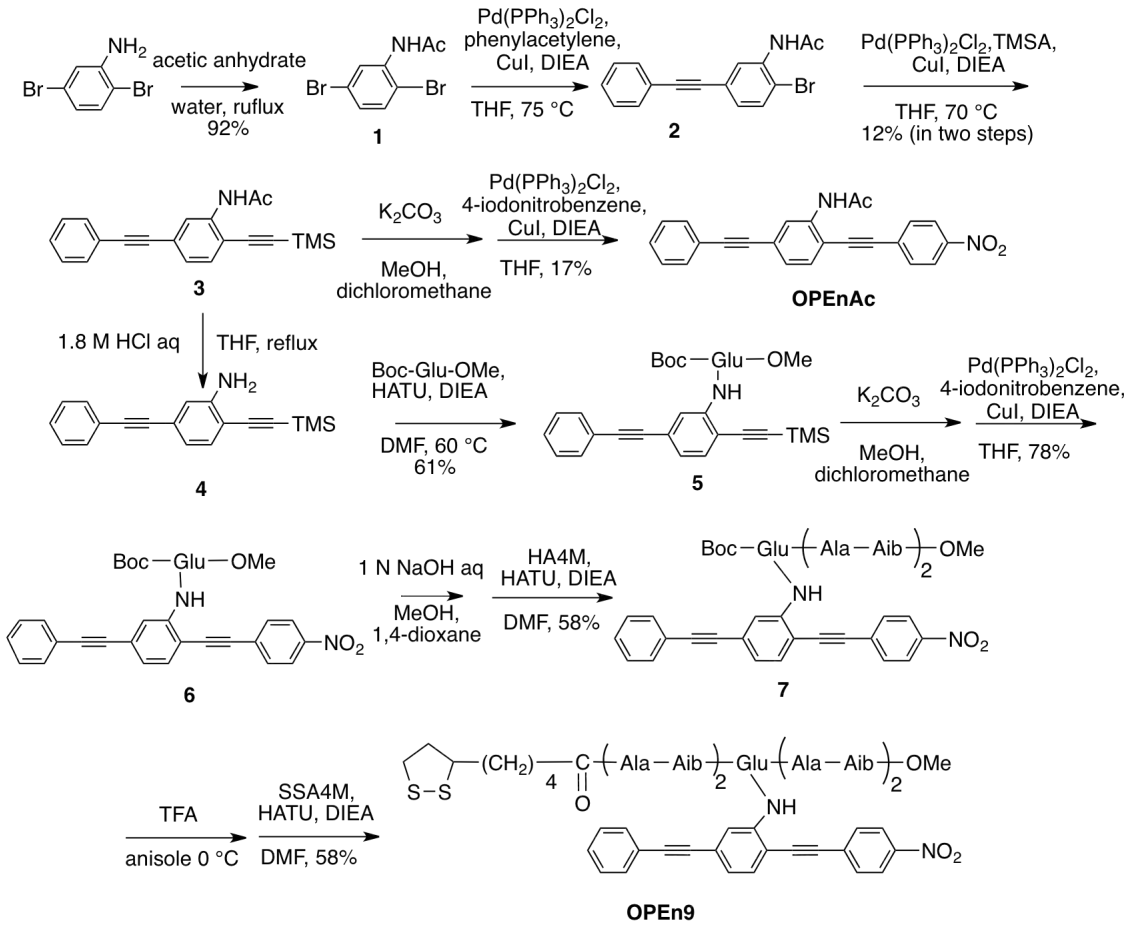

Scheme I-1. Synthetic scheme of **OPEnAc** and **OPEn9.**

generated, and the geometry was optimized by the DFT method and the frontier orbitals were visualized. The optimized geometry under no external electric field was checked by a frequency analysis. It was confirmed there is no imaginary frequency number. The geometry was re-optimized under various external electric fields (10^9 V m^{-1} at maximum) along the long axis to see its effect on the frontier orbital distributions. The direction of the electric fields (from positive to negative) is the same as the direction of the dipole moment of the OPE moiety (from negative to positive).

Preparation of LB layer. Langmuir layers of **OPEn9, OPEnAc,** and **BA8M** were prepared at the air/water interface, and the π–*A* isotherms were studied. Milli-Q water was used for the subphase. A chloroform solution of each compound (0.3–0.5 mM) was spread onto the water subphase by a microsyringe. The solvent was allowed to evaporate for at least 15 min prior to compression, and then the molecules spread on the surface were compressed at a rate of 0.1 cm^2 s^{-1}. The Langmuir layer was transferred onto a gold substrate (for IR-RAS and ellipsometry) or a slab optical waveguide of fused quartz (for UV-Vis absorption spectroscopy) by the vertical dipping method at a rate of 0.005 mm s^{-1} to prepare the LB layers. The surface pressures at transfer were 10 or 20 mN m^{-1} for **OPEn9** (LB10, LB20) and 5 mN m^{-1} for **OPEnAc.**

Preparation of SAM. A gold substrate was prepared by vapor deposition of chromium and then gold (300 and 2000 Å for IR-RAS and ellipsometry measurement, and 10 and 80 Å for UV-Vis absorption measurement, respectively) onto a slide glass by a metal deposition system. The SAM was prepared by incubating the gold substrate in a chloroform solution of **OPEn9** (0.1 mM) for 24 h. After incubation, the substrate was rinsed thoroughly with chloroform to remove physisorbed molecules and dried under a stream of nitrogen gas and in vacuum.

IR-RAS. IR-RAS of the layers on gold was performed on an infrared spectrometer with a reflection attachment. The incident angle was set at 85° for the LB layers and 80° for the SAM, respectively, from the surface normal. The number of interferogram accumulations was more than 200. The tilt angles of the helix axis from the surface normal were determined from the amide I/II absorbance ratio by using an equation in the literature.[139,138]

Ellipsometry. The thicknesses of the layers on gold were determined by an autoellipsometer with a helium–neon laser (632.8 nm) at an incident angle of 65°. The complex optical constant of the monolayer was assumed to be 1.50 + 0.00i. The thickness of the monolayer was calculated automatically by an equipped program. The thicknesses were measured on 5 different spots on the surface and the data were averaged. The typical standard deviation was ca. 1 Å.

UV-Vis absorption. The UV-Vis absorption spectrum of the **OPEn9** SAM prepared on gold was recorded on a spectrometer with a substrate sample holder attachment at the normal incidence. The absorption spectra of the LB layers prepared on a slab optical waveguide were recorded by a surface and interface spectrometer. The incident angle of the probe light was set at 17–18° from the surface, and the accumulation number of data was 10. The tilt angles of the long axis of the OPE from the surface normal were determined by the measurements with *p* and *s* polarizers inserted between the incident light and the sample. The tilt angles were determined from the absorbances for *p* and *s* polarized lights using an equation from the literature.[238]

Synthesis

General procedure for the liquid-phase peptide coupling reaction. To a two-neck RBF charged with argon or nitrogen were added a carboxyl acid, an amine, and DMF. The flask

was cooled to 0 °C. A concentrated DMF solution of DCC and HOBt or of HATU was added to the mixture. HOAt was also added when the reaction rate is supposed to be slow. TEA or DIEA was then added to the mixture. The mixture was stirred at the designated temperature for the designated period under argon or nitrogen atmosphere. The mixture was concentrated in reduced atmosphere. The residue was purified by one or combination of the following three methods: (1) take up with EtOAc or chloroform and successively wash with 4 wt % aq $NaHCO_3$ (3×), brine, 4 wt % aq $KHSO_4$ (3×), and brine, followed by drying of the organic layer over $MgSO_4$ or Na_2SO_4; (2) purify by silica gel column chromatography; or (3) purify by Sephadex LH-20 chromatography.

General procedure for the Sonogashira coupling reaction. To a two-neck RBF were added an arylhalide. The flask was charged with argon. A palladium catalyst ($Pd(II)(PPh_3)_2Cl_2$ or $Pd(II)(PhCN)_2Cl_2$) and Cu(I)I were added to the mixture. The solvent (THF or 1,4-dioxane) was added to the mixture and the mixture was stirred slowly. An alkyene was then added to the mixture. DIEA or DIA was the added. When $Pd(II)(PhCN)_2Cl_2$ was used, tri-*tert*-butylphosphine was added. The mixture was stirred under argon atmosphere at the designated temperature for the designated period. The solvent was removed in reduced atmosphere. The residue was purified by column chromatography (silica gel).

1. To a 500 mL RBF equipped with a water-cooled Dimroth condenser were added 2,5-dibromoaniline (10 g, 39.8 mmol), acetic anhydrate (40 mL), and water (40 mL). The mixture was refluxed for 4.5 h and poured into 400 mL of water. The precipitation was collected with a filter and dried in vacuum. 10.8 g (92% yield) of the desired product was obtained.

^{1}H NMR (400 MHz, $CDCl_3$): δ (ppm) 2.24 (3 H, s, $COCH_3$), 7.11 (1 H, dd, aromatic), 7.39

(1 H, d, aromatic), 7.56 (1 H, br s, aromatic), 8.59 (1 H, br s, ArN*H*$COCH_3$).

2. See the general procedure for the Sonogashira coupling reaction. **1** (10.14 g, 37.2 mmol), Cu(I)I (0.66 g, 3.46 mmol), Pd(II)$(PPh_3)_2Cl_2$, (1.46 g, 2.08 mmol), and DIEA (24.1 mL, 138 mmol) were mixed in THF (150 mL) in a 500 mL three-neck RBF equipped with a water-cooled Dimroth condenser and a dropping. The mixture was heated up to 75 °C in argon atmosphere. To the mixture was added a 40 mL of a THF solution of phenylacetylene (4.08 mL, 37.2 mmol) from the dropping funnel over 15 h, and the solution was stirred at the elevated temperature for 45 h. The residue was purified with column chromatography (EtOAc/hexane = 1/3), but it was insufficient for complete separation of the desired product and a byproduct, 2.5-di(ethynylphenyl)acetanlide. Crude mixture of 5.32 g was used in the next reaction without additional purification.

3. See the general procedure for the Sonogashira coupling reaction. Crude **2** (5.32 g, see above), TMSA (5.1 mL, 36 mmol), Cu(I)I (323 mg, 1.7 mmol), Pd(II)$(PPh_3)_2Cl_2$ (713 mg, 1.0 mmol), and DIEA (11.8 mL, 98 mmol) were reacted in THF (50 mL) in a 300 mL two-neck RBF with a water-cooled Dimroth condenser at 70 °C for 3 days. The residue was purified by column chromatography (EtOAc/hexane = 1/3). 2.53 g (22% yield) of the desired product was obtained.

^{1}H NMR (400 MHz, $CDCl_3$): δ (ppm) 0.25 (9 H, s, $(CH_3)_3SiCC$), 2.24 (3 H, s, C*H*$_3$CONH), 7.16 (1 H, dd, aromatic), 7.40 (4 H, m, aromtaic), 7.72 (2 H, m, aromatic), 7.91 (1 H, br s, CH_3CON*H*), 8.53 (s, 1H, aromatic).

FAB-MS (DTT/TG): *m*/*z* = 332.19 (calcd for $C_{21}H_{22}NOSi$ $[M + H]^+$, 332.14).

4. To a 500 mL RBF equipped with a water-cooled Dimroath condenser were added **3** (2.20 g, 6.64 mmol), THF (120 mL), 1.2 M hydrochloric acid (120 mL). The mixture was refluxed for 12 h and the solvent was removed under reduced pressure. The residue was

purified by column chromatography (silica gel, eluants: dichloromethane/hexane = 1/1 v/v, and then dichloromethane). Due to some side reactions, the product was not completely purified by column chromatography. The crude product was used in the next step without further purification.

5. See the general procedure for the peptide coupling reaction. **4** (500 mg, 1.73 mmol), Boc-Glu-OMe (1.13 g, 4.32 mmol), HATU (2.46 g, 6.49 mmol), and DIEA (1.69 mL, 9.73 mmol) were reacted in DMF (40 mL) in a 100 mL RBF at 60 °C for 12 h. The residue was purified by methods 1 and 2 (EtOAc/hexane = 1/3). 560 mg (61% yield) of the desired product was obtained.

^{1}H NMR (400 MHz, $CDCl_3$): δ (ppm) 0.244 (9H, s, $Si(CH_3)_3$), 1.38 (9 H, s, $C(CH_3)_3$), 2.49–2.04 (2 H, m, $GluC^{\gamma}$), 2.57 (2 H, m, $GluC^{\beta}$), 3.73 (1 H, s, OCH_3), 4.40 (1 H, s, $GluC^{\alpha}$), 5.21 (1 H, s, urethane-NH), 7.17 (2 H, dd, aromatic), 7.39–7.42 (4 H, m, aromatic), 7.51–7.54 (2 H, m, aromatic), 8.01 (1H, s, amide-NH), 8.52 (1 H, s, aromatic).

FAB-MS (NBA): *m*/*z* = 532.3 (calcd for $C_{30}H_{36}N_2O_5Si$ M^+, 532.24).

6. To deprotect of the trimethylsilyl group of **5,** to a 100 mL RBF were added **5** (560 mg, 1.05 mmol), potassium carbonate (435 mg, 3.15 mmol), MeOH (20 mL), and dichloromethane (20 mL). The solution was stirred under argon atmosphere for 0.5 h, and poured into water and then extracted with EtOAc. The organic layer was washed with brine (3×). The brine solution was washed with EtOAc (3×). The combined organic layer was dried over $MgSO_4$ and concentrated under reduced pressure. The residue was purified by column chromatography (silica gel, eluent: EtOAc/hexane = 1/4 v/v). The product was obtained as a white solid (300 mg, 62%). Subsequently, the deprotected product (300 mg, 0.65 mmol), 4-iodonitroaromatic (650 mg, 260 mmol), $Pd(II)(PPh_3)_2Cl_2$ (27 mg, 40 mmol), Cu(I)I (12 mg, 65 mmol), and DIEA (0.45 mL, 26 mmol) were reacted in THF (25 mL) at

40 °C for 20 h as the general procedure for the Sonogashira coupling reaction. The residue was purified by column chromatography (silica gel, eluents: EtOAc/hexane = 1/2, 1/1, and then chloroform/MeOH = 10/1 v/v). 294 mg (78% yield) of the desired product was obteind.

^{1}H NMR (400 MHz, $CDCl_3$): δ (ppm) 1.39 (9 H, s, $C(CH_3)_3$), 2.05–2.54 (2 H, m, $GluC^{\gamma}$), 2.56–2.62 (2 H, m, $GluC^{\beta}$), 3.74 (1 H, s, OCH_3), 4.42 (1 H, s, $GluC^{\alpha}$), 5.21 (1 H, s, urethane-NH), 7.27 (1 H, d, aromatic), 7.40–7.42 (3 H, m, aromatic), 7.50 (1 H, d, aromatic), 7.55–7.57 (2 H, m, aromatic), 7.97 (2 H, d, aromatic), 8.10 (1 H, s, amide-NH), 8.23 (2 H, d, aromatic), 8.66 (1 H, s, aromatic).

FAB-MS (NBA): *m*/*z* = 582.1 (calcd for $C_{33}H_{31}N_3O_7$ M^+, 582.11).

7. The methoxy group on **6** (100 mg, 17 mmol) was deprotected by treatment with 1 N aq NaOH (0.35 mL) in a mixed solvent of dichloromethane, MeOH, and 1,4-dioxane. After 4 h of stirring at RT, the solution was neutralized with 1 N hydrochloric acid and the solvent was removed under reduced pressure. The residue was washed with Et_2O. The deprotected product (100 mg, 170 mmol), a hydrochloric acid salt of HA4M (100 mg), HATU (100 mg, 22.9 mmol), and DIEA (100 mL, 61 mmol) were reacted in DMF (1 mL) in a 30 mL RBF at 0 °C for 1 day as the general procedure of the peptide coupling reaction. The residue was purified by methods 1 and 2 (chloroform/MeOH = 75/1, 50/1, 40/1, and 30/1 v/v). 86 mg (58% yield) of the desired product was obtained.

^{1}H NMR (400 MHz, $CDCl_3$): δ (ppm) 1.52–1.36 (27 H, m, $AibC^{\beta}$, Boc, $AlaC^{\beta}$), 2.18 (2 H, m, $GluC^{\beta}$), 2.72 (2 H, m, $GluC^{\gamma}$), 3.68 (3 H, s, OCH_3), 4.10–4.13 (2 H, m, $AlaC^{\alpha}$), 4.43 (1 H, t, $GluC^{\alpha}$), 6.37 (1 H, s, GluNH), 6.72 (1 H, d, AlaNH), 6.96 (1 H, d, AlaNH), 7.23 (1 H, m, aromatic), 7.30–7.33 (3 H, m, aromatic), 7.32–7.52 (3 H, m, aromatic), 7.71 (2 H, d, aromatic), 8.12 (1 H, s, aromatic), 8.24 (2 H, d, aromatic), 8.60 (1 H, s, Ar*H*$CO(CH_2)_2$).

FAB-MS (NBA): *m*/*z* = 894.4 (calcd for $C_{47}H_{56}N_7O_{11}$ $[M + H]^+$, 894.40).

OPEnAc. The trimethylsilyl group of **3** (100 mg, 0.30 mmol) was deprotected by treatment with potassium carbonate (83.4 mg, 0.60 mmol) in a mixed solvent of MeOH (5 mL) and dichloromethane (5 mL) for 1 h. The reaction solution was then pored into water and extracted with EtOAc. The organic layer was washed with brine (3×) and dried over $MgSO_4$. The solvent was removed under reduced pressure and the residue was dried in vacuum. The deprocted product, *p*-iodonitroaromatic (150 mg, 0.60 mmol), Pd(II)$(PPh_3)_2Cl_2$ (12.7 mg, 18 mmol), Cu(I)I (5.8 mg, 30 mmol), and DIEA (0.21 mL, 1.2 mmol) were reacted in THF (5 mL) as the general procedure of the Sonogashira coupling reaction. The solution was stirred at 0 °C for 1 h and then at RT for 2 h. The residue was taken up with dichloromethane and washed with 4% aq $KHSO_4$ (3×) and the brine. The organic layer was dried over $MgSO_4$. The product was then purified by a silica gel column chromatography (silica gel, dichloromethane) and Sephadex LH20 column chromatography (DMF). 20 mg (17% yield) of the desired product was obtained.

^{1}H NMR (400 MHz, $CDCl_3$): δ (ppm) 2.28 (3 H, s, NHCOC*H*$_3$), 7.27 (1 H, s, aromatic), 7.41 (3 H, m, aromatic), 7.41–7.55 (4 H, m, aromatic) 7.68 (2 H, d, aromatic), 7.98 (1 H, br s, N*H*$COCH_3$), 8.23 (1 H, d, aromatic), 8.67 (1 H, br s, aromatic).

FAB-MS (TDD/TG): *m*/*z* = 381.2 (calcd for $C_{24}H_{17}N_2O_3$ $[M + H]^+$, 381.12).

OPEn9. The Boc group on **7** (88 mg, 96 mmol) was deprotected by treatment with TFA/anisole for 0.5 h. The obtained product was washed with Et_2O. The product was added to a test tube with SSA4H (95 mg, 185 mmol), HATU (105 mg, 277 mmol), and DIEA (72 mL, 416 mmol) in DMF (10 mL) in a test tube at RT for 27 h as the general procedure for the peptide coupling reation. The residue was purified by method 3 (DMF), then by method 2 (chloroform/MeOH = 75/1, 50/1, and 10/1 v/v), and finally by method 3 (DMF). 25 mg (40% yield) of the desired product was obtained.

^{1}H NMR (400 MHz, $CDCl_3$): δ (ppm) 1.36–1.52 (45 H, m, $AibC^{\beta}$, Boc, $AlaC^{\beta}$), 1.67–1.69 (4 H, m, $SSCH_2CH_2CH(CH_2)_3CH_2CO$), 1.89–1.92 and 2.45 (1 H, m, $SSCH_2CH_2CH(CH_2)_3CH_2CO$), 2.35 (4 H, m, $GluC^{\beta}$ and $SSCH_2CH_2CH(CH_2)_3CH_2CO$), 2.63–2.75 (2 H, m, $GluC^{\gamma}$), 3.11–3.16 (2 H, m, $SSCH_2CH_2CH(CH_2)_3CH_2CO$), 3.54 (1 H, m, $SSCH_2CH_2CH(CH_2)_3CH_2CO$), 3.60 (3 H, s, OCH_3), 3.88 (1 H, m, $AlaC^{\alpha}$), 3.99 (1 H, m, $AlaC^{\alpha}$), 4.15 (2 H, m, $AlaC^{\alpha}$, $GluC^{\alpha}$), 4.23 (1 H, m, $AlaC^{\alpha}$), 6.98–6.99 (2 H, m, AlaNH, AibNH), 7.14(1 H, d, AlaNH), 7.24 (1 H, m, aromatic), 7.34–7.40 (2 H, m, aromatic, AlaNH, AibNH), 7.43 (1 H, s, AibNH), 7.48 (2 H, d, aromatic), 7.53–7.55 (2 H, m, aromatic), 7.65–7.66 (3 H, m, aromatic, GluNH), 7.73 (1 H, s, AibNH), 7.83 (1 H, d, AlaNH), 8.22 (2 H, d, aromatic), 8.32 (1 H, s, aromatic), 8.59 (1 H, s, ArNHCO(CH2)2).

FAB-MS (NBA): *m*/*z* = 1294.5 (calcd for $C_{64}H_{84}N_{11}O_{14}S_2$ $[M + H]^+$, 1294.5).

Results and discussion

Spectroscopy in solution. A CD spectrum of **OPEn9** in TFE was recorded (Figure I-2). The spectrum shows a sharp negative Cotton effect at 203 nm and a broad shoulder at 224 nm. This pattern indicates that the peptide of **OPEn9** takes right-handed 3_{10}-helical conformation[239] despite the bulky OPE moiety is introduced at the side chain. An Ala-Aib

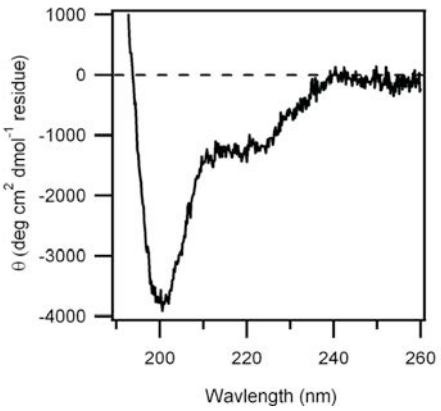

Figure I-2. CD spectrum of **OPEn9** in TFE.

repetitive sequence having no more than eight residues favors 3_{10}-helical conformation in aprotic and less polar solvents.[240] The peptide moiety of **OPEn9** thus takes 3_{10}-helical conformation in THF and chloroform, which are aprotic and less polar than TFE. In the layers, the peptide moiety takes the same conformation since they are prepared from a chloroform solution.

UV-Vis absorption spectra of **OPEn9** and **OPEnAc** in chloroform were recorded (Figure I-3a). Both spectra have a broad peak with no vibration structure, which is a typical feature of OPE having a strong electron acceptor such as a nitro group.[241,242] **OPEn9** shows λ_{max} at 364 nm, which corresponds to a red-shft of 4 nm from that of **OPEnAc** a 360 nm. This red shift was not observed in DMF (Figure I-3b), where the dipole effect of the peptide component should be weakened due to the high dielectric constant of the medium and presumably deformation of the helical structure by DMF, which acts as hydrogen-bond donor as well as acceptor. It is considered that an electric field generated by the HP dipole (Figure I-1 top) influences the electric structure of the OPE to induce the red-shift. To balidate this interpretation, ab initio calculations were performed.

Quantum Calculations. The geometry of **OPEnAc** was energetically optimized, and

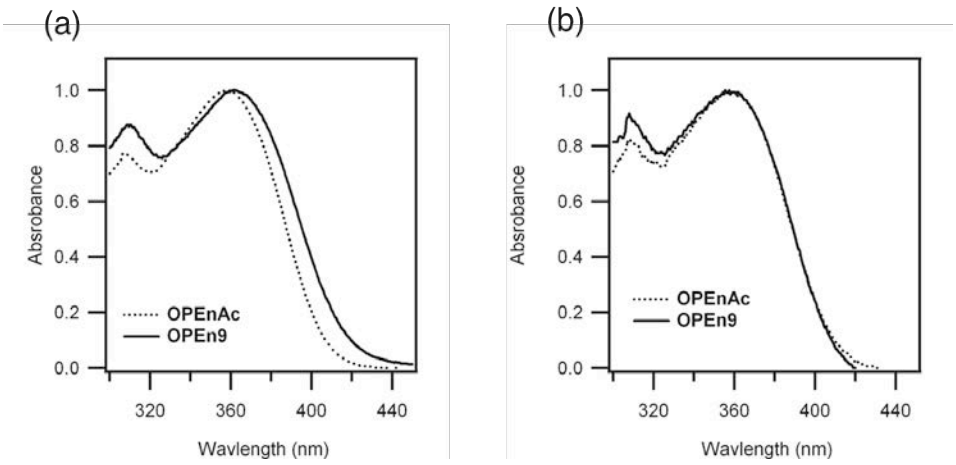

Figure I-3. UV-vis absorption spectra of **OPEn9** and **OPEnAc:** (a) chloroform, and (b) in DMF.

the electronic structure was determined under various electric fields by the DFT method on the B3LYP/6-31G(d,p) level. The spatial distributions of the HOMO and LUMO under no electric field and 1×10^9 V m^{-1} are shown in Figure I-4, respectively. In the absence of electric field (Figure I-4 top), the HOMO is localized on the left side of the molecule and the LUMO on the other side having a nitro group. When an electric field is applied (Figure I-4 bottom), this localization of the frontier orbitals is further enhanced; the contributions of the carbon atomic orbitals to the right phenyl ring to the HOMO are reduced, whereas the contributions of the carbons to the other phenyl rings are increased. The opposite behavior is observed for the LUMO, that is, the LUMO is further localized towards the left side carrying the nitro group. This orbital localization is also confirmed by a significant change in the magnitude of the dipole. The dipole increases from 3.75 D to 8.52 D upon applying an electric field of 1×10^9 V m^{-1} These results suggest that the electronic structure of the OPE component is sensitively responsive to an external electric field applied on it.

The energies of the frontier orbitals are plotted against the strength of the electric field

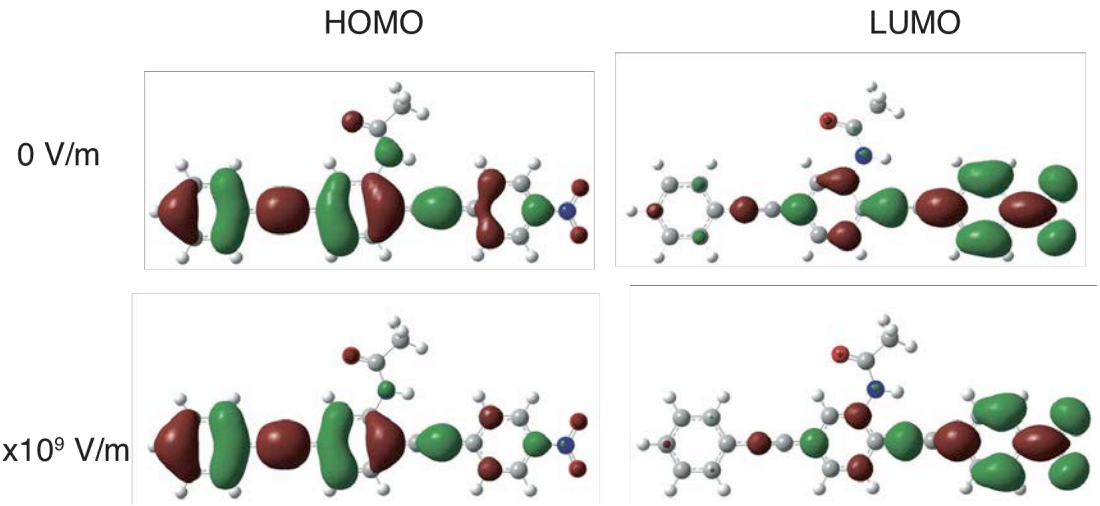

Figure I-4. Spatial distributions of the HOMO (left) and LUMO (right) of **OPEnAc** in the absence of electric field (top) and under applying an electric field of 1×10^9 V m^{-1}.

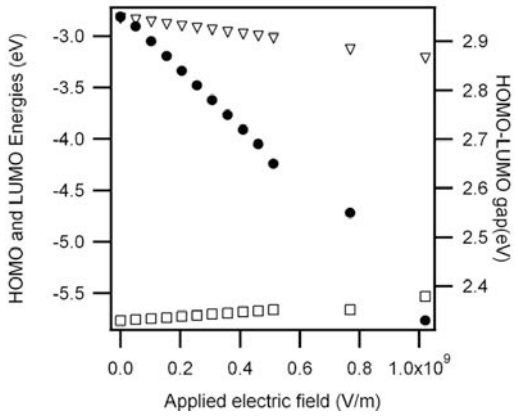

Figure I-5. Calculated energies of the HOMO (open triangle, left axis) and LUMO (open square, left axis) and HOMO–LUMO gap (filled circle, right axis) of **OPEnAc.**

in Figure I-5. The energies of the HOMO and LUMO are 5.77 and 2.18 eV, respectively, in the absence of an electric field. The HOMO energy level increases linearly with increase of the electric field, while the LUMO energy linearly decreases. Accordingly, the HOMO–LUMO gap reduces upon applying the electric field (Figure I-5). This behavior agrees well with the results reported by other groups.[197,226,243] The magnitude of the HP dipole is about 20 D. The distance between the two components in the conjugate is estimated to be 0.9 nm by a molecular modeling. With using these values, the electric field generated by the peptide dipole is calculated to be 2.5×10^8 V m^{-1} at the center of the OPE component in case that the two dipole components are arranged in the antiparallel orientation. According to the ab initio calculation (Figure I-5), the HOMO–LUMO gap decreases by 0.15 eV upon applying an electric field of 2.5×10^8 V m^{-1}. On the other hand, the experimental HOMO–LUMO gap reduction in chloroform is found to be only 0.03 eV, which is smaller than the calculated value. This discrepancy may be explained by rotational availability around the linker between the two components. The stabilization energy by the D–D interaction in the conjugate is calculated to be 6.2 kJ mol^{-1} in vacuum and 1.3 kJ mol^{-1} in chloroform (the dielectric constant of chloroform is taken to be 4.8), which is smaller

than the thermal energy of 2.5 kJ mol^{-1} at 300 K. It is thus considered that the two components are allowed to rotate around the linker over the small energy barrier in chloroform. It is therefore reasonable that the observed difference of the HOMO–LUMO gaps between **OPEn9** and **OPEnAc** becomes smaller than the calculated value, because all the molecules do not necessarily take the antiparallel conformation at a certain moment. Nevertheless, to our best knowledge, this is the first experimental observation of the electric field effect on the OPE electronic structure.

π–*A* Isotherm analysis. Figure I-6a shows the π–*A* isotherm of **OPEn9** at the air/water interface. Interestingly, the isotherm shows a phase transition around a molecular area of 2.2–1.3 nm^2 $molecule^{-1}$ and a surface pressure of 16 mN m^{-1}. The phase transition occurs reversibly either in the compression or the expansion process. We consider that this phase transition is due to the bilayer formation of the horizontally oriented conjugate on the subphase (Figure I-7b) as described in the next section. On the other hand, as shown in Figure I-6b, each model compound for the components of **OPEn9, OPEnAc,** and **BA8M** does not show such a phase transition. The hysteresis observed in the isotherm of **OPEnAc** may be due to the strong stacking tendency of the OPE by π–π interaction.[171,244,245] The peptide component of **OPEn9** thus functions to avoid π–π stacking of the OPE upon

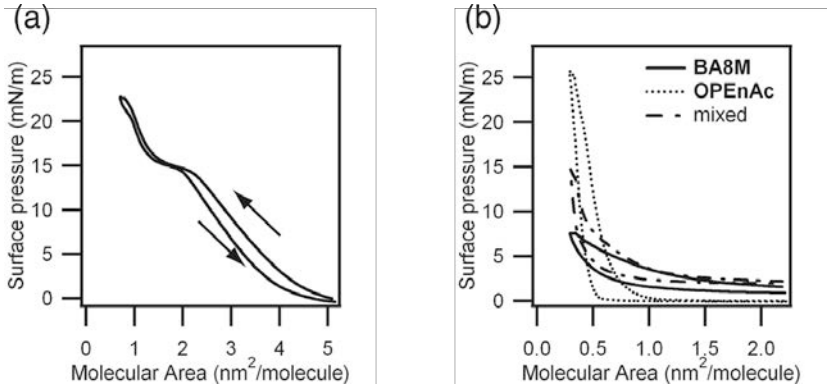

Figure I-6. π–*A* Isotherms: (a) **OPEn9;** and (b) **OPEnAc, BA8M,** and their mixture at the air/water interface.

compression on water. Furthermore, the bilayer of the conjugate does not show corruption upon compression of molecular area down to 1 nm^2 $molecule^{-1}$ with raising the surface pressure up to 20 mN m^{-1}, which makes a vivid contrast with a mixture of **OPEnAc** and **BA8M** (1/1 mol/mol) showing a very low surface pressure of 5 mN m^{-1} upon compression to the corresponding surface area. The conjugate thus forms a stable layer, suggesting that the conjugate takes a regular structure.

Characterization of the layers. The Langmuir layer was transferred on gold or fused quartz surfaces (slab optical waveguide) by the vertical dipping method to prepare the LB layers. The surface pressures at transfers of the **OPEn9** monolayer were set at 10 or 20 mN m^{-1} (the layers are named LB10 and LB20, respectively). The transfer ratios of the films were near unity (1.0–1.1). In addition, **OPEn9** SAM was prepared by immersion of a gold substrate into a chloroform solution of **OPEn9.** IR-RAS measurements were carried out to study the molecular orientation of the peptide moiety in the **OPEn9** LB layers (LB10 and LB20) and the **OPEn9** SAM prepared on gold. The spectra are shown in Figure I-8. The amides I and II are observed at ca. 1670 and 1540 cm^{-1}, respectively. The tilt angles of the

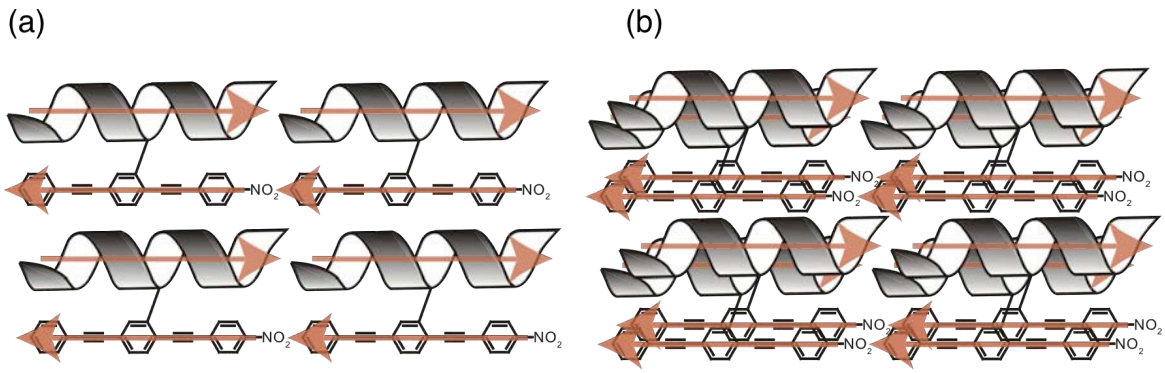

Figure I-7. Schematic representations of the top view of proposed molecular alignments of the (a) monolayer (LB10) and (b) bilayer (LB20) of **OPEn9** on a aqueous subphase or on a solid surface.

helix axis from the surface normal are determined from the amide I and II absorbance ratios to be 73° for the LB10, 69° for the LB20, and 56° for the SAM, respectively (Table I-1). These results indicate that the peptide has a horizontal orientation to the surface in the LB layers even upon compression, while random orientation in the SAM. Structural irregularity of the SAM may be explained by the mismatch of the component lengths between the HP and the OPE. The HP is too short for the OPE to take a vertical orientation on gold.

The layer thicknesses were determined by ellipsometry to be 9 Å for LB10 and 23 Å for LB20, respectively. These values are consistent with the interpretation of monolayer and bilayer formation of the conjugate with taking horizontal orientation, when we consider the following points; (i) the diameter of a 3_{10}-HP with the repeating Ala-Aib sequence is 9.4 Å.[158] (ii) the OPE component should show a thinner thickness than the peptide component, (iii) both components are tilted slightly from the surface.

UV-vis Absorption spectroscopy of layers. To study the electronic structure of the OPE in the layers, the UV-vis absorption spectra were measured. The spectra are summarized in Figure I-9. The **OPEn9** SAM shows absorption maxima at 335 nm. A

Table I-1. λ_{max} (nm) of thickness (Å), and tilt angles of the HP and the OPE in various environments.

	Thickness (Å)	Peptide tilit angle (°)	OPE tilt angle (°)	λ_{max} (nm)
OPEnAc in chloroform	—	—	—	360
OPEnAc LB	—	—	75 ± 2.0	382 ± 1.9
OPEn9 in chloroform	—	—	—	364
OPEn9 LB10	9 ± 0.5	73	74 ± 5.4	347 ± 4.6
OPEn9 LB20	23 ± 0.6	69	74 ± 3.5	358 ± 5.7
OPEn9 SAM	24 ± 0.8	56	—	335

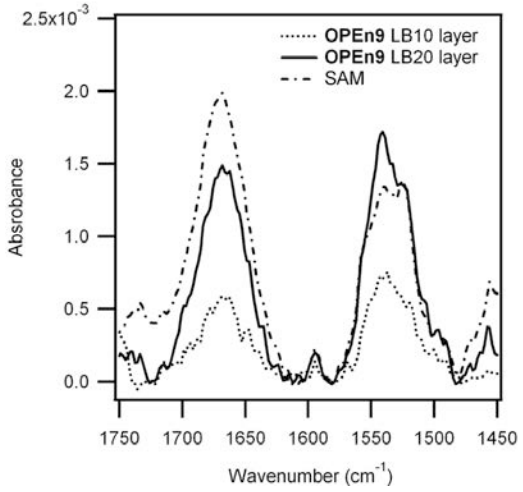

Figure I-8. IR-RAS spectra of the **OPEn9** LB10 and LB20 layers, and SAM on a gold surface.

red-shift of 10 nm in the LB10 layer (λ_{max} = 347 nm) and a further shift of 10 nm in the LB20 layer (λ_{max}= 358 nm) are observed. As the π–*A* isotherm indicates that there is no π–π stacking among the OPE components in the **OPEn9** layer, we consider the red-shift as a result of the electric field effect of the peptide dipole on the OPE component in the antiparallel arrangement. To obtain information on the orientation of the OPE component, the tilt angles of the OPE long axis from the surface normal were determined by absorption anisotropy measurements using *p* and *s* linearly polarized incident lights (Table I-1). The tilt angles are obtained as 73° for LB10 and 69° for LB20, respectively, indicating that the OPE component has a horizontal orientation similar to the HP component. In the LB10 layer, the two components have a similar horizontal orientation to the surface. Under this geometrical constraint, the two components in the conjugate should favor the antiparallel arrangement. Furthermore, head-to-tail arrangement in the layer may be prevailing because of stabilization of D–D interaction as depicted in Figure I-7a. This type of head-to-tail arrangement was previously reported in a LB monolayer of a 24mer HP.[246] The red-shift of 10 nm is thus caused by the electric field generated by the peptide dipoles neighboring the

OPE. In the LB20 layer, the conjugates are piled up to double with keeping the horizontal and the antiparallel arrangement (Figure I-7b). The electric field strength around the OPE thus becomes double to induce another red-shift of 10 nm. On the other hand, in the SAM, the peptide components orient randomly on the surface. Although the orientation of the OPE component in the SAM could not be measured, it is plausibly considered that the relative orientation of the OPE to the peptide is random because of random distribution of the surrounding dipoles.

Another possible explanation for the red-shift of the OPE component in the LB10 and LB20 layers might be due to the π–π stacking of the OPE. Indeed, in the cases of the **OPEnAc** LB layer and cast film, large red-shifts of 47 and 59 nm, respectively, from the λ_{max} in the **OPEn9** SAM were observed (Figure I-9). As described in General Introduction, optical spectra of OPEs are convolution of multiple structures. When OPEs are stacked to each other, the OPEs take only coplanar conformation, which have the lowest HOMO–LUMO transition energy.[216] In the LB layer of **OPEnAc**, the red-shift is a result of this. Hu et al. clarified this relation of λ_{max} with the coplanarity recently.[219] However, this reason is considered to be excluded from the explanation of the red shift in the **OPEn9** layers, because π–π stacking of the conjugate in those layers is not significant as revealed by the reversible π–*A* isotherms, which is described in the previous section.

Conclusion

A novel conjugate of OPE and a HP was synthesized and studied on the dipole effect of the HP on the electronic structure of the OPE and a D–D interaction in regulation of the molecular structure. In chloroform, the conjugate showed a red-shifted absorption compared to a reference OPE derivative, indicating that the electric field effect of the HP dipole on the electronic structure of the OPE in the conjugate appeared, where both components favored

the antiparallel arrangement due to the D–D interaction. This interpretation was supported by ab initio calculations. In the LB layers of the conjugate, the red-shifts of the λ_{max} became larger than that in chloroform because of the additive dipole effects from the HPs neighboring the OPE. Interesting character of the stabilized conjugate is also observed in the π–*A* isotherm. **OPEn9** forms a stable and ordered film under compression, whereas **AcOPE, BA8M,** and a mixture of the two aggregate. Such character is applicable for fabrication of aggregation-free and oriented π-conjugate films.

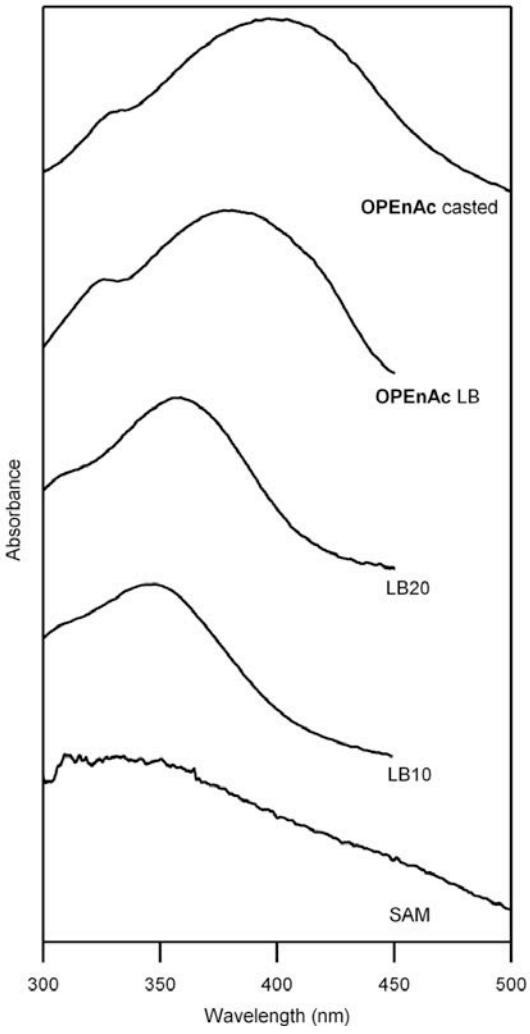

Figure I-9. UV-vis absorption spectra of **OPEnAc** and **OPEn9** in the layers.

Chapter II

Chiral Pseudotriangle Oligophenyleneethynylene Formed by Dipole–Dipole Interaction of Helical Peptides

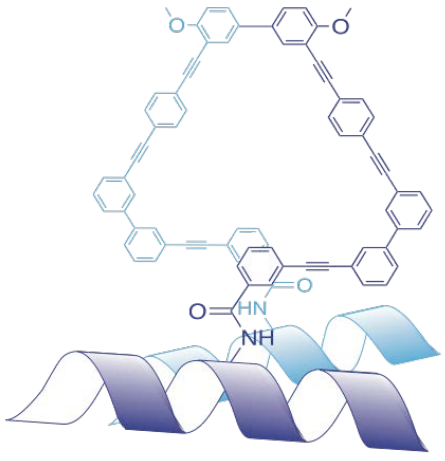

Introduction

This chapter deals with formation of a large chiral π-conjugate using D–D interaction and chirality of HPs in a concerted way. Synthesis of large functional molecules with a specified conformation has been a challenging work, because single molecule can elicit its own function by itself as demonstrated in the field of molecular electronics. Foldamers have been developed along the purpose on the basis of knowledge of protein folding.[247,234] Although foldamers are a powerful framework, they are designed generally with taking steric constrains and hydrogen bonds into consideration. In the present study, the author adopted another strategy of association of two HPs with help of D–D interaction for formation of chiral pseudotriangle structure of a π-conjugate system.

Dipole of HPs induces strong interaction with other dipolar molecules and ionic species, which contributes to several protein functions.[98,99] Ishikawa et al. have utilized D–D interaction to construct specified conformation such as a planar triangle structure containing three HPs[235] and a H-shaped conjugate of a HP and an OPE with an electron

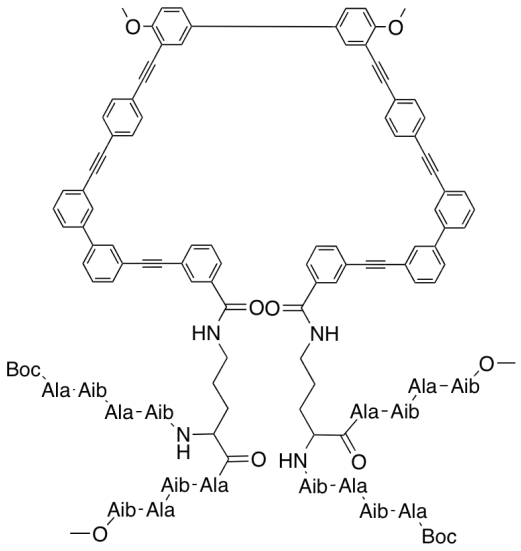

Figure II-1. Chemical structure of **f-OPEBE.**

withdrawing group (see Chapter I). In the latter case, the two dipolar moieties took antiparallel orientation, and the absorption band of OPE shifted to longer wavelength due to electric field generated by the helix dipole.

The molecular structure synthesized here is shown in Figure II-1. A triangle-like structure, OPEBE, is composed of OPEs (sides) and biphenylenes (corners). One of the three OPE sides in a triangle shape is disconnected in the middle, and each of the two terminals is connected to the side chain of Orn of nonapeptide, Boc-(Ala-Aib)$_2$-Orn-(Ala-Aib)$_2$-OMe. The OPEBE moiety is a kind of helicene, which shows chirality of helical sense. When two HPs associate together, the OPEBE moiety may take a chiral helical structure due to a specific torsion between two right-handed HPs. On the other hand, the OPEBE moiety will become a racemate of a mixture of a right-handed and a left-handed helical structures or a disordered structure upon disrupter of the two helix bundle structure because each side can rotate freely along the single bond in the biphenyl groups at the corners.

Experimental

Material. f-OPEBE was synthesized according to Schemes II-1 and 2. **f-OPEBE** was finally purified by HPLC (Showdex KD-2002.5) using DMF. See Chapter I for the general procedures of the compound identification methods. MALDI-MS was used for identification of **f-OPEBE.**

Optical Spectra. A cell of 0.1 cm optical path length was used when CD spectra of peptide absorption region was recorded. Otherwise, a cell of 1 cm optical path length was used for all optical spectroscopy.

Synthesis

General procedure of Sonogashira cross coupling: Three sets of reagents and a solvent for the coupling were used: (1) Cu(I)I, Pd(II)$(PPh_3)_2Cl_2$, and DIA (solvent); (2) Cu(I)I, Pd(II)$(PPh_3)_2Cl_2$, DIEA, and THF (solvent); (3) Cu(I)I, Pd(II)$(PhCN)_2Cl_2$, DIA, tri(*tert*-butyl)phosphine, and 1,4-dioxane (solvent). The procedure of the reaction is common: To a two-neck RBF were added an arylhalide. The flask was charged with argon.

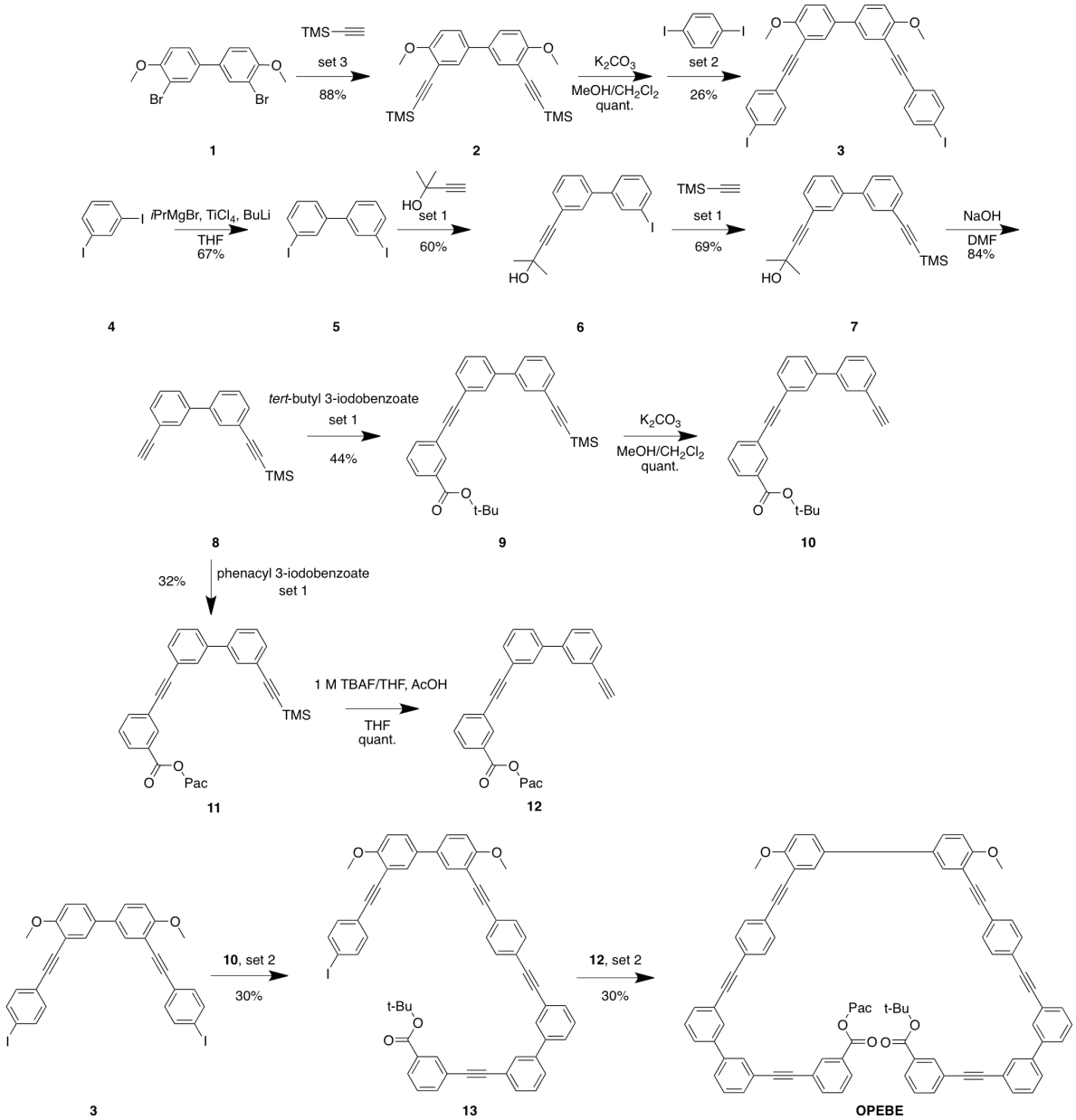

Scheme II-1. Synthetic scheme of **OPEBE.**

A palladium catalyst and Cu(I)I were added to the mixture. The solvent was added to the mixture and the mixture was stirred slowly. An alkyene was then added to the mixture. When set 2 or 3 was used, an amine and the phosphine (only in set 3) were added. The mixture was stirred under argon atmosphere at the designated temperature for designated time. The solvent was removed in reduced atmosphere. When the set 1 was used, the residue was taken up with chloroform and washed with water. The organic layer was dried over Na_2SO_4. For the all sets, the residue was finally purified with column chromatography (silica gel).

2. See the general procedure for the Sonogashira coupling with set 3. **1** (2.00 g, 5.38 mmol) TMSA (2.23 mL, 16.1 mmol), Cu(I)I (645 μmol, 122 mg), Pd(II)$(PhCN)_2Cl_2$ (247 mg, 645 μmol), DIA (4.4 mL, 32.3 mmol), and tri(*tert*-butyl)phosphine (261 mg, 1.29 mmol) were reacted in 1,4-dioxane (10 mL) at RT for 24 hr. The residue was purified by column chromatography (chloroform/hexane = 1/2 and 2/3). 2.11 g (88% yield) of the desired product was obtained.

^{1}H NMR (400 MHz, $CDCl_3$): δ (ppm) 3.90 (s, 6H, OCH_3), 6.99 (d, 2H, aromatic), 7.44 (dd, 2H, aromatic), 7.62 (d, 2H, aromatic).

EI-MS: *m*/*z* = 406.2 (calcd for $C_{18}H_{12}Br_2O_2$ M^+, 406.20).

3. The trimethylsilyl group on **2** (2.50 g, 6.15 mmol) was removed by treating with potassium carbonate (3.40 g, 24.6 mmol) in a mixture of MeOH (20 mL) and 1,4-dioxane (20 mL). According to the general procedure for the Sonogashira cross coupling wit set 2, the product was reacted with 1,4-diiodobenzene (6.07 g, 18.4 mmol), Cu(I)I (233 mg, 1.23 mmol), Pd(II)$(PPh_3)_2Cl_2$ (516 mg, 736 μM), and DIEA (8.6 mL, 49 mmol) in THF at RT for 20 hr. The residue was purified by column chromatography (chloroform/hexane = 1/2 and 1/1). 1.1 g (26% yield) of the desired product was obtained.

^{1}H NMR (400 MHz, $CDCl_3$): δ (ppm) 3.92 (s, 6H, OCH_3), 7.29 (d, 4H, aromatic), 7.50 (dd, 2H, aromatic), 7.67–7.70 (m, 6H, aromatic).

EI-MS: *m*/*z* = 666.0 (calcd for $C_{30}H_{20}I_2O_2$ M^+, 665.96).

5. To an oven dried 50 mL two-neck round-bottomed flask, which was charged with argon, were added THF (15 mL) and a 1.0 M THF solution of isopropylmagnesium bromide (3 mL, 3.0 mmol). The mixture was cooled to 0 °C and a 1.6 M hexane solution of butyllithium (3.8 mL, 6.0 mmol) was added. The mixture was cooled to –78 °C and a THF solution of 1.3-diiodobenzene (2.0 g/9 mL, 6.0 mmol). The mixture was stirred for 30 min at –78 °C and titanium(IV) tetrachloride (1.0 mL, 9.1 mmol) were added. The mixture was gradually warmed up to 0 °C and stirred for 1 hr. The mixture was then poured into saturated aqueous

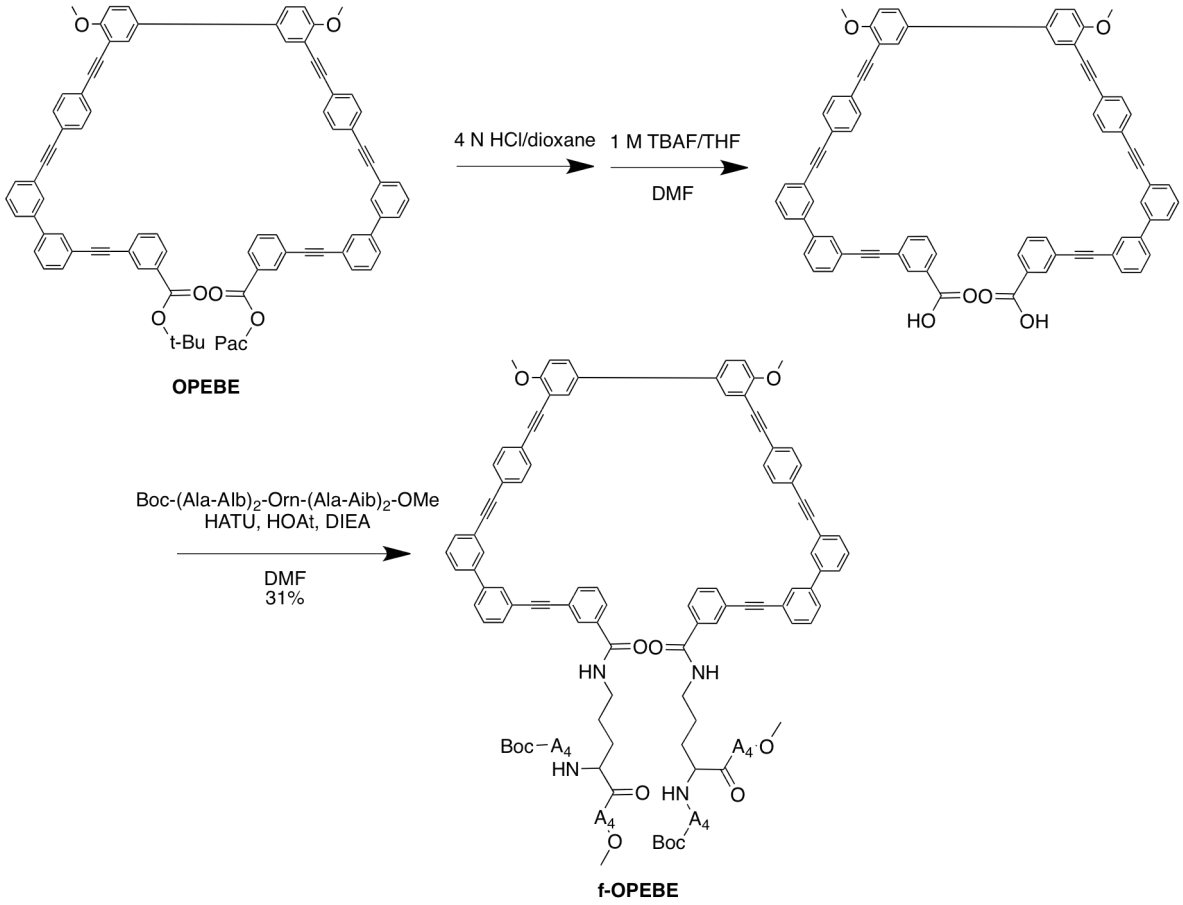

Scheme II-2. Synthetic scheme of **f-OPEBE.**

solution of ammonium chloride and extracted with ethyl acetate (3×) and dried over anhydrous sodium sulfate. 829 mg (4.06 mmol, 67%) of the desired product was obtained. 1.1 g (26% yield) of the desired product was obtained.

^{1}H NMR (400 MHz, $CDCl_3$): δ (ppm) 7.17 (t, 1H, aromatic), 7.48 (d, 1H, aromatic), 7.69 (dd, 2H, aromatic), 7.88 (d, 1H, aromatic).

EI-MS: *m*/*z* = 405.79 (calcd for $C_{12}H_8I_2$ M^+, 405.87).

6. See the general procedure for the Sonogashira cross coupling with set 1. **5** (560 mg, 1.38 mmol), 3-methyl-1-butyn-3-ol (163 μL, 1.38 mmol), Cu(I)I (1.31 mg, 6.9 μmol), and $Pd(PPh_3)_2Cl_2$ (5.4 mg, 13 μmol) in DIA (6 mL) at RT for 2 hr. The residue was purified by column chromatography (chloroform). 195 mg (60% yield) of the desired product was obtained.

^{1}H NMR (400 MHz, $CDCl_3$): δ (ppm) 1.64 (s, 6H, CH_3), 2.09 (s, 1H, OH), 7.17 (t, 1H, aromatic), 7.35–7.60 (m, 5H, aromatic), 7.67 (t, 1H, aromatic), 7.92 (t, 1H, aromatic).

EI-MS: *m*/*z* = 362.01 (calcd for $C_{17}H_{16}O$ M^+, 362.02).

7. See the general procedure for the Sonogashira cross coupling with set 1. **6** (195 mg, 538 μmol), TMSA (89 μL, 646 μmol), Cu(I)I (0.51 mg, 2.7 μmol), and $Pd(II)(PPh_3)_2Cl_2$ (2.1 mg, 5.44 μmol) were reacted in DIA (6 mL) at RT for 2 hr. The residue was purified by column chromatography (chloroform). 123 mg (69% yield) of the desired product was obtained.

^{1}H NMR (400 MHz, $CDCl_3$): δ (ppm) 0.27 (s, 9H, $Si(CH_3)_3$), 1.64 (s, 6H, CH_3), 2.09 (broad, 1H, OH), 7.34–7.52 (m, 6H, aromatic), 7.68 (s, 1H, aromatic), 7.72 (s, 1H, aromatic).

EI-MS: *m*/*z* = 332.14 (calcd for $C_{22}H_{24}OSi$ M^+, 332.16).

8. To a 100 mL two-neck round-bottomed flask with a Dimroath condenser were added **7** (1.57 mg, 4.57 mmol), toluene (60 mL), and a dry powder of NaOH (18.28 mg, 457 μmol). The mixture was heated up to ca. 120 °C and stirred overnight under nitrogen atmosphere.

The mixture was then filtered over a pad of silica. The filtrate was dried in vacuum. 1.05 g (84% yield) of the desired product was obtained.

^{1}H NMR (400 MHz, $CDCl_3$): δ (ppm) 0.27 (s, 9H, $Si(CH_3)_3$), 3.16 (s, 1H, CCH), 7.37–7.71 (m, 8H, aromatic).

EI-MS: *m*/*z* = 274.13 (calcd for $C_{19}H_{18}Si$ [M^+], 274.12).

9. See the general procedure for the Sonogashira cross coupling with set 1. **8** (550 mg, 2.0 mmol), *tert*-butyl 3-iodobenzoate (792 mg, 2.61 mmol), Cu(I)I (19 mg, 100 μmol), and Pd(II)$(PPh_3)_2Cl_2$ (84 mg, 200 μmol) were reacted in a mixture of DIA (5 mL) and THF (5 mL) at RT for 3 d. The residue was purified by column chromatography (chloroform/hexane =1/2). 396 mg (44% yield) of the desired product was obtained.

^{1}H NMR (400 MHz, $CDCl_3$): δ (ppm) 0.27 (s, 9H, $Si(CH_3)_3$), 1.61 (s, 9H, $OC(CH_3)_3$), 7.38−7.77 (m, 10H, aromatic), 7.96 (d, 1H, aromatic), 8.15 (s, 1H, aromatic).

EI-MS *m*/*z* = 450.20 (calcd for $C_{30}H_{30}O_2Si$ M^+, 450.20).

10. 9 (396 mg, 0.88 mmol) was dissolved in a mixture of MeOH (3 mL) and dichloromethane (3 mL). To the solution was added K_2CO_3 (485 mg, 3.51 mmol). The mixture was stirred for 2 h. The mixture was poured into water and extracted with dichloromethane (3×). The organic layers were dried over sodium sulfate. The solvent was removed in vacuum. The product was obtained in quantitative yield.

^{1}H NMR (400 MHz, $CDCl_3$): δ (ppm) 1.62 (s, 9H, $OC(CH_3)_3$), 3.11 (s, 1H, CCH), 7.41–7.68 (s, 7H, aromatic), 7.70 (d, 1H, aromatic), 7.77 (d, 2H, aromatic), 7.96 (d, 1H, aromatic), 8.15 (s, 1H, aromatic).

11. See the general procedure for the Sonogashira cross coupling with set 1. **8** (550 mg, 2.00 mmol), phenacyl 3-iodobenzoate (953 mg, 2.61 mmol), Cu(I)I (19 mg, 100 μmol), and

$Pd(II)(PPh_3)_2Cl_2$ (84 mg, 200 μmol) were reacted in a mixture of DIA (5 mL) and THF (7 mL) at RT for two days. The residue was purified by column chromatography (chloroform/hexane =1/2, 1/1, and then 2/1). 328 mg (0.64 mmol, 32%) of the desired product was obtained.

^{1}H NMR (400 MHz, $CDCl_3$): δ (ppm) 0.27 (s, 9H, $SiC(CH_3)_3$), 5.61 (s, 2H, OCH_2COPh), 7.36–7.64 (m, 10H, aromatic), 7.72 (s, 1H, aromatic), 7.76 (d, 2H, aromatic), 7.98 (d, 2H, aromatic), 8.11 (s, 1H, aromatic), 8.34 (s, 1H, aromatic).

12. To a 50 mL round-bottomed flask were added **11** (328 mg, 0.63 mmol), acetic acid (37 μL), 1 M THF solution of TBAF (383 μL, 0.38 mmol), and THF (10 mL). The mixture was stirred at 0 °C for 3.5 h. The mixture was passed through a pad of silica with chloroform. The solvent was removed in vacuum. The product was obtained in quantitative yield.

^{1}H NMR (400 MHz, $CDCl_3$): δ (ppm) 3.11 (s, 1H, CCH), 5.61 (s, 2H, OCH_2COPh), 7.39–7.63 (m, 10H, aromatic), 7.76 (m, 3H, aromatic), 7.98 (d, 2H, aromatic), 8.11 (d, 1H, aromatic), 8.34 (s, 1H, aromatic).

EI-MS: m/z = 440.18 (calcd for $C_{31}H_{20}O_3$ M^+, 440.14).

13. See the general procedure for the Sonogashira cross coupling with set 2. **3** (701 mg, 1.05 mmol), **10** (332 mg, 0.88 mmol), Cu(I)I (16 mg, 87 μmol), $Pd(II)(PPh_3)_2Cl_2$ (36 mg, 52 μmol), and DIEA (612 μmol, 3.51 mol) were reacted in THF (3 mL) at RT for two days. The residue was purified by column chromatography (chlorform/hexane = 2.5/1 then 3/1). 243 mg (265 μmol, 30%) of the desired product was obtained.

^{1}H NMR (400 MHz, $CDCl_3$): δ (ppm) 1.61 (s, 19H, $OC(CH_3)_3$), 3.95 (s, 3H, OCH_3), 3.96 (s, 3H, OCH_3), 6.96 (d, 2H, aromatic), 7.30 (d,2H, aromatic), 7.40–7.56 (m, 13H, aromatic), 7.68–7.72 (m, 5H, aromatic), 7.80 (d, 2H, aromatic), 7.96 (s, 1H, aromatic), 8.16 (s, 1H, aromatic).

FAB-MS (NBA): *m*/*z* = 916.3 (calcd for $C_{57}H_{41}IO_4$ M^+, 916.21).

OPEBE. See the general procedure for the Sonogashira coupling with set 2. **13** (243 mg, 0.67 mmol), **12** (281 mg, 0.63 mmol), Cu(I)I (5 mg, 26 μmol), Pd(II)$(PPh_3)_2Cl_2$ (11 mg, 15 μmol), and DIEA (185 μmol, 1.06 mol) were reacted in THF (3 mL) at 50–60 °C for two days. The residue was purified by column chromatography (chloroform/hexane = 2/1 then 1/1). Additionally, the product was purified by preparative TLC (chloroform/hexane = 3/1). 231 mg of a crude product was obtained.

^{1}H NMR (400 MHz, $CDCl_3$): δ (ppm) 1.61 (s, 9H, Boc), 3.97 (s, 3H, OCH_3), 5.61 (s, 2H, COOC*H*$_2$COPh), 6.97 (d, 2H, aromatic), 7.41–7.30 (m, 29H, aromatic), 7.56–7.73 (m, 8H, aromatic), 7.95–7.98 (m, 3H, aromatic), 8.40–8.51 (m, 2H, aromatic).

FAB-MS (NBA): *m*/*z* = 1228.5 (calcd for $C_{88}H_{60}O_7$ M^+, 1228.43).

OPEBE′. OPEBE (111 mg, 90 mmol) was dissolved in 3 mL of 4 N HCl/dioxane. The solution was stirred for two days. The soluvent was evaporated in vacuum. Removal of the *tert*-butyl group was confirmed by ^{1}H NMR and FAB-MS. The product was then dissolved in DMF (1 mL). 340 μL of 1 M THF solution of TBAF was added to the solution and stirred for 20 h. The solution was poured into 4 wt % aq $KHSO_4$ and extracted with chloroform. The organic layer was washed with brine and dried over Na_2SO_4. The organic layer was concentrated in reduced atmosphere. The residue was washed with MeOH (2×) and dried in vacuum. Removal of the Pac group was confirmed by ^{1}H NMR and FAB-MS. The product was not pure enough, but used in the next step.

f-OPEBE. See the general procedure for the peptide coupling reaction in Chapter 1. **OPEBE** (80 mg, 75 μmol), Boc-(Ala-Aib)$_2$-Orn-(Ala-Aib)$_2$-OMe (300 mg, 344 μmol), HATU (172 mg, 454 μmol), HOAt (62 mg, 454 μmol), and DIEA (132 μL, 758 μmol) were reacted in DMF at room temperature for three days. The mixture was purified by Showdex

KD-2002.5 using DMF as the eluent. The product was re-precipitated form chloroform/*i*Pr_2O/hexane. 71 mg (34% yield) of the desired product was obtained.

^{1}H NMR (400 MHz, $CDCl_3$): δ (ppm) 1.35–1.62 (m, 96H, Boc, $AlaC^{\beta}$, $AibC^{\beta}$, $OrnC^{\beta}$), 2.00 (m, 4H, $OrnC^{\gamma}$), 3.49 (m, 4H, $OrnC^{\delta}$), 3.65 (s, 6H, $COOCH_3$), 3.86 (m, 2H, $AlaC^{\alpha}$, $OrnC^{\alpha}$, or the both), 3.96 (s, 6H, Ar-OCH_3), 4.05 (m, 6H, $AlaC^{\alpha}$, $OrnC^{\alpha}$, or the both), 4.35 (m, 2H, $AlaC^{\alpha}$, $OrnC^{\alpha}$, or the both). See Figure A-II-1 in Appendix for the spectram

MALDI-MS (HR, 2,5-dihydroxylbenzoic acid): *m*/*z* = 2784.3482 (calcd for $C_{154}H_{182}N_{20}O_{28}$ $[M + Na]^+$, 2784.3397).

Results and discussion

Optical spectra. The absorption, fluorescence, and excitation spectra of **f-OPEBE** in MeOH and chloroform are shown in Figure II-2. Absorption spectra of **f-OPEBE** have several bands of nearly identical peak intensity in the 260–330 nm region. In contrast, a typical OPE absorption spectrum shows a main band around 320 nm with some subbands of weak intensities.[216] The inconsistency suggests that the OPEBE moiety may be composed of several discontinuous π-conjugate segments which sizes are shorter than an OPE unit, even though OPEBE as a whole has a possibility to constitute a long π-conjugate system. Segmentation of the π-conjugate system is also suggested from excitation spectra. As shown in Figure II-2b, the patterns of the excitation spectra are different from those of the UV spectra. The main peaks in the region of 270–300 nm in the absorption spectra become weak shoulders in the excitation spectra where the peak of a maximum intensity appears at 350 nm. The difference can be explained by segmentation of the OPEBE moiety, which comprises long and short π-conjugate segments. The photoenergy absorbed by the short segments should be transferred to the long π-conjugate segment which absorbs a light of 350 nm and fluoresces at 400 nm. Noticeably, the fluorescence spectra show only one

emission band with a high quantum yield (0.93 in MeOH, see Chapter IV for the method).[218] No aggregation is suggested based on no spectral change except intensity with varying the conjugate concentration form 3.3×10^{-6} M to 2×10^{-5} M (Appendix, Figure A-II-2–4).

CD spectra. CD spectrum of **f-OPEBE** in MeOH shows negative Cotton effects at 204 nm and a shoulder around 224 nm (Figure II-3), which are assigned to a typical pattern for a right-handed 3_{10}-helical structure.[239] The molar ellipticity ($\theta = 7.1 \times 10^3$ deg cm^2 mol^{-1} residue^{-1} at 204 nm) is agreeable with a previously report on a similar nonapeptide,[235] indicating conjugation with the OPEBE moiety has no effect on helix formation. CD spectra in THF and 1,4-dioxane also show a negative Cotton effect without a shoulder around 224 nm (Figure II-3), suggesting formation of 3_{10}-helix bundle due to helix association in these solvents of low dielectric constants.[248,249]

Conformation of f-OPEBE. CD spectra of the absorption region of the OPEBE moiety in various solvents are shown in Figure II-4. In chloroform and dichloromethane

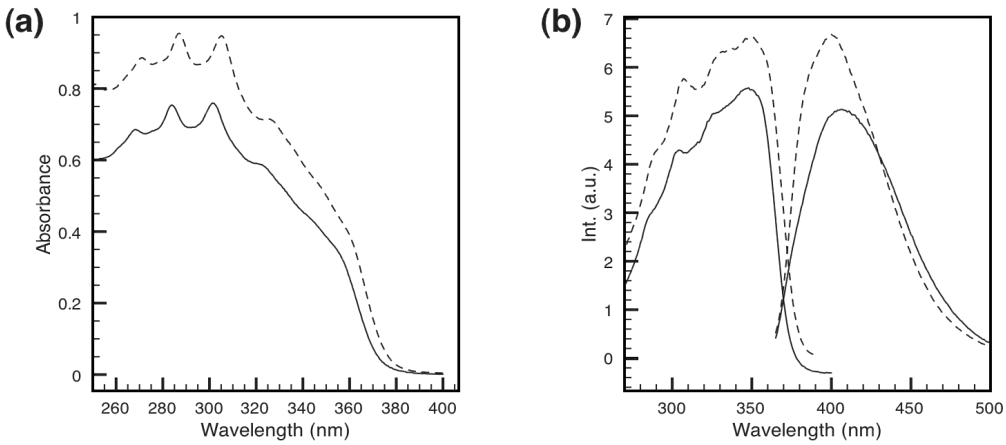

Figure II-2. Optical spectra of **f-OPEBE** in MeOH (solid) and chloroform (dash): (a) absorption spectra at 1.0×10^{-5} M for MeOH and 1.4×10^{-5} M for chloroform; (b) fluorescence and excitation spectra at 3.3×10^{-6} M for MeOH and 4.5×10^{-6} M for chloroform . The excitation wavelength was 350 nm.

solutions, negative and positive Cotton effects are observed at 290 nm and 250 nm, respectively. The OPEBE moiety thus takes a chiral structure in these solvents. Appearance of the induced Cotton effects in the relatively short wavelength region indicates that the chirality originates from the short π-conjugate segment. The exciton coupling with a pattern of a positive Cotton effect at shorter wavelength and a negative Cotton effect at longer wavelength suggests the chirality of a left-handed helix in the OPEBE moiety. The strength of the Cotton effect is linearly related with concentration of **f-OPEBE** in the range of 3.3–20 × 10^{-6} M, suggesting intermolecular association is not the reason for the chirality (Appendix, Figure A-II-3, 4). Further, no Cotton effect in the OPEBE's absorption region is observed in MeOH, even though the peptide moieties take a 3_{10}-helical conformation (Figure II-3). The chirality in the OPEBE moiety is thus not a result of addition of HP to the OPEBE moiety. Taken together, association of the two helices of **f-OPEBE** in chloroform and dichloromethane is a plausible interpretation to induce the chirality of the OPEBE moiety. Indeed, NOESY spectrum shows proximity of $AlaC^{\beta}$ protons and $AibC^{\beta}$ protons in

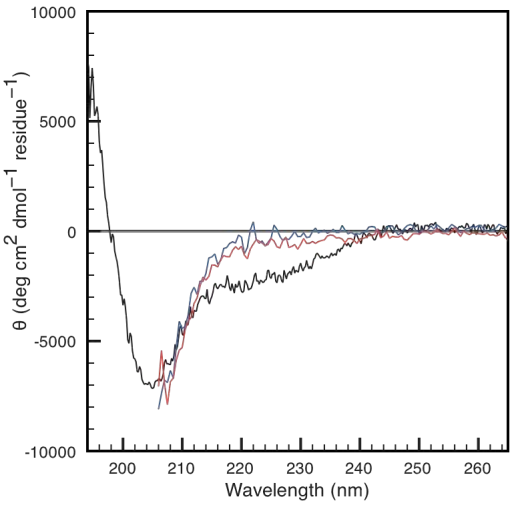

Figure II-3. CD spectrum of **f-OPEBE** in MeOH (black), THF (blue) and 1,4-dioxane (red) at 4.9–6.6 × 10^{-5} M.

chloroform-*d* but not in MeOH-d_3, supporting association of the two helices in chlorofom and not in MeOH (Appendix, Figure A-II-5, 6). The association of the two helices may be driven by D−D interaction in chloroform of a low dielectric constant of 4.8, but the interaction is not operative in MeOH of a dielectric constant of 33. In THF and 1,4-dioxane, the induced Cotton effect of the OPEBE moiety was small. Since solubility of **f-OPEBE** in these solvents is not so high, aggregation may occur as shown in Figure II-3 to obscure the induced Cotton effect.

Stability of the conformation. Stability of the association of the two helices was further studied. The addition of a left-handed helix of Boc-(D-Ala-Aib)$_4$-OMe (ten equivalents) to a chloroform solution of **f-OPEBE** did not change the intensity of the induced Cotton effect of the OPEBE moiety, indicating no inhibition effect of the helix peptide on the two helices association (Appendix, Figure A-II-7). However, the intensity of the induced Cotton effect reduced the intensity to one fourth with increasing temperature from 30 °C to 80 °C in 1,2-dichloroethane (Appendix, Figure A-II-8). The intensity was regained when the temperature was set back to 30 °C, indicating that the association of the

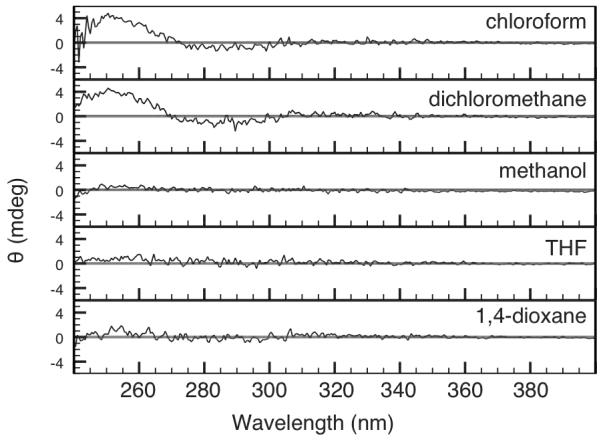

Figure II-4. CD spectra of **f-OPEBE** in various solvents at 2×10^{-5} M.

two helices is thermodynamically stable.

Conclusion

A conjugate of phenyleneethynylenes and two HPs was prepared. The conjugate, **f-OPEBE,** takes a chiral triangle structure when dissolved in chloroform or dichloromethane due to association of two HPs induced by intramolecular D−D interaction. A careful choice of solvent is necessary for observation of intramolecular D−D interaction which exceeds over other interactions.

PART II

Cyclic Conjugate of OPE and Helical Peptide

Bad artists copy, good artists steal.

—Pablo Picasso

Chapter III

Chirally Twisted Oligo(phenyleneethynylene) by Cyclization with α-Helical Peptide

Introduction

This chapter deals with chirality introduction on an OPE by clipping it with a HP. As described in General Introduction, benzene rings of OPEs rotate nearly freely. This character inspired chemists to determine precise conformation–property relationship by photophisical studies. Some OPEs and PPEs are designed to take a coplanar conformation or a twisted conformation. There are, however, no OPEs which have a main chain chirality. The author thus challenged to fabricate a chiral OPE by conjugating it with a HP. The author synthesized a novel OPE-peptide cyclic conjugate **C-OPE10** as well as a linear conjugate **L-OPE10** as a reference compound (Figure III-1). OPE having two carboxyl groups was bridged by a helical decapeptide composed of alternating Ala and Aib. The

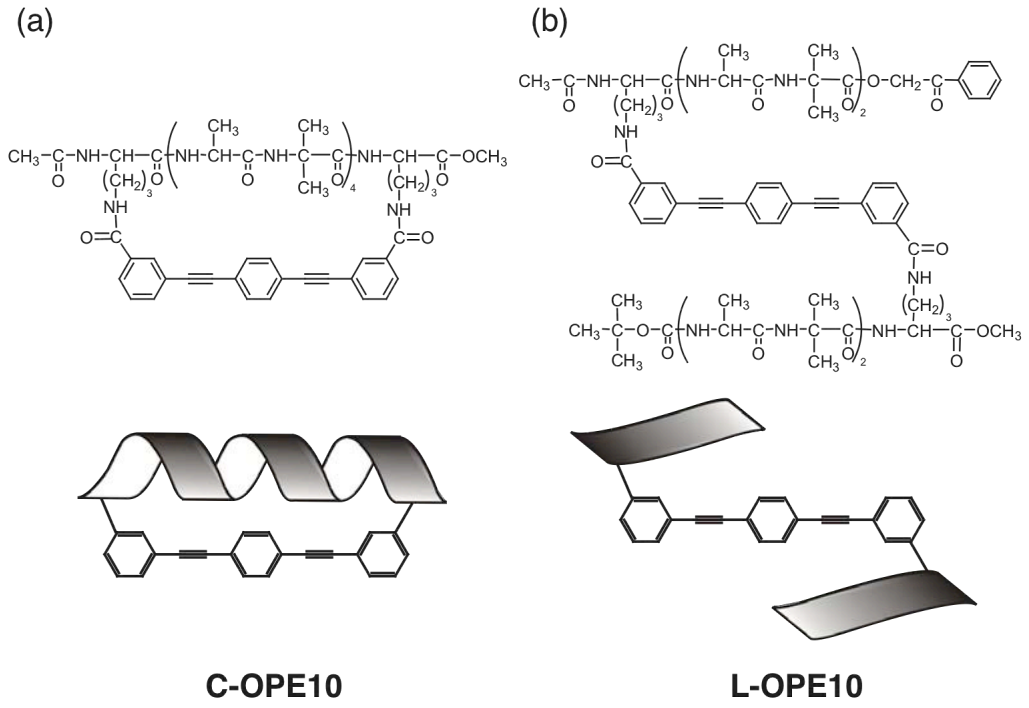

Figure III-1. Chemical structures and schematic presentations of (a) **C-OPE10** and (b) **L-OPE10.**

molecular length of a helical decamer is estimated to be 1.5–2 nm, which is close to that of OPE (1.7 nm). The HP should be effective not only for restriction of the rotational motion in OPE but also for induction of a chiral twist on it. The conformation of the peptide decamer and the OPE moiety were studied by circular dichroism (CD) spectroscopy, and the electronic structures of the OPE moiety were discussed on the basis of absorption and emission spectroscopies. For detailed discussion on CD measurements, ab initio calculations were performed using TD-DFT.

Experimental

Materials. C-OPE10 and **L-OPE10** were synthesized according to Scheme III-1. See Chapter I for general procedure of peptide and OPE synthesis and compound identifying ways. The purity of the final compounds was further analyzed by HPLC (COSMOSIL ^{5}C18-AR, eluant: CH_3CN/H_2O/TFA = 45/55/0.05 for **C-OPE10**; CH_3CN/H_2O = 90/10 for **L-OPE10**; flow rate: 1 mL/min; monitor at 355 nm).

Spectroscopy in solution. CD spectra were measured using optical cells of a 0.1 and 1 cm optical path length. An optical cell of a 1 cm optical path length was used in both absorption and emission spectroscopic measurements.

Quantum calculation. Details are described in Chapter I. No imaginary frequency number was outputted from the optimized structure. TD-DFT method was used for absorption and electric circular dichroism simulations on B3LYP/6-31G(d,p) level. Ten excited states were solved in the calculations.

Synthesis

Compounds **2–4,** and **6** were synthesized by conventional liquid phase peptide coupling (see

the general procedure in Chapter I).

5. Compound **4** (630 mg, 0.852 mmol) was treated with HBr/AcOH. The HBr salt was washed with diethlether. The deprotcetd peptide was coupled with 3-iodobenzoic acid (434 mg, 1.75 mmol) in DMF in the presence of HATU (1.33 g, 3.5 mmol), and DIEA (914 μL, 5.25 mmol) by the general procedure for the peptide coupling reaction for 30 h. The residue was purified by methods 1 and 2(chloroform/MeOH = 30/1) and washed with *i*Pr_2O. 448

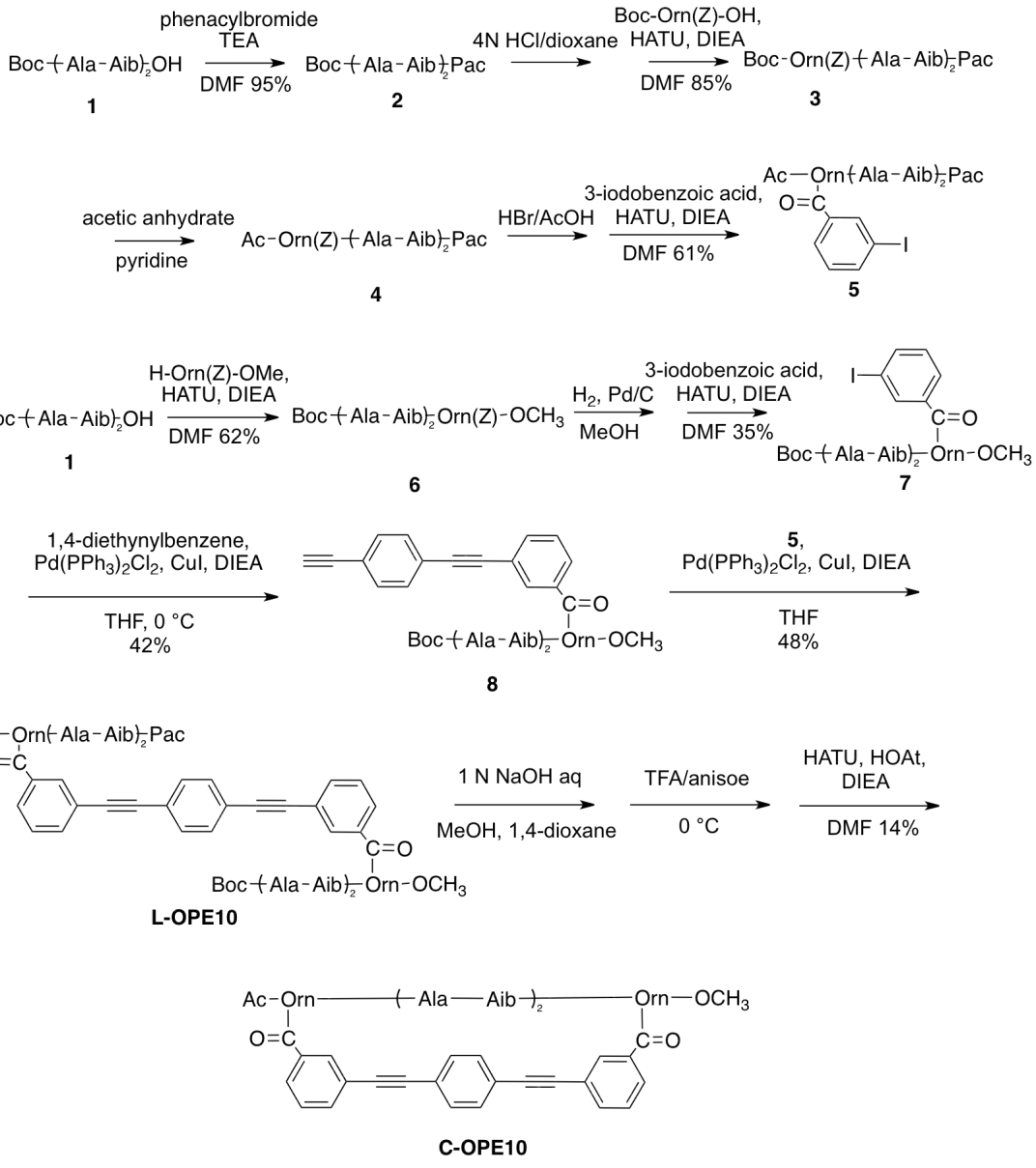

Scheme III-1. Synthetic scheme of **L-OPE10** and **C-OPE10.**

mg (61% yield) of the desired product was obtained.

^{1}H NMR (400 MHz, $CDCl_3$): δ (ppm) 1.37–1.60 (m, 20H, $AibC^{\beta}$, $AlaC^{\beta}$, $OrnC^{\beta}$), 1.81 (m, 2H, $OrnC^{\gamma}$), 2.06 (s, 3H, Ac), 3.51 (m, 2H, $OrnC^{\delta}$), 4.07 (m, 1H, $AlaC^{\alpha}$), 4.35 (m, 1H, $AlaC^{\alpha}$), 4.44 (m, 1H, $OrnC^{\alpha}$), 5.30 (dd, 2H, OCH_2COPh), 6.78–6.83 (m, 2H, $OrnNH^{\delta}$, AibNH), 7.07–7.13 (m, 2H, AlaNH, $OrnNH^{\alpha}$), 7.15-7.21 (m, 2H, AlaNH, aromatic), 7.32 (s, 1H, AibNH), 7.50 (m, 2H, aromatic), 7.62 (m, 1H, aromatic), 7.85 (d, 1H, aromatic), 7.8–7.96 (m, 3H, aromatic), 8.18 (s, 1H, aromatic).

FAB-MS (matrix: NBA): *m*/*z* = 835.3 (calcd for $C_{36}H_{48}IN_6O_9$ $[M + H]^+$, 835.24).

7. To **6** (1.3 g, 1.88 mmol) in MeOH was added Pd/C (260 mg). The reaction mixture was kept stirring under a H_2 atmosphere for 24 h. Another portion of Pd/C (50 mg) was added to the mixture and stirred for another 26 h. The catalyst was filtered off, and the filtrate was concentrated under reduced pressure. The peptide was coupled with 3-iodobenzoic acid (592 mg, 2.39 mmol) in DMF in the presence of HATU (1.51 g, 3.98 mmol), and DIEA (0.832 μL, 4.78 mmol) by the general procedure for the peptide coupling reaction for 14 h. Additional portions of HATU (600 mg, 1.6 mmol) and DIEA (554 μL, 3.2 mmol) were added to the mixture and stirred for 24 h. The residue was purified by methods 1 and 2(chloroform/MeOH = 50/1) and washed with iPr_2O. 451 mg (35% yield) of the desired product was obtained.

^{1}H NMR (400 MHz, $CDCl_3$): δ (ppm) 1.37–1.68 (m, 27H, $AibC^{\beta}$, Boc, $AlaC^{\beta}$), 1.72 (m, 2H, $OrnC^{\gamma}$), 1.98 (m, 2H, $OrnC^{\beta}$), 3.37 (m, 2H, $OrnC^{\delta}$), 3.69 (s, 3H, OCH_3), 3.93 (m, 1H, $AlaC^{\alpha}$), 4.21 (m, 1H, $AlaC^{\alpha}$), 4.50 (m, 1H, $OrnC^{\alpha}$), 6.42 (s, 1H, AlaNH), 7.12 (m, 1H, aromatic), 7.31 (m, 1H, $OrnNHC^{\alpha}$), 7.35 (s, 1H, AibNH), 7.54 (S, 1H, $OrnNHC^{\delta}$), 7.60 (d, 1H, AlaNH), 7.76 (d, 1H, aromatic), 7.92 (d, 1H, aromatic), 8.22 (s, 1H, aromatic).

FAB-MS (matrix: NBA): *m*/*z* = 789.3 (calcd for $C_{32}H_{50}IN_6O_9$ $[M + H]^+$, 789.26).

8. See the general procedure for the Sonogashira coupling reaction. **7** (308 mg, 390 μmol), 1,4-diethynylbenzene (59 mg, 468 μmol), Pd(II)(II)$(PPh_3)_2Cl_2$ (16.5 mg, 23.4 μmol), Cu(I)I (7.4 mg, 39 μmol), and DIEA (272 μL, 1.56 mmol) were reacted in THF for 2 h. The residue was purified by a column chromatography (chloroform/MeOH = 30/ 1), giving 130 mg (165 μmol, 42%).

^{1}H NMR (400 MHz, $CDCl_3$) δ (ppm) 1.35-1.57 (m, 27H, AibC$^{\beta}$, Boc, AlaC$^{\beta}$), 1.75 (m, 2H, OrnC$^{\gamma}$), 2.00 (m, 2H, OrnC$^{\beta}$), 3.17 (s, 1H, HCCPh), 3.48 (m, 2H, OrnC$^{\delta}$), 3.71 (s, 3H, OCH_3), 3.92 (m, 1H, AlaC$^{\alpha}$), 4.17 (m, 1H, AlaC$^{\alpha}$), 4.52 (m, OrnC$^{\alpha}$), 4.99 (s, 1H, AlaNH), 6.40 (s, 1H, AibNH), 7.01 (s, 1H, AibNH), 7.31–7.40 (m, 2H, OrnNH$^{\alpha}$, aromatic), 7.42–7.51 (m, 5H, AlaNH, aromatic), 7.58 (d, 1H, aromatic), 7.88 (d,1H, aromatic), 8.18 (s, 1H, aromatic).

FAB-MS (matrix: NBA) *m*/*z* = 787.4 (calcd for $C_{42}H_{55}N_6O_9$ $[M + H]^+$, 787.40).

L-OPE10. See the general procedure for the Sonogashira coupling. **8** (110 mg, 140 μmol), **5** (140 mg, 167 μmol), Pd(II)(II)$(PPh_3)_2Cl_2$ (5.9 mg, 8.4 μmol), Cu(I)I (2.7 mg, 14 μmol), and DIEA (97 μL, 560 μmol) were reacted in THF for 3 h. The residue was purified by a Sephadex LH20 column (eluant: DMF). 106 mg (48% yield at most) of the desired product was obtained. HPLC: retention time = 6.377 min (93%).

^{1}H NMR (400 MHz, $CDCl_3$): δ (ppm) 1.35–1.59 (m, 45H, AibC$^{\beta}$, Boc, AlaC$^{\beta}$), 1.59–1.90 (m, 8H, OrnC$^{\beta}$, OrnC$^{\gamma}$), 2.07 (s, 3H, Ac), 3.40-3.55 (m, 4H, OrnC$^{\delta}$), 3.71 (s, 3H, OCH_3), 3.92 (m, 1H, AlaC$^{\alpha}$, or OrnC$^{\alpha}$), 4.06 (m, 1H, AlaC$^{\alpha}$, or OrnC$^{\alpha}$), 4.14 (m, 1H, AlaCR, or OrnC$^{\alpha}$), 4.36 (m, 1H, AlaC$^{\alpha}$, or OrnC$^{\alpha}$), 4.42 (m, 1H, AlaC$^{\alpha}$, or OrnC$^{\alpha}$), 4.51 (m, 1H, AlaC$^{\alpha}$, or OrnC$^{\alpha}$), 5.20 (s, 1H, AlaC$^{\alpha}$, or OrnC$^{\alpha}$), 5.30 (dd, 2H, OCH_2COPh), 6.53 (s, 1H, NH), 6.88 (s, 1H, NH), 7.00 (d, 1H, NH), 7.35–7.95 (m, 21H, NH, and aromatic).

FAB-MS (matrix: NBA): *m*/*z* = 1493.9 (calcd for $C_{78}H_{101}N_{12}O_{18}$ $[M + H]^+$, 1493.73).

C-OPE10. L-OPE10 (74 mg, 49 μmol) in MeOH (200 μL) and 1,4-dioxane (200 μL) was treated with 1 N aq NaOH (60 μL) at 0 °C without stirring for 4 h. The mixture was neutralized with 2 N aq HCl and concentrated under reduced pressure. The product was treated with TFA (730 μL) in the presence of anisole (73 μL) at 0 °C for 1 h. The mixture was concentrated under reduced pressure, and the residue was washed with Et_2O. The identification was carried out by FAB-MS. To the TFA salt of the peptide in DMF were added HATU (205 mg, 539 μmol) and HOAt (73 mg, 539 μmol). The mixture was kept stirring under a nitrogen atmosphere at 0 °C. To the solution was added a DMF solution of DIEA (0.1 M, 10.8 mL) over 1.5 h. The temperature was then gradually raised to RT and the mixture was stirred for 24 h. Additional portions of HATU (41 mg, 108 μmol), HOAt (14.7 mg, 108 μmol), and DIEA (28 μL, 162 μmol) were added to the mixture at 0 °C followed by 33 h of stirring at RT. The mixture was concentrated under reduced pressure and purified by a Sephadex LH-20 column for two times (eluent: DMF and MeOH) and preparative TLC (eluent: chloroform/MeOH 10/1). Finally, the product was solidified with hexane. 10 mg (14% yield at most) of the desired product was obtained. HPLC: retention time) 4.713 min (~100%).

^{1}H NMR (400 MHz, MeOH-d_4) δ (ppm) 1.35–1.57 (m, 36H, AibC$^{\alpha}$, AlaC$^{\alpha}$), 1.75–1.98 (m, 8H, OrnC$^{\beta}$, OrnC$^{\gamma}$), 2.04 (s, 3H, Ac), 3.48 (m, 4H, OrnC$^{\delta}$), 3.69 (s, 3H, OCH_3), 3.92-4.04 (m, 3H, AlaC$^{\alpha}$, or OrnC$^{\alpha}$), 4.13-4.17 (m, 1H, AlaC$^{\alpha}$, or OrnC$^{\alpha}$), 4.29 (m, 1H, AlaC$^{\alpha}$, or OrnC$^{\alpha}$), 7.49–8.10 (m, 12H, aromatic).

FAB-MS (matrix: NBA): *m*/*z* = 1257.7 (calcd for $C_{65}H_{85}N_{12}O_{14}$ $[M + H]^+$, 1257.62).

Results and discussion

Conformation of peptide. To investigate the conformation of the peptide moieties of **L-OPE10** and **C-OPE10**, CD spectra were recorded in MeOH at RT (Figure III-2a). The

spectrum of **L-OPE10** showed a weak positive Cotton effect around 220 nm, suggesting that two moieties of the peptide pentamers in **L-OPE10** take a disordered conformation,[250] although some pentamers consisted of Ala and Aib residues are known to take a 3_{10}- or an α-helical structure.[251]

On the other hand, **C-OPE10** clearly showed a double-minimum pattern (peaks at 208 and 222 nm), which is characteristic of an α-helical structure.[250,252] Otoda et al. have investigated on the critical length for transition from a 3_{10}- to an α-helix of Boc-(Ala-Aib)$_n$-OMe to be eight residues on the basis of X-ray analysis of the crystalline structures.[69] The present observation for the peptide decamer in **C-OPE10** is in agreement with the previous finding.

Although the CD spectrum of **C-OPE10** showed the clear pattern of α-helix, the structure was not so stable. The helix content was determined as 23% and decreased further upon raising temperature from 10 to 50 °C (Figure III-2b). These facts indicate that the α-helical structure is most dominant in the decamer but has only a little advantage in stabilization against other structures.[138,164,161,158] Because the molar ellipticity per residue of

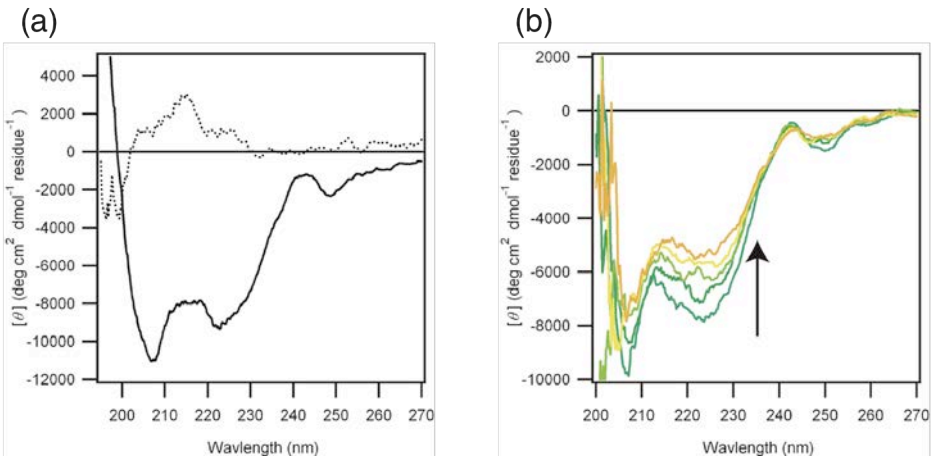

Figure III-2. CD spectra of (a) **C-OPE10** (solid) and **L-OPE10** (dot), and (b) temperature dependence of CD spectra of **C-OPE10** with raising from 10 (blue) to 50 °C (orange; every 10 °C).

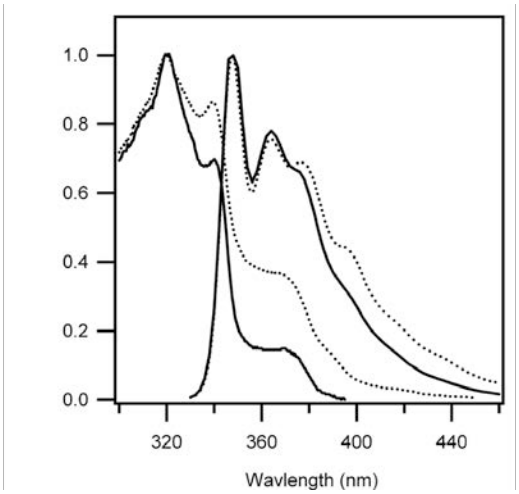

Figure III-3. Normalized absorption and emission spectra in MeOH: (solid) **C-OPE10,** and (dot) **L-OPE10.**

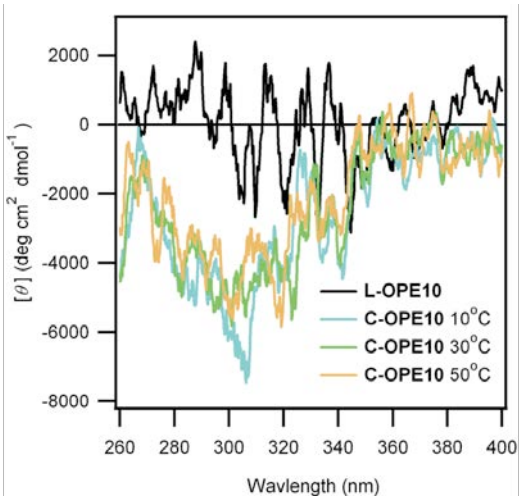

Figure III-4. CD spectra of **C-OPE10** and **L-OPE10** in MeOH.

the **C-OPE10** (ca. -1×10^4 deg cm^{-2} dmol^{-1} residue^{-1} at 222 nm) was close to that of the free dodecamer of five repeats of the Ala-Aib alternating sequence,[138] the decapeptide moiety was not stabilized in its helical structure despite the connection of a rigid rod-shaped OPE like a molecular splint. One reason for failure in stabilization of the helical structure should be unsuitable geometry for the OPE moiety to bridge the two points of the peptide with taking α-helical structure. The distance between the two terminal residues of the

α-helical decapeptide may be longer than the OPE counterpart, because the side chains of the two terminal residues make a dihedral angle of about 80° around the helix axis and are not straight along the helix axis. Another reason for instability in the α-helix may be competition between 3_{10}- and α-helical structures. When the temperature was raised to 50 °C, the peak at 222 nm nearly disappeared and became a shoulder, which is close to the typical CD spectrum pattern for 3_{10}-helical structure.[239]

Characterization of the OPE moiety. Absorption and emission spectra of **C-OPE10** and **L-OPE10** in MeOH were measured (Figure III-3). The absorption spectra of **C-OPE10** and **L-OPE10** showed well-resolved vibrational bands at 373, 340, and 320 nm, which is typical for OPE with a few functional groups.[253,216,254] No sharp band at the longer wavelength was observed in both absorption spectra under the present conditions (ca. 15

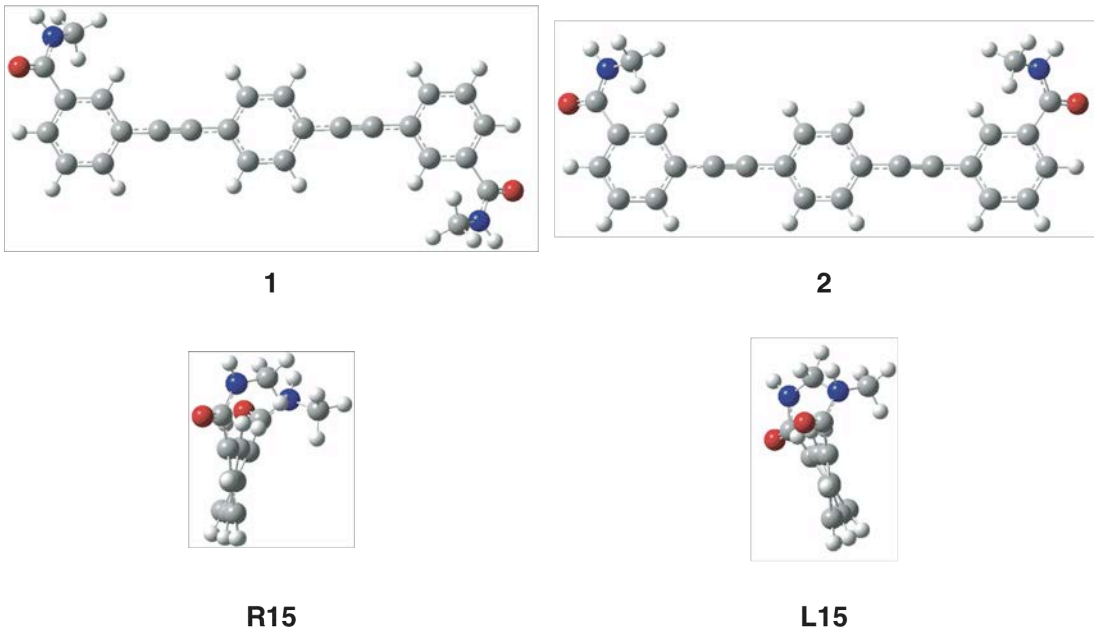

Figure III-5. Geometries of the model compounds: A gray ball represents a carbon atom, white represents hydrogen, red represents oxygen, and blue represents nitrogen.

μM for both **C-OPE10** and **L-OPE10**). The emission spectra of the both compounds also showed clear vibrational bands as the absorption spectra. The mirror image symmetry between absorption and emission spectra was broken similarly to the other reports on PPE/OPEs[216,255] as well as PPVs[244,256,257] and PPPs.[258] When the two absorption spectra were normalized by the intensity at 320 nm, **C-OPE10** shows nearly identical absorption and emission spectra with **L-OPE10.** There are two possible interpretations for the identical spectra: one is the helix bridge does not hinder the free rotation of the aromatic groups around the ethynylene axis, and the other is the fixed conformation of the OPE moiety by the helix bridge happens to show similar spectra to the average conformation of the OPE moiety in **L-OPE10,** where nearly frictionless rotation is allowed around the ethynylene axis.[173,217] We conclude the latter interpretation is applied to the present case as following.

To investigate the conformation of the OPE moiety, CD spectra were recorded in the absorption region of the OPE (260–360 nm). A negative Cotton effect was observed with **C-OPE10** (Figure III-4), whereas no peaks with **L-OPE10.** CD spectra of π-conjugate polymers such as PPE,[259] PPV,[260] and PPP[261,262] have been examined for the purpose of fabrication of circularly polarized electroluminescence materials. Cotton effects of those compounds appeared upon formation of chiral aggregation due to the chirality introduced in aliphatic side chains. This chiral aggregation is, however, not the case for **C-OPE10,** because no aggregation band in the absorption spectrum was observed in the present concentration range (13–16 μM). Both **C-OPE10** and **L-OPE10** were homogeneously dissolved in MeOH. Therefore, the negative induced CD of **C-OPE10** should reflect a twist conformation of the OPE moiety upon bridging by a right-handed helix. As far as we know, this is the first example to prepare a π-conjugated compound having main chain chirality by bridging the twisted OPE terminals with a chiral helix, which is distinctly different from the previous report by Fiesel et al. who have also synthesized soluble PPPs having main-chain

chirality.[263]

The negative Cotton effect of **C-OPE10** shows little change with increasing temperature, which is a sharp contrast to the peptide moiety. The reason may be due to the flexible linker between the OPE moiety and the HP to buffer the influence of the thermal fluctuation of the HP on the OPE moiety, but the detail remains to be solved.

Quantum calculations. The conformation of the OPE moiety is further studied by ab initio calculations on model compounds. To start with, geometry **1** (Figure III-5) was prepared by optimization with the DFT method on the B3LYP/6-31G(d,p) level. The vibration analysis revealed that **1** located at a local minimum in the energy potential. The dihedral angles of the three phenyl rings of **1** were less than 1°. Geometries **2, R15,** and **L15**

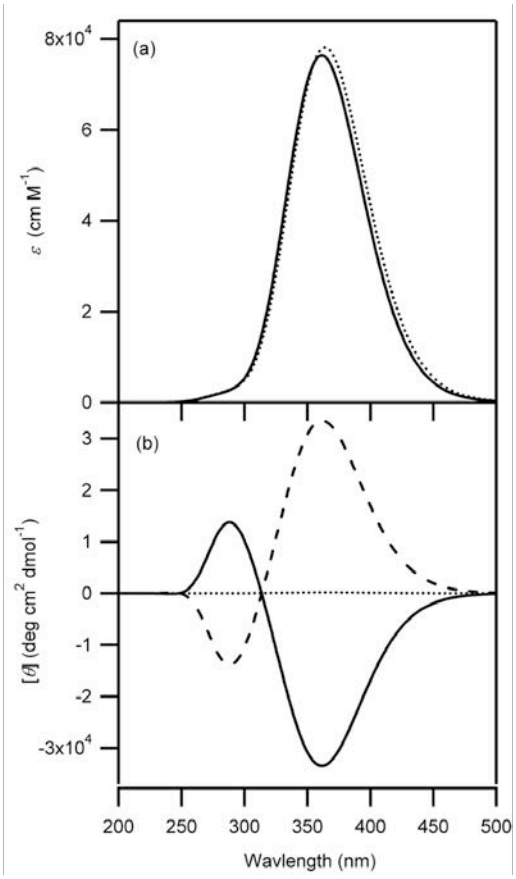

Figure III-6. Computed (a) absorption and (b) CD spectra of geometries **1** (dot), **R15** (solid), and **L15** (dash). The absorption and CD spectra of **2** are nearly identical to those of **1**. The absorption spectra of **R15** and **L15** are also

(Figure III-5) were prepared by changing the dihedral angles between the phenyl rings from **1**. Geometry **2** is a coplanar conformation, where two substituents of the OPE moiety were located at the same side. Geometry **R15** has a dihedral angle of 15° between two adjacent phenyl rings in a right-handed way, whereas **L15** in a left-handed way. Single-point calculation on the four geometries were performed using TD-DFT method using B3LYP/6-31G(d,p) basis set. The predicted absorption and CD spectra are shown in Figure III-6. The maximum absorption wavelength is 364 nm for **1** and **2**, and 361 nm for **R15** and **L15**. This reflects that the π-conjugation is weakened in **R15** and **L15** because the coplanar geometry of **2** is twisted. The calculated CD spectra of **R15** and **L15** show a negative and positive Cotton effect at the maximum absorbance wavelength, respectively (Figure III-6b). It is thus concluded that the OPE moiety in **C-OPE10** should take the right-handed conformation. However the calculated ellipticity of **R15** (-3.3×10^4 deg cm^2 dmol^{-1}) is five times larger than the measured value (ca. -6×10^3 deg cm^2 dmol^{-1}). CD spectra of **2** were calculated with varying the dihedral angles from 5 to 90° (Figure III-7). The Cotton effect at the maximum absorption wavelength increases as the twisting angle increases from 0 to 60°.

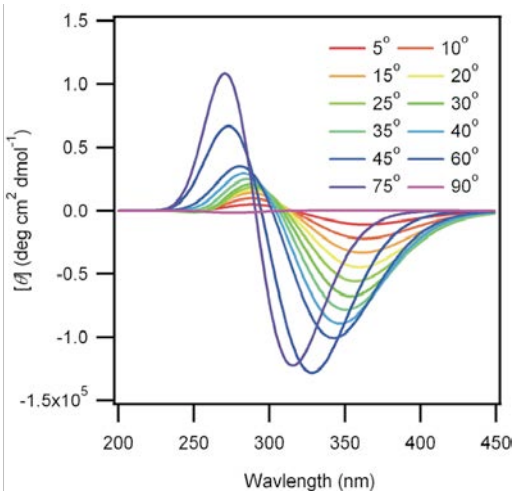

Figure III-7. Calculated CD spectra on right-hand twisted geometries with varying the dihedral angles between two phenyl rings around the molecular axis.

If the twist angle is more than 60°, the negative Cotton effect starts decreasing sharply and finally drops down to zero at 90°, where chirality disappears. When the measured molar ellipticity is compared with the computed ones, the twisted angle is estimated to be less than 5°. This estimation, however, is not reliable due to the imprecision of the calculated intensity. At the moment, the twisted angle is considered to be less than 15°.

Conclusion

Novel HP-OPE conjugates **C-OPE10** (cyclized) and **L-OPE10** (linear) were prepared. From CD measurements, the decapeptide moiety in **C-OPE10** was revealed to take α-helical structure, whereas two pentamers in **L-OPE10** took random structure. Observation of the induced negative Cotton effect of the OPE moiety in **C-OPE10** indicated a twisted conformation of the OPE moiety in **C-OPE10** because two phenyl rings were bridged by the α-helical decapeptide. Calculations showed a right-handed twist conformation of the OPE moiety. We provide here a new method to prepare a π-conjugated compound having main-chain chirality by bridging the OPE with a chiral helix. Such compounds will be applied for interesting chiroptical materials.

Chapter IV

Suppression of HOMO–LUMO Transition in a Twist Form of Oligo(phenyleneethynylene) Clamped by a Right-Handed Helical Peptide

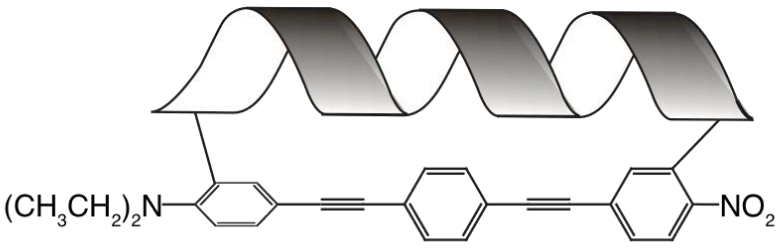

Introduction

This chapter deals with a photophysical study of an OPE based D–π–A system. The main interest is the twisting effect on HOMO–LUMO transition of the OPE. Twisting effects on OPEs with no electron donor and acceptor have been studied extensively (see General Introduction). However, the effects on a OPE based D–π–A system have not. The author thus applied the idea of twisting an OPE by clipping a HP, which is demonstrated in the previous chapter to challenge this issue. The author revised the molecular design of a cyclic conjugate between OPE and HP to increase the twist between phenyl rings, **SSA8=OPE** (Figure IV-1). The molecular arrangement of the OPE and the HP moieties becomes close together by using short linking chains, which is designed to increase the tilt in the conformation due to large steric hindrance. Eight out of nine residues of the peptide moiety consist of an alternating sequence of Ala and Aib to promote a helical structure. Asp is chosen as the N-terminal residue to introduce a connection part with lipoic acid, which is capable of being immobilized on gold, however, for the future study. In the OPE moiety, an *N*,*N*-diethylamino group and a nitro group are introduced as an electron donor and an

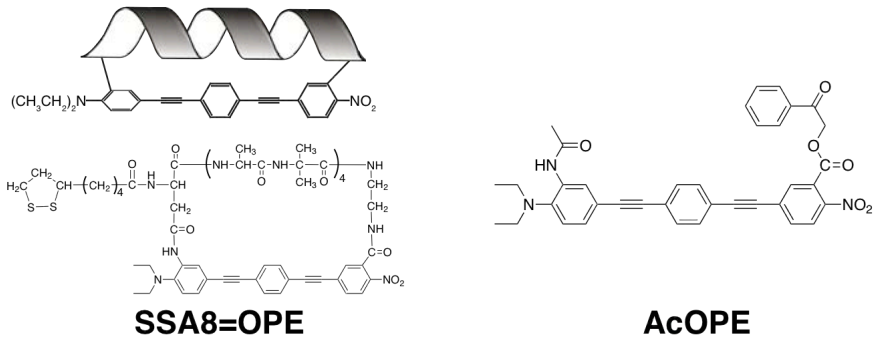

Figure IV-1. Schematic presentation of **SSA8=OPE** and chemical structures of **SSA8=OPE** and **AcOPE**.

acceptor, respectively, to build a D–π–A system. Absorption spectroscopy, fluorescence spectroscopy, CD spectroscopy, and fluorescence lifetime measurements are used to reveal the effect of the chiral twist on OPE optical properties, especially on oscillator strength of the HOMO–LUMO transition. A reference compound, **AcOPE,** which has no peptide bridge, is also synthesized and optically characterized as well. Quantum calculations based on DFT are also carried out to have detailed insights on the electronic structures and transitions of the OPE.

Experimental

Materials. SSA8=OPE and **AcOPE** were synthesized according to Schemes IV-1 and IV-2. Peptides of an alternating sequence of Ala and Aib were synthesized by the conventional liquid-phase method. The OPE moiety was synthesized by the Sonogashira coupling. See Chapter I for the general procedures of peptide and OPE synthesis and compound

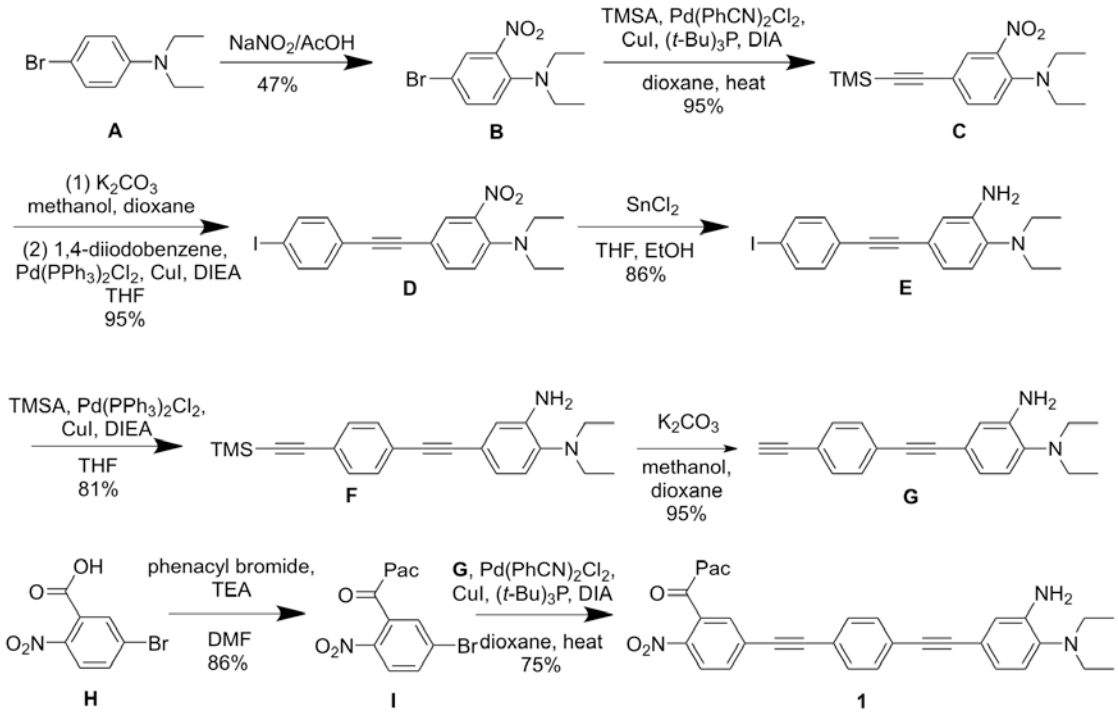

Scheme IV-1. Synthetic scheme of **1.**

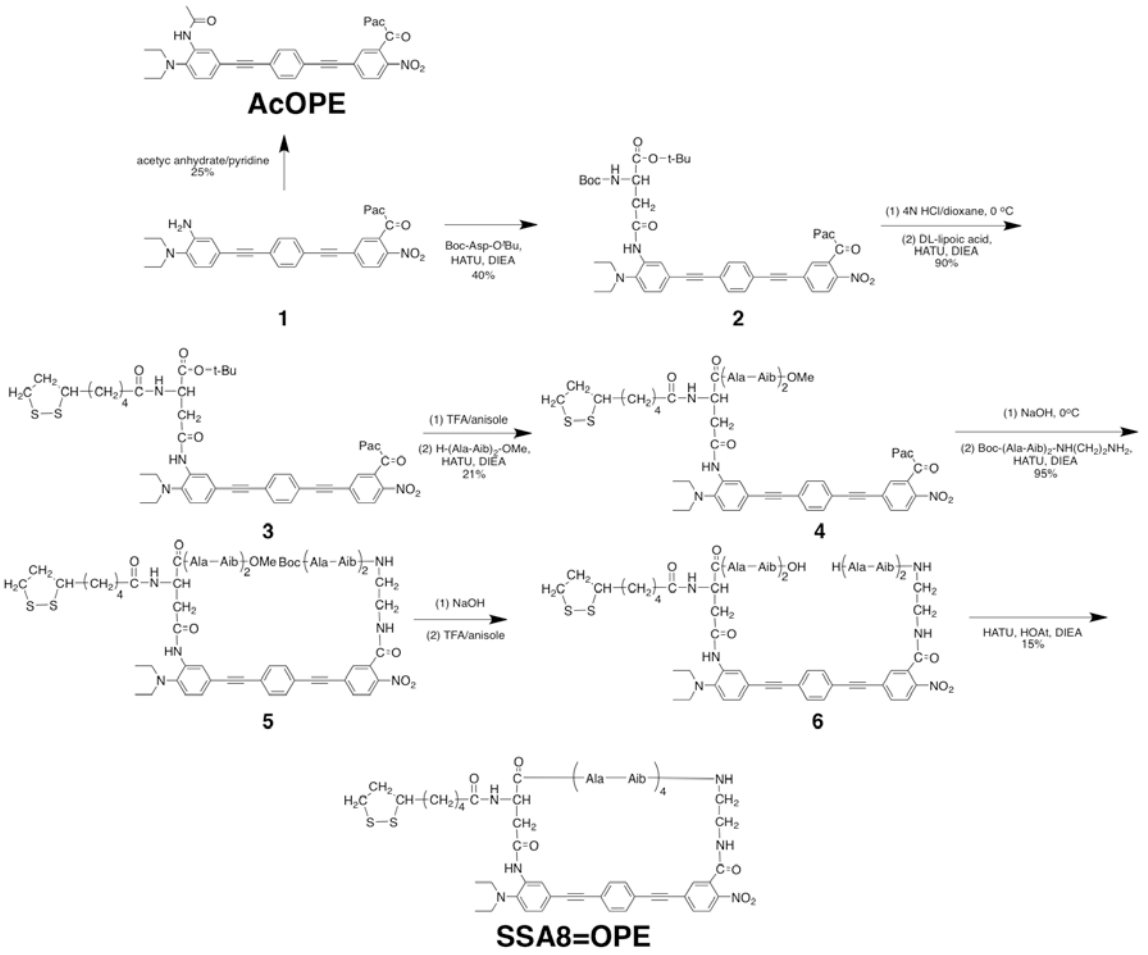

Scheme IV-2. Synthetic scheme of **SSA8=OPE** and **AcOPE.**

identification methods. The purity of the final products were checked by HPLC (Cosmosil Chorester) using MeOH and chloroform/MeOH (1/1) as an eluent for **SSA8=OPE** and **AcOPE,** respectively. The final products were characterized by high resolution mass spectrometry.

Optical spectra. CD spectra were recorded with an optical cell with 0.1 cm optical path length for the measurement of the peptide moiety and with 1 cm for the OPE moiety. An optical cell of 1 cm optical path length was used in absorption, fluorescence, and emission spectroscopy measurements. The excitation wavelength was set at 360 nm for all fluorescence spectra. The monitor wavelength was set at 460 nm for all excitation spectra.

The accumulation number was four for both fluorescence and excitation spectra. The absorbance of the solutions was kept below 0.1 when the fluorescence and excitation spectra were recorded, otherwise specified. Fluorescence quantum yield was calculated on the basis of Parker–Rees method:[264] Quantum yield (Φ) is correlated with that of a reference (Φ_r) by

$$\Phi = \Phi_r\left(\frac{K_r}{K}\right)\left(\frac{I_r}{I}\right)\left(\frac{n^2}{n_r^2}\right)\left(\frac{A}{A_r}\right), \qquad \text{(IV-1)}$$

where *K*, *I*, *n*, and *A* were absorbance at the excitation wavelength, intensity of excitation light, refractive index, and area of fluorescence signal, respectively. As a reference, a solution of quinine sulfate in 0.1 M sulfuric acid (absorbance of less than 0.1) was used. The quantum yield of the solution was set to be 0.544 for excitation at 360 nm.

Fluorescence lifetime measurement. A home built laser apparatus was used for the measurements of fluorescence decay curves. A pulse laser of 710 nm from a mode lock Ti:sapphire laser, which was excited by a continuous laser of 532 nm from a diode laser, was used as the light source. The pulse laser was introduced into a pulse selector to convert to a pulse laser of 355 nm and 8 MHz. This light was used as the excitation light. The fluorescence light was passed through a monochromator to select a light of 460 nm, which was detected by a photomultiplier. The sample solutions were degassed by bubbling nitrogen for 15 min before the measurements.

Quantum calculation. See Chapter III for the details of the geometry optimization and TD-DFT calculations.

Synthesis

4-bromo-2-nitro-*N*,*N*-dimethylaniline B. To a 1000 mL RBF were added

4-bromo-*N*,*N*-diethylaniline (6.0 g, 26.3 mmol), water (780 mL), and acetic acid (78 mL). $NaNO_2$ in water (2.0 g/130 mL) was added to the mixture dropwise. The mixture was stirred overnight and extracted with dichloromethane (3×). The organic layer was washed with brine and dried over anhydrouns magnesium sulfate. The solvent was then removed in reduced atmosphere. The product was purified by column chromatography (silica gel, chloroform/hexane 1/2). 3.37 g (47% yield) of the product was obtained.

^{1}H NMR ($CDCl_3$, 400 MHz): δ (ppm) 1.08 (6H, t, (C*H*$_3$CH$_2$)N), 3.14 (4H, q, (CH$_3$C*H*$_2$)N), 7.01 (1H, d, aromatic), 7.47 (1H, dd, aromatic), 7.80 (1H, d, aromatic).

EI-MS: *m*/*z* = 272.01 (calcd for $C_{10}H_{13}BrN_2O_2$ M^+, 272.02).

2-nitro-4-trimethylsilylethynyl-*N*,*N*-diethylaniline C. See the general procedure for the Sonogashira coupling reaction. **B** (2.45 g, 8.97 mmol), TMSA (5.0 mL, 35.88 mL), Pd(II)(II)$(PhCN)_2Cl_2$ (344 mg, 897 μmol), Cu(I)I (171 mg, 897 μmol), tri-*tert*-butylphosphine (363 mg, 1.79 mmol), and DIA (3.78 mL, 26.91 mmol) were reacted in 1,4-dioxane (8 mL) at 55 °C for one day. The residue was purified by column chromatography (chloroform/hexane = 1/2, then 1/1). 2.5 g (95% yield) of the desired product was obtained.

^{1}H NMR ($CDCl_3$, 400 MHz): δ (ppm) 0.23 (s, 9H, $(CH_3)_3Si$), 1.14 (t, 6H, (C*H*$_3$CH$_2$)$_2$N), 3.19 (q, 4H, (CH$_3$C*H*$_2$)$_2$N), 6.99 (d, 1H, aromatic), 7.42 (dd, 1H, aromatic), 7.79 (s, 1H, aromatic).

EI-MS: *m*/*z* = 290.17 (calcd for $C_{15}H_{22}N_2O_2Si$ M^+, 290.15).

4-(4′-iodophenylethynyl)-2-nitro-*N*,*N*-diethylaniline D. The trimethylsilyl group of **C** (2.90 g, 10.0 mmol) was removed with potassium carbonate in a mixture of MeOH (60 mL) and dichloromethane (60 mL, see synthesis of **G** for details). By the general procedure for the Sonogashira coupling reaction, the deprotected product (2.20 g, 10.1 mmol),

1,4-diiodobenzene (13.3 g, 40.32 mmol), Pd(II)(II)$(PPh_3)_2Cl_2$ (424 mg, 604 μmol), Cu(I)I (191 mg, 1.0 mmol), and DIEA (7.04 mL, 40.3 mmol) were racted in THF (15 mL) at 40 °C for two days. The residue was purified by column chromatography (chloroform/hexane = 1/2 then 1/1). 4.0 g (95% yield) of the desired product was obtained.

^{1}H NMR ($CDCl_3$, 400 MHz): δ (ppm) 1.14 (t, 6H, $(CH_3CH_2)_2N$), 3.22 (q, 4H, $(CH_3CH_2)_2N$), 7.04 (d, 1H, aromatic), 7.22 (d, 2H, aromatic), 7.48 (dd, 1H, aromatic), 7.68 (d, 2H, aromatic), 7.89 (s, 1H, aromatic).

EI-MS: *m*/*z* = 420.03 (calcd for $C_{12}H_{14}N_2O_2$ M^+, 420.24).

2-amino-(4′-iodophenylethynyl)-*N*,*N*-diethylaniline E. To a 200 mL RBF were added **D** (500 mg, 1.2 mmol), tin chloride dihydrate (2.7 g, 11.9 mmol), THF (6 mL), and EtOH (0.6 mL). The mixture was stirred for 3 hr. 15 mL of 50 wt % aq KOH was added to the mixture and a precipitation was filtered off. The filtrate was extracted with dichloromethane and dried over magnesium sulfate. By removing the solvent in vacuum, 400 mg (86% yield) of the desired product was obtained.

^{1}H NMR ($CDCl_3$, 400 MHz): δ (ppm) 0.96 (t, 6H, $(CH_3CH_2)_2N$), 2.96 (q, 4H, $(CH_3CH_2)N$), 4.07 (s, 2H, $ArNH_2$), 6.89–6.97 (m, 3H, aromatic), 7.21 (d, 2H, aromatic), 7.66 (d, 2H, aromatic).

EI-MS: *m*/*z* = 390.1 (calcd for $C_{18}H_{19}IN_2$ M^+, 390.06).

2-amino-(4′-4″-trimethylsilyllethynylphenylethynyl)-*N*,*N*-diethylaniline F. See the general procedure for the Sonogashira cross coupling reaction. **E** (3.71 g, 9.51 mmol), TMSA (2.63 mL, 19.0 mmol), Pd(II)(II)$(PPh_3)_2Cl_2$ (400 mg, 570 μmol), Cu(I)I (181 mg, 0.95 mmol), and DIEA (5.54 mL, 38 mmol) were reacted in THF (10 mL) at RT for 36 hr. The residue was purified by column chromatography (chloroform/hexane = 1/1). 2.81 g (81% yield) of the desired product was obtained.

^{1}H NMR ($CDCl_3$, 400 MHz): δ (ppm) 0.25 (s, 9H, $(CH_3)_3Si$), 0.99 (t, 6H, $(CH_3CH_2)_2N$), 2.96 (q, 4H, $(CH_3CH_2)_2N$), 4.06 (s, 1H, $ArNH_2$), 6.89-6.97 (m, 3H, aromatic), 7.41 (s, 4H, aromatic).

EI-MS: *m*/*z* = 360.20 (calcd for $C_{23}H_{28}N_2Si$ M^+, 360.20).

2-amino-(4′-4″-ethynylphenylethynyl)-*N*,*N*-diethylaniline G. To a 100 mL RBF were added **F** (2.81 g, 7.79 mmol), MeOH (12 mL), dichloromethane (12 mL), and potassium carbonate (2.15 g, 15.6 mmol). The mixture was stirred under nitrogen atmosphere for 2 hr. The mixture was then poured into 4 wt % aq $KHSO_4$ and extracted with dichloromethane. The organic layer was washed with brine and dried over magnesium sulfate. The solvent was removed in reduced atmosphere. 2.15 g (7.40 mmol, 95%) of the desired product was obtained. CATION: the product easily dimerizes under ambient condition. Use it immediately after production or store it in a freezer.

^{1}H NMR ($CDCl_3$, 400 MHz): δ (ppm) 0.99 (t, 6H, $(CH_3CH_2)_2N$), 2.96 (q, 4H, $(CH_3CH_2)_2N$), 3.15 (s, 1H, ArCCH), 4.07 (s, 1H, $ArNH_2$), 6.89-6.97 (m, 3H, aromatic), 7.44 (s, 4H, aromatic).

5-bromo-2-nitrobenzoic acid phenacyl ester I. To a 50 mL two-neck RBF were added 4-bromo-2-nitrobenzoic acid (**H**, 1.30 g, 5.28 mmol), phenacyl bromide (1.58 g, 7.93 mmol), DMF (10 mL), and TEA (1.45 mL, 10.57 mmol) at 0 °C. The mixture was stirred at RT under nitrogen atmosphere for 20 hr and the solvent was removed in reduced atmosphere. The residue was purified by column chromatography (silica gel, chloroform). 1.67 g (86% yield) of the desired product was obtained.

^{1}H NMR ($CDCl_3$, 400 MHz): δ (ppm) 5.61 (2H, s, OCH_2COPh), 7.51−7.55 (2H, m, aromatic), 7.63 (1H, t, aromatic), 7.80 (1H, dd, aromatic), 7.89 (1H, d, aromatic), 7.94−7.96 (2H, m, aromatic), 8.10 (1H, d, aromatic).

FAB-MS (NBA): *m*/*z* = 364.03 (calcd for $C_{15}H_{11}BrNO_5$ $[M + H]^+$, 363.97).

1. See the general procedure for the Sonogashira cross coupling reaction. **G** (1.07 g, 3.71 mmol), **I** (1.52 g, 4.17 mmol), Pd(II)(II)$(PhCN)_2Cl_2$ (85 mg, 222 μmol), Cu(I)I (42 mg, 222 μmol), tri(*tert*-butyl)phosphine (110 μL, 445 μmol), and DIA (1.56 mL, 11.1 mmol) were reacted in 1,4-dioxane (5 mL) at 40 °C for two days. The precipitation was filtered off and the filtrate was concentrated in reduced atmosphere. The residue was purified by column chromatography (silica gel, chloroform). 1.60 g (75% yield) of the desired product was obtained.

^{1}H NMR ($CDCl_3$, 400 MHz): δ (ppm) 1.00 (6H, t, $(CH_3CH_2)_2N$), 2.96 (4H, q, $(CH_3CH_2)_2N$), 4.08 (1H, s, $ArNH_2$), 5.62 (2H, s, OCH_2COPh), 6.91–6.99 (3H, m, aromatic), 7.51-7.53 (6H, m, aromatic), 7.65 (1H, t, aromatic), 7.75 (1H, dd, aromatic), 7.96 (2H, d, aromatic), 8.02 (1H, d, aromatic), 8.07 (1H, d, aromatic).

EI-MS (HR): *m*/*z* = 571.2102 (calcd for $C_{35}H_{29}N_3O_5$ M^+, 571.2107).

2. See the general procedure for the peptide coupling reaction. **1** (717 mg, 1.25 mmol), Boc-Asp-O^{t}Bu (725 mg, 2.51 mmol), HATU (1.43 g, 3.76 mmol), HOAt (512 mg, 3.76 mmol), and DIEA (876 μL 5.02 mmol) were reacted in DMF (5 mL) at 60 °C for three days. The residue was purified by methods 1 and 2 (chloroform/MeOH = 50/1). 400 mg (40% yield) of the desired product was obtained.

^{1}H NMR ($CDCl_3$, 400 MHz): δ (ppm) 0.94 (6H, t, $(CH_3CH_2)_2N$), 1.42 (9H, s, Boc), 1.46 (9H, s, O^{t}Bu), 2.90−3.10 (6H, m, AspC$^\beta$, $(CH_3CH_2)_2N$), 4.44 (1H, s, AspC$^\beta$), 5.61 (2H, s, CH_2Ph), 5.73 (1H, d, AspNH), 7.12 (1H, m, aromatic), 7.22 (1H, m, aromatic), 7.50−7.60 (6H, m, aromatic), 7.62 (1H, m, aromatic), 7.73 (1H, dd, aromatic), 7.94−8.06 (4H, m, aromatic).

FAB-MS (NBA): *m*/*z* = 842.4 (calcd for $C_{48}H_{50}N_4O_{10}$ M^+, 842.35).

3. 2 (400 mg, 474 μmol) was dissolved in a mixture of 4 N HCl/dioxane (4 mL) and toluene (2 mL) at 0 °C. The mixture was stirred for 3 hr at 0 °C, followed by evaporation of the solvent. The residue was washed with *i*Pr_2O. By the general procedure for the peptide coupling reaction, the product, D,L-lipoic acid (195 mg, 947 μmol), HATU (540 mg, 1.42 mmol), and DIEA (413 μL, 2.37 mmol) were reacted in DMF (4 mL) at RT for 30 hr. The residue was purified by methods 1 and 2 (chloroform/MeOH = 50/1). 426 mg (90% yield) of the desired product was obtained.

^{1}H NMR ($CDCl_3$, 400 MHz): δ (ppm) 0.96 (6H, t, $(CH_3CH_2)_2N$), 1.47 (11H, m, O^{t}Bu, one of $SSCH_2CH_2CH(CH_2)_3CH_2$), 1.87 (4H, m, two of $SSCH_2CH_2CH(CH_2)_3CH_2$), 1.89, 2.42 (1H, m, $SSCH_2CH_2CH(CH_2)_3CH_2$), 2.25 (2H, m, $SSCH_2CH_2CH(CH_2)_3CH_2$), 2.93 (4H, m, $(CH_3CH_2)_2N$), 3.13 (4H, m, AspC$^\beta$, $SSCH_2CH_2CH(CH_2)_3CH_2$), 3.52 (1H, m, $SSCH_2CH_2CH(CH_2)_3CH_2$), 4.76 (1H, s, AspC$^\alpha$), 5.63 (2H, s, OCH_2COPh), 6.72 (1H, d, AspNH), 7.14 (1H, m, aromatic), 7.50−7.60 (6H, m, aromatic), 7.74 (1H, m, aromatic), 7.76 (1H, dd, aromatic), 7.96−8.08 (4H, m, aromatic), 8.61 (1H, s, ArNH).

FAB-MS (NBA): *m*/*z* = 931.4 (calcd for $C_{51}H_{55}N_4O_9S_2$ $[M + H]^+$, 931.3).

4. The O^{t}Bu group on **3** (74 mg, 80 μmol) was removed by treating it with 4 N HCl/dioxane at RT for 5 hr and then with a 1/1 (v/v) mixture of TFA/anisole (10/1, v/v) and dichloromethane for 4 hr. By the general procedure for the peptide coupling reaction, the product was coupled with a hydrochloric salt of HA4M (45 mg, 118 μmol) using HATU (90 mg, 237 μmol), DIEA (109 μL, 395 μmol), and DMF (1 mL). The mixture was stirred for 15 hr at RT. The residue was purified by the methods 1 and 2 (chloroform/MeOH = 50/1, then 10/1). 20 mg (17 μmol, 21% yield) of the desired product was obtained.

^{1}H NMR ($CDCl_3$, 400 MHz): δ (ppm) 0.96 (6H, t, $(CH_3CH_2)_2N$), 1.48-1.65 (20H, m, AlaC$^\beta$, AibC$^\beta$, one of $SSCH_2CH_2CH(CH_2)_3CH_2$), 1.87 (4H, m, two of $SSCH_2CH_2CH(CH_2)_3CH_2$),

1.89, 2.42 (2H, m, $SSCH_2CH_2CH(CH_2)_3CH_2$), 2.25 (2H, m, $SSCH_2CH_2CH(CH_2)_3CH_2$), 2.93 (4H, m, $(CH_3CH_2)_2N$), 3.13 (3H m, $AspC^{\beta}$, $SSCH_2CH_2CH(CH_2)_3CH_2$), 3.52 (1H, m, $SSCH_2CH_2CH(CH_2)_3CH_2$), 3.69 (3H, s, OCH_3), 4.10 (s, 1H, $AlaC^{\alpha}$), 4.40 (s, 1H, $AlaC^{\alpha}$), 4.77 (s, 1H, $AspC^{\alpha}$), 5.63 (s, 2H, OCH_2COPh), 6.80–7.0 (m, 3H, AspNH, AlaNH), 7.14 (m, 1H, aromatic), 7.50−7.60 (m, 6H, aromatic), 7.74 (m, 1H, aromatic), 7.76 (dd, 1H, aromatic), 7.96−8.08 (m, 4H, aromatic), 8.49 (s, 1H, ArNH).

FAB-MS (NBA): m/z = 1201.5 (calcd for $C_{62}H_{73}N_8O_{13}S_2$ $[M + H]^+$, 1201.5).

5. 4 (91 mg, 75 μmol) was dissolved in a mixture of 1,4-dioxane (1.1 mL) and dichloromethane (400 μL) and a 1 N aq NaOH (151 μL) was added. The mixture was stirred at 0 °C for 2.5 hr. Dilute hydrochloric acid was added until the pH of the solution reached to 1. The solvent was removed in reduced atmosphere. The residue was washed with iPr_2O. By the general procedure for the peptide coupling reaction, the product, Boc-$(Ala\text{-}Aib)_2$-$NH_2(CH_2)_2NH_2$ (155 mg, 328 μmol), HATU (86 mg, 227 μmol), and DIEA (106 μL, 605 μmol) were reacted in DMF (1 mL) at RT for two days. The residue was purified by method 2 (MeOH) then 1.11 mg (95% yield) of the desired product was obtained.

^1H NMR ($CDCl_3$, 400 MHz): δ (ppm) 0.96 (6H, t, $(CH_3CH_2)N$), 1.18−1.39 (51H, m, $SSCH_2CH_2CH(CH_2)_3CH_2$, $AlaC^{\beta}$, $AibC^{\beta}$, Boc), 1.83, 2.39 (2H, m, $SSCH_2CH_2CH(CH_2)_3CH_2$), 2.18 (2H, m, $SSCH_2CH_2CH(CH_2)_3CH_2$) 2.90 (4H, q, $(CH_3CH_2)N$), 3.12 (2H, m, $SSCH_2CH_2CH(CH_2)_3CH_2$), 3.30−3.96 (12H, m, $SSCH_2CH_2CH(CH_2)_3CH_2$, $NH(CH_2)_2NH$, $AspC^{\beta}$, $AlaC^{\alpha}$), 4.03 (2H, m, $AlaC^{\alpha}$), 4.31 (2H, m, $AlaC^{\alpha}$), 4.68 (2H, m, $AspC^{\alpha}$), 7.20−7.30 (10H, m, NH and aromatic), 7.40−7.60 (7H, m, NH and aromatic), 7.72−7.87 (3H, m, NH and aromatic), 8.26 (1H, s, aromatic), 8.84 (1H, s, aromatic).

FAB-MS (NBA): *m*/*z* = 1559.9 (calcd for $C_{75}H_{104}N_{14}O_{17}S_2Na$ $[M + Na]^+$, 1559.7).

6. Compound **5** (110 mg, 71 μL) was dissolved in a mixture of MeOH (300 μL) and dioxane (300 μL). To the solution 1 N aq NaOH (143 μL) was added dropwise and the mixture was stirred for 1.5 days. 1 N hydrochloric acid was added to the mixture until the pH reached to 1. The solvent was then removed in reduced atmosphere. The production of the methyl group deprotected compound was checked with FAB-MS. The product was then treated with TFA/anisole (1.1 mL/0.11 mL) at 0 °C for 3 hr. The product was dried in vacuum and washed with Et_2O. The production of compound **6** was checked with FAB-MS.

SSA8=OPE. To a 50 mL RBF were added compound **6** (110 mg, 72 μL), DMF (35 mL), HATU (273 mg, 720 μmol) and HOAt (147 mg, 1.1 mmol) and the flask was charged with argon. The mixture was then cooled to 0 °C and DMF (15 mL) solution of DIEA (250 μL, 1.1 mmol) was slowly added to the mixture over 3 hr. The mixture was then stirred at RT under argon atmosphere for three days. The solvent was removed in reduced atmosphere, and the residue was purified with column chromatography (Sephadex LH-20, MeOH as eluent). Then the product was taken up with chloroform and washed with 4 wt % aq $NaHCO_3$, brine, 4 wt % aq $KHSO_4$, and brine. Then the organic layer was dried over anhydrous sodium sulfate. The product was again purified with column chromatography (Sephadex LH-20, MeOH as eluent). Finally, the product was purified with HPLC (Cosmosil Cholester, MeOH as eluent). 15 mg (15 % yield) of the desired product was obtained.

^{1}H NMR ($CDCl_3$, 400 MHz): δ (ppm) 0.96 (6H, t, $(CH_3CH_2)_2N$), 1.21−1.68 (42H, m, $AlaC^\beta$, $AibC^\beta$, $SSCH_2CH_2CH(CH_2)_3CH_2$), 1.83, 2.36 (2H, m, $SSCH_2CH_2CH(CH_2)_3CH_2$), 2.20 (2H, m, $SSCH_2CH_2CH(CH_2)_3CH_2$), 2.96 (4H, q, $(CH_3CH_2)_2N$), 3.07 (2H, m, $SSCH_2CH_2CH(CH_2)_3CH_2$), 3.25, 3.63 (2H, m, $NHCH_2CH_2NH$), 3.29−3.40 (3H, m, $AspC^\beta$,

$SSCH_2CH_2CH(CH_2)_3CH_2$), 3.84−4.00 (5H, m, $AlaC^{\alpha}$ × 3, $NH(CH_2)NH$), 4.07 (1H, m, 11 $AlaC^{\alpha}$), 4.78 (1H, s, $AspC^{\alpha}$), 6.81 (1H, s, NH), 7.14–7.16 (2H, m, NH × 2), 7.22 (1H, s, aromatic), 7.33 (1H, s, NH), 7.40–7.46 (8H, m, aromatic, NH × 4), 7.62 (1H, d, aromatic), 7.83 (2H, br, NH), 7.88 (1H, d, aromatic), 7.94 (1H, s, NH), 8.14 (2H, br, NH × 2), 8.22 (1H, s, aromatic), 8.55 (1H, s, aromatic), 8.89 (1H, s, aromatic).

FAB-MS (HR, NBA): 1404.6417 (calcd for $C_{69}H_{92}N_{14}O_{14}S_2$ M^+, 1404.6359).

AcOPE. To a test tube compound **1** (10 mg, 17 μmol), dichloromethane (2 mL), TEA (12 μL), and acetic anhydrate (5 μL) were added and the mixture was stirred for 16 hr. MeOH (500 μL) was added to the mixture and the solvent was removed in reduced atmosphere. The product was washed with Et_2O. 2.5 mg (25% yield) of the desired product was obtained. The purity was checked with HPLC (Cosmosil Cholester, chloroform/MeOH 1/1 as eluent).

^1H NMR ($CDCl_3$, 400 MHz) δ (ppm) 0.97 (6H, t, $(CH_3CH_2)_2N$), 2.21 (3H, s, $NHCOCH_3$), 2.94 (4H, $(CH_3CH_2)_2N$), 5.63 (2H, s, OCH_2COPh), 7.13 (1H, d, aromatic), 7.24 (1H, dd, aromatic) 7.51−7.54 (6H, m, aromatic), 7.65 (1H, t, aromatic), 7.75 (1H, dd, aromatic), 7.96 (1H, d, aromatic), 8.02 (1H, d, aromatic), 8.07 (1H ,d, aromatic), 8.61 (1H, d, aromatic), 8.87 (1H, s, aromatic).

FAB-MS (HR, DTT/TG): 614.2298 (calcd for $C_{37}H_{32}N_3O_6$ $[M + H]^+$, 614.2291).

Results and discussion

Absorption spectra. Absorption spectra of **SSA8=OPE** and **AcOPE** are recorded in MeOH, chloroform, DMF, and DMSO (Figure IV-2a). The absorbances of **SSA8=OPE** in all these solvents are correlated linearly with the concentrations according to the Lambert–Beer law in the range of 3.5–40 μM (Appendix, Figure A-IV-1), and the extinction coefficient is found to be 2.8×10^4 M^{-1} cm^{-1} in MeOH.

The maximum absorption wavelengths of **SSA8=OPE** (329–344 nm) are shorter than those of **AcOPE** (355–363 nm) in these solvents. **SSA8=OPE** and **AcOPE,** respectively, show a peak shift toward longer wavelength as the solvent polarity increases (a bathochromic shift).

Fluorescence and excitation spectra. Fluorescence and excitation spectra of **SSA8=OPE** are recorded in the four solvents (Figure IV-2b). The fluorescence of **SSA8=OPE** in MeOH increases the intensity linearly with the concentration up to about 32 μM (Appendix, Figure A-IV-2), indicating no aggregation of **SSA8=OPE** in this concentration range. The reference compound, **AcOPE,** also shows a medium fluorescence intensity and a linear relationship of UV absorptions with concentrations in chloroform (Figure A-IV-1), indicating that no aggregation of **AcOPE** takes place in chloroform. In contrast, fluorescence of **AcOPE** in DMF and DMSO is nearly quenched, suggesting aggregation of **AcOPE** in these solvents.

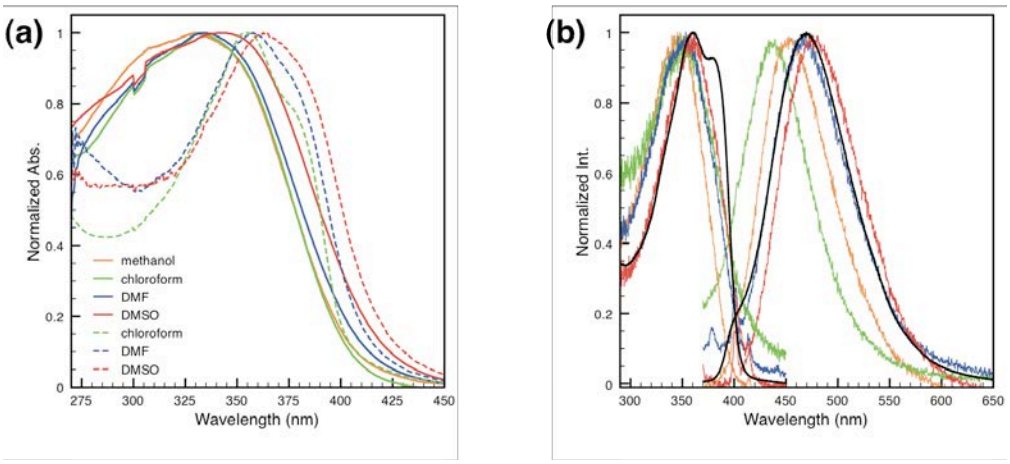

Figure IV-2. (a) Absorption spectra of **SSA8=OPE** (solid line) and **AcOPE** (dashed line) in MeOH (orange), chloroform (green), DMF (blue), and DMSO (red). (b) Fluorescence and excitation spectra of **SSA8=OPE** in MeOH (orange), chloroform (green), DMF (blue), and DMSO (red). The black lines show fluorescence and excitation spectra of **AcOPE** in chloroform.

The maximum wavelengths of fluorescence of **SSA8=OPE** are 436, 452, 465, and 476 nm in chloroform, MeOH, DMF, and DMSO, respectively. The fluorescence band of **SSA8=OPE** in chloroform is blue-shifted significantly from that of **AcOPE** (maximum at 468 nm). In contrast, the solvatochromic effect is not observed clearly in the excitation spectra of **SSA8=OPE** (maximum at 345–358 nm in these solutions). When the excitation spectra are compared between **SSA8=OPE** and **AcOPE** (maximum at 360 nm), blue-shift is not so obvious as that in florescence spectra. The Stokes shifts of 100–120 nm are observed for both compounds. This is a sharp contrast to nonsubstituted PPE/OPEs, which showed generally small Stokes shifts.[265,266,253] The florescence and excitation spectra of **SSA8=OPE** are resolved as a single Gaussian shape, indicating that only one electronic transition is involved in florescence and excitation processes. This is also true for florescence of **AcOPE**, but the excitation spectrum of **AcOPE** shows two bands, suggesting that two electronic transitions contribute to the florescence of **AcOPE**.

The quantum yield of **SSA8=OPE** is the lowest in MeOH and increases gradually in the order of DMSO < DMF < chloroform, however, much smaller than that of **AcOPE** in chloroform (Table IV-1). The quantum yield of **AcOPE** is significantly reduced when measured in DMF and DMSO because of the molecular aggregation as described before.

CD spectra. The conformation of **SSA8=OPE** in MeOH is investigated by CD

Table IV-1. Fluorescent quantum yield of **SSA8=OPE** and **AcOPE.**

	SSA8=OPE				**AcOPE**	
solvent	MeOH	chloroform	DMF	DMSO	chloroform	DMSO*
QY	0.0045	0.0168	0.0157	0.0127	0.358	0.0080

* **AcOPE** molecules associate with each other in this solution, which is suggested by an extra emission band at around 600 nm.

spectroscopy (Figure IV-3). Two negative Cotton effects are observed at 206 and 224 nm (Figure IV-3a). This double minimum pattern is assigned to α-helical structure.[250,252] The ellipticity of the largest negative peak was −18000. The α-helix content f_α is estimated to be 38% from the molar ellipticity at 222 nm.[250] The OPE moiety shows a negative Cotton effect at 357 nm and positive Cotton effects at 303 and 272 nm in CD spectrum (Figure IV-3b). These CD signals originate from a single molecule but not from chiral aggregates, because the intensities are independent of **SSA8=OPE** concentrations (Appendix, Figure A-IV-3). The absolute intensity of the Cotton effect at 303 nm after correction by absorbance increases with varying the solvent in the order of DMSO < MeOH < chloroform < DMF (Figure IV-4).

Fluorescence Lifetime. Fluorescence decay curves of **SSA8=OPE** and **AcOPE** are evaluated in chloroform, which avoids aggregation effects of these compounds, as described before (Appendix, Figure A-IV-4). The lifetimes are not determined precisely due to the fast fluorescence decay for our apparatus. However, the lifetimes of **SSA8=OPE** and **AcOPE** are similar and about 2 ns on the basis of the time required for a decrease to half

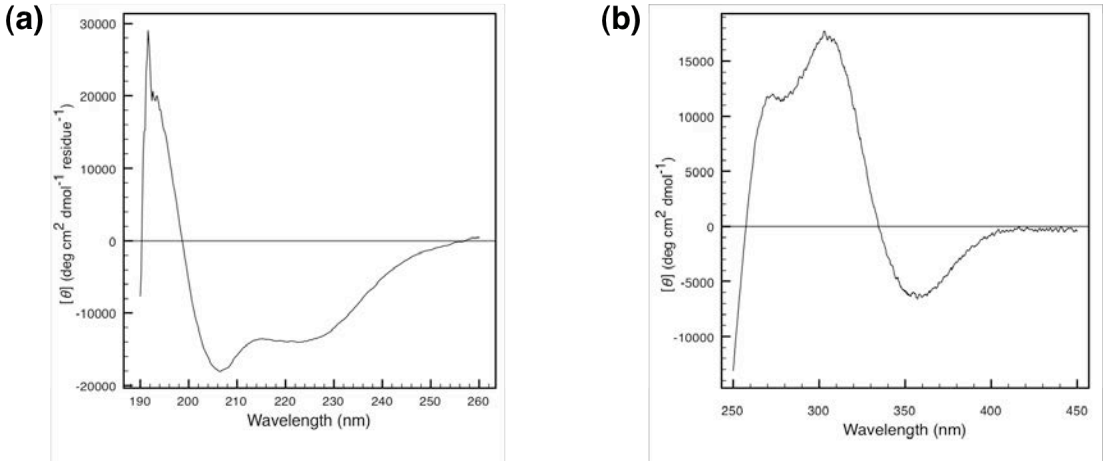

Figure IV-3. CD spectra of **SSA8=OPE** in MeOH in the range of (a) 190–260 and (b) 250–450 nm.

intensity and the pulse width of the excitation laser.

DFT Calculations. A model structure **M1,** which has the same chemical structure as **AcOPE** but the phenacyl ether is replaced by an amide, is generated and optimized. Coplanar conformation is adopted for **M1** as a representative of all conformations because the conformation should mostly contribute to the fluorescence due to extended π-conjugation. In addition to **M1**, its partial structures of the electron donor part (**Donor**) and the electron acceptor part (**Acceptor**) are also subjected to electronic structure

calculation. The orbital energy levels and spatial distributions of corresponding wave functions of HOMO − 3 to LUMO + 3 orbitals of **M1, Donor,** and **Acceptor** are illustrated in Figure IV-5. The spatial distribution of the HOMO (orbital number 126) of **M1** is nearly the same as that of the **Donor** because there are no orbitals in the **Acceptor** near the energy of the HOMO of the **Donor.** Similarly, the LUMO (orbital number 127) of **M1** is nearly the same as the **Acceptor.** The frontier orbitals are thus localized in both ends of the OPE. In contrast, the HOMO − 1 and LUMO + 1 are delocalized over the whole π-conjugate system because the energies of the HOMO − 1 of the Donor and the HOMO of the **Acceptor,** and

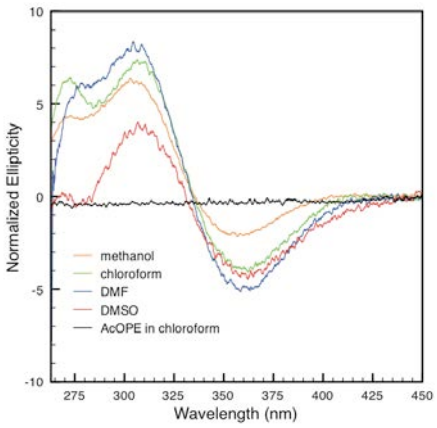

Figure IV-4. CD spcectra of **SSA8=OPE** (colored line) and **AcOPE** (black line, in chloroform.

the LUMO of the **Donor** and the LUMO + 1 of the **Acceptor** are close to each other, respectively.

The electronic transitions of **M1** with the lowest five excitation energies are listed in Table IV-2. The HOMO–LUMO transition (126 → 127) energy, which appears as a shoulder in the calculated absorption spectrum (Figure IV-6a), is by ca. 0.7 eV less than the

Table IV-2. TD-DFT calculation results on the lowest five excitation states of **M1.**

Orbital	C*	C^2*	Excitation energy (eV)	Oscillator strength
126 → 127	0.863	0.47	2.57 (481 nm)	0.84
123 → 127	0.661	0.44	3.29 (376 nm)	0.09
125 → 127	–0.187	0.03		
123 → 127	0.199	0.03	3.32 (373 nm)	0.86
125 → 127	0.603	0.36		
126 → 128	0.225	0.07		
125 → 127	–0.229	0.05	3.51 (353 nm)	0.47
126 → 128	0.613	0.37		
114 → 127	0.147	0.02	3.57 (347 nm)	0.004
120 → 127	–0.161	0.03		
121 → 127	0.644	0.41		

*The configuration interaction expansion coefficient C is normalized as the summary of C^2 is 1/2.

observed transition energy of **AcOPE** in chloroform.

The excitation energy from HOMO − 1 to LUMO transition (125 → 127), which is the main band in the calculated spectra, is also underestimated, but less prominently, by ca. 0.2 eV from the observed transition energy. As a result, the separation of the shoulder and the peak is larger in the calculated spectrum than the observed spectrum of **AcOPE.** The calculated oscillator strengths qualitatively explain the observed spectrum; the oscillator strength of the HOMO → LUMO transition is weaker than that of HOMO − 1 to LUMO transition (125 → 127).

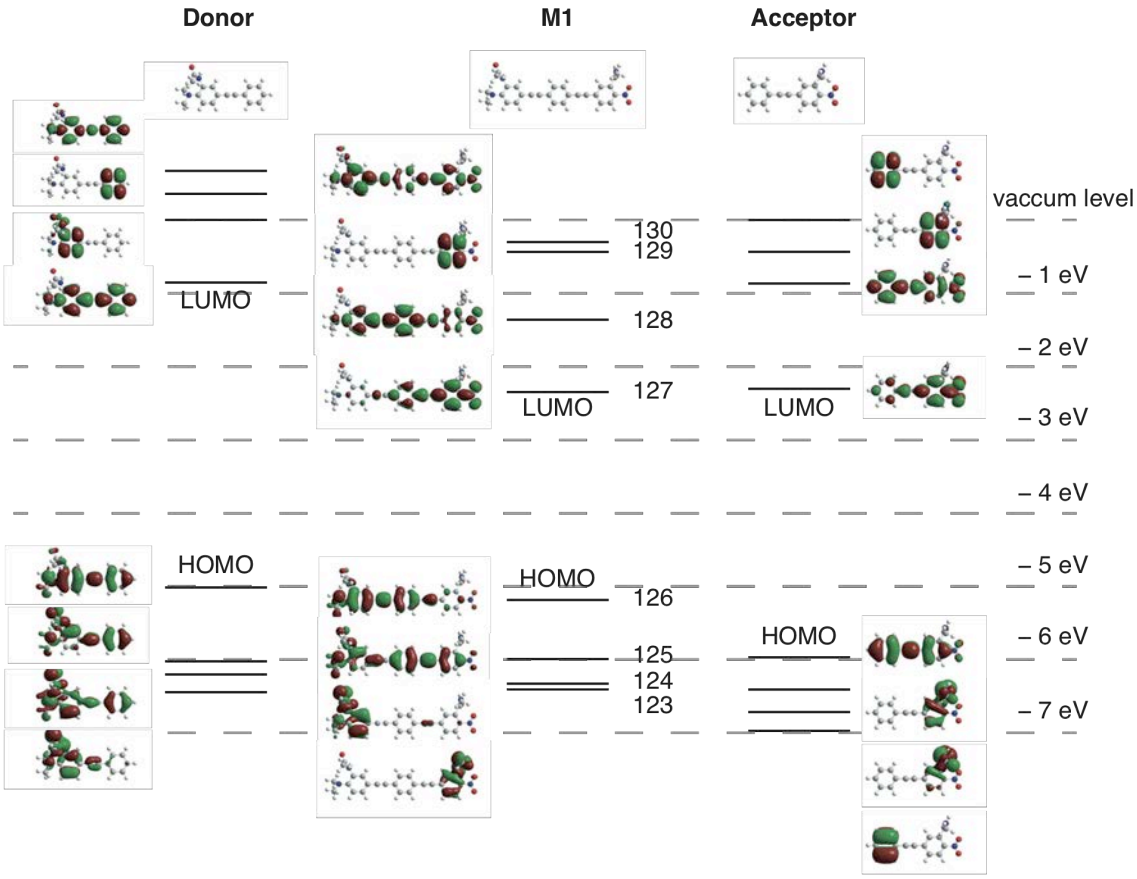

Figure IV-5. Energy level and spatial distribution of HOMO – 3 to LUMO +3 orbitals of **M1** (middle), **Donor** (left), and **Acceptor** (right) according to the DFT calculations.

Several conformations of **M1** are generated with varying the dihedral angles of adjacent phenyl rings of the optimized structure of **M1** at 15, 30, 45, 60, and 90° in a right-handed way (**R15–R90:** for example, **R45** takes a dihedral angle of 90° between the first phenyl ring and the third phenyl ring), and their optical spectra are calculated by TD-DFT (Figure IV-6). The absorption band shifts toward shorter wavelength and the shoulder diminishes with the increase of the twist in the OPE. The maximum absorption wavelength shifts from 367 nm (**M1**) to 311 nm (**R90**). The shift becomes the largest between **R45** and **R60.** The oscillator strength of the shoulder, which corresponds to the HOMO–LUMO transition, decreases dramatically from 0.84 in **M1** to 0.0003 in **R90** (Figure IV-6b). This result reveals that the twist in the main chain has a strong effect on the oscillator strength. In the twisted conformations, **R15–R60,** the absorption band with the strong oscillator strength around 350 nm is mainly composed of the HOMO to LUMO + 1 transition (126 → 128) or the HOMO − 1 to LUMO transition. **R90** has no shoulder and absorption band due to a mixture of several transitions in the region over 300 nm.

CD spectra of all the conformations with the twist in a right-handed way by TD-DFT calculations possess a negative Cotton effect at the longer wavelength and a positive one in the shorter wavelength, which agrees with the observed CD spectrum of **SSA8=OPE** in chloroform (Figure IV-4). The negative Cotton effect is assigned mainly to the HOMO–LUMO transition, HOMO − 1 to LUMO transition, and HOMO to LUMO + 1 transition in the calculations. When the phenyl rings are positioned in a left-handed way, the transitions generate a positive Cotton effect (Appendix, Figure A-IV-5). Interestingly, the Cotton effect appears even at the twist angles of 0 (**M1**) and 90° (**M90**), indicating that the amide groups on the OPE do not take coplanar orientation with the phenyl rings in the optimized structures (molecular geometries as shown in Figure IV-5). On the other hand, **R45** has the intrinsic axial chirality.

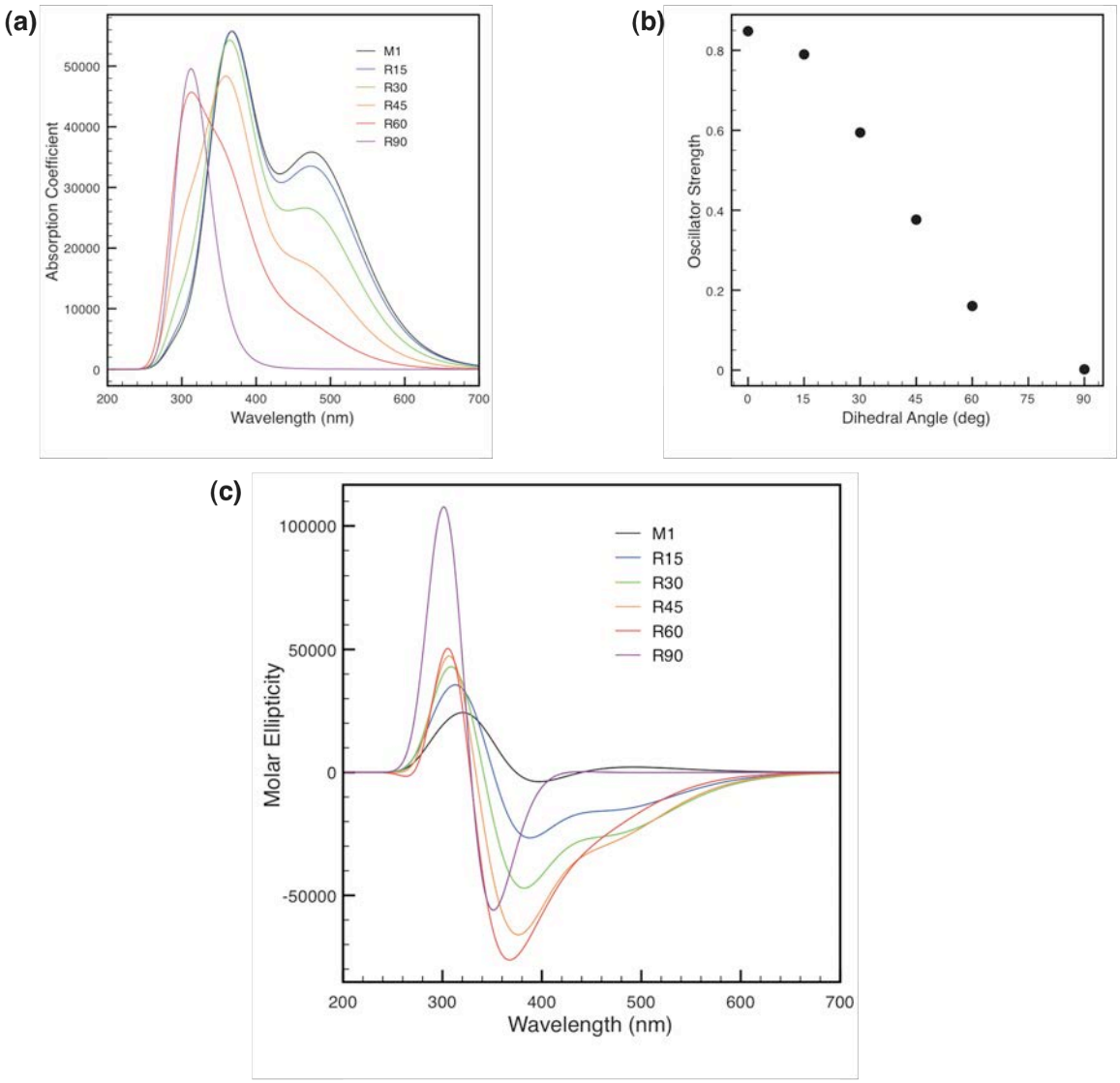

Figure IV-6. (a) Absorption spectra, (b) the oscillator strength of the HOMO–LUMO transition vs dihedral angle plot, and (c) CD spectra of **M1** and **R15–R90** obtained by the TD-DFT calculations.

Conformation of the Peptide Moiety. CD spectrum of **SSA8=OPE** in MeOH shows a double minimum pattern, which is assigned to a right-handed α-helical structure (Figure IV-3a). A previous study on the helical structure of peptide oligomers having an alternating sequence of Ala and Aib concludes that α-helical structure is prevailing when the peptide is composed of more than eight residues, while the shorter peptides favor a 3_{10}-helical structure.[69] On the other hand, Ishikawa et al.[235] reported that a nonapeptide,

(Ala-Aib)$_4$-Lys-(Ala-Aib)$_4$, takes a 3_{10}-helical structure. Further, another nonapeptide, (Ala-Aib)$_8$-Ala, is also reported to take a 3_{10}-helical structure by Yoshida et al.[267] Taken together, nonapeptides composed of multiple repeats of alternating Ala and Aib do not necessarily take an α-helical structure as the present case. Rather, we think the peptide moiety of **SSA8=OPE** takes the α-helical structure in the present case under the spatial constraint of the rigid OPE bridge between both peptide termini.

Usually, HPs are considered to reduce helical content in DMF and DMSO because these solvents are strong hydrogen bond acceptors to break the intramolecular hydrogen bonds of the α-helical structure. The conformation of the peptide moiety in DMF and DMSO cannot be evaluated directly by CD measurements. However, on the basis of the fact that the OPE moiety is shown to take a chiral conformation similarly in all the solvents examined here (Figure IV-4), the peptide moiety should keep the α-helical structure even in DMF and DMSO, meaning that this cyclic conjugate of the peptide and OPE has a rigid structure by the cyclic constraint. The peptide moiety cannot unwind the helical structure because the rigid rod-shaped OPE clamps firmly the both termini of the peptide moiety.

Oscillator Strength of HOMO–LUMO Transition. Fluorescence quantum yield of **SSA8=OPE** in chloroform is significantly lower than that of **AcOPE**. On the other hand, the fluorescence life times of **SSA8=OPE** and **AcOPE** are similar (ca. 2 ns). In chloroform, **SSA8=OPE** and **AcOPE** are molecularly dispersed under high dilution as described before, representing no molecular collision nor molecular association leading to fluorescence quench. Under these conditions, fluorescence quantum yields, fluorescence life times, the rate constants for fluorescence, k_f, and internal conversion, k_{nr}, are simply related to provide the rate constants as follows: for **SSA8=OPE,** k_f = 0.005 ns^{-1} and k_{nr} = 0.495 ns^{-1}; for **AcOPE,** k_f = 0.17 ns^{-1} and k_{nr} = 0.33 ns^{-1}.

The k_f of **SSA8=OPE** is 0.03-fold smaller than that of **AcOPE.** The small k_f and the

low quantum yield of **SSA8=OPE** suggest the small oscillator strength of the HOMO−LUMO transition because of the correlation of $k_f \approx v^2 f$,[268] where v and f are the energy gap between the ground state and the excited state and the oscillator strength of the HOMO−LUMO transition, respectively. This interpretation is consistent with the small oscillator strength of the HOMO−LUMO transition obtained by the DFT calculations. Only slight increase of k_{nr} suggests quenching effect by high concentration or clipping of peptide are not responsible for the decrease of the quantum yield, as previously reported.[269,166]

Conformation of the OPE Moiety. Even though the OPE takes multiple conformations due to the nearly free rotation of the benzene rings around the molecular axis at RT, the following discussions are subjected to the calculations on some characteristic and typical conformations, **R15–R90** and **M1,** to concisely explain the difference of the spectra of **SSA8=OPE** and **AcOPE.**

The observed CD spectra of **SSA8=OPE** (Figure IV-4) show a negative Cotton effect at 330–400 nm and a positive Cotton effect at 270–330 nm in all the solvents. This CD pattern is agreeable with the TD-DFT calculations on CD spectra of the conformations, **R15**–**R90**, with a right handed twist in the OPE (Figure IV-6c). The TD-DFT calculations on absorption spectra of conformations, **R15–R90,** are carried out (Figure IV-6a). With increase of twist in the OPE, the HOMO–LUMO transition band decreases its intensity to undetectable level, which is due to the decrease of the oscillator strength (Figure IV-6b). Taken together, **SSA8=OPE** should take the twisted form. The benzene ring at the center is still possible for free rotation, but the twisting effects are valid whatever angles the ring takes (see below for the effect of other twisted conformations on discrepancy between excitation and absorption spectra).

On the other hand, **AcOPE** should exist as a mixture of all possible conformations as no confinements are introduced. Among them, **M1** structure is the most energetically stable

conformer, which contributes mostly to the fluorescence spectrum of **AcOPE.** It is thus reasonable to represent the electronic structure of **AcOPE** with **M1** when discussing the discrepancy in optical characters between **SSA8=OPE** and **AcOPE.** With this interpretation, the shoulder around 380 nm in the absorption spectra of **AcOPE** (Figure IV-2a) is assigned to the HOMO−LUMO transition and appears at the shorter wavelength by 0.7 eV than that of the HOMO−LUMO transition band determined by the DFT calculation (Table IV-2). The strongest peaks in Figure IV-2a are assigned to HOMO to LUMO + 1 transition and HOMO − 1 to LUMO transition for **SSA8=OPE** and **AcOPE**, respectively, because these transitions possess the highest oscillator strength in the twisted form (**R15**–**R60**) and the **M1** structure, respectively.

The florescence of the two compounds in Figure IV-2b is assigned to the LUMO to HOMO transition as described before. The bathochromic shift observed in the fluorescence spectra of **SSA8=OPE** (Figure IV-2b) as well as that in absorption spectra (Figure IV-2a) are well explained by the polarized property of the excited states, as shown by localization of the LUMO orbital at the acceptor moiety (Figure IV-5).

The excitation spectra are interpretable similarly to the absorption data, where a shoulder of the HOMO−LUMO transition appears for **AcOPE** but disappears for **SSA8=OPE.** The main peak in the excitation spectra is assigned to the HOMO − 1 to LUMO or the HOMO to LUMO + 1 transition. Compared with the absorption spectra, the excitation spectra of **SSA8=OPE** show relatively weaker intensity at the shorter wavelength region (Figure IV-2). The discrepancy is explainable on the basis of the assignment of the absorption to highly twisted conformations which have low *f* leading to less contribution to fluorescence. Such discrepancy is not the case with the spectra of **AcOPE** because the dominant conformations such as **M1** are fluorescence active species.

In all the optical spectra, the peaks of **SSA8=OPE** appear at shorter wavelengths than

the corresponding peaks of **AcOPE.** The blue shifts are consistent with our interpretation that the planner conformations, which have extended π-conjugation, are excluded from the allowed conformers of **SSA8=OPE,** and twisted conformers with less electron couplings between π-orbitals[217,172] are remained in **SSA8=OPE.**

The dihedral angle of the phenyl rings at the both ends of the OPE moiety can be discussed on the basis of the fluorescence quantum yield and the intensity of Cotton effects as follows. The quantum yield in MeOH is 1/4-fold of those in the other solvents including DMF. The dielectric constants of MeOH and DMF are nearly the same (32 and 38, respectively), suggesting that the change in the conformation twist is the primary factor for the decrease of the quantum yield in MeOH. This consideration is supported by the observation that the intensities of the Cotton effects in MeOH are smaller than those in other solvents. When we consider chirality of OPE, the molecular chirality disappears at the dihedral angles of 0 and 90° between the first and the third phenyl rings because of free rotation of the second phenyl ring around the molecular axis. The conformation of the OPE at the dihedral angle of 90° is a highly twisted structure, which should give a low quantum yield because the oscillator strength is low. It is thus considered that **SSA8=OPE** should take a twisted conformation with a dihedral angle of 45–90° in MeOH. In other solvents, the dihedral angle should become smaller than that but larger than 15° for the case of the previous chapter.

Effect of Substituents of Electron Donor and Acceptor. Photophysical properties of twisted OPEs without any electron donors and acceptors have been studied in detail by Yang's group.[172,218] The latest work concluded that the optical characters of a conformer of all twisted geometry are dominated simply by the longest π-conjugate segment. The fluorescence quantum yield was explained on the basis of the torsion-induced localization of excitation and the intrachain energy transfer. However, the presence of an electron donor

and acceptor group in the current D–π–A type OPE makes the explanation different. The intramolecular electron transfer in the twisted form takes place upon photoexcitation, which should make the optical transition difficult to occur because of the poor orbital overlap due to the loss of the oscillator strength of HOMO–LUMO transition.

With the introduction of the donor and acceptor groups to OPE, fluorescence intensity changes sensitively with change in the conformation twist. The D–π–A type OPE is therefore useful as a molecular sensor, which is now under investigation.

Conclusion

A novel D–π–A system based on OPE cyclized with a nonapeptide **SSA8=OPE** as well as a D–π–A system having no peptide moiety (**AcOPE**) were synthesized. The CD spectra showed that the peptide moiety of **SSA8=OPE** takes a right-handed α-helical structure in MeOH. Due to the chirality in the peptide moiety, the dihedral angle of the phenyl rings at both ends of the OPE moiety is fixed to be 45–90° in MeOH and more than 15° in a right-handed way in the other solvents. This twist in the main chain of the OPE moiety drastically decreases the oscillator strength of the HOMO–LUMO transition, which causes the decrease in fluorescence quantum yield and the absence of the HOMO–LUMO transition band in absorption and excitation spectra. These views are supported qualitatively by DFT calculation of ground state and excited state of geometry **M1** and its derivative geometries **R15–R90**. It is therefore expected that a D–π–A system of OPE is a very sensitive sensor when the OPE part responds to the stimuli with changing the twisting angle between the phenyl ring.

PART III

Linear Conjugate of OPE and Helical Peptide

Real artist ships.

—Steve Jobs

Chapter V

Dipole Effects on Molecular and Electronic Structures in a Novel Conjugate of Oligo(phenyleneethynylene) and Helical Peptide

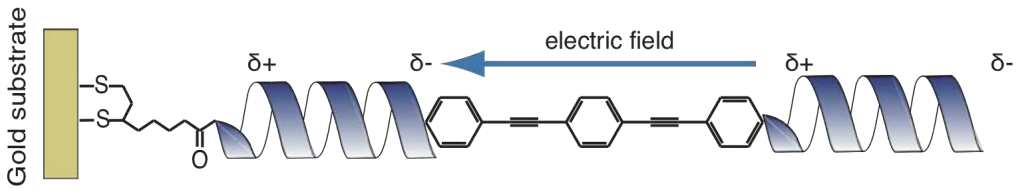

Introduction

This chapter deals with a systematic research on the external electric field effect on an OPE. This topic has been only approached by theoretical method so far. For example, Li et al. have systematically calculated the effect of electric field on polyacetylene, indicating that the HOMO–LUMO gap decreases when applying electric field along the molecular axis.[226] A similar result was obtained with OPE by Yin et al.[197] In Chapter I, the author synthesized **OPEn9** a H-character type conjugate of a HP and an OPE. The OPE moiety of **OPEn9** clearly shows a bathochromic shift due to electric field effect of the peptide dipole both in solution and in film. This is believed to be the first example of the experimental research on this issue.

In Part II, OPE and the HP were linked side by side. Since the HP generates the electric field differently between the side and the terminal of the helix, we changed the arrangement of OPE and the helix from side-by-side to a series geometry. HPs have a large

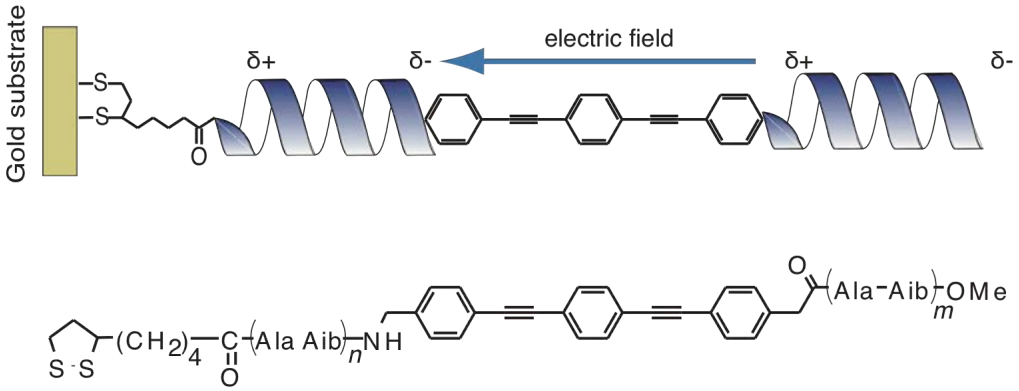

(*n*, *m*) = (0, 0), (4, 0), (8, 0), (4, 4), (8, 4), (8, 8)

Figure V-1. A schematic illustration of a SAM on a gold surface (top) and chemical structure (bottom) of HP-OPE conjugates (**2*n*OPE2*m***).

dipole along the helix axis to which direction OPE is attached as shown in Figure V-1. This linear conjugate has an advantage of forming a well-ordered SAMs on a surface due to intermolecular interaction at HP moiety. This is not the case of **OPEn9,** which forms random SAM (see Chapter I). The solvent free condition realized in SAMs is ideal for measurement of the electric field effects because dielectric constants are generally higher in solvents than in SAMs. By measuring absorption spectra of the SAMs of the conjugates with different helix lengths at one end or both ends of the OPE moiety, the effect of the electric field generated by the HPs on the electronic structure of an OPE is studied. A conjugate of 11-mercaptoundecanoic acid with OPE (**C11OPE**) is also synthesized as a reference compound. ab initio Calculations are conducted using the DFT method to obtain a thorough discussion on the electric field effect on the electronic state of the OPE moiety.

Experimental

Materials. The novel compounds consisted of HPs and OPE (**2*n*OPE2*m***) were synthesized according to Scheme V-1. A conjugate of 11-mercaptoundecanoic acid with OPE (**C11OPE**) was synthesized according to Scheme V-2. See Chapter I for the general procedures of peptide and OPE synthesis and the compound identification methods.

Spectroscopy in solution. CD spectra were measured at residue concentrations of 3–6 × 10^{-5} M with an optical cell of a 0.1 cm optical path length. Absorption spectra were recorded at a concentration of ca. 10^{-5} M. No accumulation was conducted. The emission spectra were recorded using the same solution prepared for the absorption spectroscopy. The accumulation number was eight in maximum. An optical cell of a 1 cm optical path length was used both in absorption and emission spectroscopy measurements.

Quantum calculation. Details are described in Chapter I. The optimized geometry under

no external electric field was checked by frequency analysis. It was confirmed there was no imaginary frequency number. The geometry was reoptimized under various intensities of external electric field (up to 1×10^9 V m^{-1}) along the long axis to see its effect on the energy of frontier orbitals. The direction of the electric field was parallel to the molecular axis.

Preparation of SAM. A gold substrate was prepared by vapor deposition of chromium and then gold (300 and 2000 Å for IR-RAS) and ellipsometry measurement, and 10 and 80 Å

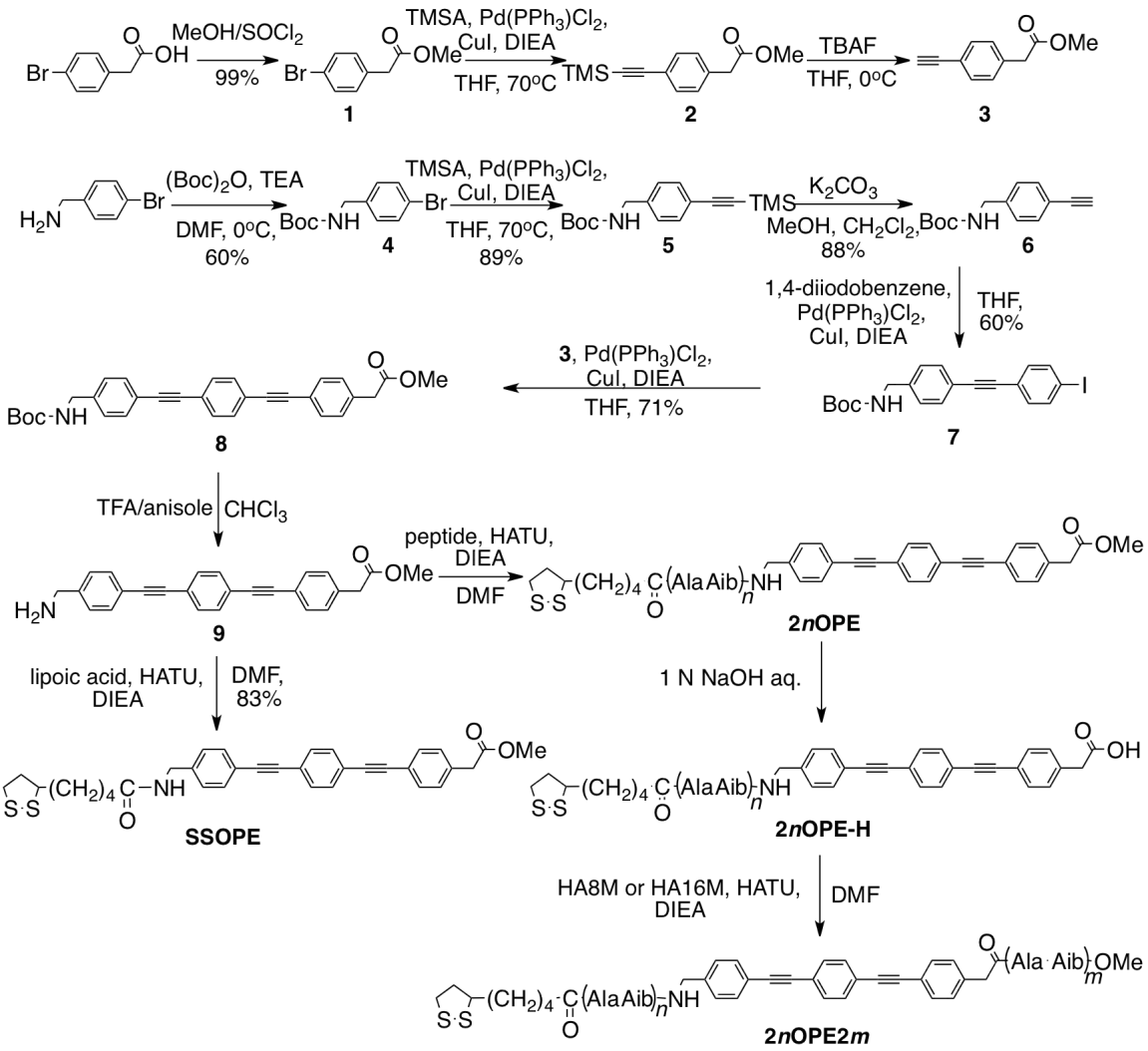

Scheme V-1. Synthetic scheme of **2*n*OPE2*m*.**

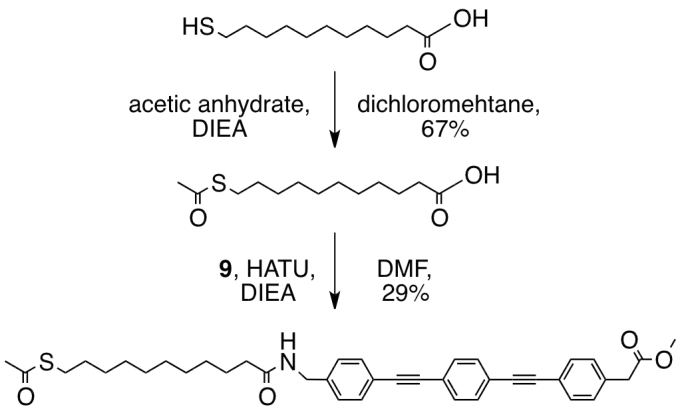

C11OPE

Scheme V-2. Synthetic scheme of **C11OPE.**

for absorption measurement, respectively) onto a slide glass or a fused quartz. The SAMs were prepared by incubating the gold substrate in an EtOH solution of the HP-OPE conjugates (0.1 mM) for 24 h. A chloroform solution (0.1 mM) was used for **C11OPE**-SAM preparation. To prepare a SAM of **16OPE16,** the incubation was carried out at 50 °C, otherwise at RT. After incubation, the substrate was rinsed thoroughly with MeOH to remove physisorbed molecules and dried under a stream of nitrogen gas and in vacuum. Chloroform was used for rinsing the SAM of **C11OPE**. For **C11OPE**-SAM, gas-phase deposition of **C12** into defects of the SAM was conducted by exposing the SAM to **C12** saturated atmosphere at 70 °C for 2 h.

Characterization and spectroscopy of the SAMs. Details of IR-RAS and ellipsometry is described in Chapter I. The relative density of the SAMs was estimated by comparison of the intensity of amide I, which was corrected to fit an assumption that all of the SAMs take tilt angle of 55°, (random orientation). The blocking experiment by CV to assess the monolayer defects was carried out in an aq $K_4[Fe(CN)_6]$ (1 mM) and KCl (1 M).

Orientation determination of the OPE moiety in SAMs. Absorption spectra of the SAMs

were recorded with a substrate sample holder attachment. Incident light was depolarized. Incident angles were changed from 0 to 50° by a step of 10°. The absorbances of the OPE moiety having a tilt angle of θ in the SAMs for *p*-polarized and *s*-polarized incident light (A_p and A_s, respectively) are described in the following equations

$$A_p = \frac{1}{2}\frac{\sin^2\theta\cos^2\phi + \cos^2\theta\sin^2\phi}{\cos\phi}, \quad \text{(V-1a)}$$

$$A_s = \frac{1}{2}\frac{\sin^2\theta}{\cos\phi} \quad \text{(V-1b)}$$

where ϕ is the effective incident angle in the SAMs, which have a relationship of the Snell's law, that is, $n_{film} \sin\phi = n_{air} \sin\phi_{exp}$ (where n_{film} and n_{air} are the refractive indices of the SAMs and air, respectively), to the equipment incident angle ϕ_{exp}. Therefore, for no-polarized incident light, the absorbance is

$$A(\theta, \phi) = A_p + A_s \quad \text{(V-2)}$$

Since the transition dipole of the π–π* absorption of OPE has the direction parallel to the molecular axis, the orientation of the OPE moiety in the SAMs is determined by plotting the area of absorption versus the incident angle and fitting the plots with the eq V-2 using the method of least-squares.

Synthesis

4-bromophenyacetic acid methyl ester (1). To a 100 mL RBF were added MeOH (30 mL) and thionyl chloride (8 mL) at 0 °C. 4-bromophenylacetic acid (2.00 g, 9.30 mmol) was then added and the mixture. The mixture was stirred at RT for two days, followed by concentration and dryid in vacuum. 2.13 g (99% yield) of the desired product was obtained as a liquid.

^{1}H NMR ($CDCl_3$, 400 MHz): δ (ppm) 3.58 (2H, s, Ar$CH_2CO_2CH_3$), 3.69 (3H, s,

$ArCH_2CO_2CH_3$), 7.15 (2H, d, phenyl), 7.45 (2H, d, phenyl).

Methyl 4-(trimetylsilylethynyl)phenylacetic acid methyl ester(2). See the general procedure for the Sonogashira coupling reaction. **1** (2.00 g, 8.73 mmol), TMSA (2.42 mL, 17.5 mmol), $Pd(II)(PPh_3)_2Cl_2$ (368 mg, 0.52 mmol), Cu(I)I (166 mg, 0.87 mmol), and DIEA (6.1 mL, 35 mmol) were reacted in THF (15 mL) at 70 °C and stirred for two days. The residue was purified by the column chromatography (chloroform/hexane = 1/2, then 1/1). The product (1.9 g) was used in the next step without further purification even though it contained some unreacted **1**.

^{1}H NMR ($CDCl_3$, 400 MHz): δ (ppm) 0.24 (9H, s, $(CH_3)_3Si$), 3.61 (2H, s, $ArCH_2CO_2CH_3$), 3.69 (3H, s, $ArCH_2CO_2CH_3$), 7.18 (2H, d, phenyl), 7.41 (2H, d, phenyl).

4-ethynylphenylacetic acid methyl ester (3). To a 100 mL RBF were added the mixture of **1** and **3** obtained above, THF (40 mL) and acetic acid (490 mL). The mixture was cooled to 0 °C and 1 M of TBAF (8.5 mL) was added dropwise. The mixture was stirred at 0 °C for 10 min and poured into water. The mixture was extracted with dichloromethane. The organic phase was washed with water (3×) and brine (2×). Then the organic phase was dried over $MgSO_4$ and dried in vacuum. A mixture of **3** and **1** was obtained as a liquid. The mixture was used in the next step without further purification.

^{1}H NMR ($CDCl_3$, 400 MHz): δ (ppm) 3.06 (1H, s, terminal alkyne), 3.61 (2H, s, $ArCH_2CO_2CH_3$), 3.69 (3H, s, $ArCH_2CO_2CH_3$), 7.22 (2H, d, phenyl), 7.43 (2H, d, phenyl).

4-((*N*-(*tert*-Butoxycarbonyl)-aminomethyl)bromobenzene (4). To a 100 mL RBF were added a hydrochloric acid salt of 4-bromobenzylamine (5.00 g, 22.5 mmol), di-*tert*-butyldicarbonate (7.36 g, 33.7 mmol), TEA (9.19 mL, 67.4 mmol), anhydrous DMF (20 mL) and water (5 mL) at 0 °C. The mixture was stirred at 0 °C for 10 min and concentrated in vacuum. The residue was purified by recrystallization from an

EtOAc/hexane system. The product (3.85 g, 60%) was obtained as a crystal.

^{1}H NMR ($CDCl_3$, 400 MHz): δ (ppm) 1.45 (9H, s, Boc), 4.26 (2H, d, ArC*H*$_2$NH), 4.84 (1H, s, ArCH$_2$N*H*), 7.15 (2H, d, phenyl), 7.44 (2H, d, phenyl).

4-(*N*-(*tert*-Butoxycarbonyl)-aminomethyl)trimethylsilylethynylbenzene (5). See the general procedure for the Sonogashira coupling reaction. **4** (2.52 g, 8.81 mmol), trimethylsilyacetylene (2.44 mL, 17.6 mmol), Pd(II)(PPh_3)$_2$$Cl_2$ (370 mg, 0.53 mmol), Cu(I)I (167 mg, 0.88 mmol), and DIEA (6.1 mL, 35 mmol) were reacted in THF (15 mL) at 80 °C for two days. The residue was purifed by column chromatography (chloroform/hexane = 1/1, then 2/1). 2.40 g (89% yield) of the desired product was obtained.

^{1}H NMR ($CDCl_3$, 400 MHz): δ (ppm) 0.24 (9H, s, $(CH_3)_3$Si), 1.45 (9H, s, Boc), 4.30 (2H, d, ArC*H*$_2$NH), 4.81 (1H, s, ArCH$_2$N*H*), 7.20 (2H, d, phenyl), 7.42 (2H, d, phenyl).

4-(*N*-(*tert*-Butoxycarbonyl)-aminomethyl)ethynylbenzene (6). To a 100 mL RBF were added **5** (2.40 g, 7.91 mmol), potassium carbonate (2.19 g, 15.82 mmol), MeOH (10 mL), and dichloromethane (10 mL). The mixture was stirred for 1.5 hr and poured into water. The product was extracted with dichloromethane and the organic layer was washed with brine. The organic layer was dried over $MgSO_4$ and dried in vacuum, yielding the product as a solid (1.62 g, 88%).

^{1}H NMR ($CDCl_3$, 400 MHz): δ (ppm) 1.46 (9H, s, Boc), 3.05 (1H, s, terminal alkyene), 4.31 (2H, d, ArC*H*$_2$NH), 4.85 (1H, s, ArCH$_2$N*H*), 7.23 (2H, d, phenyl), 7.45 (2H, d, phenyl).

4-(4′-(*N*-(*tert*-Butoxycarbonyl)-aminomethyl)phenylethynyl)iodobenzene (7). See the general procedure for the Sonogashira coupling reaction. 1,4-diiodobenzene (6.93 g, 21.0 mmol), **6** (1.62 mL, 7.00 mmol), Pd(II)(PPh_3)$_2$$Cl_2$ (294 mg, 0.42 mmol), Cu(I)I (133 mg, 0.70 mmol), DIEA (4.88 mL, 28 mmol) were reacted in THF (25 mL) at RT for one day.

The mixture was purified by column chromatography (chloroform/hexane = 2/1, then 4/1). 1.8 g (60% yield) of the desired product was obtained.

^{1}H NMR ($CDCl_3$, 400 MHz): δ (ppm) 1.46 (9H, s, Boc) 4.32 (2H, d, ArC*H*$_2$NH), 4.85 (1H, s, ArCH$_2$N*H*), 7.23 (2H, d, phenyl), 7.26 (2H, d, phenyl), 7.48 (2H, d, phenyl), 7.68 (2H, d, phenyl).

4-(4′-(4″-(*N*-(*tert*-Butoxycarbonyl)-aminomethyl)phenylethynyl)phenylethnyl)phenylacetic acid methyl ester (8). See the general procedure for the Sonogashira coupling reaction. **7** (1.80 g, 4.15 mmol), unpurified **3** (1.50g), Pd(II)$(PPh_3)_2Cl_2$ (181 mg, 0.26 mmol), Cu(I)I (82 mg, 0.43 mmol), and DIEA (3 mL, 17 mmol) were reacted in THF (20 mL) at RT for one day. The mixture was purified by column chromatography (chloroform). 1.47 g (71% yield) of the desired product was obtained.

^{1}H NMR ($CDCl_3$, 400 MHz): δ (ppm) 1.46 (9H, s, Boc) 3.65 (2H, s, ArC*H*$_2$CO), 3.71 (3H, s, OCH_3), 4.33 (2H, d, ArC*H*$_2$NH), 4.86 (1H, s, ArCH$_2$N*H*), 7.27 (4H, d, phenyl), 7.48–7.49 (8H, m, phenyl).

FAB-MS (matrix; DTT/TG) *m*/*z* = 479.24 (calcd for $C_{31}H_{29}NO_4$ M^+ 479.21).

4-(4′-(4″-(aminomethyl)phenylethynyl)phenylethnyl)phenylacetic acid methyl ester (9). To a 50 mL RBF were added **8** (700 mg, 1.46 mmol), chloroform (10 mL), TFA (7 mL), and anisole (0.7 mL) at RT. The mixture was stirred for 45 min and concentrated under reduced pressure. The residue was washed with Et_2O (3×). The TFA salt of the product was obtained as a solid with a high yield.

^{1}H NMR (MeOH-d_4, 400 MHz): δ (ppm) 3.70 (5H, s, ArC*H*$_2$CO and OCH_3), 4.15 (2H, d, ArC*H*$_2$NH), 7.31 (2H, d, phenyl), 7.49 (2H, d, phenyl), 7.53 (4H, s, phenyl), 7.62 (2H, d, phenyl).

FAB-MS (matrix; DTT/TG) *m*/*z* = 380.2 (calcd for $C_{26}H_{22}NO_2$ [M + H^+], 380.16).

8OPE. See the general procedure of the peptide coupling reaction. A TFA salt of **9** (660 mg, 1.34 mmol), SSA8H (1.95 g, 2.31 mmol), HATU (1.70 g, 4.47 mmol), and DIEA (1.21 mL, 6.92 mmol) were racted in DMF (10 mL) at RT for 10 hr and another HATU (300 mg, 0.79 mmol) and DIEA (200 μL, 1.2 mmol) were added at 0 °C. The mixture was stirred at RT for 14 hr. The mixture was purified by method 2 (chloroform/MeOH = 25/1, then 20/1). 500 mg (31% yield) of the desired product was obtained.

^{1}H NMR ($CDCl_3$, 400 MHz): δ (ppm) 1.34–1.62 (38H, m, $AlaC^{\beta}$, $AibC^{\beta}$, $SSCH_2CH_2CHCH_2C\mathit{H}_2CH_2CH_2CO$), 1.65 (4H, m, $SSCH_2CH_2CHC\mathit{H}_2CH_2C\mathit{H}_2CH_2CO$), 1.92 (1H, m, one of $SSCH_2C\mathit{H}_2CH(CH_2)_3CH_2CO$), 2.33 (2H, m, $SSCH_2CH_2CH(CH_2)_3C\mathit{H}_2CO$), 2.46 (1H, m, one of $SSCH_2C\mathit{H}_2CH(CH_2)_3CH_2CO$), 3.15 (2H, m, one of $SSC\mathit{H}_2CH_2CH(CH_2)_3CH_2CO$), 3.55 (1H, m, $SSCH_2CH_2C\mathit{H}(CH_2)_3CH_2CO$), 3.64 (s, 2H, $ArC\mathit{H}_2CO_2CH_3$), 3.71 (s, 3H, $ArCH_2CO_2C\mathit{H}_3$), 3.85 (1H, m, $AlaC^{\alpha}$), 3.95 (2H, m, $AlaC^{\alpha}$ × 2), 4.36 (2H, m, $AlaC^{\alpha}$ and one of $CONHC\mathit{H}_2Ar$), 4.58 (1H, m, one of $CONHC\mathit{H}_2Ar$), 6.34 (1H, d, amideNH), 6.58 (1H, d, amideNH), 7.28–7.53 (20H, m, amideNH and Ar), 7.78 (1H, s, amideNH).

FAB-MS (HR) (matrix: NBA) *m*/*z* = 1214.5385 (calcd for $C_{62}H_{82}N_9O_{11}S_2Na$ $[M + Na]^+$, 1214.5395).

8OPE-H. To a test tube were added **8OPE** (500 mg, 420 μmol), dioxane (1.8 mL), MeOH (1.8 mL), and 1 N aq NaOH (830 μL). The mixture was stirred at 40 °C for 30 min and at RT at 30 min. The completion of the reaction was checked by TLC. 2 N aq HCl were then added for neutralization. The mixture was concentrated under reduced pressure. The residue was taken up with chloroform and washed successively with 4% aq $KHSO_4$ (2×) and brine. The organic layer was dried over Na_2SO_4 and in vacuum.

8OPE8. See the general procedure of the peptide coupling reaction. A HCl salt of HA8M

(233 mg, 336 μmol), **8OPE-H** (220 mg, 186 μmol), HATU (107 mg, 280 μmol), and DIEA (130 μL, 746 μmol) were reacted in DMF (2.5 mL) at RT for one day and another portion of HATU (30 mg, 80 μmol) and DIEA (50 μL, 300 μmol) were added at 0 °C. The mixture was stirred at RT for 12 hr. The mixture was purified by method 3 (MeOH) and washed with Et_2O. 300 mg (88% yield) of the desired product was obtained.

^{1}H NMR (CD_3CN, 400 MHz): δ (ppm) 1.15–1.62 (78H, m, $AlaC^{\beta}$, $AibC^{\beta}$, $SSCH_2CH_2CH(CH_2)_3CH_2CO$), 1.90 (1H, m, one of $SSCH_2CH_2CH(CH_2)_3CH_2CO$), 2.28 (2H, m, $SSCH_2CH_2CH(CH_2)_3CH_2CO$), 2.42 (1H, m, one of $SSCH_2CH_2CH(CH_2)_3CH_2CO$), 3.11 (2H, m, one of $SSCH_2CH_2CH(CH_2)_3CH_2CO$), 3.55 (1H, m, $SSCH_2CH_2CH(CH_2)_3CH_2CO$), 3.58 (s, 3H, $CH_2CO_2CH_3$), 3.60 (dd, 2H, $ArCH_2CO_2CH_3$), 3.80–4.28 (8H, m, $AlaC^{\alpha}$), 4.32–4.53 (2H, m, $CONHCH_2Ar$), 7.08–7.85 (29H, m, AlaNH, AibNH, and aromatic).

FAB-MS (HR) (matrix: NBA/DTT) *m*/*z* = 1838.8976 (calcd for $C_{90}H_{129}N_{17}NaO_{19}S_2$ $[M + Na]^+$, 1838.8990).

16OPE. See the general procedure of the peptide coupling reaction. A TFA salt of **9** (100 mg, 202 μmol), SSA16H (240 mg, 163 μmol), HATU (80 mg, 228 μmol), and DIEA (85 μL, 490 μmol) were reacted in DMF (8 mL) for 16 hr. The residue was purified by method 3 (MeOH) and washed with *i*Pr_2O. 200 mg (67% yield) of the desired product was obtained.

^{1}H NMR ($CDCl_3$, 400 MHz): δ (ppm) 1.34–1.62 (78H, m, $AlaC^{\beta}$, $AibC^{\beta}$, $SSCH_2CH_2CH(CH_2)CH_2CO$), 1.92 (1H, m, one of $SSCH_2CH_2CH(CH_2)_3CH_2CO$), 2.40 (2H, m, $SSCH_2CH_2CH(CH_2)_3CH_2CO$), 2.46 (1H, m, one of $SSCH_2CH_2CH(CH_2)_3CH_2CO$), 3.15 (2H, m, $SSCH_2CH_2CH(CH_2)_3CH_2CO$), 3.55 (1H, m, $SSCH_2CH_2CH(CH_2)_3CH_2CO$), 3.64 (s, 2H, $ArCH_2CO_2CH_3$), 3.70 (s, 3H, $ArCH_2CO_2CH_3$), 3.94 (7H, m, $AlaC^{\alpha}$ × 7), 4.33–4.50 (3H, m, $AlaC^{\alpha}$ and one of $CONHCH_2Ar$) 7.29 (4H, m, amideNH and aromatic), 7.42–7.94 (23H, s, amideNH and aromatic), 8.31 (1H, s, amideNH).

FAB-MS (HR) (matrix: NBA) *m*/*z* = 1838.8962 (calcd for $C_{90}H_{129}N_{17}O_{19}S_2Na$ $[M + Na]^+$, 1838.8990).

16OPE-H. To a test tube were added **16OPE** (100 mg, 55 μmol), dioxane (220 μL), MeOH (300 μL), and 1 N aq NaOH (110 μL). The mixture was stirred at 40–45 °C for 7.5 hr. 2 N HClaq were then added for neutralization. The mixture was concentrated in reduced pressure and dried in vacuum. The residue was used in the next step without further purification.

16OPE8. See the general procedure of the peptide coupling reaction. A HCl salt of HA16M (58 mg, 83 μmol), **16OPE-H** (100 mg, 56 μmol), HATU (32 mg, 83 μmol), and DIEA (34 μL, 194 μmol) were reacted in DMF (1.5 mL) for one day. The residue was purified by method 3 (MeOH) and washed with Et_2O. 70 mg (51% yield) of the desired product.

^{1}H NMR (MeOH-d_4, 400 MHz): δ (ppm) 1.21–1.72 (114H, m, $AlaC^{\beta}$, $AibC^{\beta}$, $SSCH_2CH_2CH(CH_2)_3CH_2CO$), 1.90 (1H, m, one of $SSCH_2CH_2CH(CH_2)_3CH_2CO$), 2.34 (2H, m, $SSCH_2CH_2CH(CH_2)_3CH_2CO$), 2.47 (1H, m, one of $SSCH_2CH_2CH(CH_2)_3CH_2CO$), 3.57–3.70 (6H, m, $SSCH_2CH_2CH(CH_2)_3CH_2CO$, $CH_2CO_2CH_3$, $ArCH_2CO_2CH_3$), 3.93–4.24 (12H, m, $AlaC^{\alpha}$), 4.39–4.52 (2H, m, $CONHCH_2Ar$), 7.34–7.51 (12H, m, aromatic). FAB-MS (HR) (matrix: NBA) *m*/*z* = 2463.2527 (calcd for $C_{118}H_{177}N_{25}O_{27}S_2Na$ $[M + Na^+]$, 2463.2585).

16OPE16. See the general procedure of the peptide coupling reaction. **16OPE-H** (75 mg, 41 μmol), a hydrochloric acid salt of HA16M (86 mg, 62 μmol), HTAU (24 mg, 62 μmol), HOAt (11 mg, 81 μmol), and DIEA (25 mL, 145 μmol) were reacted in DMF (1 mL) at RT for two days. The mixture was purified by method 3 (MeOH). 60 mg (47% yield) of the desired product was obtained.

^{1}H NMR (MeOH-d_4, 400 MHz): δ (ppm) 1.0–1.7 (150H, m, $AlaC^{\beta}$, $AibC^{\beta}$,

$SSCH_2CH_2CH(CH_2)_3CH_2CO$), 1.90 (1H, m, one of $SSCH_2CH_2CH(CH_2)_3CH_2CO$), 2.35 (2H, m, $SSCH_2CH_2CH(CH_2)_3CH_2CO$), 2.46 (1H, m, one of $SSCH_2CH_2CH(CH_2)_3CH_2CO$), 3.15 (2H, m, $SSCH_2CH_2CH(CH_2)_3CH_2CO$), 3.5–3.7 (6H, m, $SSCH_2CH_2CH(CH_2)_3CH_2CO$, $COOCH_3$, $ArCH_2CONH$), 3.9–4.2 (18H, m, $AlaC^{\alpha}$, $NHCH_2Ar$), 7.3–7.6 (12H, aromatic).

FAB-MS *m*/*z* = 3088.6 (calcd for $C_{146}H_{225}N_{33}O_{35}S_2Na$ $[M + Na]^+$, 3087.6).

***S*-acetyl-11-mercaptoundecanoic acid.** To a 20 mL RBF were added 11-mercaptoundecanoic acid (200 mg, 915 μmol), acetic anhydrate (255 μL, 2.75 mmol), DIEA (479 μL, 2.75 mmol) and dichloromethane (2 mL) at 0 °C. The mixture was stirred for 7 hr and poured into 4% aq $KHSO_4$ The organic layer was washed with the acidic solution (3×) and brine. The organic layer was dried over Na_2SO_4 and concentrated under reduced pressure. The residue was purified by column chromatography (silica gel, chloroform/MeOH/acetic acid = 200/5/3). 160 mg (67% yield) of the desired product was obtained.

^{1}H NMR ($CDCl_3$ 400 MHz): δ (ppm) 1.27 (12H, br, aliphatic), 1.54–1.67 (4H, m, aliphatic) 2.31 (3H, s, OCH_3), 2.44 (2H, t, aliphatic), 2.86 (2H, t, aliphatic).

C11OPE. See the general procedure of the peptide coupling reaction. *S*-acetyl-11-mercaptoundecanoic acid (53 mg, 200 μmol), a TFA salt of **9** (38 mg, 76 μmol), HATU (106 mg, 303 μmol), and DIEA (88 μL, 506 μmol) were reacted in DMF (600 mL) at RT for 4 hr and MeOH was added to the mixture. The precipitate was collected using a centrifuge. The precipitate was washed with MeOH (3×). The precipitate was purified by method 2 (chloroform/EtOAc = 4/1). Re-precipitation from chloroform/hexane gave the product as a solid (10 mg, 20%).

^{1}H NMR ($CDCl_3$ 400 MHz): δ (ppm) 1.27 (12H, br, aliphatic), 1.54–1.67 (4H, m, aliphatic) 2.22 (2H, t, aliphatic), 2.31 (3H, s, OCH_3), 2.86 (2H, t, aliphatic), 3.62 (2H, s,

ArC*H*$_2$COOCH$_3$), 3.68 (3H, s, COOCH$_3$), 4.44 (CONHC*H*$_2$Ar), 7.26 (4H, m, aromatic), 7.47 (8H, m, aromatic).

FAB-MS *m*/*z* = 622.5 (calcd for $C_{39}H_{44}NO_4S$ $[M + H]^+$ 622.3).

Results and discussion

CD spectroscopy. CD spectra were recorded in a MeOH solution (Figure V-2). **8OPE,** which has a 8 mer peptide moiety, shows a sharp negative Cotton effect at 203 nm and a broad shoulder at 224 nm. This pattern is typical for right-handed 3_{10}-helical conformation as previously reported.[106,158] **16OPE** shows a negative Cotton effect of a double-minimum pattern (peaks at 208 and 222 nm), indicating an α-helical structure in accordance with the previous reports.[250,252] These results suggest that the attachment of an OPE moiety to the C terminal of a helix does not influence its helical structure. In contrast, the ellipticity per residue of **8OPE8** or **16OPE16** becomes smaller than **8OPE** or **16OPE**, suggesting that OPE at the N terminal may destabilize the helical structure. The reason remains to be solved

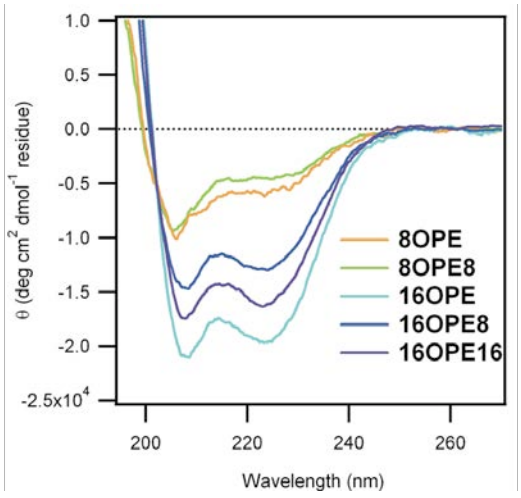

Figure V-2. CD spectra of HP-OPE conjugates in MeOH.

out.

Absorption and fluorescence measurements in chloroform solution. Absorption and emission spectra of the OPEs were recorded in chloroform (Figure V-3). All of the absorption spectra show well-resolved vibrational bands, which is typical for OPEs with a few substituents.[216,253,254] No aggregation band is observed in all the absorption spectra, and λ_{max} of these compounds are observed in a small range from 325.5 to 326.8 nm. On the other hand, the emission spectra differ significantly among the conjugates, as the fluoresence intensity longer than 380 nm becomes stronger with the increase of the total number of the residues (from above to bottom in Figure V-3). These emissions are assigned to excimer because the profiles of the excitation spectra are the same as those of the absorption spectra. Since the excimer formation is promoted in the longer peptides, association of the peptide moieties in solution should be involved in the excimer formation probably due to the D–D interaction. However, the association is fragile, because the emission around 450 nm in **16OPE16** was decreased by shaking the solution.

Quantum calculation. The effect of electric field on the electronic structure of OPE is evaluated by ab initio calculations. *p*-Di(*p*-methylphenylethynyl)benzene was selected as the model compound. The HOMO–LUMO gap of the model compound decreases in a quadratic manner with the increase of intensity of electric field (Figure V-4). This quadratic relationship is consistent with the previous calculation on polyacetylenes by Li et al. using the Hartree-Fock method with a basis set of 6-31G*.[226] The electric field of 1×10^9 V m^{-1} induces dipole of 4 D in the OPE moiety. It should be pointed out that this quadratic relationship is also applicable for π-conjugates without substituents. Generally, the HOMO–LUMO gap of OPEs having a push-pull substituent pair decreases linearly with the increase of the intensity of electric field. For example, the author has reported the HOMO–LUMO gap of OPE with a nitro group at the end and an acetoamide group at the

center decreases linearly with the increase of the intensity of electric field when the electric field directs to assist the polarization along the push-pull axis (see Chapter I). This linear relationship is also predicted by Yin et al. for OPE connected with clusters of gold using the DFT with a basis set of LANL2DZ.[197] OPEs with substituents are more susceptible to electric field than OPE alone. Indeed, our calculations show that the HOMO–LUMO gap decreases by 0.2 eV for OPE alone but by 0.5 eV for the OPE with nitro and acetoamide groups under applying electric field of 1×10^9 V m^{-1}. In the present study, we chose OPE without substituents and designed the OPE moiety isolated from the peptide moiety with an intervening methylene linker, just because our objective is to evaluate the electric field effect on the electronic structure of nonpolarized OPE.

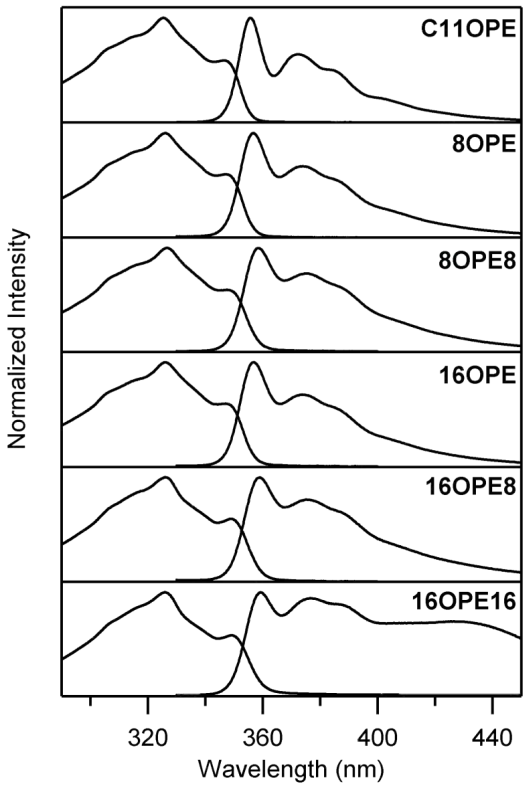

Figure V-3. Normalized absorption and fluorescence spectra of the OPE derivatives.

Blocking evaluation of SAMs by CV. The molecular packing of the SAMs on a gold surface were examined by blocking experiments using CV in aq $K_4[Fe(CN)_6]$ (1 mM) and KCl (1 M) at a scan rate of 0.1 V s^{-1} (Figure V-5). All the SAMs, including the SAM of **C11OPE** and **C12** (**C12/C11OPE**), show small redox peaks of ferricyanide/ferrocyanide, indicating that the SAMs have small defects.[158,270,271] The **C11OPE** SAM contained many defects, but the quality of the SAM was improved by exposure to an atmosphere of saturated **C12**.[271]

Spectroscopic evaluation of SAMs. IR-RAS measurements of the conjugate SAMs on a gold surface were carried out to determine the molecular tilt angles and their surface densities (Figure V-6). The obtained tilt angles and densities are summarized in Table V-1. Amide I and II bands appear around 1680 cm^{-1} and 1540 cm^{-1}, respectively. In the **C12/C11OPE** SAM, amide II band at 1550 cm^{-1} is observed, but amide I band is faint, suggesting that C=O bond of **C11OPE** should take an orientation parallel to the gold surface due to intermolecular hydrogen bonds as reported in the SAMs of amide group containing alkanethiols.[272–274] A sharp band at 1520 cm^{-1} is assigned to the stretching mode

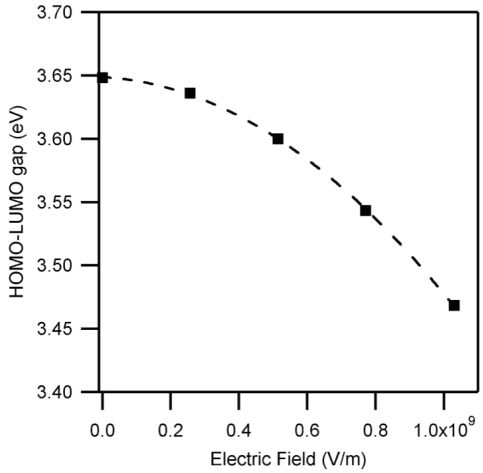

Figure V-4. Computed value of the HOMO–LUMO gap of *p*-di(*p*-methylphenyleneethynyl)benzene under several strength of electric fields.

of the OPE moiety.[275,276] The tilt angles from the surface normal of the HP moieties in the SAMs are ca. 55° in the **8OPE** and **8OPE8** SAMs, and ca. 35° in the **16OPE, 16OPE8,** and **16OPE16** SAMs (Table V-1).

The tilt angles of the OPE moieties in the SAMs are calculated from the absorption spectra obtained with varying incident angles. By fitting the data with eq V-2, the OPE moieties in the SAMs of the six HP-OPE conjugates are revealed to take tilt angles in the range of 55–70°. These larger tilt angles than those of the helical moieties can be explained

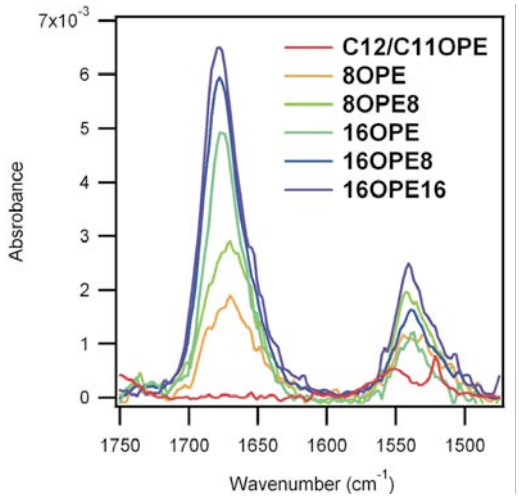

Figure V-5. Blocking experiments by CV measurements.

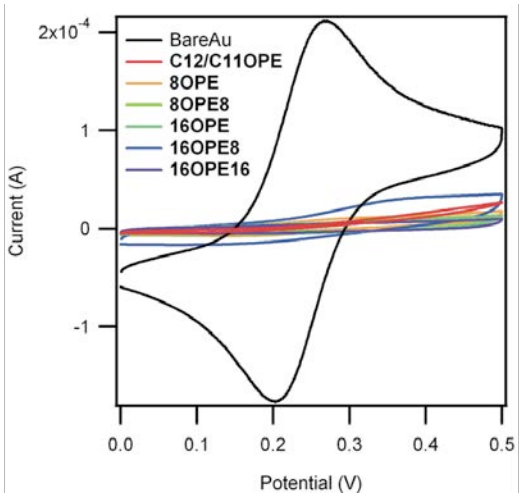

Figure V-6. IR-RAS spectra of the SAMs on a gold surface.

in two ways. The OPE moieties may overlap partially with large tilting to obtain stabilization energy due to the intermolecular van der Waals interaction and π–π stacking, even though they are separated more than 1 nm by α-HPs.[188,270] Another explanation may be head-to-tail association of the OPE moieties with taking near to horizontal orientation due to the polarized OPEs by electric field of α-HPs.

The relative molecular densities of the SAMs are also determined from IR spectra with taking the density of the **16OPE** SAM as a reference (Table V-1). The densities of the **8OPE** and **8OPE8** SAMs are 1.24- and 1.14-fold higher than that of the **16OPE** SAM, respectively, probably because of taking different types of helices between the 8mer and 16mer peptides, 3_{10}- (diameter of 0.8 nm) and α-helices (diameter of 1.1 nm), respectively. On the other hand, the densities of the **16OPE8** and **16OPE16** SAMs are lower than that of the **16OPE** SAM, even though they take an α-helical structure similarly. This observation is explainable from the bent conformation in the middle part of **16OPE8** and **16OPE16** in the SAMs, as shown that the OPE moiety tilts largely from the surface normal by 55–65°, whereas the average tilt angle of two helix moieties keeps ca. 35°. The molecular packing in

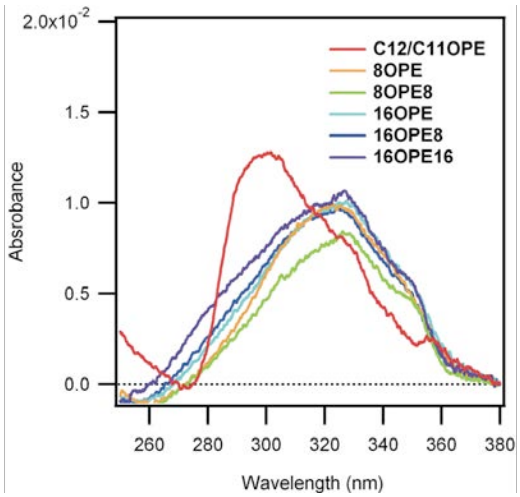

Figure V-7. Absorption spectra of the SAMs at an incident angle of 0° from the surface normal.

the **16OPE8** and **16OPE16** SAMs are therefore loose. This interpretation is consistent with the observation that the thicknesses of the **16OPE8** SAM of 34.0 Å and the **16OPE16** SAM of 39.6 Å increased just by 1.5 and 7.1 Å from that of the **16OPE** SAM, 32.5 Å (Table V-1), despite of connection of the 8mer and 16mer peptides, respectively, to **16OPE.**

Absorption spectra of the SAMs recorded with an incident angle of 0° from the surface normal are shown in Figure V-7. λ_{max} values of the spectra are summarized in Table V-1. λ_{max} values of the conjugate SAMs in a range from 323.1 to 327.0 nm are shifted significantly to longer wavelengths than that of the **C12/C11OPE** SAM at 300.7 nm. The electric field in the SAM generated by the peptide dipole is considered to influence the electronic structure of the OPE moiety as predicted by the DFT calculation described above. In the calculation, the HOMO–LUMO gap of the OPE moiety quadratically decreased with the increase of the electric field intensity (Figure V-4). The observed bathochromic shifts correspond to ca. 0.3 eV decrease of the HOMO–LUMO gap, which is theoretically explained by applying an

Table V-1. Summary of characterization results of the SAMs.

SAM	thickness (Å)[a]	helix tilit angle (°)[b]	relative density[c]	OPE λ_{max} (nm)	Energy (eV)
C12/C11OPE	29.8 ± 0.6	N/A	N/A	300.7 ± 0.7	4.11
8OPE	18.4 ± 0.8	55 ± 2.5	1.24	323.1 ± 1.6	3.82
8OPE8	25.3 ± 0.5	(60 ± 2.9)[d]	1.14	326.0 ± 0.1	3.79
16OPE	32.5 ± 2.3	32 ± 1.7	1	327.0 ± 0.6	3.78
16OPE8	34.0 ± 1.3	(35 ± 0.3)[d]	0.84	324.8 ± 0.0	3.81
16OPE16[e]	39.6 ± 0.5	(35 ± 0.1)[d]	0.85	326.7 ± 0.1	3.78

(a) measured by ellipsometory, (b) calculated from IR absorbance of amide I and II, (c) calculated from IR absorbance of amide I, (d) apparent mean value of the two helices, (e) prepared at 50 °C.

electric field of ca. 1.4×10^9 V m^{-1} to the OPE.

The 3_{10}-helical structure of the 8mer peptide generates dipole of 20 D, which means that partial charges of 1.06×10^{-19} C are separated by the helix length of 16 Å. The susceptible intensity of the electric field at the center of the OPE moiety (19 Å), which is connected to the 8mer peptide, is calculated to be 2×10^9 V m^{-1} according to the Coulomb's law (Figure V-8 top), which is in a good agreement with ca. 1.4×10^9 V m^{-1} obtained above.

This discussion is based on comparison of the conjugates with **C11OPE**, which is used as a reference compound for sensing the environmental change around the OPE moiety. This is because λ_{max} is well-known to change with the environmental change from solution to the SAM. Indeed, λ_{max} of **C11OPE** at 300.7 nm shifted significantly from that at 320 nm in chloroform.

Large hypsochromic shifts in absorption band of OPE derivatives in the SAM on a gold surface[277,278] and Langmuir–Blodgett monolayer[189,279–281] have been reported and

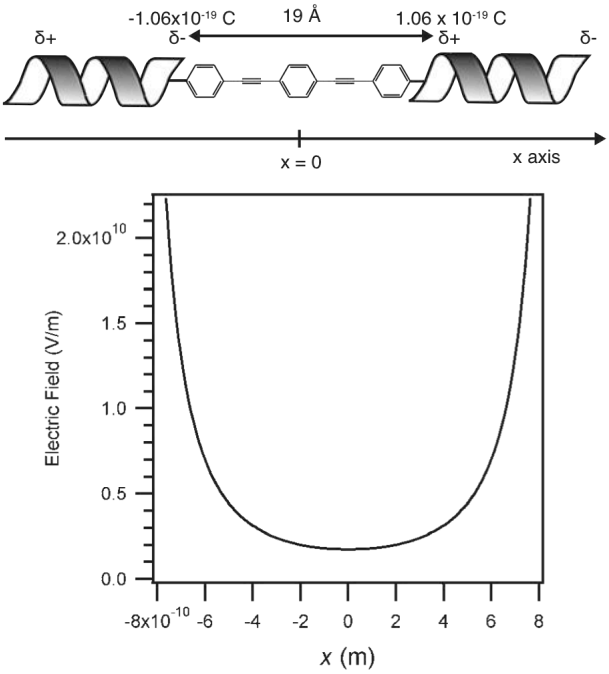

Figure V-8. Magnitude of electric field on the OPE in a simplified model.

explained by the exciton coupling of transition dipoles (H-aggregation). Generally, exciton coupling of two coplanar inclined transition dipole is described as

$$\Delta E = \frac{2|\mathbf{M}|}{r^3}\left(1 - \cos^2 \alpha\right) \qquad \text{(V-3)}$$

where ΔE is a exciton band splitting, **M** is a transition moment, r is the distance between the transition dipoles, and α is the angle between polarization axes and the line of dipole centers.[282] In the present SAMs, the molecular orientation of the OPE moiety was ca. 50°, which results in a negative value in ΔE, a bathochromic shift, according to the eq V-3. Furthermore, the absorption spectrum of the OPE moiety in the SAM of **C12/C11OPE** was unchanged by dilution of **C11OPE** with the addition of **C12** (Figure V-9), which denies the presence of intermolecular interaction between the OPE moieties in the SAM. We therefore concluded that the large hypsochromic shift in our experiment is not due to the exciton coupling but due to the environmental changes such as desolvation in the SAM leading to the absence of stabilization by solvation to the excited state of the π-conjugate.

In the **C11OPE** SAM, a minor fraction of OPE moieties takes a face-to-face stacking as indicated by a weak absorption around 355 nm with a following tailing (Figure V-7).

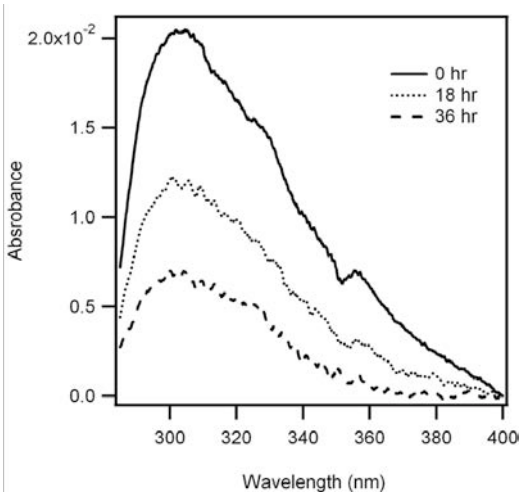

Figure V-9. Absorption spectra of the SAM of **C11OPE** on a gold surface under 0–36 h of of immersion in 1 mM chloroform solution of dodecanethiol at 60 °C.

This shift is ascribed to aggregation due to the π–π stacking among the OPE moieties, which is often observed for OPEs and PPEs in their solid phase.[171,217,244,259,283]

The λ_{max} values of the **16OPE8** and **16OPE16** SAMs are comparable with that of the **16OPE** SAM despite the presence of the additional helix moiety in the conjugate. The additional helix effect is not clearly observed probably because of the low molecular densities and poor orientation of the peptides in these **16OPE8** and **16OPE16** SAMs.

Conclusion

Novel conjugates of OPE with HPs were synthesized and their SAMs on a gold surface were characterized to experimentally demonstrate the effect of electric field on the electronic structure of the π-conjugate system. The HP moieties take 3_{10}-helical structure (for 8mer) or α-helical structure (for 16mer), which is confirmed by CD spectroscopy in MeOH solutions. The characterizations of the SAMs by IR-RAS, ellipsometry, and blocking experiment show that the SAMs of **16OPE, 16OPE8,** and **16OPE16** have a vertical orientation of the peptide moieties while **8OPE** and **8OPE8** a random orientation. The OPE moiety takes tilt angle of 55–70°. Absorption spectra of the SAMs show that the λ_{max} of the OPE moiety in the SAMs of HP-OPE conjugates is longer than that of **C11OPE,** a conjugate of 11-mercaptotundecanoic acid and the OPE moiety, by ca. 25 nm. DFT calculations show that the HOMO–LUMO gap of an OPE decreases as electric field along the molecular axis is applied and the ca. 25 nm of bathochromic shift in the absorption corresponds to the effect of an electric field of 1.4×10^9 V m^{-1}. This value of the electric field agrees with the value obtained from a simple point charge model using the Coulomb's law. Other factors leading to a bathochromic shift of the absorption spectra such as planarization of the OPE moiety are not plausible in the present case. It is therefore concluded that the bathochromic shift in the absorption spectra of the SAMs of the

conjugate is due to the effect of the electric field originated from HP moieties.

Chapter VI

Oligo(phenyleneethynylene) as a Molecular Lead for STM Measurement of Single Molecule Conductance of a helical peptide

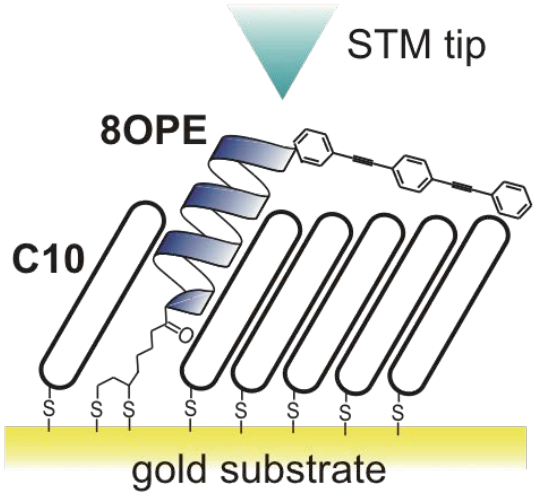

Introduction

This chapter introduces a novel application of an OPE on molecular conductance. The conjugate used is **8OPE,** a compound synthesized in Chapter V. Kimura's group have reported on the molecular conductance of various HPs measured with the latter method. HPs showed asymmetric profiles in the *I*–*V* curves.[162,163,228] However, there is one drawback in this method, which is the presence of a gap between the molecule and the STM tip. The asymmetric contact in a metal–molecule–metal junction is reported to contribute to an asymmetric profile in the *I*–*V* curve.[194,284] To eliminate the asymmetric effect of the measurement configuration, we proposed to attach a gold nanoparticle as a molecular terminal to the peptide end to confirm the intrinsic molecular rectification behavior of the HPs.[162] The asymmetric profiles of HPs are due to the dipole effect on the molecular conduction, where a large dipole moment along the helix should influence on the current oppositely on the direction through the HPs. The STS method has an advantage compared

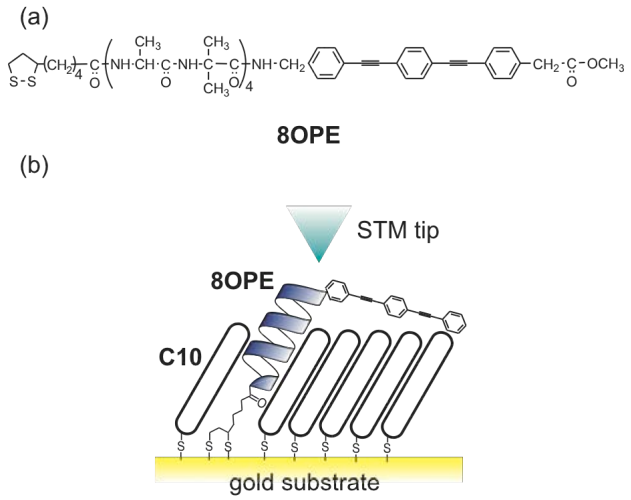

Figure VI-1. (a) Chemical structure of **8OPE**. (b) Schematic representation of STM observation of a mixed SAM of **8OPE** and **C10** (**8OPE/C10**).

with the break junction method for the asymmetric molecules, because molecules can be immobilised directionally on electrode. In the case of the gold nanoparticle method, however, it is necessary for the molecule to have thiol groups at both terminals with different protecting groups, which requires cumbersome synthetic procedures. Instead of using a gold nanoparticle as a molecular terminal, the author proposes here a molecular lead of a conjugate molecule attached to the HP end. As a result, the author found out the tip position effect on the molecular conductance.

8OPE is selected because the length of the HP moiety is compatible for insertion into **C10** (Figrue VI-1b). **16OPE** in 1-hexadecanethiol conducts too little current for reliable STS measurements. Since the OPE moiety is rich in π-electrons, the molecule–tip coupling should become strong when the STM tip is positioned very close to the molecular terminal. When this is the case, the molecule–electrode coupling is tunable by changing the gap distance between the molecule and the STM tip that can be controlled with varying the set current.

To verify this hypothesis, **8OPE** was inserted into a SAM of **C10** on a gold substrate (**8OPE/C10**, Figure VI-1b). The peptide in the alkanethiol SAM system is chosen, because a single helix or a bundle of helices are observable by STM measurements under this condition.[162,228,229] Further, the peptide moiety is buried in the **C10** SAM and the OPE moiety is exposed over the SAM as a molecular lead to be accessible with the STM tip where the molecular length of **C10** is ca. 15 Å and that of 3_{10}-helix of the octapeptide having lipoic acid at the N-terminus is ca. 24 Å.[158]

Experimental

Materials. 8OPE was synthesized as described in Chapter V. The other reagents are used as purchased.

SAM preparation. A gold substrate was prepared by vapor deposition of gold on a mica substrate. The SAM of **C10** was prepared by incubation of the gold substrate in a 3 mM EtOH solution of **C10** for 24 h. The **C10**-SAM coated substrate was rinsed thoroughly with EtOH and dried with a blow of nitrogen. The substrate was then immersed into a 0.1 mM chloroform/EtOH (1/1, v/v) solution of **8OPE** for 24 h, followed by thorough rinsing with chloroform/EtOH (1/1, v/v) and EtOH, and drying with a nitrogen blow. The obtained sample (**8OPE/C10**) was stored under high vacuum (10^{-8} Pa).

STM measurement. The STM measurements were performed under high vacuum (10^{-8} Pa) at RT. All images were obtained in the constant current mode and recorded at high impedances (50 GΩ or higher). An electrochemically polished tungsten was used as the STM tip.

Fitting with the Simmons equation. The Simmons equation is expressed as

$$I = \frac{Ce}{4\pi^2\hbar d^2}\left\{\left(\phi - \frac{eV}{2}\right)\exp\left[-\frac{2(2m)^{1/2}}{\hbar}\alpha\left(\phi - \frac{eV}{2}\right)^{1/2} d\right] - \left(\phi + \frac{eV}{2}\right)\exp\left[-\frac{2(2m)^{1/2}}{\hbar}\alpha\left(\phi + \frac{eV}{2}\right)^{1/2} d\right]\right\}, \quad \text{(VI-1)}$$

where e is the charge of an electron, $\hbar$ is Planck's constant divided by 2π, d is the tunneling distance, ϕ is the barrier height, V is the applied bias, and m is the mass of an electron. C is the proportionality constant. α is a unitless adjustable parameter used in the fitting [140,144,145]. Fittings were applied to the ±1.0 V region. By using this equation, nonlinear least-squares fitting was performed to fit eq VI-1 to the experimental results with four parameters, d, ϕ, α and C. At low bias, eq VI-1 can be approximated as

$$I = \frac{C(2m\phi)^{1/2}}{h^2 d}\alpha V \exp\left[-\frac{2(2m)^{1/2}}{\hbar}\alpha(\phi)^{1/2} d\right] \quad \text{(VI-2)}$$

The right term in this equation is not a exponential function strictly with *d*. Considering, however, that the exponential factor dominates in the equation, eq VI-2 can be regarded as $I \approx \exp(-\beta d)$ with

$$\beta = \frac{2(2m)^{1/2}}{\hbar}\alpha(\phi)^{1/2} \qquad \text{(VI-3)}$$

where β is the structure dependent attenuation factor. Thus, β values can be calculated by using ϕ and α values obtained from the fitting.

Results and discussion

STM images. A STM image of **8OPE/C10** is shown in Figure VI-2a, where pit structures of **C10**-SAM are observed as dark spots with a diameter of ca. 100 Å. Bright spots having heights of 5–10 Å (based on the STM image) over the **C10** matrix were also observed. The physical height of the spots was inaccessible since the imaged height is influenced not only by the physical height itself but also by local density of sates (LDOS).

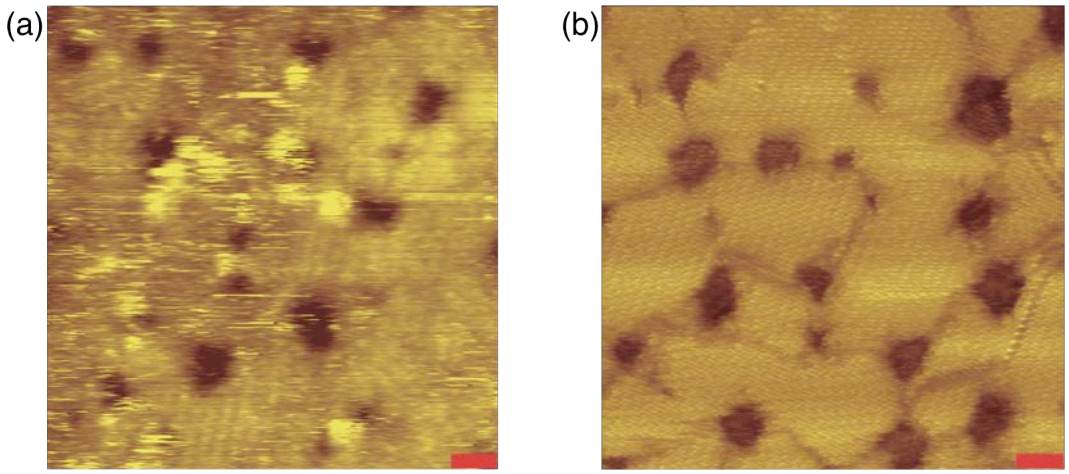

Figure VI-2. STM images of (a) **8OPE/C10** recorded under the conditions of bias of 1 V and set current of 19 pA and (b) **C10** SAM without insertion of **8OPE** molecules under the conditions of 0.9 V and 9.8 pA. The red bars represent 5 nm.

The STM images of a **C10**-SAM without **8OPE** insertion showed no such bright spots (Figure VI-2b). Thus the bright spots are assigned to **8OPE** inserted into the **C10** matrix. Most of the spots are considered to be a cluster of **8OPE** molecules as previously reported.[161,163] This interpretation explains why the bright spots are observed as isotropic circles despite of a rectangular shape of OPE as illustrated in Figure VI-1. The strip structure in the **C10** matrix having ca. 2 nm of line distance (Figure VI-2a) is a typical structure of alkanethiol SAM having relatively lower surface density.[148,285] Before insertion of **8OPE** molecules, the **C10**-SAM showed $\sqrt{3} \times \sqrt{3}$ structure (Figure VI-2b). Insertion of **8OPE** molecules and exposure to vacuum atmosphere should have induced the molecular reorganisation on the surface. In **8OPE/C10, C10** molecules declined more than in the pure **C10**-SAM but not completely lied down on the surface. The tilt angles of **8OPE** and **C10** may be aligned in the mixed SAM.

STS measurements. STS measurements were carried out to obtain *I*–*V* curves of **8OPE** and **C10,** respectively (solid lines in Figure VI-3 see Figure A-VI-1 in Appendix for the *I*–*V* curves with standard deviation). The *I*–*V* curves of **8OPE** were acquired by placing the tip on the bright spots, while those of **C10** on the area where no bright spots were observed. Two kinds of the tip–sample configurations were attained by choosing either set current of 5.5–6 pA (Figure VI-3a and b) or 19 pA (Figure VI-3c and d) under bias of 1 V. The feedback electric circuit was turned off to fix the molecule–tip distance during the voltage sweeps. The bias voltage was applied to the sample with taking the grounded tip as zero. The applied bias from zero to +2 V and from zero to 2 V was separately swept. More than 100 scans of *I*–*V* curves were collected for each sweep direction. *I*–*V* curves showing fluctuation of more than 40 pA, current response of less than 4 pA in the whole bias sweep, and no bias response were abolished. Before the measurements, the sample was imaged for several hours to confirm no thermal drift during the STS measurements. The data on the

bright spots which kept being observed for several scans were collected, and the others were abolished since they were regarded as physisorbed on gold.

***I–V* curve analysis.** To analyze the *I–V* curves of **C10** and **8OPE** in depth, the *I–V* curves were fitted with the Simmons equation (eq VI-1), which is the simplest model for tunneling behavior through a rectangular barrier in the metal–insulator–metal system

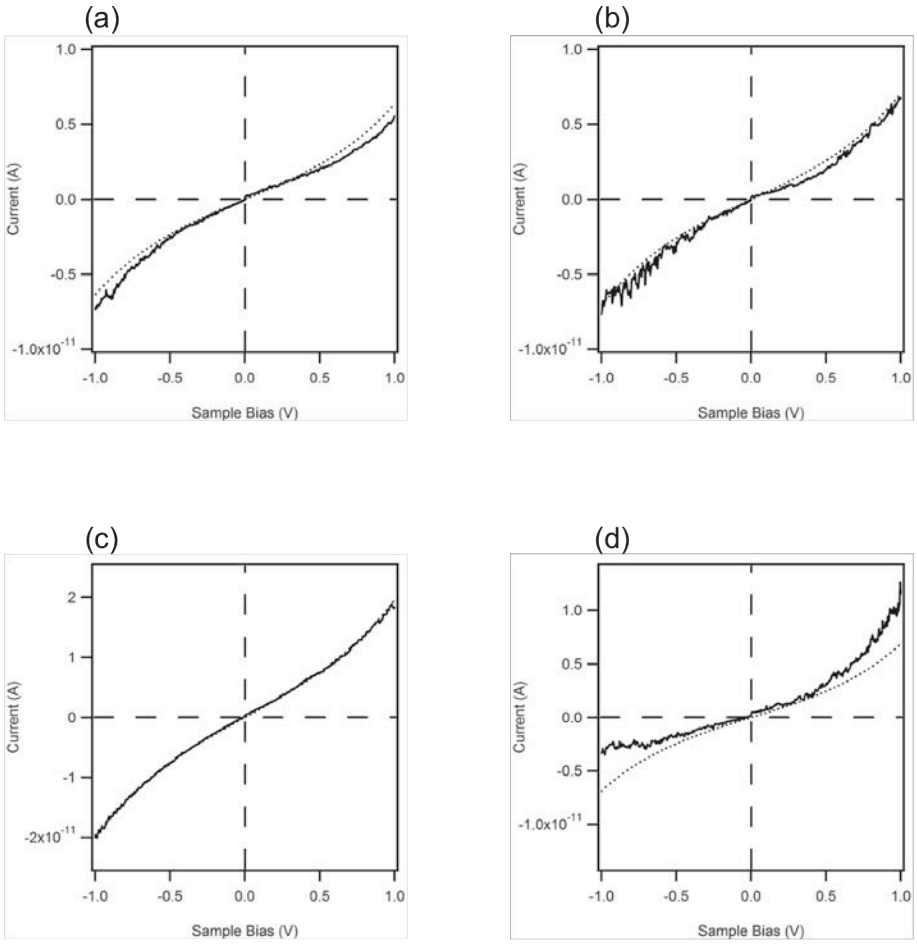

Figure VI-3. Curve fitting of the averaged experimental data of I V curves with the Simmons equation (eq III-1). (a) **C10** and (b) **8OPE** under the conditions of baias of 1 V and set current of 5.5–6 pA, and (c) **C10** and (d) **8OPE** under the conditions of 1 V and 19 pA. Solid and dotted lines represent the experimental data and the fitting curve, respectively.

(Dotted lines in Figure VI-3 and Table VI-1).[199,200] In the case of the low set current of 5.5–6 pA (a wide molecule–tip gap), the calculated curves are successfully fitted only with slight deviations of larger current in the negative sample bias for the both compounds (Figure VI-3a and b). The ϕ value of 3.31 eV and the β value of 1.36 $Å^{-1}$ for **C10** are within the values reported in the previous studies (ϕ = 1.1 $Å^{-1}$ is widely accepted for the alkane chains.[145] β = 1.36 $Å^{-1}$ is larger than that due to the gap effect and the curve fitting with 4 parameters). The weakly asymmetric profile is repeatedly reported.[145,146,229] The *I*–*V* curve of **C10** obtained under the high set current of 19 pA (a narrow molecule–tip gap) (Figure VI-3c) is fitted consistently with the equation.

The ϕ value of 2.40 eV and β of 0.85 $Å^{-1}$ for **8OPE** are good agreement with previous reports (β = 0.66 $Å^{-1}$ by Kimura et al.[163] and 0.75 $Å^{-1}$ by Sisido et al.[286]). β of 0.85 $Å^{-1}$ for **8OPE** is larger than these values probably due to the presence of lipoic acid between the helix moiety and gold [229]. Under set point of 19 pA, the curve fitting is unsuccessful for the *I*–*V* curve of **8OPE** (Figure VI-3d) because of the asymmetric profile.

Although the *I*–*V* curves are similar between **8OPE** and **C10** at the wide molecule–tip gap (Figure VI-3a and b), the molecular conductance of **8OPE** is larger than that of **C10** when we take account of the longer molecular length of **8OPE** than **C10**. This observation is consistent with the previous report,[162] which is explainable by the smaller distance decay coefficient of electron tunneling, β, for HPs than that for alkane chains.

Under the configuration of the narrow molecule–tip gap (Figure VI-3c), the *I*–*V* curve of **C10** becomes fully symmetric, which is curve-fitted completely. On the other hand, the *I*–*V* curve of **8OPE** shows three times larger current at +1 V than at 1 V (Figure VI-3d), which tendency is opposite to that under the condition of the wide molecule–tip gap (Figure VI-3b).

Origin of asymmetry. The asymmetric curves can be interpreted comprehensively

with considering two points: the relative energy level difference of the molecular orbitals (especially the HOMO and the LUMO) from the Fermi levels of two electrodes, E_{F1} (for the substrate) and E_{F2} (for the tip), and asymmetric contact of the molecule with two electrodes.[287] Electrostatic potential drop at the molecule–tip contact is generally considered to be large because of the poor electronic coupling between the molecule and the tip.

Table VI-1. Summary of fitting paramaters to the Simmons equation (eq VI-1). Condition (A) +1 V, 5.5–6 pA, (B) +1 V, 19 pA.

sample	condition	d (nm)	f (eV)	α	$C \times 10^{16}$	β (Å^{-1})
C10	A	1.50	3.31	0.72	1.15	1.36
	B	1.50	3.95	0.70	11.02	1.43
8OPE	A	2.40	3.00	0.48	3.41	0.85
	B	2.37	3.81	0.44	13.82	0.87

The HOMO level (6.5 eV) of the amide group is closer to the Fermi level of the electrodes (5.1 eV for gold and 4.55 eV for tungsten[288]) than the LUMO level (1.2 eV).[289] The HOMO level should be therefore used for electron transfer through the molecule. When this is the case, the current will become larger with more positive electrode level than the neighboring HOMO level because of larger transmission probability.[146,290] In the case of **8OPE** with a narrow molecule–tip gap, to contrary to the general consideration described above, the potential drop may be larger at the gold substrate side than the tip side. Then, the energy gap between HOMO and E^{P}_{F1} will become larger than that between HOMO and E^{n}_{F2} (Figure VI-4b). The current is thus larger at the positive bias, which successfully explains the asymmetric *I*–*V* curve of **8OPE** under the narrow molecule–tip gap (Figure VI-3d). In the case of the wide molecule–tip gap, the potential drop at the tip side may be as large as the gold substrate side because of the wide vacuum gap (Figure VI-4a), resulting in the

reversed weakly asymmetric *I*–*V* curve (Figure VI-3b).

The interpretation of the small potential drop at the tip side in the potential profile in the case of the narrow molecule–tip gap is explainable by a strong electronic coupling of the molecule–tip contact (Figure VI-4b), even though there is a gap between the molecule and the tip. Probably, the OPE moiety of **8OPE** is exposed out of the **C10** matrix, enabling the efficient electronic coupling between π-electrons delocalised over the whole area of the OPE moiety (ca. 80 $Å^2$) and the tungsten tip. This strong coupling should make the potential drop small.

Change of the molecule–tip electron coupling by controlling the tip–molecule distance should be therefore the reason for the drastic change in the *I*–*V* curves of **8OPE**. There are many reports on porphyrins, showing that the electronic coupling between large π-conjugate crowds and metal electrode is highly dependent on their distance.[291] Generally, the π-conjugate skeleton of a porphyrin is precisely imaged with STM when the compound is

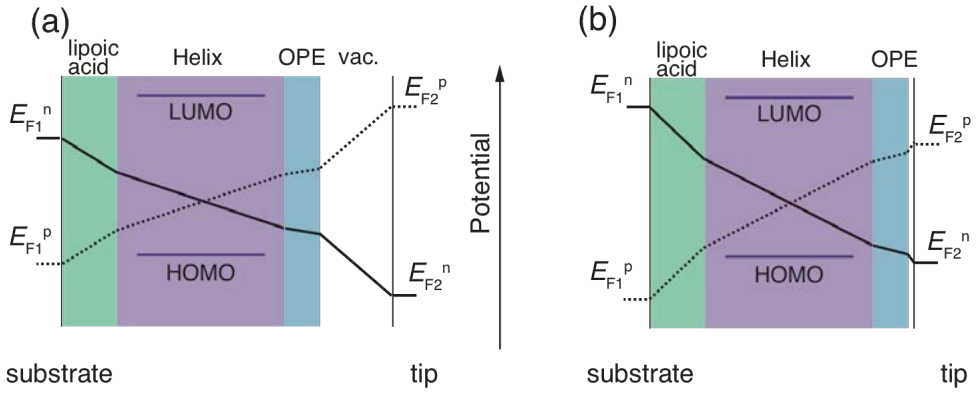

Figure VI-4. Illustration of the Fermi energy levels of electrodes and the electrostatic potential distribution at the molecule–electrode contacts for the negative (solid line) and positive (dot line) sample biases under the tip position fixed (a) at bias of 1 V and set current of 5.5–6 pA (a wide molecule–tip gap) and (b) at bias of 1 V and set current of 19 pA (a narrow molecule–tip gap). The arrow at between two diagrams directs toward the negative side of the potential.

deposited on a metal surface.[292] In the case of Cu-*tetra*-3,5-di-tert-butyl-phenyl porphyrin, however, the porphyrin moiety is not imaged. The four di-ter-butyl-phenyl (DBP) groups are rotated out of the plane of the porphyrin ring (near to a right angle) because of steric repulsion, resulting in an electronic decoupling of the delocalised π-orbital of porphyrin from the metallic surface.[293] The situation is unchanged even when the tilt angle of DBP group is reduced to 10° from the main ring.[294] In the present study, the critical point for establishing the electron coupling should exist between the two tip positions examined here.

When the coupling between the OPE moiety and the tip is established, the potential drop is the smallest at the junction. Recent ab initio calculations show potential drop is large in the order of vacuum gap > C–H bond > Au–S bond ≈ aromatic moiety.[295–297] Therefore, the potential drop at the tip side should become smaller than that between the gold substrate and the helix moiety. The OPE moiety is thus considered as a molecular lead of the HP moiety.

Conclusion

The asymmetric behavior in *I*–*V* curves of **8OPE,** a HP with an OPE as a molecular lead, was switched by controlling STM tip position from the OPE moiety. The switching behavior can be explained by the potential drop between the molecular lead of the OPE moiety and the tip, which is explained by change in electron coupling between them with the gap variation. The OPE moiety can be a good molecular lead when the STM tip is positioned closely to the OPE.

Chapter VII

Vertical Orientation with a Narrow Distribution of Helical Peptides Immobilized on Quartz Substrate by Stereocomplex Formation

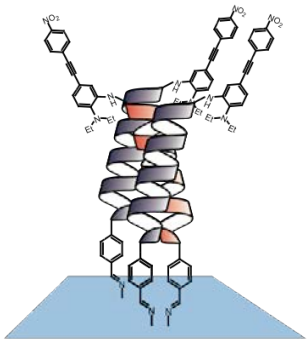

stereocomplex

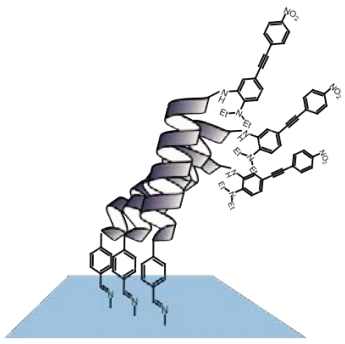

enantiopure

Introduction

This chapter deals with a SHG study to reveal the seteromixing effect on SAM quality. HPs have been reported to form densely packed SAMs with vertical orientation on gold surface.[270,159,271,298,156,299,300,160,164–166] Most of the HP-SAMs fabricated so far were generally prepared by using a right-handed helix. Recently Ueda et al. showed that a mixture of a right-handed helix and a left-handed helix formed a sheet self-assembly in a buffer solution, where a right-handed helix and a left-handed helix were aligned side-by-side with perpendicular orientation against the sheet surface. Electron diffraction from the sheet clearly showed the helices took a crystalline structure of a square lattice due to stereocomplex formation.[121,122] This finding prompted us to prepare a helix-SAM with using a mixture of a right-handed helix and a left-handed helix.

Usually HP-SAMs are characterized by molecular tilt angles from the surface normal,

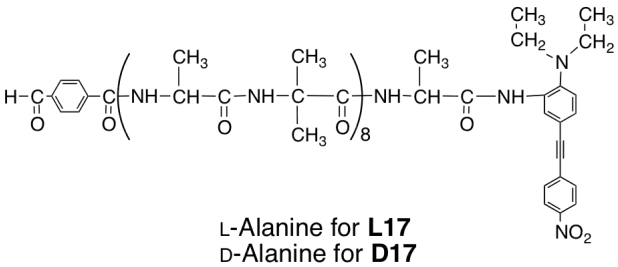

L-Alanine for **L17**
D-Alanine for **D17**

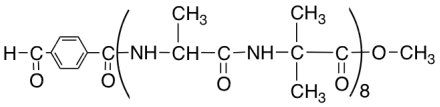

L-Alanine for **LA16**
D-Alanine for **DA16**

Figure VII-1. Chemical structures of **L17**, **D17**, **LA16**, and **DA16.**

which are analyzed by IR-RAS.[136,138,137,301] However, the tilt angle obtained from RAS reflects the average value of the SAM with no information on distribution of the tilt angle. Here, the author utilize SHG to obtain deep insights on the molecular alignment in the helix-SAMs. Taking assumptions of $C_{\infty v}$ and predominant hyperpolarizability of $\beta_{z'z'z'}$ about a chromophore in a SAM, non-vanishing components of second-order sensitivity of a SAM χ are related with $\beta_{z'z'z'}$ as eqs VII-1 and VII-2,

$$\chi_{zzz} = N_s \langle \cos^3 \theta \rangle \beta_{z'z'z'} \tag{VII-1}$$

$$\chi_{zxx} = \chi_{zyy} = \chi_{xzx} = \chi_{yyz} = \frac{1}{2} N_s \langle \cos\theta - \cos^3 \theta \rangle \beta_{z'z'z'} \tag{VII-2}$$

where N_s and θ represent surface density and tilt angle from surface normal, respectively. χ components depend on mean values of $\cos^3 \theta$ and $\cos \theta$, suggesting that information on distribution of θ can be obtained by SHG measurements.

The author designed compounds **L17** and **D17** (Figure VII-1). These compounds are linear conjugates of a D–π–A moiety with a high β value and a HP. The D–π–A moiety is a diphenylacetylene having a diethylamine group as an electron donor and a nitro group as an electron acceptor at the both ends. The peptide moiety is composed of 17 amino acids. Alternating sequence of D-Ala and Aib was adopted for **D17**. L-Ala instead of D-Ala was used for **L17**. This sequence is known to take a stable α-helical structure, which is essential for formation of well-packed and oriented SAMs. The D–π–A moiety was connected on the C-terminal of the peptide moiety through amide linkage at the *ortho* position of the diethylamino group. *p*-Formylbenzoic acid was introduced at the N-terminal of the peptide moiety as a linker to the fused quartz substrate covered with APS. Right- and left-handed HPs without the D–π–A moiety, **LA16** and **DA16**, respectively, are also synthesized. Five types of SAMs, **D17/L17**-SAM, **D17**-SAM, **L17**-SAM, **D17/LA16**-SAM, and **L17/DA16**-SAM were prepared on fused quartz substrates. On the basis of analysis of SHG

from these SAMs, structural differences (molecular density, θ, and distribution of θ) of their SAMs are discussed.

Experimental

Materials. D17 and **L17** were synthesized according to Scheme VII-1. HPs without the D–π–A compounds, **LA16** and **DA16** (see Figure VII-1) as well as the peptide moiety of **D17** and **L17** were synthesized by the conventional liquid-phase method. The purity of the final products was checked by HPLC (COSMOSIL $5C^{18}$-AR-300 for **D17** and **L17**, and COSMOSIL Cholester for **DA16** and **LA16**). See Chapter I for the general procedures of peptide and OPE synthesis and the compound identification methods.

Preparation of self-assembled monolayer. Five types of SAMs (**D17/L17**-SAM, **D17**-SAM, **L17**-SAM, **D17/LA16**-SAM, and **L17/DA16**-SAM) were prepared by the following procedures: (1) Fused quartz substrates (12 × 40 × 1 mm) were washed with a mixture of 28% aq of ammonia, 30% aq of hydrogen peroxide, and water (1/1/5, v/v/v) at 70 °C for 30 min. The substrates were then rinsed with water; (2) The substrates were immersed in a 1 wt % toluene solution of 3-aminopropyl trimethoxysilane at 60 °C for 10 min and immediately rinsed successively with toluene, a mixture of toluene and MeOH (1/1, v/v), and MeOH, followed by nitrogen blow for drying; (3) The coated substrates were immersed in a 0.1 mM 1,2-dichloroethane solution of **D17** or **L17** for preparation of **D17**-SAM or **L17**-SAM, respectively, for 24 hr at 70 °C. For **D17**/**L17**-SAM, a 1,2-dichloroethane solution of a mixture of **D17** and **L17** (0.1 mM for each) were used for immersion. **L17**/**DA16**-SAM and **D17/LA16**-SAM were similarly prepared with using the corresponding solutions. After immersion, the substrates were washed with MeOH and dried with nitrogen blow.

Optical measurements. CD spectra were measured with optical cells of 0.1 and 1 cm optical path length. Absorption spectra of solutions were recorded with an optical cell of 1 cm optical path length.

Second harmonic generation measurements: For the SHG measurements, *s*- or *p*-polarized fundamental light was focused on the sample with an incident angle of 45°, using a convex lens (f = 100 mm) after passing through an SH-cut filter to eliminate the SHG light from the various optical components. The *p*-polarized SHG light generated at the sample was filtered by a fundamental cut filter to remove intense fundamental light and was detected by a photomultiplier tube (Hamamatsu photonics: R7154) after passing though a monochromator (Shimadzu: SP-120). The signals were averaged by a Boxcar integrator (Stanford Research: SR-250). A light source ranging from 560 nm to 660 nm (0.92 eV) was obtained using an optical parametric oscillator (OPO: Continuum Surelite OPO) pumped by the third-harmonic light of a *Q*-switched Nd-YAG laser (Continuum: SureliteII-10).

Synthesis

The following descriptions are for **D17**. **L17** were synthesized similarly using L-Ala instead of D-Ala.

4-bromo-2-amino-*N*,*N*-diethylaniline (2): To a 500 mL RBF were added 4-boromo-*N*,*N*-diethynylaniline (**1**, 1.53 g, 6.71 mmol), deionized water (210 mL), and acetic acid (21 mL). To the mixture 20 mL of aqueous solution of sodium nitrite (601 mg, 8.72 mmol) were added dropwise. The mixture was stirred overnight and extracted with dichloromethane (3×) and the organic solution was dried over $MgSO_4$. The product was purified with column chromatography (silica gel, chloroform/hexane = 1/3). 1.0 g (61% yield) of the desired product was obtained.

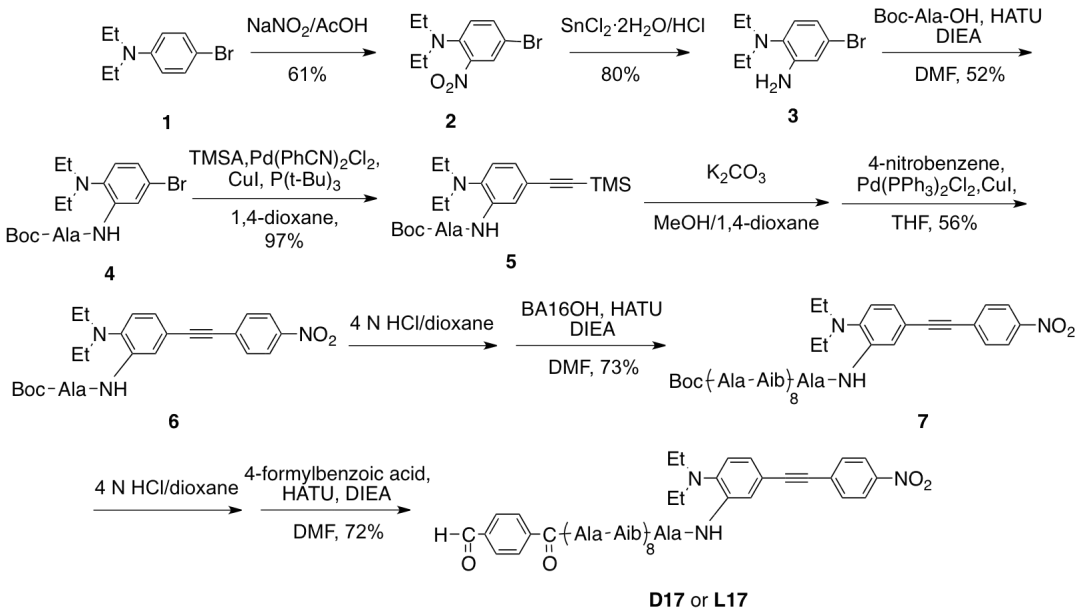

Scheme VII-1. Synthetic scheme of **D17** and **L17.**

^{1}H NMR ($CDCl_3$ 400 MHz): δ (ppm) 0.96 (6H, t, $(CH_3CH_2)_2N$), 2.90 (4H, q, $(CH_3CH_2)_2N$), 7.01 (1H, d, aromatic), 7.48 (1H, dd, aromatic), 7.79 (1H, d, aromatic).

EI-MS: *m*/*z* = 271.99 (calcd for $C_{10}H_{13}O_2N_2Br$ M^+, 272.0).

2-amino-4-bromo-*N*,*N*-diethylaniline (3): To a 100 mL RBF were added **2** (1.13 g, 4.1 mmol) and tin(II) chloride dihydrate (3.15 g, 16.55 mmol) in 8 mL of concentrated hydrochloric acid. The mixture was stirred for 30 min and 5 N aq NaOH was added until the mixture reached pH = 10. The mixture was extracted with dichloromethane (3×) and the combined organic layers were washed with brine. The organic layers was then dried over $MgSO_4$ and concentrated in reduced atmosphere. The residue was purified by column chromatography (silica gel, chloroform/hexane = 1/3 then 1/2). 800 mg (80%) of the desired product was obtained.

^{1}H NMR ($CDCl_3$ 400 MHz): δ (ppm) 0.96 (6H, t, $(CH_3CH_2)_2N$), 2.90 (4H, q, $(CH_3CH_2)_2N$), 4.14 (2H, s, (NH_2)), 6.78–6.88 (3H, m, aromatic).

EI-MS: *m*/*z* = 242.1 (calcd for $C_{10}H_{15}N_2Br$ M^+, 242.0).

4: See the general procedure for the peptide coupling reaction. **3** (1.16 g, 4.85 mmol), Boc-D-Ala-OH (918.25 mg, 4.85 mmol), HATU (2.40 g, 6.31 mmol), DIEA (1.72 mL, 9.71 mmol) were reacted in DMF (7 mL) at RT for 14 hr. The residue was purified with methods 1 and 2 (EtOAc/hexane = 1/4). 1.04 g (52%) of the desired product was obtained.

^{1}H NMR ($CDCl_3$ 400 MHz): δ (ppm) 0.94 (6H, t, (C*H*$_3$CH$_2$)$_2$N), 1.44–1.47 (12H, (C*H*$_3$)$_3$C, AlaC$^\beta$), 2.90 (4H, q, (CH$_3$C*H*$_2$)$_2$N), 4.45 (1H, s, AlaC$^\alpha$), 5.10 (1H, s, Boc-N*H*), 7.02 (1H, d, aromatic) 7.18 (1H, dd, aromatic), 8.64 (1H, d, aromatic).

FAB-MS: *m*/*z* = 413.13 (calcd for $C_{18}H_{28}BrN_3O_3$ $[M + H]^+$, 414.2).

5: See the general procedure for the Sonogashira cross coupling reaction. **4** (1.00 g, 2,41 mmol), Pd(II)(PhCN)$_2$Cl$_2$ (37.0 mg, 96.54 mmol), TMSA (467 μL, 3.38 mmol) Cu(I)I (13.8 mg, 72 μmol), tri(*tert*-butyl)phosphate (48.8 mg, 241 μmol), and DIA (847 μL, 6.03 mmol) were reacted in 1,4-dioxane (1.5 mL) at 40–45 °C for 1 d. The residue was purified by column chromatography (silica gel, chloroform) 941 mg (97%) of the desired product was obtained.

^{1}H NMR ($CDCl_3$ 400 MHz): δ (ppm) 0.22 (9H, s, (CH$_3$)$_3$Si), 0.92 (6H, t, (C*H*$_3$CH$_2$)$_2$N), 1.44–1.47 (12H, (CH$_3$)$_3$C, AlaC$^\beta$), 2.90 (4H, q, (CH$_3$C*H*$_2$)$_2$N), 4.35 (1H, s, AlaC$^\alpha$), 5.06 (1H, s, Boc-N*H*-), 7.06 (1H, d, aromatic), 7.17 (1H, d, aromatic), 8.56 (1H, s, aromatic) 9.30 (Ala-N*H*-Ar).

FAB-MS: *m*/*z* = 432.4 (calcd for $C_{23}H_{38}N_3O_3Si$ $[M + H]^+$, 431.3).

6: 5 (941 mg, 2.18 mmol) was treated with potassium carbonate (903 mg, 6.54 mmol) in a mixture of MeOH (30 mL) and dichloromethane (30 mL) for 2 hr. The mixture was extracted with dichloromethane (3×) and the organic layer was washed with brine, followed by drying in vacuum. According to the general procedure for the Sonogashira cross copling reaction, the product was reacted with 4-iodonitrobenzene (1.08 g, 4.34 mmol),

$Pd(II)(PPh_3)_2Cl_2$ (91 mg, 130 μmol), Cu(I)I (41 mg, 216 μmol), DIEA (1.45 mL, 8.68 mmol) at 0 °C for 1 hr. The residue was purified by column chromatography (chloroform/EtOAc = 45/1 then 40/1). 580 mg (56%) of the desired product was obtained.

^{1}H NMR ($CDCl_3$ 400 MHz): δ (ppm) 0.96 (6H, t, $(CH_3CH_2)_2N$), 1.44–1.47 (12H, $(CH_3)_3C$, $AlaC^{\beta}$), 2.96 (4H, q, $(CH_3CH_2)_2N$), 4.37 (1H, s, $AlaC^{\alpha}$), 5.02 (1H, s, Boc-N*H*-), 7.16 (1H, d, aromatic), 7.27 (1H, d, aromatic), 7.64 (2H, d, aromatic), 8.21 (2H, d, aromatic), 8.67 (1H, d, aromatic), 9.34 (Ala-N*H*-Ar).

FAB-MS: *m*/*z* = 481.3 (calcd for $C_{26}H_{33}N_4O_5$ $[M + H]^+$, 481.2).

7: The Boc group was deprotected by treatment with 4 N HCl/dioxane, followed by washing with *i*Pr_2O. Accoring to the general procedure for the peptide coupling, the deprotected product was reacted with Boc-(D-Ala-Aib)$_4$-OH (420 mg, 307 μmol), HATU (186 mg, 491 μmol), DIEA (241 μL, 1.39 mmol) in DMF at RT for 24 hr. The residue was purified by method 3 (MeOH). 400 mg (73% yield) of the desired product was obtained.

^{1}H NMR ($CDCl_3$ 400 MHz): δ (ppm) 0.93 (6H, t, $(CH_3CH_2)_2N$), 1.3–1.5 (84H, m, $(CH_3)_3C$, $AlaC^{\beta}$, $AibC^{\beta}$), 2.99 (4H, q, $(CH_3CH_2)_2N$), 3.90–4.0 (7H, m, $AlaC^{\alpha}$), 4.33 (1H, m, $AlaC^{\alpha}$), 4.71 (1H, m, $AlaC^{\alpha}$), 5.48 (1H, s, Boc-N*H*), 6.79 (1H, s, NH), 7.06 (1H, s, NH), 7.27–7.80 (17H, m, NH and aromatic), 8.20 (2H, d, aromatic), 8.51 (1H, s, NH), 9.31 (1H, s, NH).

FAB-MS: *m*/*z* = 1730.1 (calc. for $C_{82}H_{129}N_{20}O_{21}$ $[M + H]^+$, 1730.0).

D17. 7 (200 mg, 115 μmol) was treated with TFA/anisole (2 mL/200 μL) in dichloromethane (1 mL) at 0 °C for 4 hr. Then another TFA/anisole (1 mL/100 μL) was added and further treated at 0 °C for 3 hr. The mixture was concentrated under reduced atmosphere and washed with *i*Pr_2O. The product was dried in vacuum. According to the general procedure for the peptide coupling reaction, the product was reacted with 4-formylbenzoic acid (56 mg, 380 μmol), HATU (239 mg, 630 μmol), and DIEA (220 μL,

1.26 mmol) in DMF (1 mL) at RT for 28 hr The residue was purified by method 3 (MeOH) 160 mg (72% yield) of the desired product was obtained. Further purification was conducted by a reversed phase HPLC (MeOH/water = 9/1) before the product was used for measurements.

^{1}H NMR ($CDCl_3$ 400 MHz): δ (ppm) 0.95 (6H, t, $(CH_3CH_2)_2N$), 1.3–1.5 (75H, m, $AlaC^{\beta}$, $AibC^{\beta}$), 2.98 (4H, q, $(CH_3CH_2)_2N$), 3.96 (6H, br, $AlaC^{\alpha}$), 4.23 (2H, br, $AlaC^{\alpha}$), 4.46 (1H, br, $AlaC^{\alpha}$), 7.04 (1H, m, aromatic), 7.16 (1H, m, aromatic), 7.3–8.2 (26H, m, NH, aromatic), 9.16 (1H, s, NH), 9.94 (1H, s, CHO).

FAB-MS: (HR) *m*/*z* = 1761.9301 (calc. for $C_{85}H_{125}N_{20}O_{21}$ $[M + H]^+$, 1761.9328).

Results and discussion

UV and CD spectroscopy. Absorption spectra of **D17** and **L17** were recorded in a MeOH solution (Figure VII-2). The two spectra are completely identical to each other. Two of the three bands at 352 and 246 nm are absorption bands mainly from the D–π–A moiety, whereas the other one at 204 nm is assigned to the π–π* transition band of the peptide

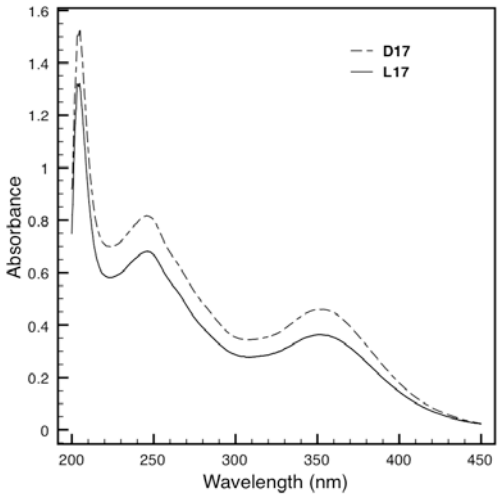

Figure VII-2. Absorption spectra of **D17** and **L17** in MeOH.

moiety.[302,303] The molecular extinction coefficients of the three bands are 1.8×10^4, 3.4×10^4, and 7.7×10^4, respectively.

CD spectra of **D17** and **L17** are shown in Figure VII-3. The peptide moiety (Figure VII-3 left) of **L17** shows two peaks of negative Cotton effects at 208 and 224 nm, which are typical for a right-handed α-helical structure.[250,252] The molar ellipticity of the peak was ca. 2.0×10^4, which is agreeable with those of $(Ala\text{-}Aib)_8$ and $(Leu\text{-}Aib)_8$ reported previously.[158,229] The spectrum of **D17** is a mirror image exactly of that of **L17** as expected, showing that **D17** takes a left-handed α-helical structure.

Induced Cotton effect of the D–π–A moiety is observed around 350 nm (Figure VII-3 right). In the spectrum of **L17**, a negative broad peak at 350 nm and a positive sharp peak at 260 nm appear. The spectrum of **D17** around 350 nm is also the mirror image of that of **L17**. TD-DFT calculations support that the induced Cotton effect originates from a twist in the D–π–A moiety.

Preparation of SAMs. The peptide SAMs were prepared on fused quartz substrates via Shiff-base formation between amino groups of APS layer on the fused quartz substrates

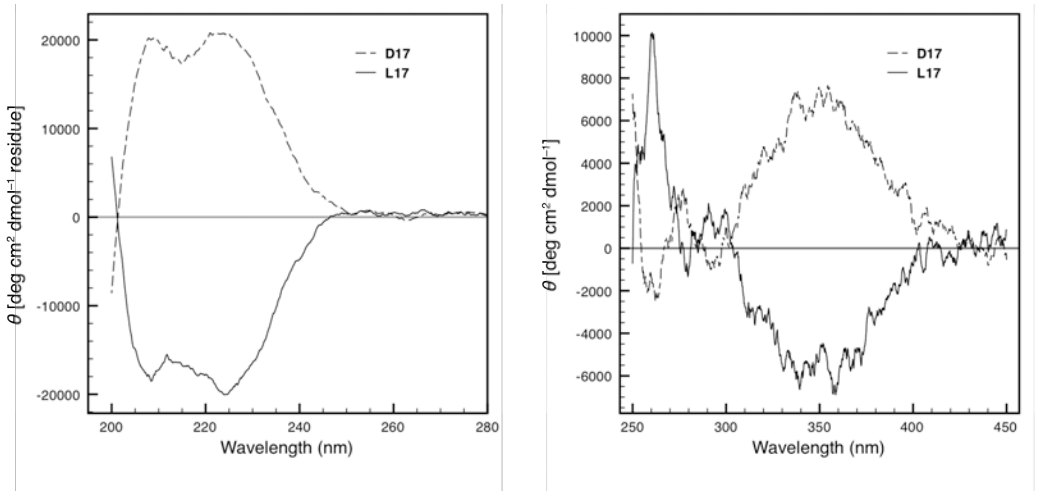

Figure VII-3. CD spectra of **D17** and **L17** in MeOH.

and formyl groups of the N-terminal of the peptides. Concentrations of peptides in a 1,2-dichloromethane solution is critical for the quality of the SAMs. When the concentrations are too high, SAMs are covered by physisorbed molecules as well. SHG from **D17**-SAM and **L17**-SAM prepared from 0.5 and 0.1 mM solutions were checked, which showed reasonable SHG intensities. The condition of 0.1 mM solution is thus adopted.

Second-order susceptibility of the D–π–A moiety. The SHG intensities from the **D17/L17**-SAM and Y-cut quartz as a function of the light incident angle ϕ_{in} ($-30 < \phi_{in} < 30$) were recorded under the *p*–*p* setup (Figure VII-4). The wavelength of the incident light was 560 nm. Maker fringes were not clearly observed for the both samples because of insufficient monochrome laser light and out of focus on the samples.

The relative SHG light intensity from the SAM against the Y-cut quartz in the *p*–*p* set up, $I_r(2\omega)^{p-p}$, is expressed as

$$I_r(2\omega)^{p-p} = \frac{1}{(\chi_q d_q)^2}\left|(A_{zzz}\chi_{zzz} + A_{xzx}\chi_{xzx} + A_{zxx}\chi_{zxx})\right|^2 \qquad \text{(VII-3)}$$

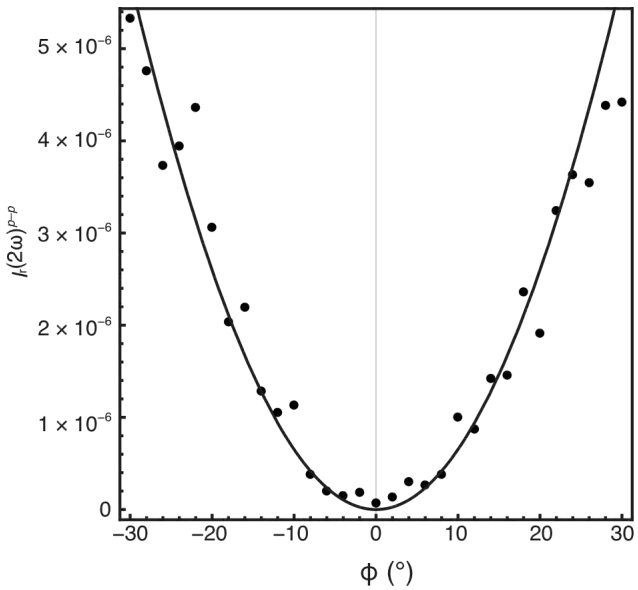

Figure VII-4. The SHG signals of **D17/L17**-SAM with a fitting line using eq (VII-3).

where $A_{zzz} = \sin\theta_{out}\sin^2\phi_{in}$, $A_{xzx} = \cos\phi_{out}\sin\phi_{in}\cos\phi_{in}$, $A_{zxx} = \sin\phi_{out}\cos^2\phi_{in}$, $n_{air}\sin\phi_{in} = n_{silica}\sin\phi_{out}$, $n_{air} = 1$, $n_{silica} = 1.5$, χ_q is the second-order susceptibility of the Y-cut quartz (=0.6 pm/V), and d_q is the thickness of the Y-cut quartz (20 μm). Note that the Fresnel factors are excluded in the all three *A* components since they have little contribution. Assuming normal distribution having a standard deviation (SD, σ) of 0.2 rad (12°), 41° of a mean value of the tilt angle θ, and $N_s = 8.4 \times 10^{17}$ m^{-2} (14×10^{17} mol/cm^{-2}),[270] $\beta_{z'z'z'}$ is calculated to be 1.3×10^{-37} m^4/V (3.0×10^{-28} esu), which is in the range of typical values for the D–π–A compounds ($1–5 \times 10^{-28}$ esu).[304,305]

Relative intensity of the SHG signal. SHG intensities of all the SAMs were recorded under the *p–p* setup ($I(2\omega)^{p-p}$, Table VII-1). The wavelength and angle of the incident light were 660 nm and 45°, respectively. The SHG intensities of the SAMs are sufficiently larger than that of the quartz substrate treated by APS at this wavelength. When the SH intensities are compared among the stereomixed SAMs of the right-handed helix and the left-handed helix, the SHG intensity of **D17/L17**-SAM becomes four times larger than those of **D17/LA16**-SAM and **L17/DA16**-SAM, where the latter two SAMs are an equimolar mixture of the HPs with the D–π–A chromophore and without. This observation is understandable since the SHG intensity is related with square of the surface density of the SHG chromophore N_s according to the eqs VII-1–3.[306–308] At the same time, the SAM structures of the tilt angle and its distribution of the SHG chromophore are considered to be similarly reserved among the SAMs composed of a mixture of the righ-handed helix and the left-handed helix irrespective of the SHG chromophore concentration. The scaffolds of the stereomixed right-handed and the left-handed HP SAMs are therefore very effective to align regularly the chromophores attached to the helices.

When the SHG intensity is compared between the enatiopure SAM and the stereomixed SAM, the SHG intensities of **D17**-SAM and **L17**-SAM become about half and

one-fourth of that of **D17/L17**-SAM, respectively, despite of the D–π–A chromophore being attached all to the HP in these SAMs. A plausible explanation for the difference is suggested that the surface density of the D–π–A chromophore of the enantiopure SAMs may be smaller than that of the stereomixed **D17/L17**-SAM due to the different tilt angle θ of the D–π–A chromophore. In the present system, the quartz substrate is used, which cannot be subjected to the IR-RAS to obtain information of the tilt angle of the helix from the surface normal. On the basis of our experience, however, the tilt angle of helices became smaller with mixing a HP with the opposite helical sense, supporting this explanation.

Another factor contributing to the second-order susceptibility of a SAM can be the local field factor *f*. *f* is generally described by the Lorentz–Lorenz correction, $f = (n^2 + 2)/3$, where *n* is the refractive index at the optical frequency. The correction, however, presumes

Table VII-1. Observed and calculated SH intensity of the SAMs.

	D17/L17	**D17**	**L17**	**D17/LA16**	**L17/DA16**
$I(2\omega)^{p-p}$ [a] (relative, experimental)	100	47	27	25	24
$I(2\omega)^{s-p}/I(2\omega)^{p-p}$ (experimental)	0.21	0.23	0.23	0.23	0.23
σ (rad, assumption)	0.2	0.5	0.5	0.2	0.2
θ[b] (deg, calculation)	41	59	59	41	41
N_s (relative, assumption)	1.0	0.87	0.67	0.5	0.5
$I(2\omega)^{p-p}$ [c] (relative, calculation)	100	47	27	25	25

(a) the value of **D17/L17**-SAM is set to be 100; (b) calculation of eq. VII-4 (shown in Figure VII-5a) with the assumption of σ; (c) products of the term $|(A_{zzz}\chi_{zzz} + A_{zzz}\chi_{zzz} + A_{zzz}\chi_{zxx})|^2$ in eq VII-3 (showen in Figure VII-5b and N_s assumed. Normalized to the value of **D17/L17.**

a crystal structure, which is not the case of the SAMs. This factor is thus ommited from eq VII-3.

Morecular orientation and its distribution. SHG measurements were conducted to obtain information on θ and σ using an incident light of 560 nm. Under the assumptions of the $C_{\infty v}$ symmetry of the D–π–A moiety and $\beta_{z'z'z'}$ as the major nonlinear optical molecular polarizability, the ratio of SHG signals can be expressed as

$$\frac{I(2\omega)^{s-p}}{I(2\omega)^{p-p}} = \frac{4\left(\langle\cos\theta\rangle - \langle\cos^3\theta\rangle\right)^2}{5\langle\cos\theta\rangle^2 - 6\langle\cos\theta\rangle\langle\cos^3\theta\rangle + 5\langle\cos^3\theta\rangle^2} \qquad \text{(VII-4)}$$

where $I(2\omega)^{s-p}$ and $I(2\omega)^{p-p}$ represent the intensities of *p*-polarized SHG light obtained from *s*-polarized incident light and *p*-polarized incident light, respectively.[309] The SHG signal ratios are thus dependent on θ and its distribution σ. Indeed, Figure VII-5a shows the calculated curves of eq VII-4 with different σ (σ = 0.01–0.5 rad), showing that the ratio monotonically increases as θ increases, and decreases as σ increases. Figure VII-5b shows calculated SHG intensity of eq VII-3 as a function of θ with different σ. (Note that ϕ_{in} = 45°, and the term of $1/(\chi_q d_q)^2$ is omitted for simplicity.) The curves show again the decrease of the SHG intensity with the increase of σ.

Two kinds of experimental values, $I(2\omega)^{p-p}$ and $I(2\omega)^{s-p}/I(2\omega)^{p-p}$, are not enough to determine uniquely the three parameters, θ, σ, and N_s, of the SAMs. The author therefore try to find out the self-consistent set of these values with reasonable assumptions. First assumption is to set σ values of 0.2 and 0.5 for the stereomixed and the enantiopure SAMs, respectively. As described before, the author found out the stereomixed SAMs were composed of more vertically oriented helices than the enantiopure SAMs, suggesting the smaller θ value and the smaller σ value of the stereomixed SAMs than the enatiopure SAMs. With using the experimental values of $I(2\omega)^{s-p}/I(2\omega)^{p-p}$ and these σ values, θ values were

determined from eq VII-4 (Table VII-1). Second assumption is to set the relative values of N_s of 1.0, 0.87, 0.67, 0.5, and 0.5 for **D17/L17**, **D17**, **L17**, **D17/LA16**, and **L17/DA16** SAMs, respectively. These values are in agreeable with the previous interpretation that the stereomixed SAMs should have similar structural paprameters of θ and σ, and the helices in the enantiopure SAMs should more tilted with smaller N_s. As listed at the first and sixth rows in Table 1, the experimental result can be well explained by the calculation under these assumptions. On the other hand, when the author assume the same σ value of 0.2 for all the SAMs, θ is estimated to be 41° for all the SAMs, and the relative molecular densities should be 0.68 and 0.51 for **D17**-SAM and **L17**-SAM, respectively. However, the density of 0.51 is too sparse to form the helical SAMs with θ of 41°. The stereomixed SAMs therefore should be composed of more vertically oriented helices with smaller θ and σ than those of the enatiopure SAMs, even though the σ values used here do not have quantitative accuracy.

The above conclusion is supported by the observation of the stereomixed helical membrane recently reported by Ueda et al.[121,122] They prepared a sheet-shaped molecular

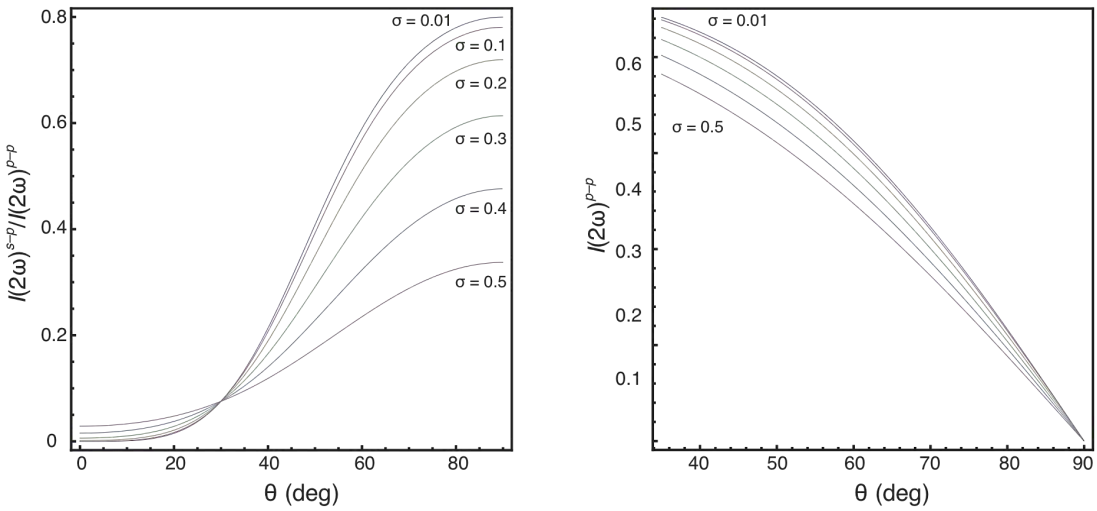

Figure VII-5. Calculated curves of SHG intensity vs θ assuming the normal distribution of δ = 0.01–0.5 rad in molecular orientation: (a) calculation of eq VII-4 and (b) calculation of the term $|(A_{zzz}\chi_{zzz} + A_{zzz}\chi_{zzz} + A_{zzz}\chi_{zxx})|^2$ in eq VII-3.

assembly from a mixture of right-handed and left-handed helices in the hydrophobic blocks of amphiphilic peptides. TEM observation clearly showed a square lattice arrangement of the helices in the sheet-shaped membrane, whilst the enantiopure membrane was less ordered. Taken together, a mixture of right-handed and left-handed helices has a strong tendency to form a well ordered structure with stacking side-by-side to be a checkered pattern.

Conclusion

Novel linear conjugates of HPs and a D–π–A chromophore, **D17,** and **L17,** were synthesized. SHG measurements of the five kinds of SAMs, **D17/L17**-SAM, **D17**-SAM, **L17**-SAM, **D17/LA16**-SAM, and **L17/DA16**-SAM were carried out. β of the D–π–A moiety in **D17/L17**-SAM is estimated to be 1.3×10^{-37} m^4/V (3.0×10^{-28} esu), which is comparable to the reported values of D–π–A compounds. $I(2\omega)^{p-p}$ values of the enantiopure SAMs were as low as 47% and 27% of that of the **D17/L17**-SAM. Not only the tilt angle θ but also its distribution σ become smaller in the stereomixed SAMs than the enantiopure SAMs. The stereocomplex formation between the right-handed helix and the left-handed helix should be the reason for the regular structure of the stereomixed SAMs.

Concluding Remarks

The dissertation deals with researches on the compounds obtained by conjugating OPEs and HPs. Each of the conjugates showed unprecedented characters, which can be realized only by neither. Such characters are applicable to fundamental studies of OPEs and HP-SAMs.

In Chapter I, a H-character type conjugate, **OPEn9,** was synthesized and characterized. The OPE moiety and HP moiety are found to take the antiparallel conformation in chloroform solution and a LB layer due to D–D interaction. The effect of external electric field generated by the HP moiety influences the electronic structure of the OPE moiety, narrowing the HOMO–LUMO gap. This effect is also confirmed by DFT calculations. This finding is predicted by previous computational researches but experimentally observed for the first time in this research. **OPEn9** does not aggregate easily, which is in contrast to the each moiety. This character enables **OPEn9** to form a well-ordered alignment in a LB monolayer assisted by intermolecular D–D interaction. D–D interaction is proved to be effective in regulating alignment of two relatively large moieties.

In Chapter II, an OPE based pseudotriangle with two HPs was synthesized (**f-OPEBE**). The OPEBE moiety makes no Cotton effect in methanol, suggesting the compound take random conformation. In contrast, in chloroform and dichloromethane, Cotton effect is observed in the absorbing region of the OPEBE. Association of two HP driven by intramolecular D–D interaction should induce a chiral pseudotriangle conformation of the OPEBE. In, THF and 1,4-dioxane, where dielectric constant is less than dichloromethane, CD spectra of the peptide absorbing region shows a negative Cotton effect but no shoulder around 224 nm. This indicates that HPs aggregate by intermolecular interaction in these solvent. Indeed, far weaker Cotton effect is observed in the OPEBE absorbing region in

these solvents. D–D interaction between HPs are found to be effective not only in inducing a specific conformation but also inducing chirality in the conformation.

In Chapter III, an O-character conjugate, or a macrocycle, of an OPE and a HP is synthesized. The both ends of the OPE and HP moieties were clipped. Due to right-handed helicity in the HP moiety, the OPE is twisted in a right-handed way. This twist was confirmed by CD spectroscopy and by interpretation of TD-DFT calculations. Clipping the both side of an OPE with a HP is proved to be a good way to introducing the main-chain chirality in a OPE.

In Chapter IV, the main-chain twisting conjugation designed in Chapter III was revised and applied to twist an OPE based D–π–A moiety. **SSA8=OPE**, the conjugate of the OPE moiety and a HP, showed the Cotton effect at the absorption range of the HP moiety and the OPE moiety. The dihedral angle of the phenyl rings at both ends of the OPE moiety is fixed to be 45–90° in MeOH and more than 15° in a right-handed way in the other solvents. Due to the twist, the oscillator strength of the HOMO–LUMO transition is considerably decreased, resulting in the decrease in fluorescence quantum yield and the absence of the HOMO–LUMO transition band in absorption and excitation spectra. The oscillator strength of the HOMO–LUMO transition of the D–π–A is found to be highly sensitive to the alignment of the donor part and the acceptor part even if the two parts are separated by a free rotating *p*-diethynylphenyl group.

In Chapter V, linear conjugates, **2*n*OPE2*m*,** were synthesized for a systematic research on the external electric field effect on an OPE. The SAMs of **2*n*OPE2*m*** were prepared on a gold surface. The absorption spectra of the SAMs show a bathochromic shift of ca. 25 nm from the reference **C11OPE**-SAM. DFT calculations show that the HOMO–LUMO gap of an OPE decreases as electric field along the molecular axis is applied and the ca. 25 nm of bathochromic shift in the absorption corresponds to the effect of an electric field of 1.4 ×

10^9 V m^{-1}. This value of the electric field agrees with the value obtained from a simple point charge model using the Coulomb's law. Other factors leading to a bathochromic shift of the absorption spectra such as planarization of the OPE moiety are not plausible in the present case. The external electric field generated from HP-SAMs is thus useful tool for controlling the electronic structure of a π-conjugate system.

In Chapter VI, **8OPE,** one of the linear conjugates designed in Chapter V, was inserted in a SAM of **C10** and STS measurements were performed. The *I–V* curves is symmetric when the tip–molecule distance is far but asymmetric when the distance is close. In contrast, no asymmetric curves were recorded form the STS measurements of **C10.** The switching behavior can be explained by the potential drop between the molecular lead of the OPE moiety and the tip. Since the OPE moiety is exposed on the **C10**-SAM and has delocalized π-electrons, the moiety can electronically couple with the tip, resulting in small potential drop in the interface when the tip–OPE distance is close. The OPE moiety can be a good molecular lead when the STM tip is positioned closely to the OPE.

In Chapter VII, two linear conjugates of a D–π–A and a HP (**D17** for left-handed helix and **L17** for right-handed helix) were synthesized. SHG signal of enantiopure SAMs, **D17**-SAM and **L17**-SAM, are 47% and 27% of that of a stereocomplex SAM, **D17/L17**-SAM. Intensity ratio of *p–p* and *s–p* polarized setup was 0.23 for all the SAMs. On the basis of these experimental results and assumptions that molecular tilt angle has normal distribution θ and the standard deviation of the molecular tilt angle is 0.2 rad for **D17/L17**-SAM and 0.5 rad for the enantiopure SAMs, θ is calculated to be 41° for **D17/L17**-SAM and 59° for the enantiopure SAMs. Molecular density of **D17**-SAM and **L17**-SAM is calculated to be 87% and 67% of **D17/L17**-SAM, respectively. HPs in a stereocomplex SAM are thus more vertically and uniformly oriented than in an enantiopure SAM. Linear conjugate of a D–π–A and a HP is useful for investigation of structure of

HP-SAMs using SHG.

There results clearly validate the idea of conjugating two functional moieties. This idea is not limited to OPEs and HPs but can be extended to many other functional organic structures. The author believes that the dissertation suggests a novel viewpoint in organic molecule designing and will contribute in our quest for new materials.

References

(1) Grignard, V. *Compt. Rend.* **1900**, *130*, 1322.

(2) Diels, O.; Alder, K. *Justus Liebigs Ann. Chem.* **1928**, *460*, 28.

(3) Pellissier, H. *Tetrahedron* **2009**, *65*, 2839–2877.

(4) Juhl, M.; Tanner, D. *Chem. Soc. Rev.* **2009**, *38*, 2983–2992.

(5) Coates, G.; Hustad, P.; Reinartz, S. *Angew. Chem. Int. Ed.* **2002**, *41*, 2236–2257.

(6) Sobota, P.; Szafert, S. *J. Chem. Soc., Dalton Trans.* **2001**, 1379–1386.

(7) Corradini, P.; Guerra, G.; Cavallo, L. *Acc. Chem. Res.* **2004**, *37*, 231–241.

(8) Brown, H. C.; Zweifel, G. *J. Am. Chem. Soc.* **1961**, *83*, 486–487.

(9) Brown, H.; Prasad, J. *Heterocycles* **1987**, *25*, 641–657.

(10) Wittig, G.; Rieber, M. *Justus Liebigs Ann. Chem.* **1949**, *562*, 187–192.

(11) Hajós, G.; Nagy, I. *Curr. Org. Chem.* **2008**, *12*, 39–58.

(12) Palacios, F.; Alonso, C.; Aparicio, D.; Rubiales, G.; de los Santos, J. *Tetrahedron* **2007**, *63*, 523–575.

(13) Merrifield, R. B. *J. Am. Chem. Soc.* **1963**, *85*, 2149–2154.

(14) Jansen, M. *Angew. Chem. Int. Ed.* **2002**, *41*, 3746–3766.

(15) Corey, E. J. *Chem. Soc. Rev.* **1988**, *17*, 111–133.

(16) Corey, E. J. *Angew. Chem. Int. Ed. Engl.* **1991**, *30*, 455–465.

(17) Wilson, R. M.; Danishefsky, S. J. *J. Org. Chem.* **2007**, *72*, 4293–4305.

(18) Vineyard, B. D.; Knowles, W. S.; Sabacky, M. J.; Bachman, G. L.; Weinkauff, D. J. *J. Am. Chem. Soc.* **1977**, *99*, 5946–5952.

(19) Katsuki, T.; Sharpless, K. B. *J. Am. Chem. Soc.* **1980**, *102*, 5974–5976.

(20) Ohkuma, T.; Ooka, H.; Hashiguchi, S.; Ikariya, T.; Noyori, R. *J. Am. Chem. Soc.* **1995**, *117*, 2675–2676.

(21) Knowles, W. S. *Angew. Chem. Int. Ed.* **2002**, *41*, 1998–2007.

(22) Tsogoeva, S. *Chem. Commun.* **2010**, *46*, 7662–7669.

(23) Schrock, R. *Chem. Rev.* **2002**, *102*, 145–179.

(24) Monsaert, S.; Lozano Vila, A.; Drozdzak, R.; Van Der Voort, P.; Verpoort, F. *Chem. Soc. Rev.* **2009**, *38*, 3360–3372.

(25) Vougioukalakis, G. C.; Grubbs, R. H. *Chem. Rev.* **2010**, *110*, 1746–1787.

(26) Negishi, E.; Huang, Z.; Wang, G.; Mohan, S.; Wang, C.; Hattori, H. *Acc. Chem.*

Res. **2008**, *41*, 1474–1485.

(27) Suzuki, A. *Chem. Commun.* **2005**, 4759–4763.

(28) Heck, R. *Synlett* **2006**, 2855–2860.

(29) Burke, M. D.; Schreiber, S. L. *Angew. Chem. Int. Ed.* **2004**, *43*, 46–58.

(30) Kroto, H. W.; Heath, J. R.; O'Brien, S. C.; Curl, R. F.; Smalley, R. E. *Nature* **1985**, *318*, 162–163.

(31) Chen, Z.; King, R. B. *Chem. Rev.* **2005**, *105*, 3613–3642.

(32) Babu, S. S.; Mohwald, H.; Nakanishi, T. *Chem. Soc. Rev.* **2010**, *39*, 4021–4035.

(33) Guldi, D. M.; Illescas, B. M.; Atienza, C. M.; Wielopolski, M.; Martin, N. *Chem. Soc. Rev.* **2009**, *38*, 1587–1597.

(34) Dong, H.; Wang, C.; Hu, W. *Chem. Commun.* **2010**, *46*, 5211–5222.

(35) Chen, L.; Hong, Z.; Li, G.; Yang, Y. *Adv. Mater.* **2009**, *21*, 1434–1449.

(36) Saunders, B. R.; Turner, M. L. *Adv. Colloid Interface Sci.* **2008**, *138*, 1–23.

(37) Thompson, B.; Fréchet, J. *Angew. Chem. Int. Ed.* **2008**, *47*, 58–77.

(38) Segura, J. L.; Martin, N.; Guldi, D. M. *Chem. Soc. Rev.* **2005**, *34*, 31–47.

(39) Vougioukalakis, G. C.; Roubelakis, M. M.; Orfanopoulos, M. *Chem. Soc. Rev.* **2010**, *39*, 817–844.

(40) Hammett, L. P. *Chem. Rev.* **1935**, *17*, 125–136.

(41) Hammett, L. P. *J. Am. Chem. Soc.* **1937**, *59*, 96–103.

(42) Hansch, C.; Leo, A.; Taft, R. W. *Chemical Reviews* **1991**, *91*, 165–195.

(43) Balzani, V.; Credi, A.; Venturi, M. *Molecular Devices and Machines*; WILEY-VCH Verlag GmbH & Co. KGaA, Weinheim, 2008.

(44) Alberts, B.; Jhonson, A.; Lewis, J.; Raff, M.; Roberts, K.; Walter, P. *Molecular Biology of the Cell*; Forth Edition.; Garland Science, 2002.

(45) Access Protein Data Bank (http://www.rcsb.org/pdb/home/home.do) for details.

(46) Taylor, H. S. *Proc. Am. Phil. Soc.* **1941**, *85*, 1–12.

(47) Huggins, M. L. *Chem. Rev.* **1943**, *32*, 195–218.

(48) Pauling, L.; Corey, R. B.; Branson, H. R. *Proc. Natl. Acad. Sci. USA* **1951**, *37*, 205–11.

(49) Chothia, C. *Annu. Rev. Biochem.* **1984**, *53*, 537–572.

(50) Branden, C.; Tooze, J. *Introduction to Protein Structure*; Garland Science, 1999.

(51) Zhou, Y.; Morais–Cabral, J. H.; Kaufman, A.; MacKinnon, R. *Nature* **2001**, *414*, 43–48.

(52) MacKinnon, R.; Cohen, S. L.; Kuo, A.; Lee, A.; Chait, B. T. *Science* **1998**, *280*,

106–109.

(53) Doyle, D. A.; Cabral, J. M.; Pfuetzner, R. A.; Kuo, A.; Gulbis, J. M.; Cohen, S. L.; Chait, B. T.; MacKinnon, R. *Science* **1998**, *280*, 69–77.

(54) Bordag, N.; Keller, S. *Chem. Phys. Lipids* **2010**, *163*, 1–26.

(55) Beevers, A. J.; Dixon, A. M. *Chem. Soc. Rev.* **2010**, *39*, 2146–2157.

(56) Strömstedt, A. A.; Ringstad, L.; Schmidtchen, A.; Malmsten, M. *Curr. Opin. Colloid Interface Sci.* **2010**, *15*, 467–478.

(57) Mahalka, A. K.; Kinnunen, P. K. *Biochim. Biophys. Acta, Biomembr.* **2009**, *1788*, 1600–1609.

(58) Crisma, M.; Formaggio, F.; Moretto, A.; Toniolo, C. *Biopolymers* **2006**, *84*, 3–12.

(59) Barlow, D. J.; Thornton, J. M. *J. Mol. Biol.* **1988**, *201*, 601–619.

(60) Bolin, K. A.; Millhauser, G. L. *Acc. Chem. Res.* **1999**, *32*, 1027–1033.

(61) Millhauser, G. L. *Biochemistry* **1995**, *34*, 3873–3877.

(62) Millhauser, G. L.; Stenland, C. J.; Hanson, P.; Bolin, K. A.; van de Ven, F. J. *J. Mol. Biol.* **1997**, *267*, 963–974.

(63) Long, H. W.; Tycko, R. *J. Am. Chem. Soc.* **1998**, *120*, 7039–7048.

(64) Karle, I. L.; Balaram, P. *Biochemistry* **1990**, *29*, 6747–6756.

(65) Karle, I. L.; Flippen-Anderson, J. L.; Gurunath, R.; Balaram, P. *Protein Sci.* **1994**, *3*, 1547–1555.

(66) Karle, I. *Biopolymers* **1996**, *40*, 157–180.

(67) Toniolo, C.; Benedetti, E. *Trends Biochem. Sci* **1991**, *16*, 350–353.

(68) Toniolo, C.; Crisma, M.; Formaggio, F.; Peggion, C. *Biopolymers* **2001**, *60*, 396–419.

(69) Otoda, K.; Kitagawa, Y.; Kimura, S.; Imanishi, Y. *Biopolymers* **1993**, *33*, 1337–1345.

(70) Moretto, A.; Formaggio, F.; Kaptein, B.; Broxterman, Q. B.; Wu, L.; Keiderling, T. A.; Toniolo, C. *Pept. Sci.* **2008**, *90*, 567–574.

(71) Marqusee, S.; Baldwin, R. L. *Proc. Natl. Acad. Sci. U. S. A.* **1987**, *84*, 8898–902.

(72) Scholtz, J. M.; Qian, H.; Robbins, V. H.; Baldwin, R. L. *Biochemistry* **1993**, *32*, 9668–9676.

(73) Jackson, D. Y.; King, D. S.; Chmielewski, J.; Singh, S.; Schultz, P. G. *J. Am. Chem. Soc.* **1991**, *113*, 9391–9392.

(74) Peczuh, M. W.; Hamilton, A. D.; Sanchez-Quesada, J.; de, M.; Haack, T.; Giralt, E. *J. Am. Chem. Soc.* **1997**, *119*, 9327–9328.

(75) Haack, T.; Peczuh, M. W.; Salvatella, X.; Sanchez-Quesada, J.; de, M.; Hamilton, A. D.; Giralt, E. *J. Am. Chem. Soc.* **1999**, *121*, 11813–11820.

(76) Blackwell, H. E.; Grubbs, R. H. *Angew. Chem. Int. Ed.* **1998**, *37*, 3281–3284.

(77) Boal, A. K.; Guryanov, I.; Moretto, A.; Crisma, M.; Lanni, E. L.; Toniolo, C.; Grubbs, R. H.; O'Leary, D. J. *J. Am. Chem. Soc.* **2007**, *129*, 6986–6987.

(78) Phelan, J. C.; Skelton, N. J.; Braisted, A. C.; McDowell, R. S. *J. Am. Chem. Soc.* **1997**, *119*, 455–460.

(79) Ousaka, N.; Sato, T.; Kuroda, R. *J. Am. Chem. Soc.* **2008**, *130*, 463–465.

(80) Ousaka, N.; Sato, T.; Kuroda, R. *J. Am. Chem. Soc.* **2009**, *131*, 3820–3821.

(81) Butterfield, S. M.; Patel, P. R.; Waters, M. L. *J. Am. Chem. Soc.* **2002**, *124*, 9751–9755.

(82) Orner, B. P.; Salvatella, X.; Sanchez, Q. J.; De, M. J.; Giralt, E.; Hamilton, A. D. *Angew Chem Int Ed Engl* **2002**, *41*, 117–9.

(83) Shi, Z.; Olson, C. A.; Kallenbach, N. R. *J. Am. Chem. Soc.* **2002**, *124*, 3284–3291.

(84) Albert, J. S.; Hamilton, A. D. *Biochemistry* **1995**, *34*, 984–90.

(85) Wilson, D.; Perlson, L.; Breslow, R. *Bioorg. Med. Chem.* **2003**, *11*, 2649–2653.

(86) Chapman, R. N.; Dimartino, G.; Arora, P. S. *J. Am. Chem. Soc.* **2004**, *126*, 12252–12253.

(87) Wang, D.; Chen, K.; Kulp, J. L.; Arora, P. S. *J. Am. Chem. Soc.* **2006**, *128*, 9248–9256.

(88) Tashiro, S.; Tominaga, M.; Yamaguchi, Y.; Kato, K.; Fujita, M. *Angew. Chem., Int. Ed.* **2006**, *45*, 241–244.

(89) Tashiro, S.; Tominaga, M.; Yamaguchi, Y.; Kato, K.; Fujita, M. *Chem. Eur. J.* **2006**, *12*, 3211–3217.

(90) Hatakeyama, Y.; Sawada, T.; Kawano, M.; Fujita, M. *Angew. Chem., Int. Ed.* **2009**, *48*, 8695–8698.

(91) Dolain, C.; Hatakeyama, Y.; Sawada, T.; Tashiro, S.; Fujita, M. *J. Am. Chem. Soc.* **2010**, *132*, 5564–5565.

(92) Bernal, F.; Tyler, A. F.; Korsmeyer, S. J.; Walensky, L. D.; Verdine, G. L. *J. Am. Chem. Soc.* **2007**, *129*, 2456–2457.

(93) Moellering, R. E.; Cornejo, M.; Davis, T. N.; Bianco, C. D.; Aster, J. C.; Blacklow, S. C.; Kung, A. L.; Gilliland, D. G.; Verdine, G. L.; Bradner, J. E. *Nature* **2009**, *462*, 182–188.

(94) Wang, D.; Liao, W.; Arora, P. S. *Angew. Chem. Int. Ed.* **2005**, *44*, 6525–6529.

(95) Wang, D.; Lu, M.; Arora, P. *Angew. Chem. Int. Ed.* **2008**, *47*, 1879–1882.

(96) Henchey, L. K.; Kushal, S.; Dubey, R.; Chapman, R. N.; Olenyuk, B. Z.; Arora, P. S. *J. Am. Chem. Soc.* **2010**, *132*, 941–943.

(97) Wada, A. *Adv. Biophys.* **1976**, 1–63.

(98) Hol, W. G. J.; van Duijnen, P. T.; Berendsen, H. J. C. *Nature* **1978**, *273*, 443–446.

(99) Hol, W. G. J. *Prog. Biophys. Mol. Biol.* **1985**, *45*, 149–195.

(100) Hol, W. G. *Adv. Biophys.* **1985**, *19*, 133–165.

(101) Datta, A.; Pati, S. K. *Chem. Soc. Rev.* **2006**, *35*, 1305–1323.

(102) Würthner, F.; Yao, S. *Angew. Chem. Int. Ed.* **2000**, *39*, 1978–1981.

(103) Würthner, F.; Yao, S.; Debaerdemaeker, T.; Wortmann, R. *J. Am. Chem. Soc.* **2002**, *124*, 9431–9447.

(104) Würthner, F.; Yao, S.; Beginn, U. *Angew. Chem. Int. Ed.* **2003**, *42*, 3247–3250.

(105) Yao, S.; Beginn, U.; Gress, T.; Lysetska, M.; Würthner, F. *J. Am. Chem. Soc.* **2004**, *126*, 8336–8348.

(106) Ishikawa, T.; Shimasaki, T.; Akashi, H.; Iwanaga, T.; Toyota, S.; Yamasaki, M. *Bull. Chem. Soc. Jpn.* **2010**, *83*, 220–232.

(107) Yashima, E.; Maeda, K.; Iida, H.; Furusho, Y.; Nagai, K. *Chem. Rev.* **2009**, *109*, 6102–6211.

(108) Sanda, F.; Terada, K.; Masuda, T. *Macromolecules* **2005**, *38*, 8149–8154.

(109) Sakurai, S.; Okoshi, K.; Kumaki, J.; Yashima, E. *J. Am. Chem. Soc.* **2006**, *128*, 5650–5651.

(110) Okoshi, K.; Sakurai, S.; Ohsawa, S.; Kumaki, J.; Yashima, E. *Angew. Chem. Int. Ed.* **2006**, *45*, 8173–8176.

(111) Fujiki, M. *J. Am. Chem. Soc.* **2000**, *122*, 3336–3343.

(112) Cheon, K. S.; Selinger, J. V.; Green, M. M. *Angew. Chem. Int. Ed.* **2000**, *39*, 1482–1485.

(113) Tabei, J.; Nomura, R.; Sanda, F.; Masuda, T. *Macromolecules* **2004**, *37*, 1175–1179.

(114) Nishiyama, N.; Kataoka, K. *Pharmacol. Ther.* **2006**, *112*, 630–648.

(115) Branco, M. C.; Schneider, J. P. *Acta Biomater.* **2009**, *5*, 817–831.

(116) Osada, K.; Kataoka, K. In *Peptide Hybrid Polymers*; Advances in Polymer Science; Springer Berlin / Heidelberg, 2006; Vol. 202, pp. 113–153.

(117) Hamley, I. W. *Soft Matter* **2011**, *7*, 4122–4138.

(118) Kanzaki, T.; Horikawa, Y.; Makino, A.; Sugiyama, J.; Kimura, S. *Macromol.*

Biosci. **2008**, *8*, 1026–1033.

(119) Ueda, M.; Makino, A.; Imai, T.; Sugiyama, J.; Kimura, S. *J. Pept. Sci.* **2011**, *17*, 94–99.

(120) Ueda, M.; Makino, A.; Imai, T.; Sugiyama, J.; Kimura, S. *Langmuir* **2011**, *27*, 4300–4304.

(121) Ueda, M.; Makino, A.; Imai, T.; Sugiyama, J.; Kimura, S. *Chem. Commun.* **2011**, *47*, 3204–3206.

(122) Ueda, M.; Makino, A.; Imai, T.; Sugiyama, J.; Kimura, S. *Soft Matter* **2011**, *7*, 4143–4146.

(123) Love, J. C.; Estroff, L. A.; Kriebel, J. K.; Nuzzo, R. G.; Whitesides, G. M. *Chem. Rev.* **2005**, *105*, 1103–1170.

(124) Sekitani, T.; Yokota, T.; Zschieschang, U.; Klauk, H.; Bauer, S.; Takeuchi, K.; Takamiya, M.; Sakurai, T.; Someya, T. *Science* **2009**, *326*, 1516 –1519.

(125) Lee, J.; Chang, H.; Kim, S.; Bang, G.; Lee, H. *Angew. Chem. Int. Ed.* **2009**, *48*, 8501–8504.

(126) Fabre, B. *Acc. Chem. Res.* **2010**, *43*, 1509–1518.

(127) Bhosale, R.; Misek, J.; Sakai, N.; Matile, S. *Chem. Soc. Rev.* **2010**, *39*, 138–149.

(128) Kondo, T.; Uosaki, K. *J. Photochem. Photobiol., C* **2007**, *8*, 1–17.

(129) Imahori, H.; Mori, Y.; Matano, Y. *J. Photochem. Photobiol., C* **2003**, *4*, 51–83.

(130) Samanta, D.; Sarkar, A. *Chem. Soc. Rev.* **2011**, *40*, 2567–2592.

(131) Whitesell, J. K.; Chang, H. K. *Science* **1993**, *261*, 73 –76.

(132) Whitesell, J. K.; Chang, H. K.; Whitesell, C. S. *Angew. Chem. Int. Ed. Engl.* **1994**, *33*, 871–873.

(133) Fujita, K.; Kimura, S.; Imanishi, Y.; Rump, E.; Ringsdorf, H. *Langmuir* **1994**, *10*, 2731–2735.

(134) Fujita, K.; Kimura, S.; Imanishi, Y.; Rump, E.; Ringsdorf, H. *Langmuir* **1995**, *11*, 253–258.

(135) Fujita, K.; Kimura, S.; Imanishi, Y.; Okamura, E.; Umemura, J. *Langmuir* **1995**, *11*, 1675–1679.

(136) Miura, Y.; Kimura, S.; Imanishi, Y.; Umemura, J. *Langmuir* **1998**, *14*, 2761–2767.

(137) Miura, Y.; Kimura, S.; Imanishi, Y.; Umemura, J. *Langmuir* **1999**, *15*, 1155–1160.

(138) Miura, Y.; Kimura, S.; Imanishi, Y.; Umemura, J. *Langmuir* **1998**, *14*, 6935–6940.

(139) Gremlich, H. U.; Fringeli, U. P.; Schwyzer, R. *Biochemistry* **1983**, *22*, 4257–4264.

(140) Holmlin, R. E.; Haag, R.; Chabinyc, M. L.; Ismagilov, R. F.; Cohen, A. E.; Terfort,

A.; Rampi, M. A.; Whitesides, G. M. *J. Am. Chem. Soc.* **2001**, *123*, 5075–5085.

(141) Wold, D. J.; Frisbie, C. D. *J. Am. Chem. Soc.* **2001**, *123*, 5549–5556.

(142) Beebe, J. M.; Engelkes, V. B.; Miller, L. L.; Frisbie, C. D. *J. Am. Chem. Soc.* **2002**, *124*, 11268–11269.

(143) Wold, D. J.; Haag, R.; Rampi, M. A.; Frisbie, C. D. *J. Phys. Chem. B* **2002**, *106*, 2813–2816.

(144) Wang, W.; Lee, T.; Reed, M. A. *Phys. Rev. B* **2003**, *68*, 035416.

(145) Lee, T.; Wang, W.; Klemic, J. F.; Zhang, J. J.; Su, J.; Reed, M. A. *J. Phys. Chem. B* **2004**, *108*, 8742–8750.

(146) Engelkes, V. B.; Beebe, J. M.; Frisbie, C. D. *J. Am. Chem. Soc.* **2004**, *126*, 14287–14296.

(147) Morita, T.; Lindsay, S. *J. Am. Chem. Soc.* **2007**, *129*, 7262–7263.

(148) Seo, K.; Lee, H. *ACS Nano* **2009**, *3*, 2469–2476.

(149) Sachs, S.; Dudek, S.; Hsung, R.; Sita, L.; Smalley, J.; Newton, M.; Feldberg, S.; Chidsey, C. *J. Am. Chem. Soc.* **1997**, *119*, 10563–10564.

(150) Dudek, S. P.; Sikes, H. D.; Chidsey, C. E. D. *J. Am. Chem. Soc.* **2001**, *123*, 8033–8038.

(151) Sikes, H. D.; Smalley, J. F.; Dudek, S. P.; Cook, A. R.; Newton, M. D.; Chidsey, C. E. D.; Feldberg, S. W. *Science* **2001**, *291*, 1519–1523.

(152) Choi, S. H.; Risko, C.; Delgado, M. C. R.; Kim, B.; Brédas, J.; Frisbie, C. D. *J. Am. Chem. Soc.* **2010**, *132*, 4358–4368.

(153) Eckermann, A. L.; Feld, D. J.; Shaw, J. A.; Meade, T. J. *Coord. Chem. Rev.* **2010**, *254*, 1769–1802.

(154) Salomon, A.; Cahen, D.; Lindsay, S.; Tomfohr, J.; Engelkes, V.; Frisbie, C. *Adv. Mater.* **2003**, *15*, 1881–1890.

(155) Selzer, Y.; Allara, D. L. *Annu. Rev. Phys. Chem.* **2006**, *57*, 593.

(156) Long, Y.; Abu-Irhayem, E.; Kraatz, H. *Chem. Eur. J.* **2005**, *11*, 5186–5194.

(157) Boussicault, F.; Robert, M. *Chem. Rev.* **2008**, *108*, 2622–2645.

(158) Kai, M.; Takeda, K.; Morita, T.; Kimura, S. *J. Pept. Sci.* **2008**, *14*, 192–202.

(159) Arikuma, Y.; Nakayama, H.; Morita, T.; Kimura, S. *Angew. Chem. Int. Ed.* **2010**, *49*, 1800–1804.

(160) Arikuma, Y.; Nakayama, H.; Morita, T.; Kimura, S. *Langmuir* **2011**, *27*, 1530–1535.

(161) Kitagawa, K.; Morita, T.; Kimura, S. *J. Phys. Chem. B* **2004**, *108*, 15090–15095.

(162) Kitagawa, K.; Morita, T.; Kimura, S. *Thin Solid Films* **2006**, *509*, 18–26.

(163) Kitagawa, K.; Morita, T.; Kimura, S. *Langmuir* **2005**, *21*, 10624–10631.

(164) Morita, T.; Kimura, S.; Kobayashi, S.; Imanishi, Y. *J. Am. Chem. Soc.* **2000**, *122*, 2850–2859.

(165) Yasutomi, S.; Morita, T.; Imanishi, Y.; Kimura, S. *Science* **2004**, *304*, 1944–1947.

(166) Morita, T.; Yanagisawa, K.; Kimura, S. *Polym. J* **2008**, *40*, 700–709.

(167) Okamoto, S.; Morita, T.; Kimura, S. *Langmuir* **2009**, *25*, 3297–3304.

(168) Okamoto, S.; Morita, T.; Kimura, S. *Chem. Lett.* **2009**, *38*, 126–127.

(169) Wakabayashi, M.; Fujii, S.; Morita, T.; Kimura, S. *Chem. Lett.* **2008**, *37*, 702–703.

(170) Tada, Y.; Morita, T.; Umemura, J.; Iwamoto, M.; Kimura, S. *Polym. J.* **2005**, *37*, 599–607.

(171) Miteva, T.; Palmer, L.; Kloppenburg, L.; Neher, D.; Bunz, U. *Macromolecules* **2000**, *33*, 652–654.

(172) Yang, J.; Yan, J.; Hwang, C.; Chiou, S.; Liau, K.; Gavin Tsai, H.; Lee, G.; Peng, S. *J. Am. Chem. Soc.* **2006**, *128*, 14109–14119.

(173) Seminario, J.; Zacarias, A.; Tour, J. *J. Am. Chem. Soc.* **1998**, *120*, 3970–3974.

(174) Facchetti, A. *Chem. Mater.* **2011**, *23*, 733–758.

(175) Grimsdale, A. C.; Leok Chan, K.; Martin, R. E.; Jokisz, P. G.; Holmes, A. B. *Chem. Rev.* **2009**, *109*, 897–1091.

(176) Grimsdale, A.; Chan, K.; Martin, R.; Jokisz, P.; Holmes, A. *Chem. Rev.* **2009**, *109*, 897–1091.

(177) Cheng, Y.; Yang, S.; Hsu, C. *Chem. Rev.* **2009**, *109*, 5868–5923.

(178) Chen, J.; Cao, Y. *Acc. Chem. Res.* **2009**, *42*, 1709–1718.

(179) Bunz, U. *Chem. Rev.* **2000**, *100*, 1605–1644.

(180) Weder, C.; Sarwa, C.; Bastiaansen, C.; Smith, P. *Adv. Mater.* **1997**, *9*, 1035–1039.

(181) Hirohata, M.; Tada, K.; Kawai, T.; Onoda, M.; Yoshino, K. *Syn. Met.* **1997**, *85*, 1273–1274.

(182) Montali, A.; Bastiaansen, C.; Smith, P.; Weder, C. *Nature* **1998**, *392*, 261–264.

(183) Tour, J. M.; Rawlett, A. M.; Kozaki, M.; Yao, Y.; Jagessar, R. C.; Dirk, S. M.; Price, D. W.; Reed, M. A.; Zhou, C.; Chen, J.; Wang, W.; Campbell, I. *Chem. Eur. J.* **2001**, *7*, 5118–5134.

(184) Bumm, L. A.; Arnold, J. J.; Cygan, M. T.; Dunbar, T. D.; Burgin, T. P.; Jones, L.; Allara, D. L.; Tour, J. M.; Weiss, P. S. *Science* **1996**, *271*, 1705–1707.

(185) Tour, J. M. *Acc. Chem. Res.* **2000**, *33*, 791–804.

(186) Blum, A. S.; Kushmerick, J. G.; Pollack, S. K.; Yang, J. C.; Moore, M.; Naciri, J.; Shashidhar, R.; Ratna, B. R. *J. Phys. Chem. B* **2004**, *108*, 18124–18128.

(187) Blum, A. S.; Yang, J. C.; Shashidhar, R.; Ratna, B. *Appl. Phys. Lett.* **2003**, *82*, 3322.

(188) Davis, W. B.; Svec, W. A.; Ratner, M. A.; Wasielewski, M. R. *Nature* **1998**, *396*, 60–63.

(189) Huber, R.; González, M. T.; Wu, S.; Langer, M.; Grunder, S.; Horhoiu, V.; Mayor, M.; Bryce, M. R.; Wang, C.; Jitchati, R.; Schönenberger, C.; Calame, M. *J. Am. Chem. Soc.* **2008**, *130*, 1080–1084.

(190) Wautelet, P.; Le Moigne, J.; Videva, V.; Turek, P. *J. Org. Chem.* **2003**, *68*, 8025–8036.

(191) Leroy-Lhez, S.; Parker, A.; Lapouyade, P.; Belin, C.; Ducasse, L.; Oberle, J.; Fages, F. *Photochem. Photobiol. Sci.* **2004**, *3*, 949–959.

(192) Pettersson, K.; Kyrychenko, A.; Rönnow, E.; Ljungdahl, T.; Mårtensson, J.; Albinsson, B. *J. Phys. Chem. A* **2006**, *110*, 310–318.

(193) Khairul, W. M.; Fox, M. A.; Schauer, P. A.; Yufit, D. S.; Albesa-Jove, D.; Howard, J. A. K.; Low, P. J. *Dalton Trans.* **2010**, *39*, 11605–11615.

(194) Kushmerick, J. G.; Holt, D. B.; Yang, J. C.; Naciri, J.; Moore, M. H.; Shashidhar, R. *Phys. Rev. Lett.* **2002**, *89*, 086802.

(195) Selzer, Y.; Cai, L.; Cabassi, M.; Yao, Y.; Tour, J.; Mayer, T.; Allara, D. *Nano Lett.* **2005**, *5*, 61–65.

(196) Haiss, W.; Wang, C.; Grace, I.; Batsanov, A. S.; Schiffrin, D. J.; Higgins, S. J.; Bryce, M. R.; Lambert, C. J.; Nichols, R. J. *Nat. Mater.* **2006**, *5*, 995–1002.

(197) Yin, X.; Li, Y.; Zhang, Y.; Li, P.; Zhao, J. *Chem. Phys. Lett.* **2006**, *422*, 111–116.

(198) Wang, W.; Lee, T.; Reed, M. A. *Rep. Prog. Phys.* **2005**, *68*, 523–544.

(199) Simmons, J. G. *J. Appl. Phys.* **1963**, *34*, 1793–1803.

(200) Simmons, J. G. *J. Appl. Phys.* **1963**, *34*, 2581–2590.

(201) Ho, S. C.; Kim, B.; Frisbie, C. D. *Science* **2008**, *320*, 1482–1486.

(202) Lu, Q.; Liu, K.; Zhang, H.; Du, Z.; Wang, X.; Wang, F. *ACS Nano* **2009**, *3*, 3861–3868.

(203) Smalley, J. F.; Sachs, S. B.; Chidsey, C. E. D.; Dudek, S. P.; Sikes, H. D.; Creager, S. E.; Yu, C. J.; Feldberg, S. W.; Newton, M. D. *J. Am. Chem. Soc.* **2004**, *126*, 14620–14630.

(204) Tomfohr, J.; Sankey, O. F. *J. Chem. Phys.* **2004**, *120*, 1542–1554.

(205) Reed, M. A.; Chen, J.; Rawlett, A. M.; Price, D. W.; Tour, J. M. *Appl. Phys. Lett.* **2001**, *78*, 3735–3737.

(206) Yeganeh, S.; Galperin, M.; Ratner, M. A. *J. Am. Chem. Soc.* **2007**, *129*, 13313–13320.

(207) Chen, J.; Reed, M. A.; Rawlett, A. M.; Tour, J. M. *Science* **1999**, *286*, 1550–1552.

(208) D. Le, J.; He, Y.; Hoye, T. R.; Mead, C. C.; Kiehl, R. A. *Appl. Phys. Lett.* **2003**, *83*, 5518–5520.

(209) Moroni, M.; Le Moigne, J.; Pham, T. A.; Bigot, J. *Macromolecules* **1997**, *30*, 1964–1972.

(210) Weder, C.; Wrighton, M. S. *Macromolecules* **1996**, *29*, 5157–5165.

(211) Li, H.; Powell, D. R.; Hayashi, R. K.; West, R. *Macromolecules* **1998**, *31*, 52–58.

(212) Walters, K. A.; Ley, K. D.; Schanze, K. S. *Langmuir* **1999**, *15*, 5676–5680.

(213) McQuade, D. T.; Kim, J.; Swager, T. M. *J. Am. Chem. Soc.* **2000**, *122*, 5885–5886.

(214) Halkyard, C. E.; Rampey, M. E.; Kloppenburg, L.; Studer-Martinez, S. L.; Bunz, U. H. F. *Macromolecules* **1998**, *31*, 8655–8659.

(215) Levitus, M.; Garcia-Garibay, M. A. *J. Phys. Chem. A* **2000**, *104*, 8632–8637.

(216) Levitus, M.; Schmieder, K.; Ricks, H.; Shimizu, K.; Bunz, U.; Garcia-Garibay, M. *J. Am. Chem. Soc.* **2001**, *123*, 4259–4265.

(217) Kim, J.; Swager, T. M. *Nature* **2001**, *411*, 1030–1034.

(218) Yang, J.; Yan, J.; Lin, C.; Chen, C.; Xie, Z.; Chen, C. *Angew. Chem. Int. Ed.* **2009**, *48*, 9936–9939.

(219) Hu, W.; Zhu, N.; Tang, W.; Zhao, D. *Org. Lett.* **2008**, *10*, 2669–2672.

(220) McQuade, D.; Pullen, A.; Swager, T. *Chem. Rev.* **2000**, *100*, 2537–2574.

(221) Zhou, Q.; Swager, T. M. *J. Am. Chem. Soc.* **1995**, *117*, 7017–7018.

(222) Zhou, Q.; Swager, T. M. *J. Am. Chem. Soc.* **1995**, *117*, 12593–12602.

(223) Yang, J.; Swager, T. *J. Am. Chem. Soc.* **1998**, *120*, 5321–5322.

(224) Yang, J.; Swager, T. *J. Am. Chem. Soc.* **1998**, *120*, 11864–11873.

(225) Meyers, F.; Marder, S. R.; Pierce, B. M.; Bredas, J. L. *J. Am. Chem. Soc.* **1994**, *116*, 10703–10714.

(226) Li, Y.; Zhao, J.; Yin, X.; Yin, G. *J. Phys. Chem. A* **2006**, *110*, 11130–11135.

(227) Staykov, A.; Nozaki, D.; Yoshizawa, K. *J. Phys. Chem. C* **2007**, *111*, 3517–3521.

(228) Kitagawa, K.; Morita, T.; Kimura, S. *Angew. Chem. Int. Ed.* **2005**, *44*, 6330–6333.

(229) Kitagawa, K.; Morita, T.; Kimura, S. *J. Phys. Chem. B* **2005**, *109*, 13906–13911.

(230) Steed, J. W.; Turner, D. R.; Wallace, K. *Core Concepts in Supramolecular Chemistry and Nanochemistry*; 1st ed.; Wiley, 2007.

(231) Zayed, J. M.; Nouvel, N.; Rauwald, U.; Scherman, O. A. *Chem. Soc. Rev.* **2010**, *39*, 2806–2816.

(232) Zhang, X.; Wang, C. *Chem. Soc. Rev.* **2011**, *40*, 94–101.

(233) Hill, D.; Mio, M.; Prince, R.; Hughes, T.; Moore, J. *Chem. Rev.* **2001**, *101*, 3893–4011.

(234) Goodman, C. M.; Choi, S.; Shandler, S.; DeGrado, W. F. *Nat. Chem. Biol.* **2007**, *3*, 252–262.

(235) Ishikawa, T.; Morita, T.; Kimura, S. *Bull. Chem. Soc. Jpn.* **2007**, *80*, 1483–1491.

(236) Becke, A. D. *J. Chem. Phys.* **1993**, *98*, 5648–5652.

(237) Ditchfield, R.; Hehre, W. J.; Pople, J. A. *J. Chem. Phys.* **1971**, *54*, 724–728.

(238) Li, F.; Zare, R. *J. Phys. Chem. B* **2005**, *109*, 3330–3333.

(239) Toniolo, C.; Polese, A.; Formaggio, F.; Crisma, M.; Kamphuis, J. *J. Am. Chem. Soc.* **1996**, *118*, 2744–2745.

(240) Kennedy, D. F.; Crisma, M.; Toniolo, C.; Chapman, D. *Biochemistry* **1991**, *30*, 6541–6548.

(241) Meier, H.; Mu"hling, B.; Kolshorn, H. *Eur. J. Org. Chem.* **2004**, *2004*, 1033–1042.

(242) Risko, C.; Zangmeister, C. D.; Yao, Y.; Marks, T. J.; Tour, J. M.; Ratner, M. A.; van Zee, R. D. *J. Phys. Chem. C* **2008**, *112*, 13215–13225.

(243) Staykov, A.; Nozaki, D.; Yoshizawa, K. *J. Phys. Chem. C* **2007**, *111*, 11699–11705.

(244) Halkyard, C.; Rampey, M.; Kloppenburg, L.; Studer-Martinez, S.; Bunz, U. *Macromolecules* **1998**, *31*, 8655–8659.

(245) Masuo, S.; Yoshikawa, H.; Asahi, T.; Masuhara, H.; Sato, T.; Jiang, D.; Aida, T. *J. Phys. Chem. B* **2003**, *107*, 2471–2479.

(246) Morino, N.; Kitagawa, K.; Morita, T.; Kimura, S. *Thin Solid Films* **2005**, *479*, 261–268.

(247) Horne, W. S.; Gellman, S. H. *Acc. Chem. Res.* **2008**, *41*, 1399–1408.

(248) Vijayakumar, E. K. S.; Sudha, T. S.; Balaram, P. *Biopolymers* **1984**, *23*, 877–886.

(249) Balaram, H.; Sukumar, M.; Balaram, P. *Biopolymers* **1986**, *25*, 2209–2223.

(250) Chen, Y.; Yang, J. T.; Martinez, H. M. *Biochemistry* **1972**, *11*, 4120–4131.

(251) Vijayakumar, E. K. S.; Balaram, P. *Tetrahedron* **1983**, *39*, 2725–2731.

(252) Holzwarth, G.; Doty, P. *J. Am. Chem. Soc.* **1965**, *87*, 218–228.

(253) Liu, L. T.; Yaron, D.; Sluch, M. I.; Berg, M. A. *J. Phys. Chem. B* **2006**, *110*, 18844–18852.

(254) James, P.; Sudeep, P.; Suresh, C.; Thomas, K. *J. Phys. Chem. A* **2006**, *110*, 4329–4337.

(255) Sluch, M.; Godt, A.; Bunz, U.; Berg, M. *J. Am. Chem. Soc.* **2001**, *123*, 6447–6448.

(256) Cornil, J.; Beljonne, D.; Heller, C.; Campbell, I.; Laurich, B.; Smith, D.; Bradley, D.; Müllen, K.; Brédas, J. *Chem. Phys. Lett.* **1997**, *278*, 139–145.

(257) Gierschner, J.; Mack, H.; Luer, L.; Oelkrug, D. *J. Chem. Phys.* **2002**, *116*, 8596–8609.

(258) Heimel, G.; Daghofer, M.; Gierschner, J.; List, E. J. W.; Grimsdale, A. C.; Mullen, K.; Beljonne, D.; Bredas, J.; Zojer, E. *J. Chem. Phys.* **2005**, *122*, 054501.

(259) Fiesel, R.; Halkyard, C. E.; Rampey, M. E.; Kloppenburg, L.; Studer-Martinez, S. L.; Scherf, U.; Bunz, U. H. F. *Macromol. Rapid Commun.* **1999**, *20*, 107–111.

(260) Peeters, E.; Christiaans, M. P. T.; Janssen, R. A. J.; Schoo, H. F. M.; Dekkers, H. P. J. M.; Meijer, E. W. *J. Am. Chem. Soc.* **1997**, *119*, 9909–9910.

(261) Oda, M.; Nothofer, H.; Lieser, G.; Scherf, U.; Meskers, S. C. J.; Neher, D. *Adv. Mater.* **2000**, *12*, 362–365.

(262) Fiesel, R.; Scherf, U. *Acta Polym.* **1998**, *49*, 445–449.

(263) Fiesel, R.; Huber, J.; Apel, U.; Enkelmann, V.; Hentschke, R.; Scherf, U.; Cabrera, K. *Macromol. Chem. Phys.* **1997**, *198*, 2623–2650.

(264) Parker, C. A.; Rees, W. T. *Analyst* **1960**, *85*, 587–600.

(265) Nakayama, H.; Kimura, S. *J. Org. Chem.* **2009**, *74*, 3462–3468.

(266) Beeby, A.; Findlay, K.; Low, P. J.; Marder, T. B. *J. Am. Chem. Soc.* **2002**, *124*, 8280–8284.

(267) Yoshida, K.; Kawamura, S.; Morita, T.; Kimura, S. *J. Am. Chem. Soc.* **2006**, *128*, 8034–8041.

(268) Cuthbert, J. D.; Thomas, D. G. *Phys. Rev.* **1967**, *154*, 763.

(269) Yanagisawa, K.; Morita, T.; Kimura, S. *J. Am. Chem. Soc.* **2004**, *126*, 12780–12781.

(270) Takeda, K.; Morita, T.; Kimura, S. *J. Phys. Chem. B* **2008**, *112*, 12840–12850.

(271) Arikuma, Y.; Takeda, K.; Morita, T.; Ohmae, M.; Kimura, S. *J. Phys. Chem. B* **2009**, *113*, 6256–6266.

(272) Clegg, R.; Hutchison, J. *Langmuir* **1996**, *12*, 5239–5243.

(273) Tam-Chang, S.; Biebuyck, H. A.; Whitesides, G. M.; Jeon, N.; Nuzzo, R. G.

Langmuir **1995**, *11*, 4371–4382.

(274) Sek, S.; Palys, B.; Bilewicz, R. *J. Phys. Chem. B* **2002**, *106*, 5907–5914.

(275) Dunbar, T. D.; Cygan, M. T.; Bumm, L. A.; McCarty, G. S.; Burgin, T. P.; Reinerth, W. A.; Jones, L.; Jackiw, J. J.; Tour, J. M.; Weiss, P. S.; Allara, D. L. *J. Phys. Chem. B* **2000**, *104*, 4880–4893.

(276) Cygan, M. T.; Dunbar, T. D.; Arnold, J. J.; Bumm, L. A.; Shedlock, N. F.; Burgin, T. P.; Jones, L.; Allara, D. L.; Tour, J. M.; Weiss, P. S. *J. Phys. Chem. B* **1998**, *120*, 2721–2732.

(277) Dhirani, A.; Lin, P.; Guyot-Sionnest, P.; Zehner, R. W.; Sita, L. R. *J. Chem. Phys.* **1997**, *106*, 5249–5253.

(278) Stapleton, J. J.; Harder, P.; Daniel, T. A.; Reinard, M. D.; Yao, Y.; Price, D. W.; Tour, J. M.; Allara, D. L. *Langmuir* **2003**, *19*, 8245–8255.

(279) Villares, A.; Lydon, D. P.; Robinson, B. J.; Ashwell, G. J.; Royo, F. M.; Low, P. J.; Cea, P. *Surf. Sci.* **2008**, *602*, 3683–3687.

(280) Villares, A.; Lydon, D. P.; Low, P. J.; Robinson, B. J.; Ashwell, G. J.; Royo, F. M.; Cea, P. *Chem. Mater.* **2008**, *20*, 258–264.

(281) Villares, A.; Lydon, D. P.; Porres, L.; Beeby, A.; Low, P. J.; Cea, P.; Royo, F. M. *J. Phys. Chem. B* **2007**, *111*, 7201–7209.

(282) Kasha, M.; Rawls, H. R.; El-Bayoumi, M. A. *Pure Appl. Chem.* **1965**, *11*, 371–392.

(283) Kim, J.; McQuade, D.; McHugh, S.; Swager, T. *Angew. Chem. Int. Ed.* **2000**, *39*, 3868–3872.

(284) Datta, S.; Tian, W.; Hong, S.; Reifenberger, R.; Henderson, J. I.; Kubiak, C. P. *Phys. Rev. Lett.* **1997**, *79*, 2530.

(285) Qian, Y.; Yang, G.; Yu, J.; Jung, T. A.; Liu, G. *Langmuir* **2003**, *19*, 6056–6065.

(286) Sisido, M.; Hoshino, S.; Kusano, H.; Kuragaki, M.; Makino, M.; Sasaki, H.; Smith, T. A.; Ghiggino, K. P. *J. Phys. Chem. B* **2001**, *105*, 10407–10415.

(287) Li, X.; He, J.; Hihath, J.; Xu, B.; Lindsay, S. M.; Tao, N. *J. Am. Chem. Soc.* **2006**, *128*, 2135–2141.

(288) Michaelson, H. B. *J. Appl. Phys.* **1977**, *48*, 4729.

(289) Watanabe, J.; Morita, T.; Kimura, S. *J. Phys. Chem. B* **2005**, *109*, 14416–14425.

(290) Beebe, J. M.; Kim, B.; Frisbie, C. D.; Kushmerick, J. G. *ACS Nano* **2008**, *2*, 827–832.

(291) Otsuki, J. *Coord. Chem. Rev.* **2010**, *254*, 2311–2341.

(292) Auwarter, W.; Weber-Bargioni, A.; Riemann, A.; Schiffrin, A.; Groning, O.; Fasel, R.; Barth, J. V. *J. Chem. Phys.* **2006**, *124*, 194708–6.

(293) Jung, T. A.; Schlittler, R. R.; Gimzewski, J. K.; Tang, H.; Joachim, C. *Science* **1996**, *271*, 181–184.

(294) Moresco, F.; Meyer, G.; Rieder, K.; Tang, H.; Gourdon, A.; Joachim, C. *Phys. Rev. Lett.* **2001**, *86*, 672.

(295) Liang, G. C.; Ghosh, A. W.; Paulsson, M.; Datta, S. *Phys. Rev. B* **2004**, *69*, 115302.

(296) Bevan, K.; Zahid, F.; Kienle, D.; Guo, H. *Phys. Rev. B* **2007**, *76*.

(297) Bevan, K.; Kienle, D.; Guo, H.; Datta, S. *Phys. Rev. B* **2008**, *78*.

(298) Galka, M. M.; Kraatz, H. *ChemPhysChem* **2002**, *3*, 356–359.

(299) Mandal, H. S.; Kraatz, H. *Chem. Phys.* **2006**, *326*, 246–251.

(300) Sek, S.; Misicka, A.; Swiatek, K.; Maicka, E. *J. Phys. Chem. B* **2006**, *110*, 19671–19677.

(301) Miura, Y.; Xu, G.; Kimura, S.; Kobayashi, S.; Iwamoto, M.; Imanishi, Y.; Umemura, J. *Thin Solid Films* **2001**, *393*, 59–65.

(302) Olah, G. A.; Huang, H. W. *J. Chem. Phys.* **1988**, *89*, 2531.

(303) Bode, K. A.; Applequist, J. *J. Am. Chem. Soc.* **1996**, *100*, 17825–17834.

(304) Li, D.; Marks, T. J.; Ratner, M. A. *J. Phys. Chem.* **1992**, *96*, 4325–4336.

(305) Kanis, D. R.; Ratner, M. A.; Marks, T. J. *Chem. Rev.* **1994**, *94*, 195–242.

(306) Girling, I. R.; Cade, N. A.; Kolinsky, P. V.; Jones, R. J.; Peterson, I. R.; Ahmad, M. M.; Neal, D. B.; Petty, M. C.; Roberts, G. G.; Feast, W. J. *J. Opt. Soc. Am. B* **1987**, *4*, 950–954.

(307) Yokoyama, S.; Nakahama, T.; Otomo, A.; Mashiko, S. *Thin Solid Films* **1998**, *331*, 248–253.

(308) Decher, G.; Tieke, B.; Bosshard, C.; Gunter, P. *J. Chem. Soc., Chem. Commun.* **1988**, 933–934.

(309) Manaka, T.; Taguchi, D.; Nakamura, D.; Higa, H.; Iwamoto, M. *Colloids Surf., A* **2005**, *257–258*, 319–323.

List of Publications

Chapter I

Dipole Effects on Molecular and Electronic Structures in a Novel Conjugate of Oligo(phenyleneethynylene) and Helical Peptide
Hidenori Nakayama, Tomoyuki Morita, and Shunsaku Kimura
Phys. Chem. Chem. Phys., **2009**, *11*, 3967–3976.
DOI: 10.1039/b817685j

Chapter II

Chiral Pseudotriangle Oligophenyleneethynylene Formed by Dipole–Dipole Interaction of Helical Peptides
Hidenori Nakayama and Shunsaku Kimura
Chem. Commun., submitted.

Chapter III

Chirally Twisted Oligo(phenyleneethynylene) by Cyclization with α-Helical Peptide
Hidenori Nakayama and Shunsaku Kimura
J. Org. Chem., **2009**, *74*, 3462–3468.
DOI: 10.1021/jo9001905

Chapter IV

Suppression of HOMO–LUMO Transition in a Twist Form of Oligo(Phenyleneethynylene) Clamped by a Right-Handed Helical Peptide
Hidenori Nakayama and Shunsaku Kimura
J. Chem. Phys. A, **2011**, 115, 8960–8968.
DOI: 10.1021/jp200997c

Chapter V

Electric Field Effect of Helical Peptide Dipole in Self-Assembled Monolayers on Electronic Structure of Oligo(Phenyleneethynylene)
Hidenori Nakayama, Tomoyuki Morita, and Shunsaku Kimura
J. Phys. Chem. C, **2010**, *114*, 4669–4674.
DOI: 10.1021/jp101021d

Chapter VI Oligo(phenyleneethyylene) as a molecular lead for STM measurement of single molecule conductance of helical peptide
Hidenori Nakayama and Shunsaku Kimura
Chem. Phys. Lett., **2011**, *508*, 281–284.
DOI: 10.1016/j.cplett.2011.04.063

Chapter VII Vertical Orientation with a Narrow Distribution of Helical Peptides Immobilized on Quartz Substrate by Stereocomplex Formation
Hidenori Nakayama, Takaaki Manaka, Mitsumasa Iwamoto, and Shunsaku Kimura
Soft Matter submitted.

Other publications

Electric field effect of helical peptide dipole on oligo-(phenyleneethynylene) in the conjugate with respect to its electronic structure, molecular orientation, and assembly formation
Hidenori Nakayama, Tomoyuki Morita, and Shunsaku Kimura
PMSE Preprints, **2008**, *99*, 525–526.

Electric-field effect of helical peptide dipole in self-assembled monolayers on electronic state of oligo(phenyleneethynylene)
Hidenori Nakayama, Tomoyuki Morita, and Shunsaku Kimura
Polymer Preprints, **2009**, 50, 472–473.

Molecular dipole engineering. Modulation of π-conjugate system by molecular dipole with OPE-peptide composite
Hidenori Nakayama, Tomoyuki Morita, and Shunsaku Kimura
Kyoto Daigaku Nippon Kagaku Sen'i Kenkyusho Koenshu I, **2010**, *67*, 7–12.

Electron Hopping over 100 Å Along an α-Helix
Yoko Arikuma, Hidenori Nakayama, Tomoyuki Morita, and Shunsaku Kimura
Angew. Chem. Int. Ed., **2010**, *49*, 1800–1804.

DOI: 10.1002/anie.200905621

Ultra-Long-Range Electron Transfer through a Self-Assembled Monolayer on Gold Composed of 120-Å-Long α-Helices
Yoko Arikuma, Hidenori Nakayama, Tomoyuki Morita, and Shunsaku Kimura
Langmuir, **2011**, *27*, 1530–1535.
DOI: 10.1021/la103882r

Appendix

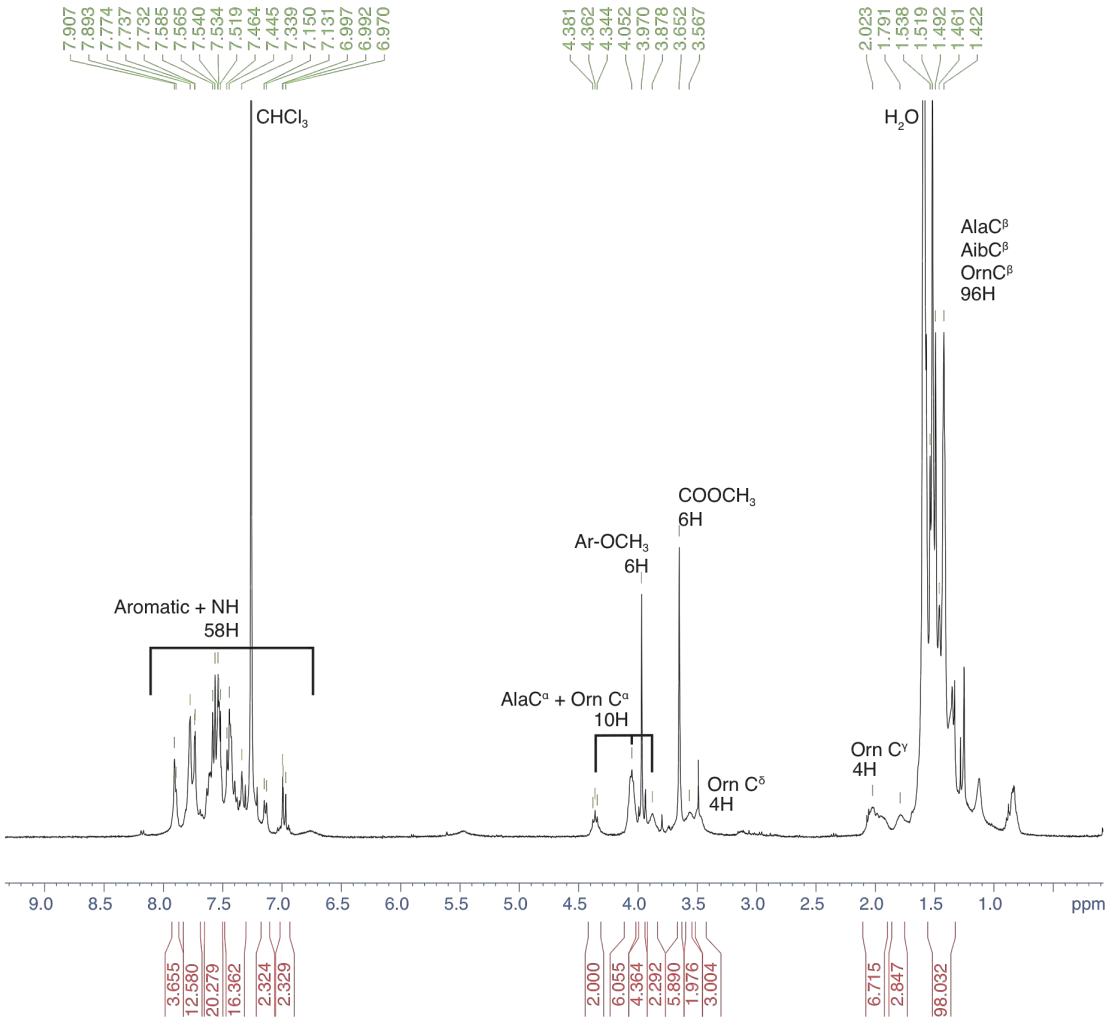

Figure A-II-1. ^{1}H NMR spectrum of **f-OPEBE** in chloroform-*d*.

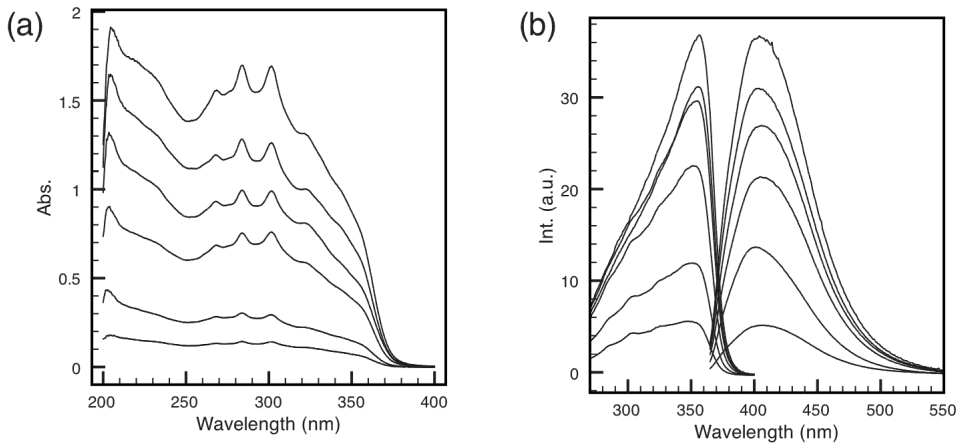

Figure A-II-2. Optical spectra of **f-OPEBE** in methanol at 2–20 × 10^{-6} M: (a) absorption spectra, and (b) fluorescence (excited at 355 nm) and excitation spectra (fluorescence at 410 nm).

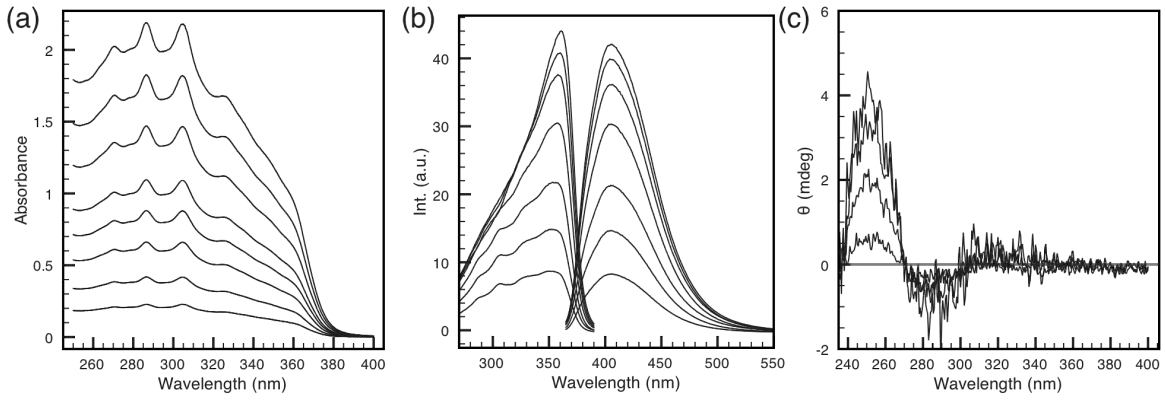

Figure A-II-3. Optical spectra of **f-OPEBE** in dichloromethane: (a) absorption spectra at 2.6–26 × 10^{-6} M, (b) fluorescence (excited at 355 nm) and excitation spectra (fluorescence at 405 nm) 2.6–26 × 10^{-6} M, and (c) circular dichroism spectra at 9–35 × 10^{-6} M.

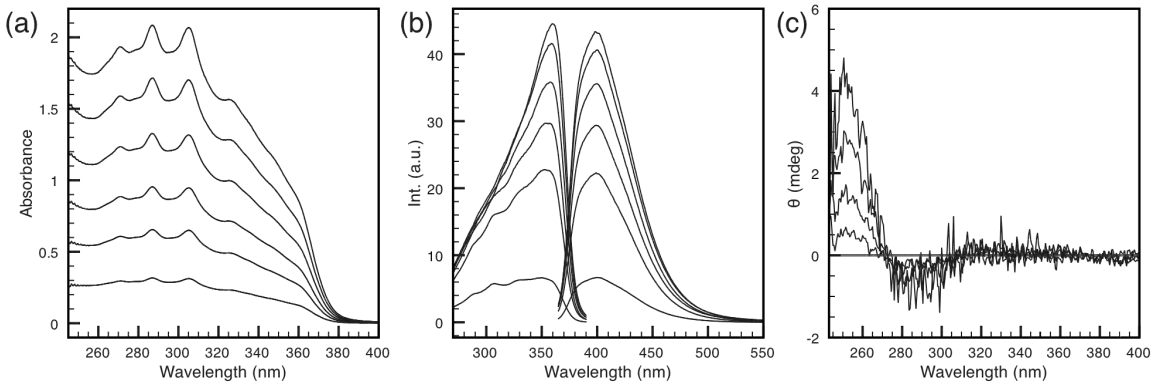

Figure A-II-4. Optical spectra of **f-OPEBE** in methanol: (a) absorption spectra at 4.5–26 × 10^{-6} M, (b) fluorescence (excited at 355 nm) and excitation spectra (fluorescence at 405 nm) 4.5–26 × 10^{-6} M, and (c) circular dichroism spectra at 9–35 × 10^{-6} M.

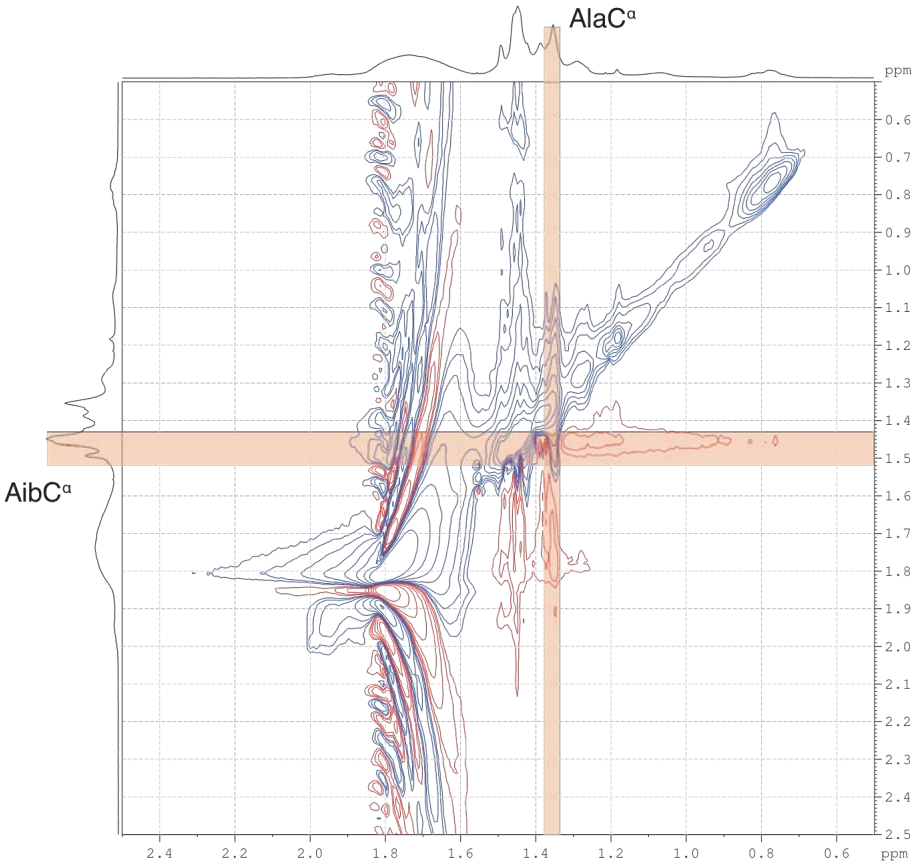

Figure A-II-5. NOESY of **f-OPEBE** in chloroform-*d*. A little amount of methanol was added to shift a peak of water from 1.56 ppm to 1.7 ppm

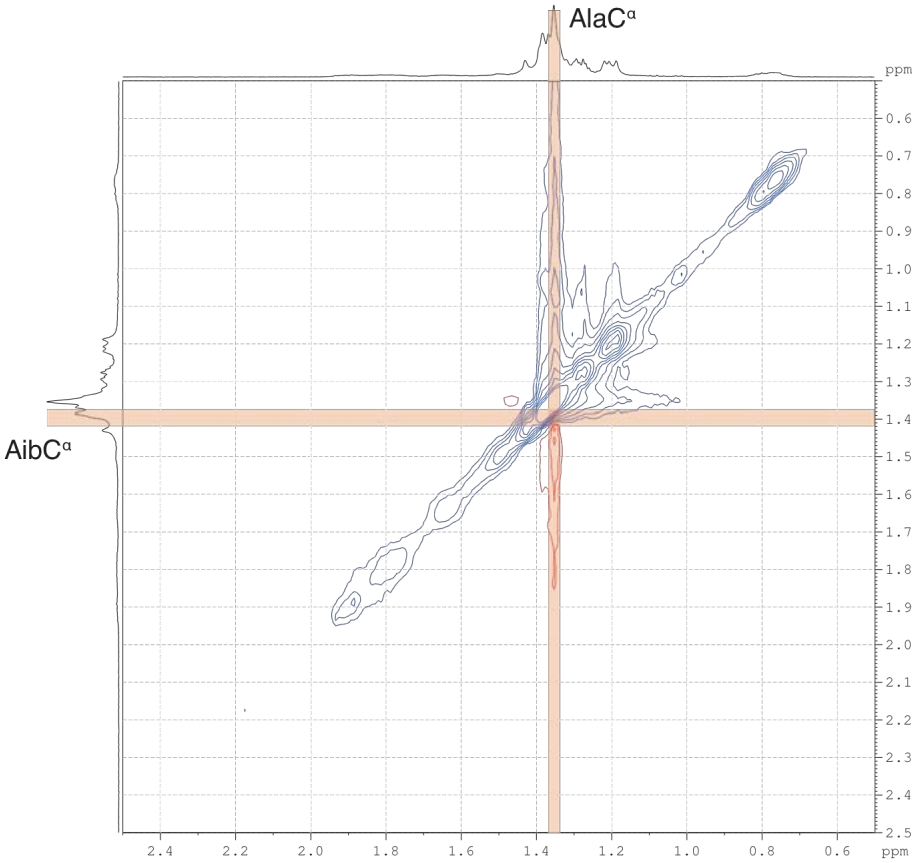

Figure A-II-6. NOESY of **f-OPEBE** in methanol-d_4.

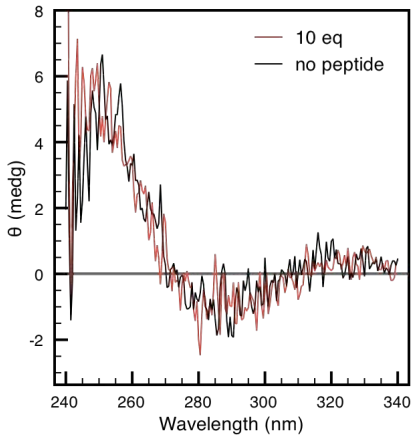

Figure A-II-7. Circular dichroism of **f-OPEBE** in chloroform with the addition of ten equivalents of Boc-(D-Ala-Aib)$_4$-OMe (red) and without (black).

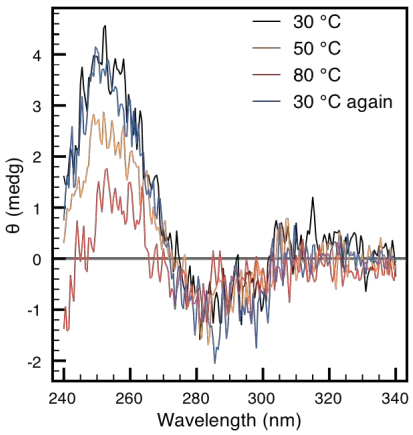

Figure A-II-8. Circular dichroism spectra of **f-OPEBE** in 1,2-dichloroethane with varying temperature in the range of 30to 80 °C (2.6×10^{-5} M).

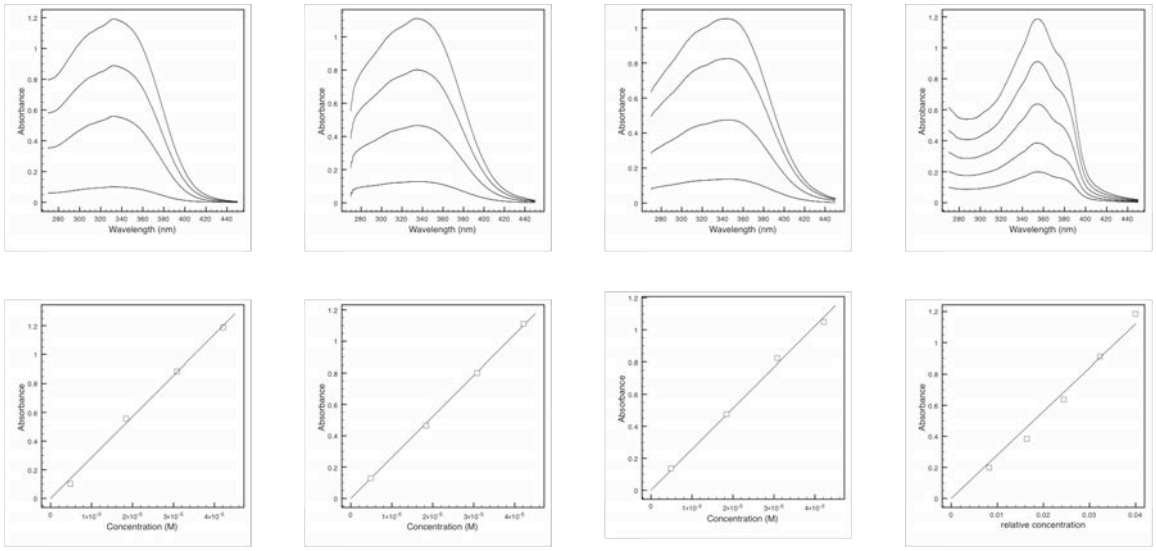

SSA8=OPE in chloroform | **SSA8=OPE** in DMF | **SSA8=OPE** in DMSO | **AcOPE** in chloroform

Figure A-IV-1. Absorption spectra of **SSA8=OPE** in chloroform, DMF, and DMSO, and that of **AcOPE** in chloroform in various concentrations.

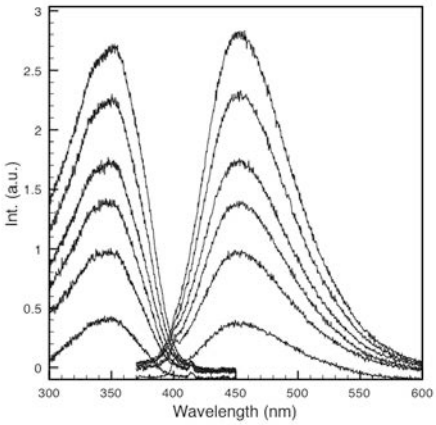

Figure A-IV-2. Fluorescence and excitation spectra of **SSA8=OPE** in MeOH in the concentration of 3.5–32 mM.

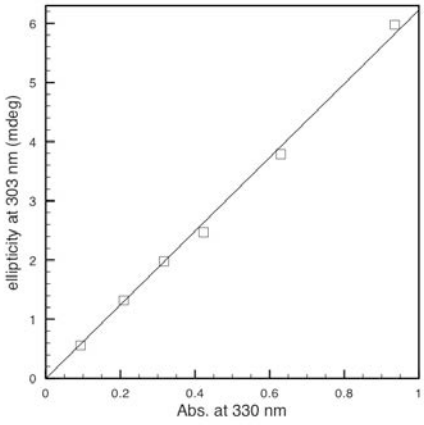

Figure A-IV-3. Absorption vs. ellipticity plot of **SSA8=OPE** in MeOH.

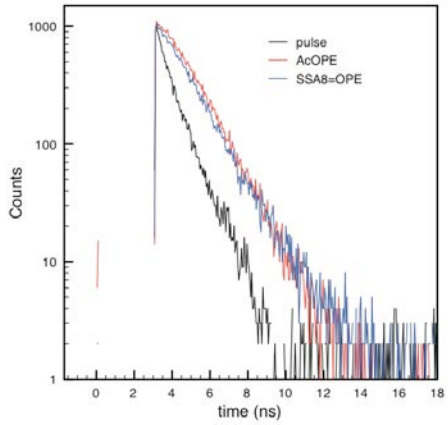

Figure A-IV-4. Fluorescence decay curves on **SSA8=OPE** and **AcOPE** in chloroform.

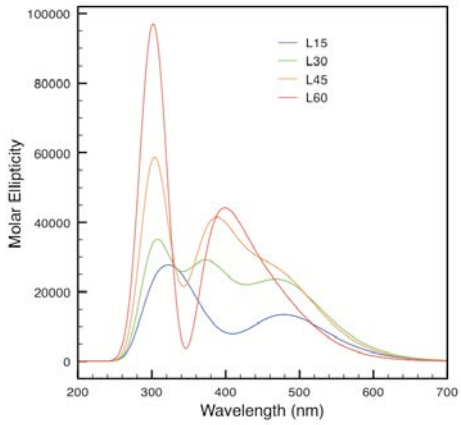

Figure A-IV-5. Circular dichroism spectra obtained with TD-DFT calculations on left-handed twisted structure of **M1**. Four twisted geometries having dihedral angle of 15°, 30°, 45°, and 60° between adjacent benzene rings were generated (named **L15**, **L30**, **L45**, and **L60**, respectively) and lowest ten excited states were calculated for each geometry.

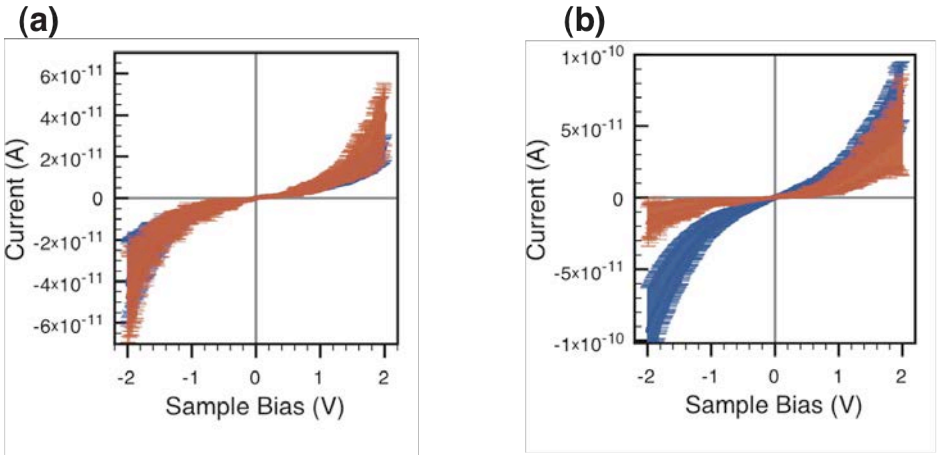

Figure A-VI-1. *I–V* curves of **8OPE** (red) and **C10** (blue) by STS measurements at conditions of (a) +1 V, 5.5–6 pA and (b) +1 V, 19 pA. The distribution of the curves shows the standard deviation.

Acknowledgement

The present research has been carried out under the supervision of Prof. Dr. Shunsaku Kimura from April 2006 to March 2012 at the Department of Material Chemistry, Graduate School of Engineering, Kyoto University.

The author owes his deepest gratitude to Prof. Dr. Kimura. He gave the author a lot of chances to challenge researches with the author's ideas. On the other hand, he kindly supported the author whenever he lost his way. The author positively acknowledges that it is Prof. Dr. Kimura's balanced guidance drew out the author's passion and ability to complete his researches. Prof. Dr. Kimura also allowed the author to make several presentations abroad. The feedbacks and discussions during the presentations were meaningful. The author shall reply to Prof. Dr. Kimura's kindness by contributing to the development of science and technology in the future.

The author is grateful to Dr. Tomoyuki Morita for his constructive discussions and introduction on theories on physical chemistry and experimental equipment. The author would have not been able to expand his research to the area of computational chemistry and photochemistry without instructions by Dr. Morita.

The author is grateful to Prof. Dr. Toshikazu Takigawa, Department of Material Chemistry, and Prof. Dr. Kazuyoshi Tanaka, Department of Molecular Engineering, for their valuable comments on the dissertation.

The author is grateful to Dr. Hitoshi Ohmae and Dr. Akira Makino. Advices on organic synthesis from Dr. Ohmae were helpful. Dr. Makino encouraged the author in the time of difficulties.

The author would like to show his graduate to Dr. Futoshi Fujimura and Mr. Takahito

Ishikawa. Dr. Fujimura introduced the author how his mind should be when he tackles experimental difficulties. Mr. Ishikawa was a kind tutor of the very rudiments of scientific experiments and writings. Their guidance has been the solid basis of the author's technique and philosophy on scientific research.

The author is grateful to Yusuke Ishihara for his helpful discussions and for sharing the joys and sorrows.

The author appreciates Liang Bing for her contribution for correction of grammatical mistakes in the manuscript.

It is a great pleasure of express his appreciation to all members of the Kimura Laboratory in Kyoto University for their active and enjoyable collaboration. The author shared peaceful time with each of the members in the laboratory.

The author is grateful to the Japan Society for the Promotion of Science for financial support.

The author would like to express his appreciation to his father, Dr. Takenori Nakayama and his mother, Mrs. Keiko Nakayama. Dr. Nakayama insinuated the importance of hardworking to complete a tough job. Mrs. Nakayama expanded the author's interest to cultural and social matters. She also has repeatedly taught the author how to prevent mistakes and reduce uncertainty when he executes his task. The author was not aware of the importance of well-preparation and risk management when he was young, but now he acknowledges that these are essential to survive hardships. Their devoted education throughout the author's life as well as financial support was essential to run the researches.

January 2012

Hidenori Nakayama